In vitro and *in vivo* analysis of the CXC chemokine receptor 6 in leukocyte recruitment and allergic lung inflammation

Von der Fakultät für Mathematik, Informatik und Naturwissenschaften der RWTH Aachen University zur Erlangung des akademischen Grades einer Doktorin der Naturwissenschaften genehmigte Dissertation

vorgelegt von

Diplom-Biologin

Andrea Koenen

aus Kempen

Berichter: Universitätsprofessor Dr. rer. nat. Andreas Ludwig

Universitätsprofessor Dr. rer. nat. Hermann Wagner

Tag der mündlichen Prüfung: 13.05.2016

Meiner Familie

Table of contents

1 Introduction

1.1 Cell migration in health and disease

Directional cell movement within the body of higher organisms represents a critical cell function and is regulated by both biochemical and mechanical interactions. Tight regulation of cell migration is necessary because the induction of cell migration is critical during many different mechanisms in health and disease. Embryonic development[1], cancer metastasis[2], angiogenesis[3], the regeneration of peripheral nerves[4], wound healing[5] and inflammation are highly dependent on migratory processes. During an immune response, recruitment of leukocytes from the vasculature into inflamed tissue is a major process and essential for immunological defence. Recruitment of leukocytes comprises several steps, including adhesion to endothelial cells of the blood vessels followed by the transmigration through the endothelial cell layer and migration into the tissue to sites of inflammation. Directional migration of leukocytes is called chemotaxis and involves the activity of chemotactic factors secreted by different cells, such as endothelial cells, smooth muscle cells and other leukocytes. Chemotactic factors are a diverse group of chemicals that include lipids, formylated peptides, proteolytic fragments of complement proteins, and chemokines, which represent a family of small, chemoattractant cytokines. By interaction with their receptors on the cell surface, chemokines induce chemotactic cell migration of a target cell. Chemotaxis is a highly regulated process and induces a polarisation of the leukocytic cell on the leading edge, resulting in a functional specialisation of this cell domain in signal transduction and further migration[6].

1.2 Chemokines

The chemokine system, consisting of seven transmembrane receptors and chemokine ligands is essential to coordinate migration, activation, differentiation and survival of many cells in vertebrates[7–9]. About 45 chemokines are expressed by different cell types, including leukocytes[10], epithelial cells[11], interstitial cells[12], fibroblasts[13] and endothelial cells[14]. The physiologic importance of this family of chemotactic cytokines is derived from their specificity to interact with distinct receptors. There are four major chemokine sub-families including the XC-, CC-, CXC- and CX_3C-chemokines which differ upon the position of highly conserved cysteine residues of the N-terminal site of the chemokine domain. The chemokine family can also be

subdivided with respect to the function of these chemokine members in health and disease. Some chemokines are expressed during an immune response at a site of infection due to interleukin-1 (IL-1) or tumour necrosis factor (TNF) stimulation and act inflammatory by attracting immune effector cells[15,16]. Besides, chemokines are involved in controlling directional cell migration during tissue development[1,7] and homeostasis to maintain tissue function. Most chemokines are produced and released as soluble mediators of low molecular weight (8—10 kDa). By contrast, CX_3CL1 and CXCL16 are expressed as transmembrane glycoproteins of 95 and 50-60 kDa[11,15,17], respectively. Their chemokine domain is linked to a heavily glycosylated mucin-like stalk followed by a transmembrane domain and a short cytoplasmic C-terminal domain. These transmembrane chemokines can be released from the cell membrane by proteolytic cleavage close to the cell surface. This process is termed shedding and is mediated by members of the a disintegrin and metalloproteinase (ADAM) family.

As mentioned, chemokines play key roles in the accumulation and recruitment of diverse cells in physiological processes during embryonic development and in pathophysiological processes such as cancer and inflammation. Most cancers express a complex array of chemokines, thereby influencing the local microenvironment through recruitment of stromal cells and by stimulating angiogenesis[18]. Besides the role of chemokines in cancer, chemokines contribute to inflammatory processes by mediating the recruitment of different leukocyte subsets to sites of inflammation by specific chemokine–chemokine receptor interactions resulting in migration and adhesion of chemokine receptor expressing cells. Chemokines can become immobilised on the surface of endothelial cells by interaction with e.g. glycosaminoglycans or heparan sulphate proteoglycans[19,20] or they are expressed as transmembrane proteins (CXCL16/CX_3CL1) and are presented to leukocytes. Activation of leukocytes by chemokines leads to their extravasation into the inflamed tissue. Thereafter, leukocytes are guided by directional cues provided by localised sources of chemokines and emerging chemokine gradients to move towards sites of inflammation or infection. Therefore, many diseases, which are linked to increased amounts of inflammatory cells, like rheumatoid arthritis, atherosclerosis and asthma, are dependent on the release of chemokines and the recruitment of chemokine receptor expressing cells. For example, CCL2 (also called monocyte chemotactic protein 1 (MCP-1)) is rapidly produced by stromal cells and immune cells after pattern-recognition receptor activation or after cytokine stimulation during arteriosclerosis, leading to monocyte recruitment[9]. In addition, CXCL16 is reported to be

important during the progression of rheumatoid arthritis[21] and is also suspected to induce T cell recruitment into healthy lung tissue[11,22].

1.3 Chemokine receptors

Chemokines exert their function by the interaction with their cognate receptors. Chemokine receptors belong to the rhodopsin-like family of seven transmembrane receptors and are classified by different features. XC-, CC-, CXC- and CX_3C-chemokine receptors only bind XC-, CC-, CXC- and CX_3C-chemokines respectively. Eighteen of the known chemokine receptors are GTP binding protein coupled receptors (GPCRs), which interact with $G\alpha_i$-subunits of the heterotrimeric G proteins to induce intracellular signalling upon chemokine binding. Some chemokine receptors of this GPCR group are also capable of interacting with the $G\alpha_q$-subunit. An additional group of chemokine receptors consists of seven atypical chemokine receptors, which do not interact with G proteins[8]. Instead of interacting with G proteins, this type of chemokine receptors are described to interact with β-arrestin, Rab GTPases and kinases[23]. Furthermore atypical chemokine receptors scavenge their cognate ligands and thereby influence chemokine concentrations and immune response[24]. Therefore, atypical chemokine receptors were initially called decoy receptors, interceptors, scavenger receptors or chemokine-binding proteins.

Some chemokine receptors are able to bind several chemokines, for example CXCR2, which binds CXCL1-3 and 5–8[25]. Other receptors bind only a single chemokine. Chemokines on the other hand can also be specific for just one receptor. This was shown for CXCR6 which uniquely binds CXCL16 and *vice versa*. Other chemokines can bind to different receptors, exhibiting diverse specificities. One example is CXCL8, which binds to the chemokine receptors CXCR1 as well as CXCR2. Interestingly, CXCR2, compared with CXCR1, internalizes more rapidly and recovers more slowly in response to CXCL8[26]. As such, receptors that bind several ligands display ligand specific affinities and activation patterns. Regulation of receptor activity may also occur at the level of affinity regulation. Structure function studies indicate that all chemokine ligands interact with their receptor using two different regions in two steps, which is either called two-site or two-step model[27,28]. During binding, the chemokine first binds with its core region, including the N-loop of the chemokine to the N-terminus and extracellular loops of the receptor (this is called “site-I” of chemokine and receptor interaction). This first binding step is dominated by ionic interactions between positively charged residues of the ligand and negatively charged residues of the chemokine receptor. In the second step, the N-terminus of the chemokine is

positioned in a way that it is capable of interacting with parts of the transmembrane region and parts of the extracellular domain of the receptor (generating "site-II" of interaction). Binding of site-II finally leads to activation of the receptor which is mainly characterised by conformational changes of the seven transmembrane domains of the receptor. Interestingly, the majority of these conformational changes are highly conserved for all GPCRs[29]. Most prominent during the activation of GPCRs is the alteration of non-covalent contacts of transmembrane helix VI (TM-VI) with other TM regions ("global toggle switch"). As a direct consequence of TM-VI switching, the G protein binding site of the receptor is presented, which leads to activation of intracellular signalling cascades induced by the G protein[30].

1.4 G protein signalling of chemokine receptors

The activation cycle of chemokine receptors interacting with the corresponding G protein follows a highly conserved process common for GPCRs. The heterotrimeric G protein of chemokine receptors consists of a α_i–subunit (sometimes also α_q) and a $\beta\gamma$–dimer. The exchange of guanosindiphosphat (GDT) to guanosintriphosphat (GTP) influences the conformation of the α_i–subunit. This exchange allows the bound heterotrimeric G protein to be released from the receptor and to dissociate into active α_i–subunit (GTP-bound) and the $\beta\gamma$-dimer. The α_i–subunit and the $\beta\gamma$-dimer activate distinct downstream effectors, thereby reducing the activity of the adenylyl cyclase, activating phosphodiesterases (PDE) and phospholipase C (PLC), which lead to altered activation of ion channels, e.g. leading to calcium influx. Moreover, the intracellular proteinkinases Akt (proteinkinase B) as well as the extracellular-signal regulated kinase (ERK) are phosphorylated. All those effects, especially increasing calcium influx, are prominent for chemokine receptors and induce migration. The cycle of receptor activation is completed by the hydrolysis of α_i–subunit-bound GTP to GDP, resulting in the re-association of the α and $\beta\gamma$-subunits and their binding to the receptor, which terminates receptor signalling. Beside G protein dependent signalling cascade, the association of β-arrestin due to C-terminal receptor phosphorylation might be involved in signalling mechanisms independent of G protein interaction[31]. It is well known that β-arrestin is responsible for desensitisation and endocytosis of GPCRs and chemokine receptors. Recent studies indicate that β-arrestin activates downstream signalling mechanisms, such as the mitogen-activated protein kinase (MAPK) pathway. Both, receptor desensitisation and the MAPK pathway can influence chemotactic migration independent of G proteins[32,33]. Nevertheless, the interaction of GPCRs with the corresponding

G protein is essential for distinct signalling cascades. This is evidenced by the inhibition of $G\alpha_i$ coupled chemokine receptors by pertussis toxin (PTX). PTX catalyses the adenosine diphosphate (ADP)-ribosylation of α_i-subunits of G proteins, preventing G proteins from interaction with GPCRs. This abrogates intracellular signalling events such as calcium signalling and cell migration in response to chemotactic stimuli. As highly conserved interaction site for G proteins, an asparagine-arginine-tyrosine (DRY) motif has been discovered at the interface of TM-III and the beginning of the second intracellular loop of several GPCRs[29,34] (Figure 1). The high conservation of this DRY motif may indicate that it is critical for GPCR functions, since several studies showed complete knock-down of signalling events due to mutations of this motif[35,36].

1.5 Importance of the DRY motif of GPCRs

In case of the $D^{3.49}R^{3.50}Y^{3.51}$ motif at the interface of TM-III and the second intracellular loop, each amino acid is important for different mechanisms. Especially the aspartic acid ($D^{3.49}$) and the arginine ($R^{3.50}$) are known to be involved in stabilising the interaction of inactive and active conformational states of the receptor and most important for the binding of the Gα–subunit (Figure 1). In detail, $R^{3.50}$ is responsible for the interaction with the intracellular Gα–subunit of the heterotrimeric G protein and thereby is the most conserved residue in all GPCRs[29,30,36,40]. The mutation of endogenous DRY motif into DNY of the chemokine receptor CX_3CR1 led to a abrogation of intracellular signalling of this receptor, indicated by inhibition of calcium influx[35]. Since the ligand binding was not impaired but signalling was inhibited by PTX treatment, the decreased signalling of CX_3CR1 DNY is thought to be a consequence of disturbed interaction with the Gα-subunit. In the inactive state, $R^{3.50}$ further interacts via hydrogen bonds with the neighbouring $D^{3.49}$ of the DRY motif, which stabilizes the inactive conformation. Upon activation of the receptor, $R^{3.50}$ is rotated to interact with $Y^{5.58}$ on TM-V. In this new position between TM-III, TM-V and TM-VI, the guanidine group of $R^{3.50}$ builds the binding pocket for the Gα-subunit and forms hydrogen bonds to interact with this peptide. However, in many GPCRs, $R^{3.50}$ is also responsible for the interaction with an acidic residue on TM-VI ($D/E^{6.30}$) in the inactive state. This interaction is often called “the ionic lock”, since the non-covalent binding stabilizes the inactive conformation of many receptors[29,36]. Importantly, chemokine receptors contain a basic residue at position 6.30, leading to a lack of the ionic lock. Besides the importance of $R^{3.50}$, different analysis of the aspartic acid ($D^{3.49}$) of the DRY motif revealed inconsistent results, but $D^{3.49}$ has been shown to be involved in activity regulation and ligand binding[26,41,42]. The last

amino acid of the DRY motif is the least conserved and the least studied one among GPCRs. It has been shown, that mutations at this position often do not or just weakly affect receptor function[34]. However, in one study it was proposed that the $Y^{3.51}$ of CCR2 is essential for receptor activation due to phosphorylation of this amino acid[43]. In contrast, $Y^{3.49}A$ mutation of the chemokine receptor CXCR4 did not show significant differences upon ligand binding or receptor activation[44]. However, conformational changes caused by the $Y^{3.49}A$ mutation of CXCR4 were assumed, since receptor dimerisation seemed to be slightly impaired[44].

Interestingly, CXCR6 is the only chemokine receptor that carries an asparagine-arginine-phenylalanine (DRF) motif instead of the common DRY motif. This special motif of CXCR6 is not only found in humans but also in several other species (Table 1). Up to now, it is still unclear whether this characteristic motif represents a special functional adaptation of the receptor CXCR6.

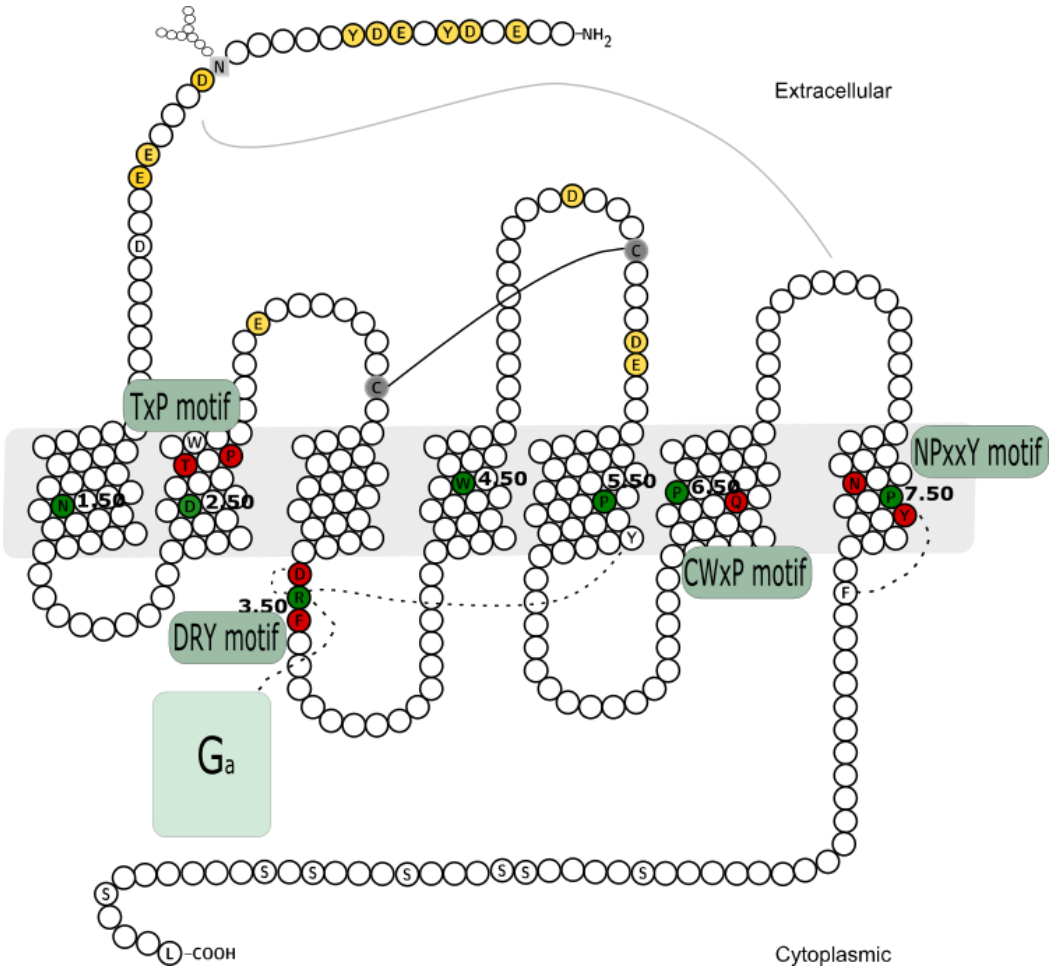

Figure 1 Highly conserved residues of G protein coupled chemokine receptors
Schematic description of highly conserved motifs and interactions in GPCRs and chemokine receptors on the basis of CXCR6. GPCRs consist of seven transmembrane regions (TMI to TMVII), an extracellular N-terminus and an intracellular C-terminus (sometimes building one more helix close to the membrane). Three extracellular loops are supposed to be important for ligand interaction, and two intracellular loops are important for interaction with the intracellular G protein. Yellow: acidic residues located in extracellular loops. Green: most conserved residues of each transmembrane domain (also marked with Ballosteros Weinstein labelling[37]. The first number denotes the helix and the second number denotes the residue position relative to the most conserved position, which is assigned by the number 50). Grey circles with black solid line: cysteine residues, responsible for disulphide bonds. Lighter grey line: existence of a second disulphide bond in other chemokine receptors, except of CXCR6. Red: residues building important micro switches (each micro switch is named by the canonical sequence in green quarters) which regulate receptor conformation and conformational changes due to receptor activation: In addition to the global toggle switch, there are more highly conserved micro switches. The TxP motif of TM II plays an important role in chemokine receptor activation. The CWxP motif, found in TM VI is highly conserved in rhodopsin-like receptors, although in some chemokine receptors, this motif consists of xQxP. Furthermore, there is the NPxxY(x)F motif in TM VII. Ga: α-subunit of heterotrimeric G proteins interacting with the chemokine receptor. Dotted lines indicate molecular interaction between different amino acids ($D^{3.49}$ and $R^{3.50}$; $R^{3.50}$ and $Y^{5.58}$; $R^{3.50}$ and Gαi) (modified from Nomiyama et al.[38], generated using Protter[39] (http://wlab.ethz.ch/protter/start/).

Table 1 Conservation of the DRF/DRY motif in CXCR6 (right) and other human chemokine receptors (left)

Receptor	Position and Sequence
CCR1	^{129}DRY
CCR2	^{139}DRY
CCR5	^{108}DRY
CXCR3	^{149}DRY
CXCR5	^{101}DRY
CXCR6	^{126}DRF
CX3CR1	^{126}DRY

Species	Position and Sequence
Homo sapiens	^{126}DRF
Mus musculus	^{135}DRF
Rattus norvegicus	^{135}DRF
Bos taurus	^{125}DRF
Erinaceus europaeus	^{128}DRF
Pan troglodytes	^{126}DRF
Macaca fascicularis	^{127}DRF
Callorhinchus milii	DRY

1.6 CXCR6-CXCL16 axis

CXCR6 is the exclusive receptor for CXCL16, which does not interact with any other chemokine receptor. CXCR6, also called BONZO (CD186), is located on chromosome 3 in a cluster that contains CC, XC, and CX_3C chemokine receptors. Interestingly, there are no other CXC receptors located in this cluster[8]. The protein CXCR6 with a molecular mass of 40 kDa consists of 342 amino acids and carries one N-glycosylation site at the N-terminal domain (Figure 2). Initially, CXCR6 was identified as an entry co-receptor on T cells for strains of HIV-1 and simian immunodeficiency virus, before its role as a chemokine receptor was discovered. In humans and mice, CXCR6 is expressed on activated T cells, especially on cytotoxic T cells, T helper cells type 1 and 2 (T_H1, T_H2) and memory T cells as well as on macrophages, natural killer T cells (NKT), fibroblast and smooth muscle cells[8,11,45,46]. As a GPCR, CXCR6 expresses different important motifs, but interestingly CXCR6 shows additional anomalies within the family of GPCRs and especially within the family of chemokine receptors. First, CXCR6 does not build a second disulphide bond at the extracellular side of the receptor (Figure 2). There is one covalent binding between the extracellular loops 1 and 2, but no covalent interaction between the N-terminus and the extracellular loop 3[47]. For the present study, the most important difference is the existence of the DRF motif instead of the conserved DRY motif at the interface of TM-III and the second intracellular loop.

Initially, the only known ligand for CXCR6, the chemokine CXCL16 was not only discovered as a chemokine, but also as scavenger protein for phosphatidyle serine and low density lipoproteins. Therefore, CXCL16 was called SR-PSOX (scavenger receptor for phosphatidyle serine and oxidised low-density lipoprotein)[48]. The protein CXCL16 consists of 254 amino acids (Figure 2) and is synthesised as an intracellular precursor that undergoes glycosylation and transport to the cell surface as a 60 kDa transmembrane glycoprotein. Mature CXCL16 protein can then be released from the cell surface as soluble form due to proteolytic cleavage by ADAM10 or

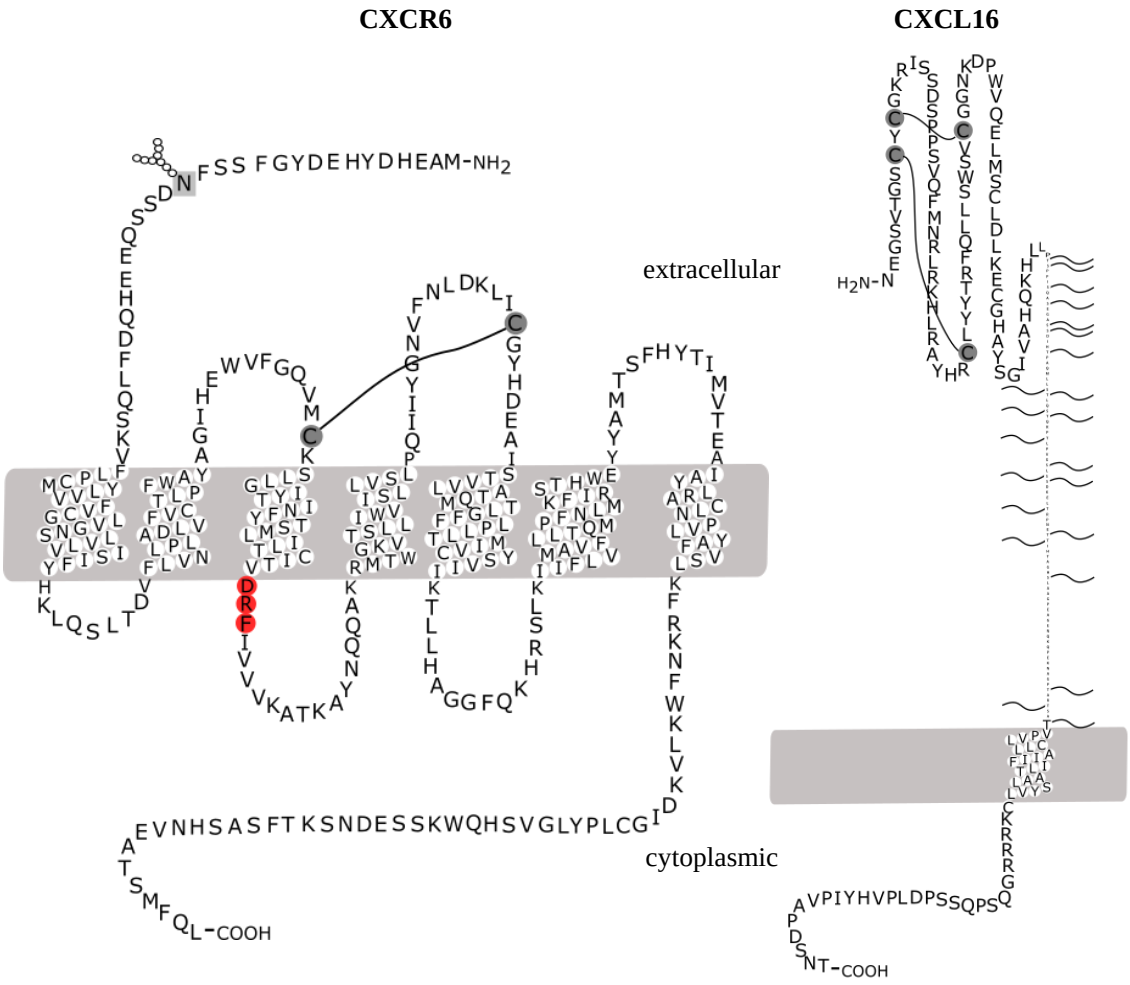

Figure 2 Schematic description of CXCR6 and its endogenous ligand CXCL16
Left: Chemokine receptor CXCR6. The DRF motif beginning at amino acid 126 is marked red and the N-glycosylation site is indicated. Right: Chemokine CXCL16. Disulphide bonds of the receptor and chemokine domain of CXCL16 are indicated as black lines linking cysteine residues (grey circles) and possible O-glycosylation sites of the mucin-like stalk of CXCL16 are shown as waved lines (figures generated by Protter[39] (http://wlab.ethz.ch/protter/start/)).

ADAM17[49–51]. In addition, a soluble form of CXCL16 may be generated by alternative splicing[52]. CXCL16 is expressed on antigen presenting cells, dendritic cells, monocytes and macrophages, fibroblastic reticular cells, epithelial cells and endothelial cells[8,11].

The interaction of CXCL16 and CXCR6 expressing cells induces adhesion and intracellular signalling mechanisms in CXCR6 expressing cells. As such, interaction can lead to adhesion of CXCR6 expressing monocytes or platelets to the transmembrane form of CXCL16, which is expressed for example by endothelial cells[14,53–55]. This CXCR6-CXCL16-mediated adhesion can be important during the diapedesis of leukocytes in the course of cell recruitment during inflammation[19]. Moreover, activation of CXCR6 induces intracellular signalling cascades, such as increased phosphorylation of the protein kinase Akt and mammalian target of rapamycin (mTOR)[56,57] as well as increased calcium influx into the cytoplasm[35]. Besides, the activation of the phosphatidylinositide 3-kinase (PI3K)/Akt signalling pathway in platelets[53] and the activation of the ERK1/2/RhoA/cofilin/F-actin pathway in breast cancer cells was shown to be activated by CXCR6 activity[58]. Thus, the signalling pathway of activated CXCR6 has been linked to different cellular functions such as migration and proliferation[59,60] and recruitment of different CXCR6 expressing cells such as NKT and T helper cell subsets[22,45]. The outcome of CXCR6-CXCL16 interaction has been linked to inflammatory diseases and cancer progression.

1.7 CXCR6 in inflammatory diseases

Accumulating evidence indicates a critical role of the CXCR6-CXCL16 axis in inflammation and cancer. CXCR6 is associated with the development of rheumatoid arthritis[21], liver fibrosis[61], glomerulonephritis[59] and renal fibrosis[46,62]. Expression of CXCL16 is up-regulated in inflamed tissue and can be up-regulated by IFNγ and TNFα stimulation[15] in different cell types, as endothelial cells[55], macrophages[10,63], smooth muscle cells[64] and astroglial cells[65]. Additionally, the activity of ADAM10 is increased in inflamed murine lung tissue which correlates with increased concentration of soluble CXCL16[50,66]. Inflammatory diseases are driven and controlled by immune cells, recruited into inflamed tissue. CXCR6 could be identified to be responsible for these recruitment processes in different inflammatory diseases. CXCR6 was found to be highly expressed on lymphocytes isolated from synovium of joints from human rheumatoid arthritis patients. In line with this, CXCR6 knock-out mice demonstrated that during collagen-induced arthritis, recruitment of T cells was impaired, leading to decreased disease syndromes[21]. In addition, during renal fibrosis, CXCR6 has been reported to be expressed by circulating fibroblast

precursors, whose recruitment drives renal fibrosis progression. Studies using CXCL16 knock-out mice[46] as well as CXCR6 knock-out mice[62] confirmed the importance of CXCR6-CXCL16-induced recruitment of fibroblast precursors. Other studies described the importance of CXCR6-mediated NKT cell recruitment during liver fibrosis. Both, CXCR6 knock-out and pharmacological inhibition of CXCL16 by antibody treatment reduced liver inflammation and fibrosis[45,61]. Moreover, CXCR6 was found on the cell surface of T_H2 cells[22] in blood and the expression was shown to be increased in T cells recruited into lung tissue in comparison to peripheral leukocytes[67]. These results were even more obvious in asthmatic patients[22,67]. In accordance with this, CXCL16 has been reported to be constitutively expressed by lung epithelial cells[11]. Although the chemokine receptor has been reported to have an impact on the mentioned inflammatory diseases and although CXCR6 is expressed in lung leukocytes, until now, there are only rare reports dealing with the analysis of CXCR6 in acute inflamed lung tissue or the role of CXCR6 during chronic lung diseases.

1.8 Progression of allergic asthma

Asthma is a chronic illness of the lung, which consists of several subtypes, including allergic and severe steroid-resistant asthma[68,69]. The development of asthma can be induced by different pathologic mechanisms. It is thought that asthma is caused by a combination of genetic pre-disposition and environmental factors, including tobacco smoke, exposure to air pollution[70] or viral infections. In case of allergic asthma, inflammation and airway obstruction are triggered by allergen exposure in atopic individuals[71]. The characteristics of allergic asthma include increased recruitment of eosinophils into the lung tissue (eosinophilia), cytokine release from many different cell types, as most important T_H2 cells, increased mucus production, airway hyperresponsiveness (AHR), and tissue remodelling. The reasons for the development of allergic asthma are still not fully understood, but a current model for allergic inflammation leading to allergic asthma is briefly described as follows (Figure 3)[71].

Initiation of an allergic response in the airways is often started by airway epithelial cells lying at the interface between the host and the environment and thereby representing the first line of defence against microorganisms, gases and allergens. Allergens cause allergic reactions due to binding to immunoglobulins. In addition, allergens and other environmental stimuli can have proteolytic activity, which can affect the epithelial barrier function and thereby activate epithelial cells directly. Epithelial cells express toll-like receptors, pattern recognition receptors and other proteins capable of detecting environmental stimuli on the cell surface[72]. Hence, epithelial cells get stimulated by environmental stimuli and then secrete cytokines like thymic stromal lymphopoietin (TSLP), IL-33, and IL-25, which activate dendritic cells (DCs). TSLP mediates

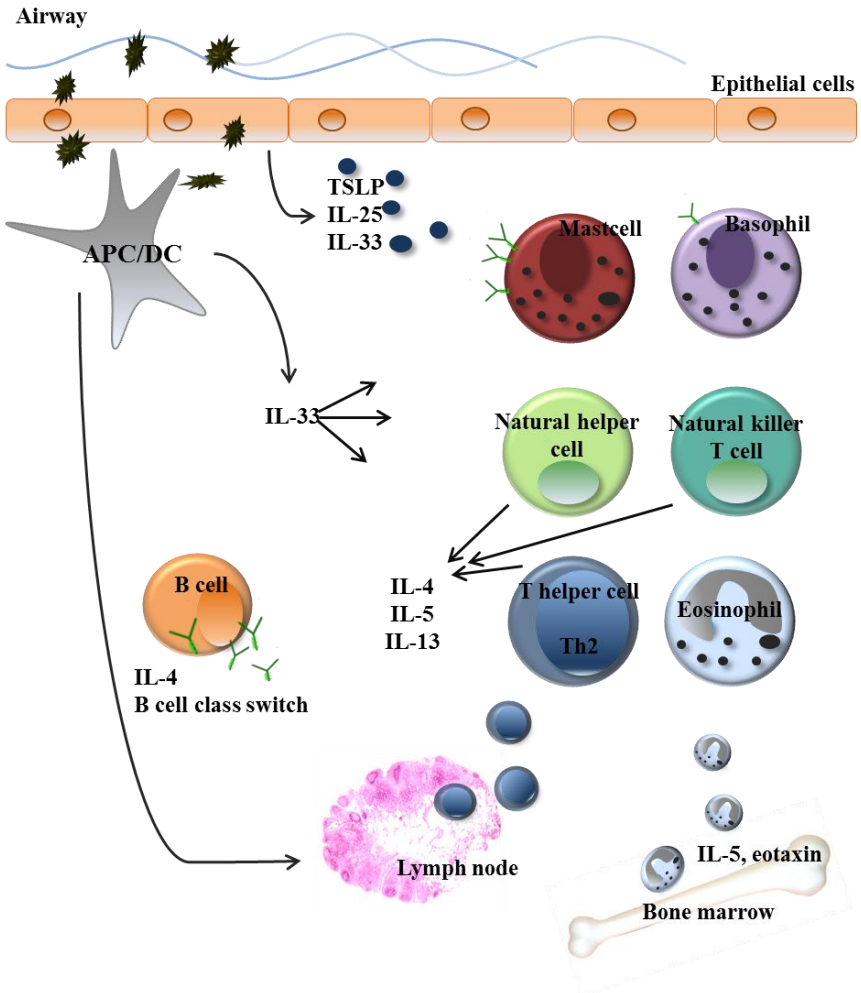

Figure 3 Cells and cytokines involved in bronchial asthma
Different cell types and secreted cytokines are involved in allergic asthma. The dark green particles indicate allergens entering the lung, detected by epithelial cells and APC/DC. Expression of CXCL16 by epithelial cells and APC/DC is indicated by black structures as well as expression of CXCR6 by natural killer cells and T_H2 cells. Abbreviations: TSLP: thymic stromal lymphopoietin, IL: Interleukin, APC: antigen presenting cell, DC: dendritic cell. For detailed explanation see text (Modelled after Kim et al.[77]).

migration of DCs, which present antigenic structures of the entered allergens and promote stimulation and differentiation of T_H cells, partially recruited of neighbouring lymph nodes into lung tissue. Interestingly, antigen presenting cells (APC) and DCs express CXCL16, the ligand of CXCR6 which might be relevant for interaction with CXCR6 expressing cells. Due to activation by APCs, stimulated T_H cells release IL-4, which mediates immunoglobulin E (IgE)-isotype switching in B cells. Antigen specific-IgE, released from B cells, binds to mast cells and basophils in the airways, augmenting local allergic responses. In addition, IL-33 and IL-25 produced by epithelial cells promote IL-13 and IL-5 release from natural helper cells in the airways, which then promote T_H2 cell differentiation. T_H2 cells produce the characteristic cytokines IL-4, IL-5, and IL-13. The downstream consequences of IL-13 exposure on resident lung cells in asthma include goblet cell metaplasia and increased mucus production, airway fibrosis and remodelling. T_H2 cells are recruited to the lung tissue via the activity of chemokines and express different chemokine receptors e.g. CXCR3, CCR6, CXCR6[22,73]. Another hallmark of asthma is the strong accumulation of eosinophils. Eotaxin (also called CCL11; ligand for CCR3), together with IL-5, are responsible for the recruitment of eosinophils from the bone marrow. Eotaxin is expressed by airway epithelial cells, airway smooth muscle cells, vascular endothelial cells, macrophages as well as eosinophils themselves[74]. Further cell types, which were recently discussed to be important for the development of asthma, are innate like lymphoid cells[75], including natural killer T cells (NKT cells). NKT cells were described to produce T_H2 cytokines including IL-4, IL-5 and IL-13, thereby pushing the allergic response similar to T_H cells. Interestingly, NKT cells were often described to express CXCR6 and migrate in response to CXCL16 gradients[45,76].

As described in detail, development of inflammatory diseases, including asthma, is orchestrated by the interplay of different cytokines and chemokines. This requires a fine regulation by the involvement of specialised chemokine receptors and their ligands. In the past, some chemokine receptors were discussed to be potential pharmacological targets for the treatment of asthma in human patients. As such, CCR3, the receptor for eotaxin is one possible target in asthmatic diseases. The role of CCR3 in asthma was demonstrated by generating knock-out mice and provocation of ovalbumin (OVA)-induced asthma in these animals[78]. In the mentioned study, eosinophil recruitment to the lung after allergen challenge was significantly reduced in CCR3 knock-out mice but AHR was unexpectedly increased, which is thought to be caused by

compensatory processes by mast cells[78]. By contrast, blockade of the CXCL12 receptor CXCR4 with the specific antagonist AMD3100 effectively abrogates both, leukocyte recruitment and AHR in a murine model of allergic inflammation[79]. However, since the receptor is widely expressed on all T cells, monocytes and also stem cells, such inhibition may induce undesired side effects. In summary, asthma is an inflammatory T_H2 driven disease, also implicating NKT cells, which both express CXCR6. Furthermore, CXCL16 is highly expressed by lung epithelial and endothelial cells. Therefore an involvement of CXCR6 in asthmatic lung inflammation seems very feasible, but has not been investigated so far.

As mentioned, the endothelial expression of CXCL16 might have an impact on homing of CXCR6 expressing cells from the blood stream into the lung tissue. The protease ADAM10 constitutively sheds the transmembrane form of CXCL16. Furthermore this protease sheds other mediators which have shown to be important during asthma development[80,81]. Thus, ADAM10 might be involved in cell recruitment during the progression of asthmatic lung inflammation as well.

1.9 ADAM10 in allergic asthma development

A disintegrin and metalloproteinase 10 (ADAM10), is a member of the zinc protease superfamily of ADAM proteases. ADAMs are cell surface proteins with a unique molecular structure. The N-terminal prodomain is linked to a metalloproteinase domain followed by a desintegrin, a cysteine-rich domain and an EGF-like domain. The transmembrane domain connects these extracellular parts with a cytoplasmic domain (Figure 4). Within the active site the metalloproteinase domain carries a zinc atom, which is essential for the proteolytic activity[81]. ADAM10 shows constitutive activity, which can be rapidly and post-translationally enhanced by several stimuli. ADAM10 mediates shedding of epidermal growth factor (EGF), neuregulin, E-cadherin, vascular endothelial cadherin (VE-cadherin), CD23, Notch and chemokines such as CX_3CL1 and CXCL16[17,50,80,81]. These membrane-expressed substrates are cleaved close to the extracellular cell surface leading to the release of their soluble ectodomains. The proteolytic processing of substrates by ADAM10 was shown to regulate key functions in inflammatory responses and embryogenesis. In fact, full ADAM10 knock-out is lethal and mice died during embryogenesis with multiple defects of the developing central nervous system, somites, and cardiovascular system[82]. Therefore, tissue specific knock-out models were generated and used to investigate the role of ADAM10 in pathological processes[80,81,83,84].

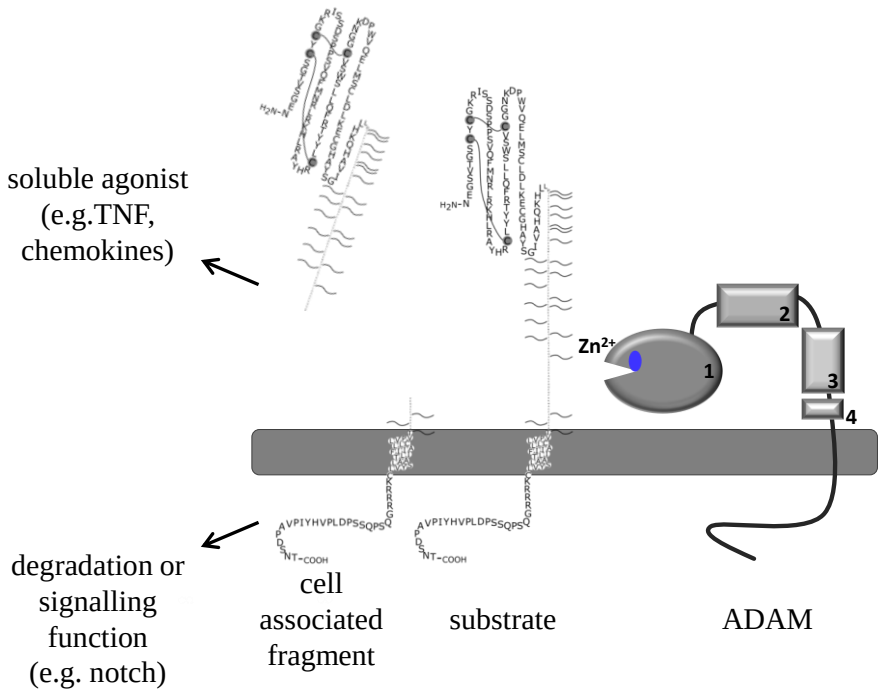

Figure 4 Schematic description of ADAM10 and shedding processes
The structure of ADAMs contain the following domains: metalloproteinase domain (1), disintegrin domain (2), a cysteine-rich domain (3) and an EGF-like domain (4). The transmembrane domain connects these extracellular parts with the cytoplasmic domain. Proteolytic cleavage of surface proteins such as chemokines, is indicated (modified from Dreymueller et al.[81]).

As mentioned, the majority of chemokines are expressed as soluble proteins, except of CXCL16 and CX_3CL1, which are expressed as transmembrane proteins. CXCL16 and CX_3CL1 either interact with their receptors as a transmembrane chemokine, leading to adhesion of receptor expressing cells, or they can be proteolytically processed by ADAM10 and ADAM17[17], leading to secretion of the soluble form of the chemokines. While ADAM10 promotes constitutive shedding of the chemokines, ADAM17-mediated shedding only occurs after induction of its protease activity[50]. These shedding mechanisms are critically involved in recruitment of leukocytes to sites of inflammation, as shown for CXCL16 dependent recruitment of inflammatory cells to malignant and inflamed astroglial cells[50]. The importance of ADAM10 for chemokine-induced cell migration was also shown *in vitro* by pharmacological inhibition and genetic ablation of the protease. These studies confirmed that ADAM10 is important for the migration of neutrophils and monocytes through endothelial cell layers. Moreover, similar observations were made by *in vivo* experiments, showing that mice lacking ADAM10 in hematopoietic cells were protected in an LPS-induced lung inflammation model[84]. It was also reported that ADAM10 expressed by B cells is crucial during asthma development[80]. This could

be mediated by impaired B cell migration. It was found that ADAM10 deficiency leads to the loss of CD23 (low-affinity IgE receptor) in B cells. Because this receptor acts as a natural regulator of IgE synthesis, inhibition of CD23 cleavage can be correlated with decreased IgE synthesis[80]. Further evidence for a role of ADAM10 in asthma was obtained by an *in vitro* study demonstrating that ADAM10 is responsible for secretion of CCL20 and other chemokines from bronchial epithelial cells[85], which could be crucial for asthma development.

Endothelial cells are responsible for the regulation of vascular permeability and extravasation of immune cells to sites of inflammation[20]. Inflammatory stimuli mediate increased expression of surface adhesion molecules by endothelial cells, like ICAM-1, which increases bronchial cellular influx[86]. Furthermore, changes in the bronchial microvasculature contribute to airway wall remodelling, driven by new vessel formation, due to an activation of endothelial cells[87,88]. Beside this remodelling processes, endothelial dysfunction is characterised by disturbed relaxation of resistant vessels and this has been reported for asthma[89]. Thereby, endothelial cells are strongly involved in lung inflammation. As described, ADAM10 is important for shedding of the transmembrane form of CXCL16, which might be relevant for the progression of asthma as well. Endothelial ADAM10 cleaves transmembrane CX_3CL1 which is thought to be important for cell detachment during transendothelial migration of leukocytes[17]. Moreover, endothelial ADAM10 cleaves VE-cadherin which is directly associated with mechanisms leading to increased permeability of endothelial cells[90].

2 Aim of the study

The aim of this study was to investigate the function of the chemokine receptor CXCR6 in inflammatory cell recruitment *in vitro* and *in vivo*. The focus of the *in vitro* investigations was on the role of the DRF motif in CXCR6 for signalling of cell migration. Subsequent *in vivo* studies addressed the role of CXCR6 in different stages of experimental murine asthma. Since the CXCR6 ligand CXCL16 is cleaved by ADAM10 on endothelial cells, the role of this protease in experimental asthma was also addressed. Hence, this thesis was divided into three different parts.

Part 1:

It is still unclear why the DRF motif of CXCR6 is conserved in many species whereas other chemokine receptors express the canonical DRY motif. The DRF motif might represent an adaptation to specialised functional characteristics of CXCR6. In order to determine characteristic features of the DRF motif, CXCR6 variants were generated carrying the canonical DRY motif or a functionally inactive DNF motif. The effect of these mutations was studied in terms of ligand binding, receptor internalisation and recycling, calcium and Akt signalling, adhesion, and migration. For this purpose, human embryonic kidney cells (HEK293) and the monocytic cell line THP-1 were used as expression systems. Furthermore, CX_3CR1, another chemokine receptor, was chosen to confirm results regarding the effect of DRF/DRY expression on chemokine-induced migration.

Part 2:

CXCR6 is expressed on various T lymphocytes, like NKTs and T helper cells and by regulating recruitment of these cells the receptor can contribute to several inflammatory diseases. However, the function of the receptor in asthma remains unknown. Therefore, the CXCR6-CXCL16-axis in asthmatic disease development was studied. CXCR6 knock-out mice, which express GFP under the control of the CXCR6 promotor, were analysed in different *in vivo* models of experimental asthma-induced by OVA-sensitisation. OVA-sensitisation was performed for either 35 days resulting in a subchronic asthmatic disease or for 110 days resulting in a more chronic lung disease. Cell recruitment and cytokine composition were analysed as well as lung physiology and histological modifications.

Part 3:

On endothelial cells ADAM10 sheds transmembrane CXCL16 constitutively and this could represent a pathway how endothelial ADAM10 can affect asthma development. Experiments with mice lacking endothelial ADAM10 indicate a pro-inflammatory role for ADAM10 in the early phase of LPS-induced lung inflammation[91], but these animals were not yet studied in models of asthma. Therefore, mice with Tie2 promotor-driven knock-out of ADAM10 in endothelial cells (ADMA10flox/flox/Tie2-Cre mice (Tie2 *Adam*10)) were studied for disease development in the 35-days model of OVA-induced asthma.

3 Materials and Methods

3.1 Consumables, chemicals, kits and buffer

3.1.1 Consumables

All cell culture consumables (cell culture dishes, cell culture flaks, multi-well plates, flow cytometry tubes) were purchased from Sarstedt (Nürnberg, Ger), BD Bioscience (NJ, USA) or Falcon (Corning Incorporated New York, USA).

BD, Microlane, 20 gauge needle	Becton Dickinson GmbH, Fraga, ESP
BD, Plastipak, syringe 1 mL	Becton Dickinson GmbH, Madrid, ESP
Capillaries sodium heparinised, 9 µl	Hirschmann Laborgeraete GmbH& Co. KG, Eberstadt, Ger
CountBright™ Absolute Counting Beads, for flow cytometry	Life Technologies, New York, USA
Filter pipet tips Tip One	Starlab, Merenschwand, CH
Omnican F, Single use syringe 1 mL	B. Braun Melsungen AG, Melsungen, Ger
Polycarbonate ultra-centrifugation tubes	BD biosciences, Heidelberg, Ger
RT-qPCR-plates (96 wells)	BIO Plastics, Landgraaf, NL

3.1.2 Chemicals

All chemicals used in this study had the degree of purity *pro analysis* (p.a.) at least and were ordered from either Sigma-Aldrich (St.Louis, MO, USA) or Roth (Karlsruhe, Ger), if not specified otherwise. All enzymes for cloning were purchased from Fermentas (St.Leon-Rot, Ger). Further chemicals are listed below.

Biozym LE Agarose	Biozym Scientific GmbH, Oldendorf, Ger
Agarose LM (low melting)	GERBU Biotechnik GmbH, Heidelberg,

	Ger
Aluminium Hydroxid Gel Adjuvant	InvivoGen, San Diego, USA
Albumin from chicken egg white	Carl Roth GmbH & Co. KG, Karlsruhe, Ger
Calcein-AM	BIOTREND Chemikalien GmbH, Cologne, Ger
Collagen-G	Biochrome GmbH, Berlin, Ger
Collagenase typ II	Biochrome GmbH
Complete protease inhibitor	Roche, Penzberg, Ger
p-Nitrophenyl β-D-glucoronide	Calbiochem EMD Chemicals, San Diego, USA
Pluronic F-127	Biotium, Hayward California, USA
Probenicid	Carl Roth GmbH

3.1.3 Kits

Kits for Enzyme link Immunosorbent Assays (ELISAs) for the determination of soluble chemokines, cytokines and inflammatory proteins were purchased from R&D and used according to manufacturers' protocols. Further kits, for plasmid DNA purification, cloning, PCR and RT-qPCR methods etc. and their origin are mentioned in each method section.

3.1.4 Buffer and Solutions

Annealing-buffer for shRNA-oligos (x2)	200 nm potassium-acetate 60 nM HEPES 4 mM magnesium-acetate pH 7.4
Blocking buffer for western blot	3% BSA TBST

Ca2+-influx assay buffer	HBSS 10 mM HEPES 710 ng/ml Probenicid
Ca2+-assay Fluo-4-AM staining buffer	Ca2+-influx assay buffer 2 nM Pluronic F-127 2 nM Fluo-4-AM
Chemotaxis assay buffer	RPMI1640 0.2% BSA
Erythrocyte lysis buffer	4.145 g NH_4Cl 0.5 g $KHCO_3$ 0.02 g EDTA ad 0.5 l H_2O bidest.
FACS-buffer (cell culture)	Dulbecco's PBS (PAA) 0.2% BSA
FACS-buffer for cells isolated from mouse tissue	Dulbecco's PBS (PAA) 1% FCS 1 mM EDTA
Glucoronidase substrate buffer	100 mM sodium-acetate 10 mM p-nitrophenyl-β-D-glucoronide pH 4
Glucoronidase stopping buffer	400 mM glycin pH 10.3
LB medium	10 g bakto-tryptone

	5 g yeast extract 10 g NaCl ad 1 l H_2O bidest. pH 7.0
Lysis buffer for phosphorylation analysis	1 mM Na_3PO_4 10 mM pNPP 1 mM benzamidin 30 nM NaF 5 mM DTT 10 nM glycerophosphat 20 nM Tris 150 nM NaCl 4 mM EDTA 1 MM PMSF 1% Triton-x-100 complete (1x) ad 10 mL H_2O bidest.
PBS	150 mM NaCl 120 mM KCl 10 nM Na_2HPO_4/KH_2PO_4 pH 7.4
PBST	PBS 0.1% Tween 20
Running-buffer (SDS-PAGE)	25 mM Tris/HCl 200 mM glycine 3.5 mM SDS pH 7.5

Separation gel buffer (SDS-PAGE)	90.85g Tris/HCl 2 g SDS ad 500 mL H_2O bidest. pH 8.8
SDS-sample buffer (SDS-PAGE)	20% glycine 4.5% SDS 125 mM Tris/HCl a spatula tip of bromphenol blue pH 6.8 for reducing conditions: 5% mercapto-ethanol
Stacking gel buffer (SDS-PAGE)	30.28 g Tris/HCl 2 g SDS ad 500 ml H_2O bidest. pH 6.8
Stripping-buffer (for PVDF-membrane)	0.1% SDS 0.2 M glycine in H_2O bidest. pH 2.2
TAE (x50)	57.1 ml glacial acetic acid 242g Tris 1 mM EDTA ad 1 l H_2O bidest. pH 7.4
TBST	8.75 g NaCl 3.152 g Tris HCL

	0.29 g EDTA ad 1 L H_2O bidest pH 7.4
Transferbuffer (wet blot)	192 mM glycine 25 mM Tris/HCl 10% methanol

3.1.5 Chemokines

MCP-1 (MCP, CCL2)	PeproTech GmbH, Hamburg, Ger
Recombinant human or murine CXCL16 (chemokine domain)	PeproTech GmbH
Recombinant human or murine CX3CL1 (chemokine domain)	R&D-Systems GmbH, Wiesbaden-Nordenstadt, Ger
Recombinant murine CX3CL1 (chemokine domain)	R&D-Systems GmbH

3.1.6 Antibodies

Table 2 Antibodies
Listed are primary and secondary antibodies (sec AB) used in this study for fluorescence activated cell sorting (FACS), western blot analysis, and for functional assays.

Name	Company	Isotype (clone number)	Concentration	Application
monoclonal anti-human CXCR6-phycoerythrin (PE)	R&D systems	mouse IgG2b (clone 56811)	1 µg/ml	FACS
monoclonal anti-mouse CXCR6-PE	R&D systems	rat IgG2B (clone 221002)	1 µg/ml	FACS
monoclonal anti-mouse CD4-allophycocyanin APC-H7	BD Biosciences	rat IgG2b kappa (clone 131922)	2 µg/ml	FACS

monoclonal anti-mouse CD8a-Pacific Blue	BD Biosciences	rat IgG2a kappa (clone 53-6.7)	2 µg/ml	FACS
monoclonal anti-mouse IFNγ-Fluor450 (detectable: Pacific Blue)	eBioscience	rat IgG1 kappa (clone XMG1.2)	1 µg/ml	FACS
monoclonal anti-mouse ST2-APC (IL-1 receptor4)	R&D systems	rat IgG2B (clone 245707)	2 µg/ml	FACS
monoclonal anti-mouse NK-1.1-PE- Cyanine7 (Cy7)	BD Biosciences	mouse IgG2a kappa (clone PK136)	2 µg/ml	FACS
monoclonal anti-mouse CD25-APC (IL-2 receptor alpha chain, p55)	BD Biosciences	rat IgG2 kappa (clone 3C7)	2 µg/ml	FACS
monoclonal anti-mouse CD3ε-PE-Cy5	BD Biosciences	armenian hamster IgG (clone 145-2C11)	2 µg/ml	FACS
monoclonal anti-mouse lymphocyte antigen 6G PE-Cy5	Miltenyi Biotech	rat IgG2b kappa (clone 1A8)	8 µg/ml	FACS
monoclonal anti-mouse F4/80-RPE	Serotec	rat IgG2b (CI:A3-1)	1:25	FACS
monoclonal anti-mouse CD11b-PE-Cy7 (Integrin alpha M, CR3A)	BD Biosciences	Rat IgG2b (clone M1/70)	2 µg/ml	FACS
monoclonal anti-mouse IL-17A-PE	BD Biosciences	rat IgG1 kappa (clone TC11-18H10)	2 µg/ml	FACS
monoclonal anti-mouse CD127-PE-Cye5 (IL-7 receptor alpha chain)	BD Biosciences	rat IgG2a kappa (clone A7R34)	2 µg/ml	FACS
monoclonal anti-mouse CD19-RPE	BD Biosciences	rat IgG2a kappa (1D3)	2 µg/ml	FACS
monoclonal anti-human-alpha5 integrin (CD49e (230307))	R&D systems	mouse IgG1 (clone 238307)	4µg/ml	FACS
monoclonal anti-human beta1 integrin	R&D systems	mouse IgG1 (clone 4B7R)	4µg/ml	FACS
monoclonal anti-beta 1 integrin, active conformation	Millipore	mouse IgG2b (clone HUTS-4)	4µg/ml	FACS
monoclonal isotype mouse IgG2b	R&D systems	mouse IgG2b (clone 20116)	4µg/ml	FACS

monoclonal isotype IgG2b PE	R&D systems	mouse IgG2b (clone 133303)	4 µg/ml	FACS
monoclonal anti-Akt	Cell signaling	rabbit IgG (clone C67E7)	dilution: 1:1000	Western blot
monoclonal anti-Akt phosphorylation (site Ser473)	Cell signaling	rabbit IgG (clone D9E)	dilution: 1:1000	Western blot
polyclonal anti-human IgG gamma chain	Serotec	goat IgG	2µg/ml	adhesion assay
polyclonal anti-human CXCL16	R&D systems	goat IgG	50 ng/ml	proliferation assay
polyclonal goat anti-human IgG Fc gamma- APC	Jackson Immuno Research	goat IgG	2.5 µg/ml	FACS (sec AB)
polyclonal goat anti-mouse IgG-APC	Jackson Immuno Research	goat IgG	5 µg/ml	FACS (sec AB)
polyclonal goat anti-rabbit IgG-Horseradish peroxidase (HRP)	Jackson Immuno Research	goat IgG	0.02µg/ml	Western blot (sec AB)

3.1.7 Oligonucleotides

Synthesised oligonucleotides were purchased from Eurofins MWG Operon (Ebersberg, Ger) with HPLC purified grade. Table 3 includes primer sequences used for mRNA expression analysis and oligonucleotides for mutagenesis via site directed mutagenesis (3.3.1.4) are given in Table 4

Table 3 Oligonucleotides used for quantitative RT-qPCR
(For: forward primer, Rev: reverse primer, IL: Interleukin, GAPDH: Glyceraldehyde 3-phosphate dehydrogenase, RPS29: 40S ribosomal protein S29, TGFβ: Transforming growth factor beta).

Name	Sequence (5´→3´)	Annealing temperature
GAPDH_For	CGGGGCTCTCCAGAACATCATCC	60 °C
GAPDH_Rev	CCAGCCCCAGCGTCAAAGGTG	
Human CXCR6_For	ATGCCATGACCAGCTTTCACT	60 °C
Human CXCR6_Rev	TTAAGGCAGGCCCTCAGGTA	
Human CXCL16_For	TGTCTATACTACACGAGGTTCCA	60 °C
Human CXCL16_Rev	AGCATGTCCACATTCTTT	

Murine CX3CR1_For	ACCTCCTTCCCTGAACTGGA	60 °C
Murine CX3CR1_Rev	ATTTCCCACCAGACCGAACG	
Murine RPS29_For	CCTTTCTCCTCGTTGGGC	61 °C
Murine RPS29_Rev	GAGCAGACGCGGCAA	
Murine eotaxin_For	ATTGTGTTGTTTGTTTGCTTGC	60 °C
Murine eotaxin_Rev	GTCAGCCTGGTCTACACAGTGA	
Murine CXCL16_For	CCTTGTCTCTGGCGTTCTTCC	60 °C
Murine CXCL16_Rev	TCCAAAGTACCCTGCGGTATC	
Murine IL5_For	AGCACAGTGGTGAAAGAGACCTT	60 °C
Murine IL5_Rev	TCCAATGCATAGCTGGTGATTT	
Murine IL13_For	AGACCAGACTCCCCTGTGCA	60 °C
Murine IL13_Rev	TGGGTCCTGTAGATGGCATTG	
Murine IL4_For	ACAGGAGAAGGGACGCCAT	60 °C
Murine IL4_Rev	GAAGCCCTACAGACGAGCTCA	
Murine TGFβ_For	TGACGTCACTGGAGTTGTACGG	60 °C
Murine TGFβ_Rev	GGTTCATGTTACGGATGGTGC	
Murine Collagen1A-For	CTGGCGGTTCAGGTCCAAT	63 °C
Murine Collagen1A-Rev	TTCCAGGCAATCCACGAGC	

Table 4 Oligonucleotides for site directed mutagenesis
Marked letters of the sense sequence: a grey background indicates induced point mutations leading to mutations of the DRF/DRY motif and underlined letters indicate silent mutations used for identification of positive mutation by adding restriction sites as indicated (Tm,no: melting temperature, Bp: base pairs).

Starting gene	Sequence (5´→ 3´)	Bp length Tm,no	Resulting mutation
Murine CXCR6 wild type	Sense: CAGTGGATCGATACATTGTAG TGGTCCAGGCTACCAAGGCCT TC	44 55,5 °C	Murine CXCR6 F137Y (+2. ClaI site)
	Antisense: CTACAATGTATCGATCCACTG TGATGCAGGTGAGAGTGAGC ATGGAC	47 56 °C	
Murine CXCR6 wild type	Sense: GTGGATAATTTCATTGTAGTG GTCCAGGCTACCAAAGCTTTC AACCG	47 54,2 °C	Murine CXCR6 R136N (+3. HindIII site)
	Antisense: CCACTACAATGAAATTATCCA CTGTGATGCAGGTGAGAGTG AGCATG	47 54,1 °C	
Murine CX3CR1 wild type	Sense: CATCGATCGGTTCCTTGCCAT CGTCCTGGCCGCCAACTCCAT GAAC	46 69,3 °C	Murine CX3CR1 Y129F (+2. ClaI site)
	Antisense: GATGGCAAGGAACCGATCGA TGCTGATGACGGTGATGAAG AATATGCCCC	50 67,7 °C	

3.1.8 Plasmids

Table 5 shows abbreviations of plasmids used in this thesis together with a short description of their properties. Plasmid maps are listed in the appendix.

Table 5 Plasmids

Name	Properties
pLVX-IRES-Neo	HIV-1-based, lentiviral expression vector
pMD2	Lentiviral envelope plasmid encoding VSV-G
psPAX	Lentiviral packaging plasmid encoding the HIV gag-pol gene and further auxiliary HIV proteins
pLVX-IRES-Neo-empty vector	Lentiviral expression vector with G418 resistance (Neo^r), control

	vector for overexpression
pLVX-IRES-Neo hCXCR6	Lentiviral expression vector for overexpression of human CXCR6
pLVX-IRES-Neo hCXCR6-DRY	Lentiviral expression vector for overexpression of human CXCR6 with the point mutation F128Y
pLVX-IRES-Neo hCXCR6-DNF	Lentiviral expression vector for overexpression of human CXCR6 with the point mutation R127N
pLVX-IRES-Neo mCXCR6	Lentiviral expression vector for overexpression of murine CXCR6
pLVX-IRES-Neo mCXCR6-DRY	Lentiviral expression vector for overexpression of murine CXCR6 with the point mutation F128Y
pLVX-IRES-Neo mCXCR6-DNF	Lentiviral expression vector for overexpression of murine CXCR6 with the point mutation R127N
pLVX-IRES-Neo mCX_3CR1-	Lentiviral expression vector for overexpression of murine CX_3CR1
pLVX-IRES-Neo mCX_3CR1-DRF	Lentiviral expression vector for overexpression of murine CX_3CR1 with the point mutation Y128F
pLVX-IRES-Neo mCX_3CR1-DNY	Lentiviral expression vector for overexpression of murine CX_3CR1 with the point mutation R127N
pcDNA3.1+ hCXCL16-FC	Expression vector for soluble human CXCL16 fused to the Fc-part of human IgG1
pcDNA3.1+ mCXCL16-FC	Expression vector for soluble murine CXCL16 fused to the Fc-part of human IgG1
pcDNA3.1+ hCX_3CL1-FC	Expression vector for soluble CX3CL1 that is fused to the Fc-part of human IgG1

3.2 Cell culture methods

3.2.1 Cell line propagation

Cells were cultured at 37 °C and 5 Vol.-% CO_2 in a humidified atmosphere (*Cell culture incubator C150*, Binder, Tuttlingen, Ger). Cell culture media were supplemented with 10% foetal bovine serum (FBS), penicillin (100 U/ml) and streptomycin (100 µg/ml). Human embryonic kidney 293 cells (HEK293) were cultured in DMEM, and when confluence was reached cells were sub-cultured using trypsin/EDTA. For the monocytic cell line THP-1, which growth in suspension, RPMI 1640 medium was used and changed twice a week. THP-1 cells were seeded in concentrations of $2x10^5$/ml. Transfected and transduced cells were cultured in medium supplemented with additional 1 mg/ml geneticin (G418, Calbiochem EMD Chemicals, San Diego, USA) for selection. Prior to experiments, transduced cells were cultured G418 free for at

least one week. Cells were cryopreserved in liquid nitrogen using cell culture medium supplemented with 20% FCS and 10% DMSO. After thawing, cells were immediately dissolved in pre-warmed culture medium and centrifuged at 300 x g for 5 min (*Centrifuge Avanti J-25*, Beckman Coulter, Krefeld, Ger) to remove DMSO. The number of viable cells was counted by trypan blue dye exclusion (0.2% trypan blue end concentration) using Neubauer chambers (Brand GmbH, Wertheim, Ger). Cell line propagation and further treatments were performed under the *Cell culture bench Hera Safe KS 12* (Thermo Fischer, Waltham, MA USA).

3.2.2 Transduction of target cells

Cells were transduced with concentrated lentiviral particles. Before transduction, cells were seeded with a density of $2.5x10^5$ cells per six-well containing 1 ml standard medium, and 5-10 µl of concentrated lentivirus were added. To increase the transduction rate, polybrene was added to the medium at a final concentration of 4 µg/ml. 24 h after transduction, the medium was replaced. 24 h later, G418 was added at a final concentration of 1 mg/ml to select transduced cells.

3.3 Molecular biology methods

3.3.1 Cloning and production of lentiviral particles

E. coli strain DH5α genotype: supE44 ΔlacU 169(φ80lacZ ΔM15) hsd R17 recA1 end A1 gyr196 thi-1 relA1.v. was used for the cloning and propagation of plasmids.

3.3.1.1 Transformation of bacteria

100 µl aliquots of chemical competent DH5α *E. coli* bacteria (*Z-Competent™ E.Coli Transformation Buffer Set*, Set, Zymo Research, Irvine, USA) were thawed on ice. After thawing, 5 µl of PCR or ligation product or 200 ng of plasmid DNA were added to the *E. coli* DH5α cells. The mixture was incubated on ice for 15 min. The transformed bacteria were plated out on LB-agar plates containing 50 µg/ml ampicillin and incubated for 24 h at 37 °C.

3.3.1.2 DNA plasmid purification

4 ml LB medium containing 50 µg/ml ampicillin were inoculated with a single bacteria colony and cultured for 16 h at 37 °C and 300 rpm. Afterwards, 2 ml of bacterial suspension were used for miniprep plasmid purification using the *NucleoSpin Plasmid kit* (Macherey-Nagel). Plasmids were analysed via restriction analysis and after verification of plasmid accuracy, a maxi-plasmid-

preparation using *NucleoBond PC 500* (Macherey-Nagel) was performed to maximize plasmid concentration.

3.3.1.3 **Production and concentration of lentiviral protein overexpressing particles**

A variant of HEK293 cells, stably expressing the large T-antigen, HEK293T cells, were used as producer cell line for production of lentiviral particles. $2x10^6$ HEK293T cells were seeded on a collagen coated 10 cm culture dish and cultured for 48 h. The medium was changed at least 2-3 h prior to transfection. 5 µg pLVX-IRES-Neo, 3.25 µg pMD2 and 1.75 µg psPAX2 were mixed prior to addition of 20 µl *jetPEI* (Poly Plus Transfections, Illkirch, F) in 250 µl NaCl solution (150 nM). The combined transfection mixture was incubated for 15-30 min at room temperature and then added drop wise to HEK293T cells. 24 h after transfection the medium was replaced by 10 ml of fresh medium. Lentiviral particles containing supernatant was collected after additional 48 h. The supernatant was centrifuged at 500 x g to remove cell debris and sterile filtered using a 0.2 µm filter. To produce larger amounts of lentiviral containing supernatant, 15 cm dishes were used and the amount of cells, DNA, NaCl solution, jetPEI and medium was scaled up by factor 2.5.

Concentration of lentiviral particles was performed via ultracentrifugation using *Ultracentrifuge L7-65* (Beckman Coulter, Krefeld, Ger). 10-30 ml of supernatant was centrifuged in screw-top ultracentrifuge tubes at 50,000 x g for 2 h. After centrifugation the medium was discarded and the pellet containing the lentiviral particles was dissolved in 50 µl PBS. The concentrated lentivirus was aliquoted and stored at -80 °C.

3.3.1.4 **Site-Directed Mutagenesis**

QuikChange Site-Directed Mutagenesis was used to induce point mutations in the DRF motif of murine CXCR6 and DRY motif of CX_3CR1. Synthetic mutagenic oligonucleotide primers were designed (see Table 4) containing the desired mutation and a silent mutation to identify positively mutated plasmids by restriction analysis. Site directed mutagenesis was performed using 25 µl of *Phusion® High-Fidelity PCR Master Mix with HF Buffer* (New England BioLabs, Ipswich, USA), 5 nmol of each designed primer and 50 ng of the target plasmid in a total volume of 50 µl H_2O. This mixture was incubated for 1 min at 95 °C, followed by 12 cycles of 1 min 95 °C, 1 min x °C (x=Tm,no-5 °C) and 1 min/kb 72 °C, and a final cycle of 1 min x °C and 30 min at 72 °C in the *PCR-cycler* (Biometra Analytik GmbH, Göttingen, Ger). Afterwards, the initial plasmid was

digested by adding 1 µl of *DpnI* restriction enzyme for 1 h at 37 °C. Finally 5 µl of the resulting PCR product was transformed as described in section 3.3.1.1. To verify the correct mutation of each plasmid by site directed mutagenesis, resulting plasmids were treated with restriction enzymes mentioned in Table 4 and analysed via agarose gel electrophoresis. Correct mutagenesis was further verified by plasmid sequencing (Eurofins MWG Operon) in case of positive restriction analysis. Site directed mutagenesis of human CXCR6-DRF motif has been performed by Nicole Schwarz for expression via pcDNA3.1(+) plasmids and have been cloned into pLVX-IRES-Neo plasmids by Christine Haselier.

3.3.1.5 **Plasmid cloning by restriction enzyme digest**

For overexpression, murine CXCR6 and CX_3CR1 were cloned out of pcDNA3.1+ vectors into pLVX-IRES-Neo vectors using restriction enzymes *EcoRI* and *XhoI* (CX_3CR1) or *EcoRI* and *XbaI* (CXCR6). 1 µg of each vector was restricted simultaneously by 0.5 µl (5/10U) of each restriction enzyme in a total volume of 50 µl H_2O containing 1x or 2x buffer *Tango* for 1 h at 37 °C. Restriction was stopped by heating the mixture for 5 min at 80 °C. The excised fragment was purified by agarose gel electrophoresis and isolated with the *NucleoSpin Extract II kit* (Macherey-Nagel). The fragment and the target vector pLVX-IRES-Neo were ligated with T4 ligase for 1 h at RT in a ratio of 3:1. 4 µl of the ligation product was transformed into *E.coli DH5α* as described in section 3.3.1.1. Correct cloning was verified by plasmid sequencing (Eurofins MWG Operon).

3.3.2 Messenger RNA (mRNA) isolation and cDNA synthesis

mRNA was isolated with the *RNeasy Mini Kit* (Qiagen, Hilden, Ger) according to the manufacturer's protocol. For mRNA isolation either $3x10^6$ cells or lung tissue powder was used. Both, tissue and cells were added to a *QIAshredder spin column* (Qiagen), and RNA isolation was continued as recommended. To avoid contamination by genomic DNA, DNase-treatment was performed during the isolation. The RNA was eluted with 20 µl RNase free water. The RNA content of the samples was determined using the *NanoDrop-ND-100* (PEQLAB Biotechnologie GmbH, Erlangen, Ger) and the samples were stored at -80 °C. cDNA synthesis was performed with the *RevertAid™ H Minus First Strand-Kit* (Fermentas GmbH, St. Leon-Rot, Ger) according to the manufacturer's protocol using 250 ng of isolated RNA per reaction.

3.3.3 Quantitative PCR (RT-qPCR)

The mRNA expression level was analysed by quantitative RT-PCR using the *LightCycler480 DNA SYBR Green I Master* (Roche) and specific primer pairs (6.25 nM each). A serial dilution of pooled cDNA products of all samples was used as gold standard to prepare relative standard curves for target genes and reference genes (glyceraldehyde 3-phosphate dehydrogenase (GAPDH) for human samples and 40S ribosomal protein S29 (RPS29) for murine samples). Samples (1 µl of 1:10 diluted cDNA) and standards were run in duplicates on 96-well plates. Quantitative RT-PCR was run on *LightCycler 480* (Roche) for 40 to 45 cycles consisting of 10 sec denaturation at 95 °C, 10 sec annealing (temperature see Table 3), and 15 sec amplification at 74 °C. Data were obtained as the crossing point value normalised according to the e-method using the *LightCycler®480* software 1.5 (Roche) and used for statistical analysis.

3.4 Biochemical methods

3.4.1 Generation of chemokine-FC constructs

Human CX_3CL1-Fc and murine/human CXCL16-Fc constructs were used for ligand binding and adhesion assays with chemokine receptor expressing cells. To produce these constructs HEK293T cells were transfected via *jetPEI* with pcDNA3.1+ vectors coding for the extracellular domain of each chemokine, C-terminally fused to the Fc-part of human IgG1a, as described before[35,92,93]. 48 h after transfection, HEK 293T cells were washed twice with PBS and kept in FCS free medium for 24 h. Cell supernatant was collected and 1:15 concentrated by *Vivaspin sample concentrators* (Sigma-Aldrich). Concentrated supernatant containing chemokine-Fc constructs was stored at -20 °C in aliquots until usage.

3.4.2 Protein staining for fluorescence activated cell sorting (FACS)

Flow cytometric analysis was used to determine the surface expression of cell markers, CXCR6, and CX_3CR1, as well as the intracellular expression of cytokines and transcription factors. $2x10^5$ cells were transferred into FACS-tubes, centrifuged (300 x g for 5 min) and resuspended in 1% paraformaldehyde (PFA) for fixation of intra- and extracellular antigens. Cells were washed once and after centrifugation resuspended in 50 µl of primary antibody solution (against target protein, Table 2). For staining of intracellular antigens, cells were permeabilised using 0.1% Triton X-100 for 5 min. Samples were incubated in the dark on ice for 45-60 min and afterwards washed twice with 300 µl ice-cold FACS-buffer. Cells were either resuspended in 200 µl PBS or

incubated with 50 µl secondary antibody solution (see Table 2). Cells were incubated in the dark on ice for 30-45 min, washed twice with 300 µl ice-cold FACS-buffer and after centrifugation resuspended in 200 µl ice-cold PBS and analysed by flow cytometry *(LSRII Fortessa*, BD Biosciences, Heidelberg, Ger) using *FACS Diva software 6.2* (BD Biosciences). For further data processing *Flowjo 6.5.5 software* (FlowJo, LLC, Oregon, USA) was used.

3.4.3 Sodium dodecyl sulphate - polyacrylamide gel electrophoresis (SDS-PAGE)

SDS-PAGE allows the separation of proteins according to their molecular mass in a denaturing discontinuous polyacrylamide gel electrophoresis (PAGE) system. Proteins were separated on self-made 10% (1.5 mm) mini SDS-PAGE gels (see Table 6) using a polyacrylamide gel electrophoresis chamber (BIO-RAD, Hercules, USA).

Table 6 Composition of separating and stacking gels

Compound	Separating gel 10%	Stacking gel 5%
Rothiphorese® Gel 30 (37,5:1)	3.3 ml	0.85 ml
1.5 M Tris Buffer pH 8.8 (separating gel buffer)	2.5 ml	-
0.5 M Tris Buffer pH 8.8 (stacking gel buffer)	-	1.25 ml
10% SDS	100 µl	50 µl
MilliQ H20	3.97 ml	2.8 ml
10% APS	100 µl	50 µl
TEMED	10 µl	5 µl

Separation was performed at constant 120 V for 80 min at room temperature. The size of the protein bands was determined using 5 µl *PageRuler^{TM} Prestained Protein Ladder* (Fermentas GmbH) per line on each SDS-PAGE.

During this study, SDS-PAGE was performed for analysis of Akt phosphorylation, and information concerning protein amount and cell number is listed in 3.4.4.

3.4.4 Western blotting and phosphorylation analysis

After protein separation via SDS-PAGE, proteins were electrophoretically transferred to polyvinylidenfluorid (PVDF) membrane (GE Healthcare, Munich, Ger) at constant 85 V for

120 min using the *Mini Trans-Blot® Cell set up* (Biorad Laboratories, Munich, Ger). The membranes were blocked with corresponding blocking buffer listed in 3.1.4 and according to the protein of interested for 1 h at room temperature or overnight at 4 °C. The primary antibodies against the protein of interest were added to the membranes at the concentrations and incubation conditions listed in Table 2. Membranes were washed three times for 5-10 minutes with TBST and incubated with the corresponding secondary antibodies for 1 h at room temperature. Secondary antibodies conjugated with horseradish peroxidase (HRP) were diluted in blocking buffer. After three washes with TBST, the *ECL Plus HRP substrate solution* (Amersham, Little Chalfont, UK) was added to the membranes. The HRP signals were detected using the chemiluminescence reader *LAS-3000-scanner (*Fujifilm, Düsseldorf, Ger). For analysis of Akt phosphorylation $1.5x10^6$ cells per well were cultured in the absence of serum for 12 h. After stimulation of cells, cells were cooled on ice, centrifuged at 300 x g for 10 min and resuspended in 200 µl lysis buffer for phosphorylation analysis (see section 3.1.43.1.4). After 30 min, cell homogenates were centrifuged at 16,000 x g for 10 min. 150 µl of the supernatant was supplemented with 1x SDS sample buffer and boiled for 5 min at 95 °C. 25 µl of cellular lysates were subjected to SDS-PAGE followed by Western blotting. Membranes were first incubated with the antibody specifically recognizing phosphorylated Akt. After detection, bound antibodies were removed by incubation in stripping buffer for 10 min at room temperature. The membrane was blocked again with blocking buffer, and antibody for total Akt was used. Akt activation was expressed as phosphorylated Akt versus total Akt. Antibodies were used according to Table 2.

3.4.5 Filamentous (F)-Actin staining via phalloidin

Phalloidin is a bicyclic peptide belonging to a family of toxins isolated from the toxic basidiomycete fungus *Amanita phalloides* and is used in this study to selectively detect F-actin without binding to monomeric G-actin. For F-actin analysis, THP-1 cells were harvested, washed once with HBSS, counted and resuspended in HBSS to a density of $1x10^6$ cells/ml. After resting periods of 20 min at 37 °C, cells were fixed by adding 4% PFA in a 1:2 ratio, yielding an end concentration of 2% PFA. Cells were centrifuged and resuspended in 0.5% Triton X-100 in PBS to permeabilize cell membranes. Triton X-100 was washed out by centrifugation. Finally cells were stained with 2 U/ml phalloidin Alexa 488 (Lifetechnologies, Carlsbad, USA) in HBSS containing 0.2% BSA for 15 min on ice. Cells were washed once and resuspended in PBS for flow cytometry analysis.

3.5 Functional *in vitro* assays

3.5.1 Ligand binding assay

To analyse the ability of stable ligand binding by chemokine receptors in dependence on mutations of the DRF/DRY motif, binding assays were performed using the CXCL16-Fc and CX_3CL1-Fc constructs described in 3.4.1. Receptor expressing cells were harvested, washed once with HBSS and resuspended in HBSS to a concentration of $1x10^6$ cells/ml. The assay was performed either with THP-1 cells or with HEK293 cells.

For THP-1 cells, the assay was performed at room temperature and on ice in parallel to HEK cells, where cells were fixed before treatment, as described below. The chemokine-Fc fusion proteins were diluted 1:10 (absolute concentration was not measured, but production of Fc-fusion proteins was standardised according to 3.4.1) to THP-1 cell suspension and incubated for 10 min or 1 h on ice or at room temperature. Subsequently, cells were fixed with, 1% PFA end concentration to stop the assay and to stabilise the receptor-ligand-binding. All cells were placed on ice and washed with ice cold HBSS followed by centrifugation and washing with FACS-buffer. Finally cells were stained with anti-human IgG Fc gamma-APC antibody for 1 h on ice to detect bound chemokine-Fc proteins and analysed by flow cytometry. If indicated, binding specificity was approved by adding soluble recombinant chemokine (10 nM) to the cells immediately after chemokine-Fc application for competitive binding. For HEK293 cells, the assay was performed with slight modifications. Cells were fixed with 1% PFA after harvesting via accutase treatment, washed two times with FACS-buffer and incubated with chemokine-Fc proteins for 1 h on ice. Finally, cells were stained with anti-human IgG Fc gamma-APC antibody to detect bound chemokine-Fc proteins for 1 h on ice.

3.5.2 Internalisation and recycling assay

To analyse the surface regulation of the different CXCR6 mutants after ligand binding, an internalisation and recycling assay was performed for receptor variant expressing HEK293 cells. Cells were harvested via accutase treatment, washed once with PBS and resuspended in PBS with a final concentration of $1x10^6$ cells/ml. For the internalisation assay, all cells instead of those treated at 37 °C later on, were placed on ice. For inhibition of internalisation, cells were either pretreated with the dynamin inhibitor dynasore (100 µM for 15 min) or with the cytochrome oxidase inhibitor sodium azide (NaN_3, 0.2%, 15min). Internalisation of CXCR6 was provoked by

treatment with 20 nM human CXCL16 for 15 min. Subsequently, all samples were placed on ice and transferred to FACS-tubes, washed once with 300 µl PBS and centrifuged. After centrifugation, cells were treated with 1% PFA for fixation and then stained for surface CXCR6 detection as described in 3.4.2. For the measurement of receptor recycling, internalisation of the receptor was provoked by incubation with 20 nM CXCL16 for 15 min at RT. Then, 500 µl of preheated PBS (37 °C) was added and cells were centrifuged. Cells were again resuspended in preheated PBS to allow recycling of the receptor to the cell surface until recycling progress was stopped by placing the cells on ice for 10 min. Finally cells were treated with 1% PFA for fixation and then stained for surface CXCR6 detection as described in 3.4.2

3.5.3 Proliferation assay

For real-time analysis of cell proliferation, 10000 THP-1 cells expressing different human CXCR6 variants were seeded in 100 µl in 96-well plates. To analyse the role of CXCR6 expression, cells were either coincubated with recombinant human CXCL16 (10 nM) or anti-human CXCL16 capture antibody (50 ng/ml). Cell proliferation was measured as increase of cell density within the *IncuCyte^{TM} Zoom* (Essen Biosciences, Hertfordshire, UK) taking 1 picture per well every 2 h for 72 h. For statistical analysis, the fold increase in density within 72 h was calculated using the *IncuCyte^{TM}* software (Essen Biosciences, Hertfordshire, UK).

3.5.4 Intracellular calcium-influx assay

Intracellular calcium signalling was measured using Fluo-4-acetoxymethylester (Fluo-4-AM, Life Technologies, New York, USA). This is a labelled calcium indicator that exhibits an increase in fluorescence upon binding of Ca^{2+}. AM is an uncharged group making sure the Fluo-4-AM can permeate cell membranes easily. Once inside the cell, AM is cleaved by nonspecific esterases, resulting in a charged form of Fluo-4 that leaks out of cells more slowly.

THP-1 cells were harvested, washed once with HBSS and resuspended in calcium-staining buffer at a density of $2x10^6$ cells/ml. After an incubation of 15 min at 37 °C in the dark, the cells were washed twice (300 x g for 5 min) with 5 ml of prewarmed (37 °C) calcium-assay buffer. Cells were resuspended at a density of $2x10^6$ cells/ml and 100 µl of the cell suspension were added to a black 96-well-plate with a clear bottom. Calcium-influx upon stimulation with CXCL16 and MCP-1 was measured at 37 °C in the *FLUOstar OPTIMA plate-reader (*BMG-Labtech, Ortenberg, Ger). After establishing the fluorescent baseline of the cells for 10 s, either 20 µl of a

15 nM MCP solution (2.3 nM MCP-1 final) or 7-15 µl of a 15 or 150 nM CXCL16 solution (1-20 nM CXCL16 final) was injected to the labelled cells. As buffer control, 20 µl of calcium-assay buffer containing 0.5% BSA was injected. The fluorescence was constantly measured at an excitation wavelength of 488 nm and an emission wavelength of 526 nm. After stimulation of the cells, labelling of the THP-1 with Fluo-4-AM was verified by injecting the detergent Triton X-100 (0.1% final), which lead to a maximum increase of the signal. Because of permeabilisation of the cell membrane the Fluo-4-AM stored inside the cells could bind to free calcium of the assay buffer. To determine the background fluorescence, EGTA (15 mM final) was injected to disrupt the complex and capture all free calcium.

Calcium influx assay was performed with HEK293 as well. Therefore HEK293 cells were harvested via accutase treatment. The following procedure was performed as described for THP-1 cells.

3.5.5 Chemotaxis assay

Chemotaxis against CXCL16 or CX_3CL1 was analysed using a *Boyden chamber* (Neuroprobe, Gaithersburg, MD), which allows the parallel investigation of eight different conditions. THP-1 cells were harvested, washed with chemotaxis assay buffer and resuspended at a concentration of $2x10^6$ cells/ml. Lower chambers of the *Boyden chamber* were filled with 28.5 µl assay buffer containing 0.3 – 33 nM chemokine, increasing logarithmically. 3 nM MCP-1 was used as positive control. Upper and lower chamber were separated by a filter membrane with 8 µm pores. 30 µl of cell suspension were filled into the upper chamber. After migration for 2 h at 37 °C, the migrated cell number was determined using the glucoronidase-assay as described before[84]. Therefore, 3 wells of the lower chamber were pooled, measuring each condition as duplicate. For quantification of the cell number a 1:2 serial dilution of non-migrated cells was used. Migration experiments with PBMC, murine cells and THP-1 experiments analysing the chemotactic response to human and murine CX_3CL1 were performed in *Transwell® Permeable Supports*, (Corning incorporated life science, Lowell, USA*)* with an insert diameter of 6.5 mm and a pore size of 8 µm. THP-1 cells were prepared as described above. For the isolation of murine blood cells, 400 µl of blood, collected from *vena cava,* was added to ice cold 1.4 ml PBS containing 1 mM EDTA. Then 8 ml of erythrocyte lysis buffer were added and incubated at 37 °C until the suspension appeared clear. 40 ml PBS were added and the suspension was centrifuged for 5 min at 4 °C and 300 x g. Cells were resuspended in 2 ml prewarmed (37 °C) migration buffer at a

concentration of $2x10^6$ cells/ml. PBMC were isolated of fresh blood supplemented with 0.4% calcium citrate of healthy volunteers as described before[35]. Transwells were placed into 24-well plates filled with 600 µl chemokine containing migration buffer, and 100 µl of cell solution was applied to the upper well. After incubation for 2 h at 37 °C the number of migrated cells was again determined using the β-glucoronidase-assay.

3.5.6 Adhesion assay

The influence of the different chemokine receptor variants on cell adhesion was analysed by investigating the adhesion to immobilised human/murine CXCL16-Fc or CX_3CL1-Fc. 48-well cell culture plates were coated with 120 µl PBS containing 2 µg/ml anti-human-Fc antibody overnight at 4 °C. To minimize unspecific adhesion, the wells were washed twice and blocked with PBS containing 1% BSA for 1 h at room temperature. Finally the wells were coated with CXCL16-Fc or CX_3CL1-Fc cell supernatant (see 3.4.1), which were diluted 1:20 in PBS containing 1% BSA, for 1 h at RT. Unbound Fc-constructs were removed by washing with HBSS. Cells were harvested and washed once with PBS. To enable visualisation of adherent cells, $2x10^6$ cells/ml were stained with 1 µM calcein-AM for 15 min in PBS. After washing with PBS, cells were kept in HBSS (HEK293 cells 15 min, THP-1 cells 4 h) until $1x10^5$ cells in 200 µl HBSS were transferred to the wells containing immobilised chemokine-Fc. Cell culture plates were centrifuged for sedimentation of the cells for 1 min at 300 x g without impulse or break. After another 15 min (HEK293) or 30 min (THP-1) of rest at 37 °C, fluorescence intensity was measured for quantification of starting cell number. Then, the medium was discarded by inversion of the plates and wells were washed with 200 µl warm PBS. After repeating this washing step twice, cell number of remaining cells was determined. For the quantification of the cell number, a 1:2 serial dilution of labeled cells was measured. Fluorescence was measured by the *FLUOstar OPTIMA plate-reader* at an excitation wavelength of 488 nm and an emission wavelength of 526 nm.

3.5.7 Apoptosis assay

The influence of the different CXCR6 chemokine receptor mutants on cell apoptosis was determined using the *Annexin V Apoptosis Dection Kit eFluor 450* (eBioscience) according to the manufacturer's protocol. Cells were harvested and $5x10^5$ cells were resuspended in 500 µl cell culture medium containing 10% fresh FCS. To induce apoptosis, cells were treated with 100 mU/ml bleomycin or 100 mU/ml bleomycin plus 50 ng/ml anti-human CXCL16 antibody

(neutralising antibody). After incubation for 24 h $1x10^5$ cells were transferred to FACS-tubes and stained with Annexin V and 7-AAD to distinguish between early apoptosis (Annexin V positive, 7-AAD negative), late stage apoptosis (Annexin V and 7AAD positive) and necrosis (Annexin V negative, 7-AAD positive). Cell staining was measured using flow cytometry analysis.

3.6 Analysis of allergic lung disease in an ovalbumin-induced asthma model

3.6.1 Mice

CXCR6 GFP knock-in mice were purchased from *The Jackson Laboratory* (strain 005693) and constructed as described by Unutmaz et al.[94]. Homozygous $CXCR6^{GFP/GFP}$ mice are deficient for CXCR6 expression and express GFP under control of CXCR6 promotor. Heterozygous $CXCR6^{+/GFP}$ mice, expressing GFP in addition to CXCR6, were used as control animals. The mice have a C57BL/6 background. Genotypes were proven by standardised genotyping for each animal (data not shown).

To generate mice lacking ADAM10 in endothelial cells, ADAM10flox/flox mice[95] were mated with Tie2-Cre (Angiopoietin receptor) transgenic mice[96] (provided by Dr. Tom Sato). ADMA10flox/flox/Tie2-Cre mice (Tie2 $Adam10^{-/-}$) were maintained on a mixed genetic background (129Ps/C57BL/6)[97]. Littermates, negative for Cre recombinase were used as control animals. Genotypes were proven by standardised genotyping for each animal (data not shown).

All animal experiments were approved by the local authority Landesamt für Natur, Umwelt und Verbraucherschutz (LANUV NRW, 87-581.04.2010.A370 and appendices and 84.02.04.2011.A335 and appendices). Animals were hosted in a pathogen-free environment within the animal facility of the Medical Faculty of RWTH Aachen University and were transferred to individually ventilated cages for each experimental condition (ovalbumin treatment and control treatment) within the Institute of Pharmacology and Toxicology of RWTH Aachen University. Sensitisation was performed with 6- to 8-week old female mice.

3.6.2 OVA-induced lung inflammation

The OVA model was used to investigate the influence of CXCR6 or endothelial ADAM10 on the development of experimental asthma. Mice were sensitised by intraperitoneal injection of ovalbumin (aluminium hydroxide gel as vehicle control) over a period of 21 days followed by nebulisation to induce allergic reaction. The 35 days-model was used as subchronic model

dominated by eosinophil recruitment and mast cell reaction, whereas the 110 days-model mimicked the establishment of more severe asthma including tissue remodelling.

For sensitisation mice were treated as followed (see also Figure 5): on days 0, 14 and 21 0.2 ml of an OVA/aluminium hydroxide gel solution containing 60 µg OVA and 2.25 mg of aluminium hydroxide was injected intraperitoneally to mice in the asthma group. 0.2 ml 2% aluminium hydroxide gel alone was injected intraperitoneally in the control groups. On days 28, 29 and 35 OVA nebulisation was performed with 5 ml 0.9% sodium chloride containing 1% OVA for 20 minutes. Control groups were nebulised with 0.9% sodium chloride at the same time points. In case of the 110 days-model, nebulisation was performed twice a week, until day 110. Mice were sacrificed on day 36/111 to analyse lung inflammation. For this purpose serum, bronchoalveolar lavage (BAL) fluid, and lung tissue were collected for histological staining, ELISAs, and RT-qPCR and cells of BAL were subjected to flow cytometry analysis (see section 3.6.3).

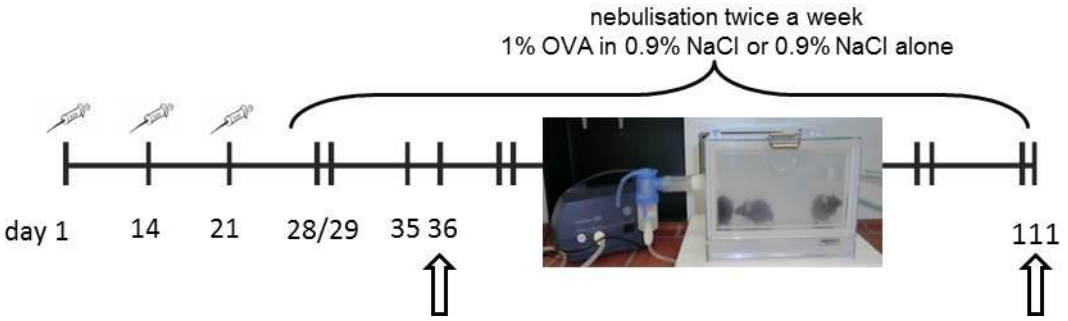

Figure 5 Sensitisation protocol for OVA-induced asthma
Schematic description of the sensitisation protocol for induction of subchronic (sacrifice at day 36) and chronic (sacrifice at day 111) lung inflammation by OVA-treatment. Equipment: Nebulizer plastic box for mice (Sanplatec corporation, Osaka City, JP) and PARI LC SPRINT nebulizer (PARI GmbH, Starnberg, Ger).

3.6.3 Operating procedure and sample collection

Mice were euthanised under anaesthesia (500 mg/kg ketamin and 50 mg/kg xylazine). Mice were fixed in the supine position and the cervical trachea was fully exposed. The trachea was opened with a small horizontal cut between the cartilage of the trachea and a 20 G tracheal cannula was inserted and fixed by tightening the ligature. Blood for serum collection and analysis of blood cell composition was collected from the vena cava. Afterwards the thoracic cavity was opened by rupturing the midriff and a part of post-caval lobe and the whole left lobe were ligated immediately. BAL fluid of the right lobe was collected by flushing the tissue intratracheally (i.t.) with 500 µl ice-cold PBS. Afterwards ligation of the left lobe was opened and the vascular

system was perfused with ice-cold PBS to obtain blood-free lung tissue. The right lobe was ligated and 400 µl *Roti-Fix* (Carl Roth GmbH & Co. KG) were filled into the left lobe by i.t. instillation. After 5 minutes the whole lung was removed. Tissue of the left lobe was put in liquid nitrogen for later analysis. To determine the wet-to-dry ratio, the separated tissue of the post-caval lobe was removed and weighted immediately to define the weight of the wet lung tissue. After 48 hours of drying at 60 °C, the weight of the dry lung tissue was measured again and wet-to-dry ratio was calculated to examine oedema formation. The left lung was embedded in *Roti-Fix* for another 48 hours, and then tissue was dehydrated, embedded in paraffin, and cut in 3 µm slices. Haematoxylin and eosin (HE) stain, Ladewig trichrome (TRC) and Periodic acid–Schiff (PAS) staining were performed by *Immunohistochemistry and Confocal Microscopy facility* Aachen using standard protocols. Ten images per animal were taken with the *AxioLab.A1* Zeiss microscope (Carl Zeiss Microscopy GmbH) and analysed for thickness of alveolar septa, collagen layers and amount of PAS positive cells using the *AxioVision 4.8. software* (Carl Zeiss Microscopy GmbH).

Blood was centrifuged for 10 min, 3000 x g and 4 °C to obtain serum, which was directly frozen and stored at -80 °C until analysis. In the case of differential blood cell analysis, 100 µl blood were added to 1 ml PBS supplemented with 0.5 mM EDTA directly after removal of blood and processed after termination of sample collection. 4 ml of erythrocyte lysis buffer were added and incubated at 37 °C until the suspension appeared clear. Then 15 ml ice cold PBS were added and the suspension was centrifuged for 5 min at 4 °C and 400 x g. Afterwards 1ml of 1% PFA were used for 5 min to fix the cells. Fixation was stopped by adding 10 ml PBS and centrifugation for 5 min at 400 g. Blood cells were subjected to antibody staining as indicated in Table 7. Despite characterisation of blood cells via flow cytometry analysis, the ability of chemotactic migration in response to soluble murine CXCL16 was tested as well (described in 3.5.5).

BAL fluid was centrifuged for 10 min, 400 x g and 4 °C to collect BAL cells. The supernatant was separated, centrifuged again for 10 min, 16000 x g and 4 °C, and the resulting supernatant was collected for analysis of cytokine and total protein content using *BCA assay kit* (Interchim, Montlucon Cedex, F). The pelleted cells were fixed with 1 ml 1% PFA for 5 min. 150 µl of cell fixing suspension was separated for subsequent cell counting. To determine the absolute amount of cells isolated from BAL, *CountBright™ Absolute Counting Beads* were used as recommended by the manufacturer. Remaining cells were washed with 300 µl FACS-buffer and divided into

different cell populations (for specification see results section) for diverse antibody staining mixtures (Table 7) and flow cytometry analysis.

To detect basal phenotypical differences between CXCR6$^{+/GFP}$ and CXCR6$^{GFP/GFP}$, lung tissue and spleen were subjected to differential analysis of cellular composition. Lung tissue of control treated animals was isolated, dissected by scalpels and incubated for 1 h at 37 °C in 0.1% collagenase in PBS. Afterwards the tissue was further hackled by drawing into a syringe with a 20 G cannula. Resulting tissue was put onto a 70 µm filter. The flow through was collected, centrifuged at 4 °C and 400 x g for 5 min, and the cell pellet was used for antibody staining (Table 7) and flow cytometry analysis. The spleen was separated from remaining connective tissue and dissected by scalpels and crushed by the plunger of a syringe, resuspended in 15 µl ice cold PBS and put onto a 40 µm filter. The flow through was collected and centrifuged for 5 min at 4 °C and 400 x g. Afterwards cells were fixed via 1% PFA and stained with a mixture of antibodies (Table 7) and analysed by flow cytometry.

Table 7 Antibody mixtures for investigation of cell composition of different tissues by flow cytometry analysis.
Each analysis assigned a special antibody mixture. CXCR6 expressing cells were identified by detection of GFP expression during flow cytometry analysis (PacBlue: Pacific Blue).

lung tissue (basal analysis)	CD4-APC Cy7 CD25-APC IL17-Pe IFNγ-PacBlue CXCR6-GFP	CD4-APC Cy7 ST2-APC CD127-PeCy5 IL17-Pe IFNγ-PacBlue CXCR6-GFP	CD8-PacBlue NK1.1-PeCy7 CD3-PeCy5 CD25-APC CXCR6-GFP	Ly6G-APC F4/80-Pe CD4-APC Cy7 CD8-PacBlue CD11b-Pe Cy7 CXCR6-GFP
blood (basal analysis)	CD3-PeCy5 CD11b-Pe Cy7 Ly6G-APC CD45-PacBlue CD19-Pe CXCR6-GFP	Ly6G-APC F4/80-Pe CD4-APC Cy7 CD8- PacBlue CXCR6-GFP		
spleen (basal analysis)	CD4-APC Cy7 CD3-PeCy5 CD8-PacBlue CXCR6-GFP			
BAL of CXCR6$^{+/GFP}$//$^{GFP/GFP}$ (35 days of sensitisation)	CD4-APC Cy7 CD25-APC CD127-PeCy5 IL17-Pe IFNγ-PacBlue	CD4-APC Cy7 ST2-APC CD127-PeCy5 IL17-Pe IFNγ- PacBlue	CD8-PacBlue NK1.1-PeCy7 CD3-PeCy5 CXCR6-GFP	Ly6G-APC F4/80-Pe CD4-APC Cy7 CD8-PacBlue CD11b-Pe-Cy7

	CXCR6-GFP	CXCR6-GFP		CXCR6-GFP
BAL of $CXCR6^{+/GFP}//^{GFP/GFP}$ (110 days of sensitisation)	CD4-APC Cy7 CD25-APC NK1.1-Pe.Cy7 F4/80-Pe IFNγ-PacBlue CXCR6-GFP	CD4-APC Cy7 CD8-PacBlue ST2-APC CD11b-Pe Cy7 CXCR6-GFP		
BAL of $Tie2ADAM10^{\pm//-/-}$ (35 days of sensitisation)	CD4-APC Cy7 Ly6G-APC CD11b-Pe-Cy7 CD8-PacBlue F4/80-Pe	CD4-APC Cy7 IFNγ-PacBlue ST2-APC CD127-Pe-Cy5		

3.6.4 Lung imaging

To visualize the existence of CXCR6/GFP positive cells in lung tissue and analyse potential differences in the positioning of CXCR6/GFP-positive cells, lungs of $CXCR6^{+/GFP}$ and $CXCR6^{GFP/GFP}$ mice were isolated and analysed by the *Lightsheet Z.1 microscope* (Carl Zeiss Microscopy GmbH). Mice were euthanised and prepared as described above. After perfusion with ice-cold PBS lungs were filled with preheated (37 °C) 1% low melting agarose in PBS through the tracheal cannula. For faster hardening of the agarose, lungs were covert with ice for about 25 min. Afterwards lungs were removed and cut into smaller pieces for analysis with the *Light sheet Z.1 microscope.* For further analysis of images, *Zen* software (Carl Zeiss Microscopy GmbH) was utilised.

3.6.5 Physiological lung measurements

3.6.5.1 Tracheotomy

After 110 days of OVA sensitisation, mice were anaesthetised by intraperitoneal injection of Narcoren (70 mg/kg). A subcutaneous injection of 50 µl xylazine 1% was used for local anaesthesia of the operation area. After checking for sufficient sedation, throat skin was treated with iodide solution for disinfection. Subsequently the skin was opened with a vertical cut and the trachea was bared carefully. A suture was pulled around the trachea before it was opened with a small horizontal cut. A 20 G tracheal cannula was inserted and fixed by tightening the ligature.

3.6.5.2 Measurement of lung function parameters

After tracheotomy, mice were connected to the *flexiVent* (Scireq, Montreal, Can) ventilation setup. This ventilation setup allows the measurement of lung mechanics by forced oscillation

technique (FOT). The FOT interrupts the standard ventilation mode by inducing a low frequency oscillatory waveform to the respiratory system. Thereby, two different types of oscillatory measurements were conducted: Initially, the resistance (R) and the elastance (E) of the respiratory system were calculated by the murine response to a sinusoidal waveform (SnapShot-manoeuvre with duration of 1.25 seconds and a frequency of 2.5 Hz). Additionally, a broadband forced oscillation manoeuvre (QuickPrime with duration of 3.0 seconds and frequencies between 1 and 20 Hz) was used to measure the input impedance (Z). Z was further analysed using the constant phase model to obtain a parametric distinction between the airway and tissue mechanics. The resulting parameters were the newtonian resistance and the tissue damping. Parameters were calculated using the flexiVent software *Flexiware 7.0.1* (Scireq).

Mice were mechanically ventilated with a V_{total} of 10 ml/kg, a positive end-expiratory pressure of 2 cm H_2O and a frequency of 150/min. During the entire ventilation period, the body temperature of mice was controlled by rectal measurement and adjusted to 37.0 ± 0.5 °C. Continuous data recording of heart rate and ECG was performed to monitor the function of the cardiovascular system and was used to control the depth of anaesthesia. During the first 30 min of ventilation, basal lung function was measured in a standardised script. Lung function parameters were recorded every 30 seconds. Every 5 min, short volume controlled recruitment manoeuvres (with duration of 3 seconds and a maximal pressure of 30 cmH2O) were used to avoid atelectasis. After basal ventilation, airway hyperresponsiveness was induced by nebulizing increasing concentrations of acetylcholine (AcCh) (0, 0.1, 1, 3.16, 5.62, 10, 31.6, 56.2 and 100 mg/ml).

3.7 Statistical analysis

Quantitative data are shown as mean and SD calculated from at least three independent experiments or cell isolates. Homoscedasticity was tested by the Bartlett test and analysed using parametric Student´s t-test. In the case of no homoscedasticity data were transformed: Otherwise, data were analysed using the nonparametric Mann-Whitney U test. Statistical analyses were performed using *PRISM5.0* (GraphPad Software, La Jollla, CA) and *Statistical Analysis System* (SAS, SAS Institute GmbH, Cary North Carolina, USA). All p-values were corrected for multiple comparisons using false discovery rate (FDR) control and differences were indicated by asterisks or hashes. More information is indicated in each figure legend.

4 Results

4.1 Functional analysis of the DRF motif of CXCR6

The family of G protein coupled chemokine receptors consists of 18 different proteins. 17 of these GPCR proteins carry the typical DRY motif at the interface of the transmembrane region three and the second intracellular loop. Only in CXCR6 the DRF is replaced by the DRY motif. The aim of the first part of this study was to investigate physiological consequences and explanations for this unique specialty in the family of chemokine receptors. Therefore, the endogenous DRF motif of CXCR6 was mutated into the more common DRY motif and into the DNF motif, which has been shown to abrogate signalling in other GPCR. The different variants of CXCR6 were first analysed in HEK293 cells as these cells do overexpress proteins very efficiently. Three different human receptor variants were generated and designated as follows: 1) Wild type CXCR6 termed DRF 2) CXCR6 mutant F128Y, termed DRY and 3) CXCR6 mutant R127N, termed DNF.

4.1.1 Analysis of CXCR6 variants in HEK293 cells

4.1.1.1 Analysis of CXCL16 binding by different CXCR6 variants

HEK293 cells were lentivirally transduced with pLVX-IRES-Neo plasmids coding for human CXCR6-DRF, -DRY and -DNF variants. After a period of 14 days of G418 selection, HEK293 cells were analysed for their surface expression of human CXCR6 variants. The surface expression of CXCR6 variants by HEK293 cells was then confirmed by antibody staining. Flow cytometric analysis revealed no specific binding of the anti-CXCR6 to HEK293 cells transduced with empty vector (EV) control indicating that these cells express no or undetectable levels of CXCR6. In contrast, the CXCR6 specific fluorescence intensity was strongly increased in HEK293 cells transduced with CXCR6-DRF, CXCR6-DRY and CXCR6-DNF. A narrow and uniform fluorescence distribution was obtained for all receptor variants (Figure 6A). The HEK293 quantification of three independent batches of transduced HEK293 cells (Figure 6B) revealed that the different receptor variants were expressed on the cell surface of HEK293 cells at a comparable level. Thus, mutation of the DRF motif in CXCR6 did not affect surface expression of the receptor.

Next, CXCR6 variants were tested for binding of CXCL16. For this purpose, a CXCL16-Fc fusion protein was used as a ligand, which was then detected with an anti human-Fc antibody. Flow cytometry analysis showed strong homogenous labelling on the whole population of

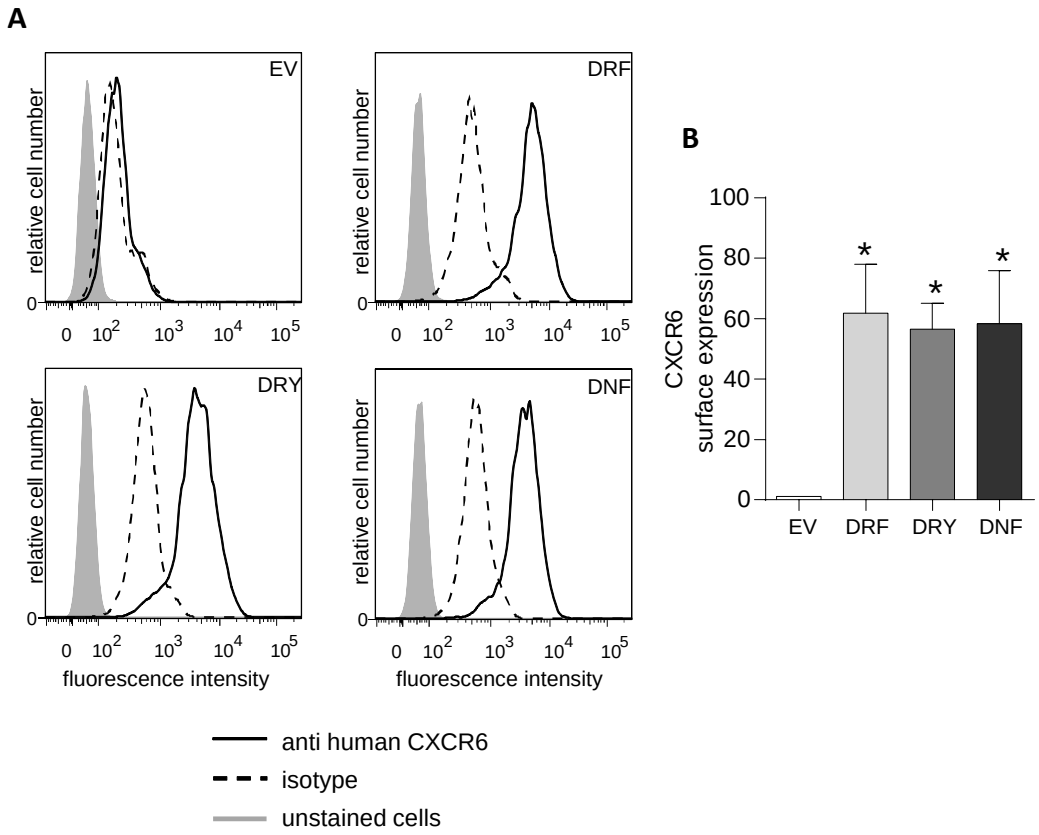

Figure 6 Human CXCR6 cell surface expression on HEK293 cells
HEK293 cells were transduced with lentivirus encoding human CXCR6 variants (wild type (126DRF), F128Y (DRY), R127N (DNF)) or with empty vector control (EV). Efficiency of overexpression and cell surface expression was controlled by flow cytometry using PE-labelled antibody against human CXCR6 in comparison to the appropriate isotype control. A) Representative histograms of flow cytometry analysis of three independent experiments. B) CXCR6 expression was measured as geomean of fluorescence signal. Unspecific fluorescence determined by isotype control was subtracted. Signals were expressed in relation to control (EV), and data of three independent experiments are shown as mean + SD. Statistical analysis was performed by one sample t-test (hypothetical value = 1) and corrected for multiple comparison by FDR. Significant differences are indicated by asterisks (*$p<0.05$).

HEK293 cells transduced with the different receptor variants but only slight labelling of HEK293 cells transduced with empty vector (Figure 7A). Thus, each of the receptor variants was able to bind the CXCL16-Fc fusion protein. The quantification of three independent experiments indicated an equal binding of CXCL16-Fc to all receptor variants, also pointing towards a similar expression of all receptor variants on the cell surface of HEK293 cells. Therefore, HEK293 cells

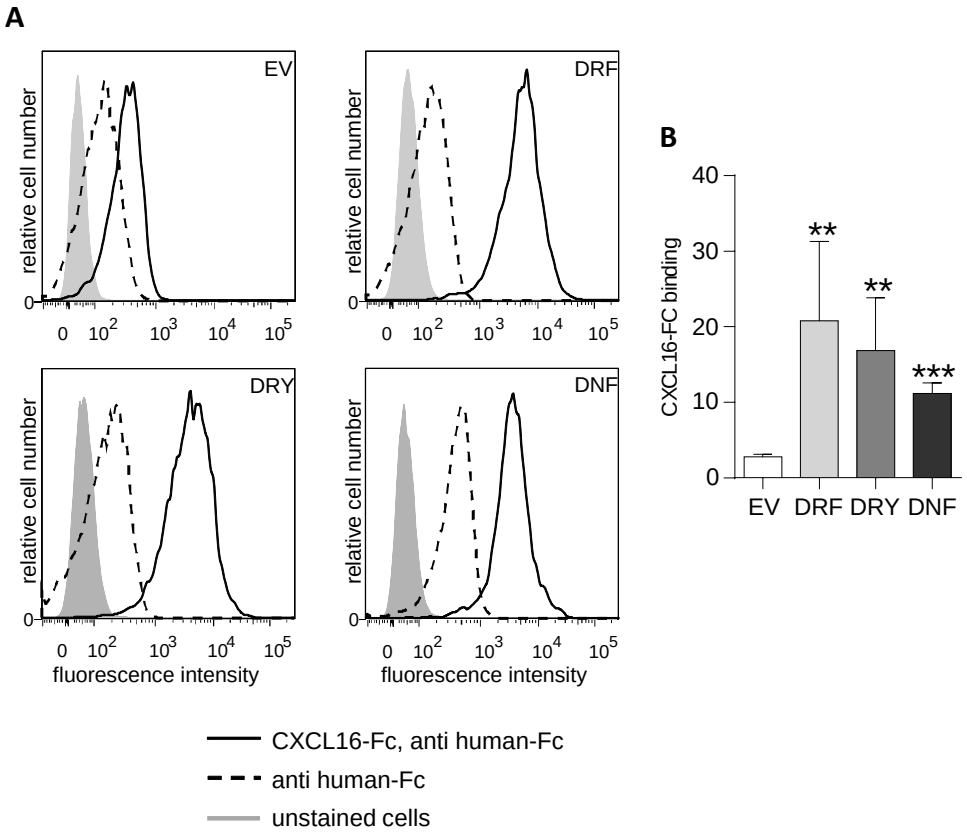

Figure 7 CXCL16-Fc binding by HEK 293 cells expressing CXCR6 variants
HEK293 cells were transduced with lentivirus encoding human CXCR6 variants. Ligand binding ability of receptor mutants was analysed by incubation with CXCL16-Fc fusion protein, followed by antibody stain against human Fc fragment and flow cytometry analysis. A) Representative histograms B) CXCL16-Fc binding was measured as geomean of fluorescence signals. Signals were expressed in relation to background binding of anti human-Fc and data are shown as mean + SD (n=3-4). Statistical analysis was performed by one tailed Student's t-test and corrected for multiple comparison by FDR (**p<0.01, ***p<0.001).

were suitable for expression of CXCR6 variants and for their further functional analysis in response to stimulation with CXCL16.

4.1.1.2 Role of the ^{126}DRF motif in CXCR6 internalisation and recycling

All chemokine receptors undergo a basal level of internalisation and degradation or recycling in the absence of endogenous ligands. Upon ligand binding, internalisation and trafficking of chemokine receptors can be greatly enhanced[98]. The clathrin-mediated endocytosis is the major trafficking pathway of chemokine receptors, also involving β-arrestin. It was shown that the DRY motif of CCR5 is involved in β-arrestin interaction[31] suggesting that this motif may also play a role for CXCR6 internalisation via β-arrestin. Therefore, HEK293 cells expressing the different receptor variants were analysed for CXCL16-dependent receptor internalisation and recycling (Figure 8 and 9). Incubation with 20 nM CXCL16 at 4 °C did not change surface staining via

anti-CXCR6 antibody leading to the conclusion that there is no internalisation of the receptor under these conditions. In contrast, when cells were stimulated with 20 nM CXCL16 for 15 min at 37 °C, surface staining of CXCR6 was strongly reduced. In comparison to untreated cells, surface expression for CXCR6 was less intense (25% (DRF), 38% (DRY), 28% (DNF)), indicating removal of the receptor from the cell surface. Interestingly, mutations of the ^{126}DRF motif did not result in detectable differences of receptor down-regulation. Even the signalling-dead mutant CXCR6-DNF showed down-regulated surface expression. Preincubation with 0.2% cell toxic NaN_3 blocked this processes for all three receptor variants. Moreover, when cells were pretreated with 100 µM dynasore to inhibit dynamin-dependent endocytosis prior to CXCL16 stimulation, down-regulation of all receptor variants was inhibited.

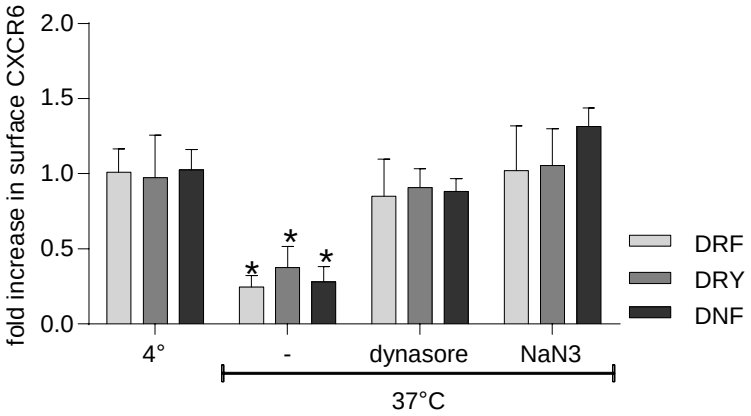

Figure 8 Internalisation of CXCR6 after stimulation with CXCL16
HEK293 cells were transduced with lentivirus encoding human CXCR6 variants. Internalisation of CXCR6 was analysed by surface staining with anti-human CXCR6 antibody. Cells were investigated at 4° or 37 °C during incubation with 20 nM CXCL16 to investigate temperature dependency or pretreated either with 100 µM dynasore or with 0.2% NaN_3 for 15 min to inhibit internalisation. Positive staining was expressed in relation to untreated HEK293 cells expressing the particular receptor variants. Data represent mean + SD of three independent experiments. Statistical analysis was performed by one-sample t-test to show the difference from staining of untreated HEK293 cells stained with anti-human CXCR6 antibody, (hypothetical value defined as 1) and corrected for multiple comparison by FDR (*$p<0.05$).

Once a receptor is internalised it either gets degraded in the lysosome or the protein is recycled to the cell surface[31]. In order to analyse such a trafficking process, HEK293 cells expressing CXCR6 variants were investigated for reexpression of CXCR6. Cells were stimulated with soluble CXCL16 to induce receptor internalisation. CXCL16 was removed by one washing step and subsequently cells were further incubated in the absence of the chemokine ligand for different time periods. The cells were then analysed for surface expression of CXCR6 (Figure 9).

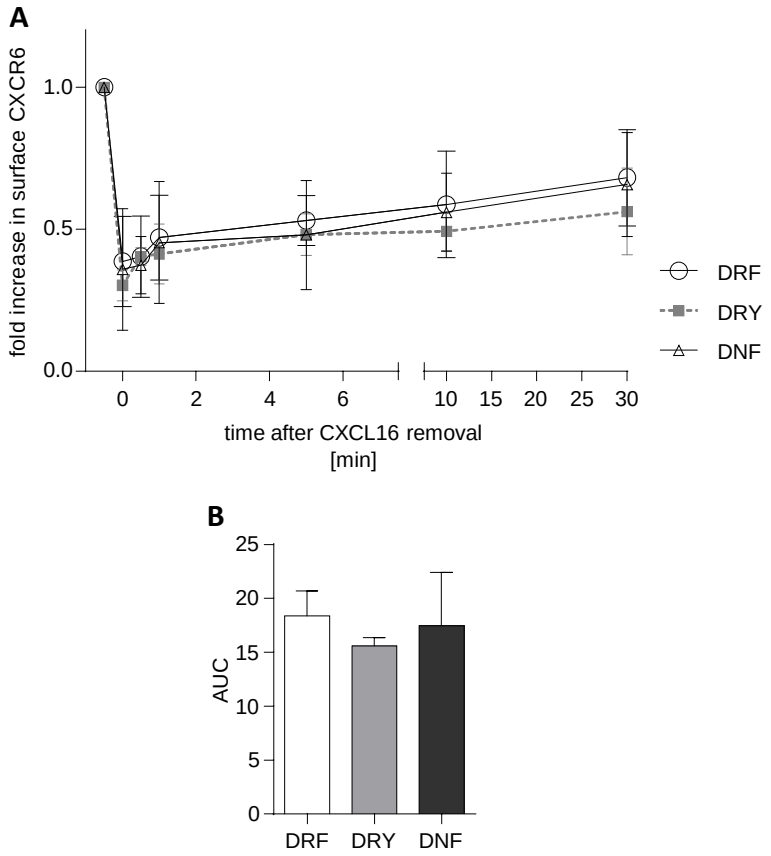

Figure 9 Recycling of CXCR6
HEK293 cells were transduced with lentivirus encoding human CXCR6 variants. Recurrence of staining possibility after removal of CXCL16 was equalised to recycling of the receptor to the cell surface. A) Recycling of CXCR6 was analysed 15 min after pretreatment with 20 nM CXCL16 dependent on the time after removal of the chemokine. Data are expressed in relation to the respective cell type stained with anti-human CXCR6 under standard conditions and represent mean ± SD of three independent experiments B) Areas under the curve (AUC) of data shown in A to quantify the recycling process. Data represent mean + SD. Statistical analysis was performed by Student's t-test and corrected for multiple comparison by FDR. No significant differences were observed.

Stimulation with CXCL16 resulted in a reduction of CXCR6 surface expression at 0 min after CXCL16 removal (0.39 (DRF), 0.3 (DRY), 0.36 (DNF) fold increase in surface CXCR6). Reexpression of the different CXCR6 receptor variants predominantly occurred in the first 5 min after the removal of soluble CXCL16. At 5 min after CXCL16 removal, surface staining of CXCR6 was increased in comparison to the expression at 0 min (DRF: 0.14, DRY: 0.18, and DNF: 0.12) fold increase in surface expression) (Figure 9A). Again, this process was independent of the mutations within the ^{126}DRF motif (Figure 9B). 30 min after removal of soluble CXCL16 stronger increase of CXCR6 surface expression was detectable again, resulting in 0.68 (DRF), 0.56 (DRY) and 0.66 (DNF) fold increase in surface CXCR6 in relation to untreated cells. Since all receptors were reexpressed at a comparable level it can be concluded that their recycling to the

cell surface is not different. During the observation time, no full restoration of CXCR6 expression was observed, which might be due to low concentrations of soluble CXCL16 still remaining in the cell suspension.

In summary, the investigated CXCR6 variants, expressed by HEK293 cells, were all capable of binding the ligand CXCL16, which led to internalisation and recycling of the receptor in a ^{126}DRF motif independent manner.

4.1.1.3 Influence of DRF-mediated signalling on CXCR6-dependent adhesion to immobilised CXCL16

CXCL16 is endogenously expressed as a transmembrane chemokine on endothelial and epithelial cells. It has been shown that the interaction between transmembrane CXCL16 and the receptor CXCR6 leads to adhesion of cells to sites of inflammation[53], which represents an essential step during immune cell recruitment. To determine a possible interaction of the ^{126}DRF motif

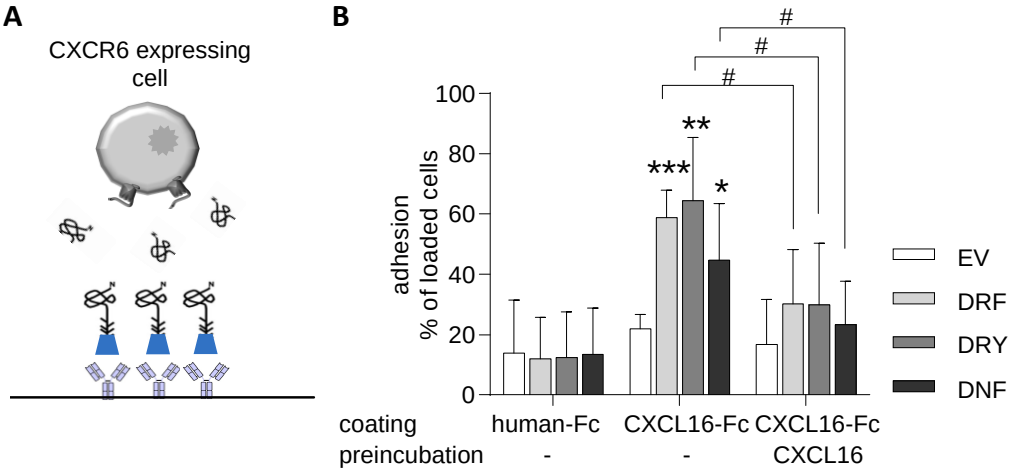

Figure 10 CXCR6-mediated adhesion of HEK293 cells
A) Schematic description of experimental setup. 48-well cell culture plates were coated with anti-human-Fc antibody. After blocking with 1% BSA, murine CXCL16-Fc construct was added. If indicated, HEK293 cells were preincubated with 20 nM CXCL16 to analyse the specificity of interaction. Then cells were transferred onto prepared culture plates, centrifuged and incubated for 15 min. Finally, cells remaining on the cell culture plates after three washing steps were measured. B) HEK293 cells were transduced with lentivirus encoding murine CXCR6 variants. Quantification of adhesion of HEK293 cells expressing murine CXCR6 mutants to immobilised murine CXCL16-Fc. Data are shown as mean + SD of percentage of loaded cells (100000) of three independent experiments. Statistic was performed by Student's t-test and corrected for multiple comparison by FDR. Statistical differences compared to adhesion of the respective cell type to anti-human-Fc are indicated by asterisks (*p<0.05, **p<0.01, ***p<0,001). Statistical differences comparing different treatments are indicated by hashes (#p<0.05).

ofCXCR6 during adhesion processes, the adhesion of HEK293 cells expressing CXCR6-DRF, -DRY and -DNF variants to immobilised CXCL16-human-Fc fusion protein was investigated (Figure 10). These investigations were complicated by the fact that HEK293 cells can express low quantities of endogenous CXCL16[99] which may interact with human CXCR6 variant and potentially prevent cell adhesion to immobilised CXCL16. Thus, murine CXCR6 and murine CXCL16-Fc were used to prevent undesired interactions with endogenously expressed human CXCL16 in HEK293 cells. HEK293 cells expressing murine CXCR6 variants adhered to immobilised murine CXCL16-Fc (59% (DRF, 65% (DRY), 45% (DNF) of loaded cells), which was significant in comparison to the unspecific binding of the respective cells to anti-human-Fc alone. Furthermore, HEK293-EV cells did not show increased binding to immobilised CXCL16-Fc. Preincubation of HEK293 cells with soluble murine CXCL16 decreased the adhesion mediated by either receptor variant to almost background, indicating a specific CXCR6-CXCL16 interaction (Figure 10B). In contrast, preincubation of HEK293 cells with pertussis toxin (PTX) did not inhibit CXCR6-mediated adhesion to immobilised CXCL16 (Figure 11). PTX specifically blocks the activation of $G\alpha_i$-subunits, which is essential for CXCR6-mediated signalling[60]. These results indicated that adhesion of HEK293 via the interaction of CXCR6 and CXCL16 is independent of $G\alpha_i$ protein-mediated signalling and this adhesion is not affected by mutation of the DRF motif into DRY or DNF.

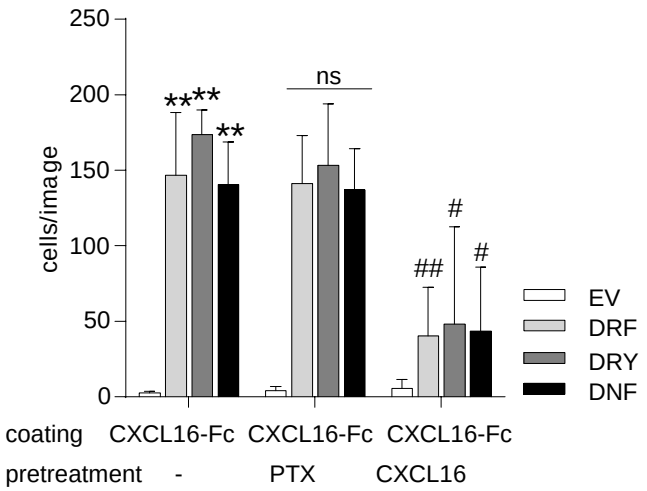

Figure 11 G protein signalling dependency of CXCR6-mediated adhesion of HEK293 cells
HEK293 cells were transduced with lentivirus encoding murine CXCR6 variants. Quantification of adhesion of HEK293 cells expressing murine CXCR6 mutants to immobilised murine CXCL16-Fc was performed using the *IncuCyte Zoom* microscope. Adhesive cells were imaged after the third washing step, and cells were counted in 16 images of each 48-well. Data are shown as mean + SD of cells per image (n=5-6). Statistic was performed by Student's t-test with Welch's correction and corrected for multiple comparison by FDR. Statistical differences compared to adhesion of EV cells are shown by asterisks (**p<0.01). Statistical differences comparing differences from the corresponding cells to CXCL16-Fc are indicated by hashes (#p<0.05, ##p<0.01). This assay was performed by D. Dreymueller.

4.1.1.4 **Analysis of calcium influx as function of CXCR6-DRF modifications**

Activation of chemokine receptors leads to activation of intracellular signalling cascades. One of the first steps is the activation of G proteins at the intracellular part of the receptor, followed by activation of phospholipase C and the influx of calcium into the cytoplasm, which itself leads to regulation of further signalling cascades[8,27,100]. Since the interaction of a chemokine receptor with the G protein is mediated mainly by the DRY motif, this motif also influences the induction of calcium signals as a consequence of G protein activation[29]. It was therefore assumed that the ^{126}DRF motif of CXCR6 would also affect the induction of calcium signals by CXCL16. To investigate this hypothesis, HEK293 cells expressing human CXCR6 variants were analysed for the intracellular calcium influx in response to the chemokine domain of human CXCL16. After application of 10 nM CXCL16, HEK293 cells expressing both CXCR6-DRF and CXCR6-DRY showed an increase in Fluo-4-fluorescence, indicating an influx of free calcium into the cytoplasm. By contrast, HEK293 cells expressing the signalling-dead mutant CXCR6-DNF or control cells receiving empty vector did not show a calcium signal when exposed to CXCL16. The maximal activation of HEK293 cells expressing CXCR6-DRF or -DRY occurred rapidly

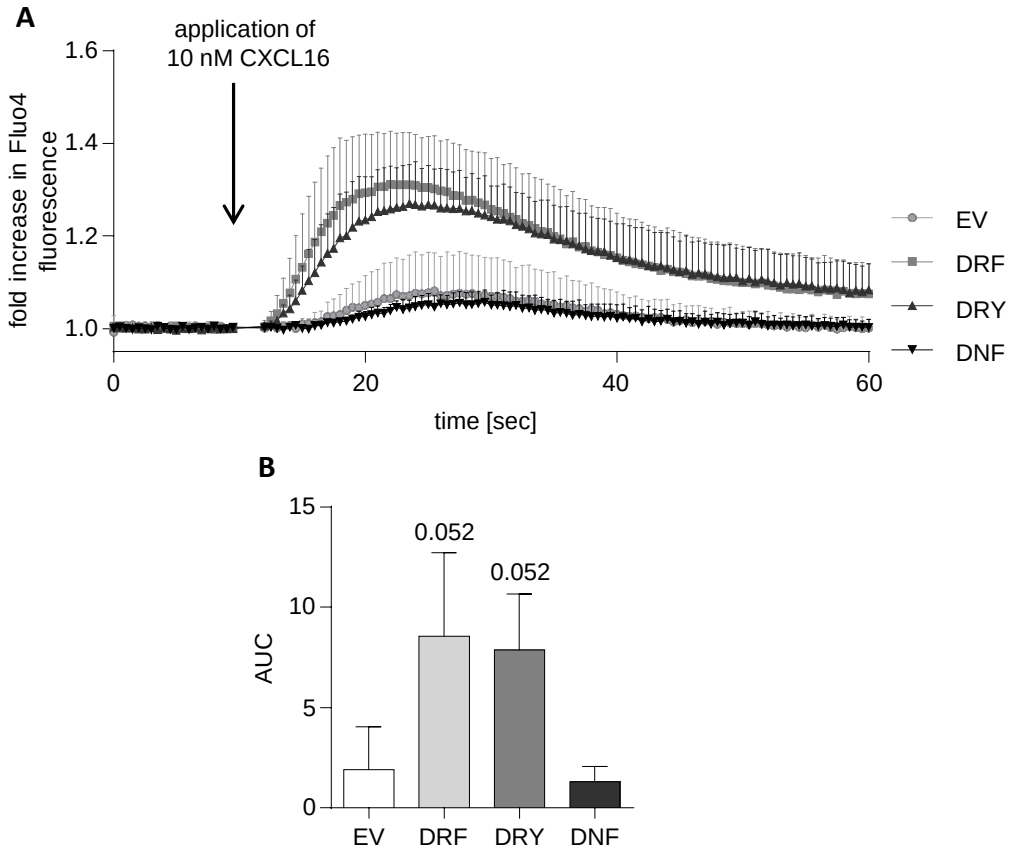

Figure 12 CXCL16-dependent calcium signalling in HEK293 cells expressing CXCR6 variants
HEK293 cells were transduced with lentivirus encoding human CXCR6 variants. Cells were loaded with Fluo-4-AM and stimulated with 10 nM CXCL16. A) Increase of the Ca^{2+} signal measured as increase in Fluo-4-AM-fluorescence over time (8 sec prior to and 51 sec after application of CXCL16) dependent on receptor variant expression. To simplify comparison of signalling curves, data were normalised to signals at 9 sec and expressed as means + SD of three independent experiments. B) AUC + SD of signalling curves shown in A. Statistic was performed by Student's t-test and corrected for multiple comparison by FDR (n=3). Statistical differences comparing differences from EV cells are indicated.

after 15-20 s. The calcium level declined approximately 15 s after CXCL16 stimulation and after 60 s a slight elevation was detectable in comparison to DNF or EV expressing cells.

To determine the best stimulus concentration for investigation of this process, HEK293 cells were stimulated with different concentrations of soluble human CXCL16 ranging from 1.5 to 15 nM. 1.5 nM CXCL16 did not lead to a detectable calcium influx. At 2 nM CXCL16 an increase of Fluo-4-fluorescence was visible but did not reach significance due to high variance. 10 nM CXCL16 induced a significant calcium signal in HEK293 cells expressing CXCR6-DRF and DRY mutant, which was absent in HEK293 cells expressing CXCR6-DNF mutant or EV (Figure 13, for comparison see Figure 12). Treatment with 15 nM CXCL16 induced a significant calcium influx in HEK293 cells expressing CXCR6-DRF or -DRY. Again, there was no

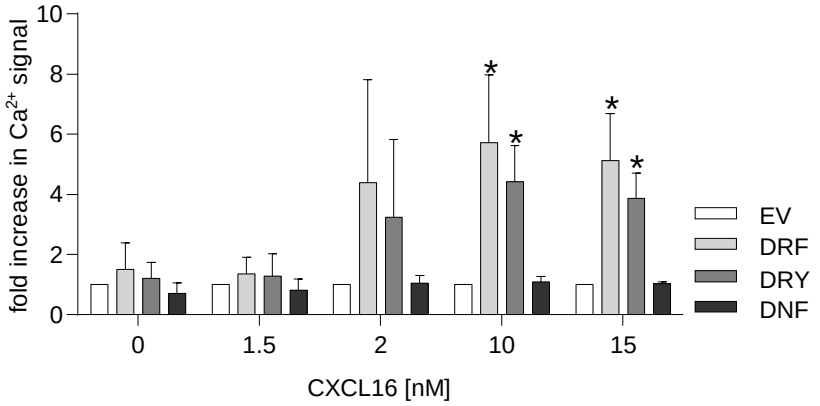

Figure 13 Concentration dependency of calcium signalling in HEK293 cells expressing CXCR6 variants

HEK293 cells were transduced with lentivirus encoding murine CXCR6 variants. Cells were loaded with Fluo-4-AM and stimulated with increasing concentrations of human CXCL16. For each calcium response the maximal fluorescence intensity was determined and minimal fluorescence intensity was subtracted. Data were expressed in relation to the response of HEK293-EV cells for each stimulation and represent mean + SD (n=3). Statistical analysis was performed with box-cox-transformed raw data using Student's t-test and corrected for multiple comparison by FDR. Asterisks indicate significant differences from the equivalent 0 nM CXCL16 control (*$p<0.05$).

significant difference between activation levels of CXCR6-DRF and -DRY. HEK293 cells expressing CXCR6-DNF or receiving EV control did not respond to any concentration of CXCL16. In summary, calcium signalling is clearly affected by compete disruption of the DRF motif via its mutation into DNF, but not by its mutation into DRY. The limitation of results described above is that they were obtained in HEK293 cells, which are kidney cells that grow as adherent cells and do not express endogenous CXCR6. Further, they show no relevant migratory potential *in vivo*. Thus, these cells are not an adequate model system for the investigation of CXCR6-mediated cell migration under homeostatic and inflammatory conditions.

4.1.2 CXCR6 in monocytic cells

CXCR6 is highly expressed on human leukocytes, especially T-lymphocytes. These cells respond to CXCL16 by increased migration[22,45,76]. As indicated by recent reports CXCR6 knock-out also affects the migratory response of monocytes[61]. To test and compare T cells and monocytes for CXCL16-induced migration, freshly isolated peripheral blood mononuclear cells (PBMC) were investigated for their chemotactic response to 3 nM CXCL16. In parallel 3 nM MCP-1 was used as a positive control, since MCP-1 was previously shown to induce chemotactic migration of these cells[35,84]. Migrated cells were differentiated by flow cytometry before and after migration using forward and side scatter (Figure 14). CXCL16 induced a chemotactic response in PBMCs, which was comparable to the response of monocytes to MCP-1 as control stimulus. Flow

cytometric analysis of migrated cells revealed that both lymphocytes and monocytes migrated to CXCL16. This experiment indicated a physiological relevance of CXCR6 not only for chemotaxis of T-lymphocytes as described previously, but also for monocytes.

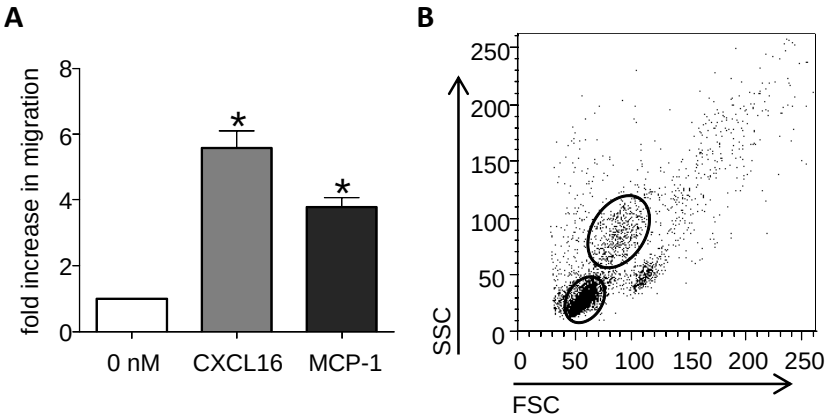

Figure 14 Migration of PBMCs in response to CXCL16 and MCP-1
A) PBMCs were isolated of human blood and migration was tested performing transwell assays in response to either 3 nM CXCL16 or 3 nM MCP-1. Data are shown as mean + SD. B) PBMCs were analysed concerning size and granularity (using SSC/FSC) by performing flow cytometry analysis before and after migration. Circles indicate populations of lymphocytes (bottom) and granulocytes identified via morphology. Statistical analysis was performed with raw data using Student's t-test and were corrected for multiple comparison by FDR (n=3). Asterisks indicate significant differences from the 0 nM control (*$p<0.05$). This assay was performed by D. Dreymueller.

.

4.1.2.1 **Analysis of CXCR6 variants in a monocytic cell line**

THP-1 cells are a well-known cell model for human monocytic cells. These cells migrate in response to chemokines like MCP-1 and they can be transduced to overexpress certain proteins like CXCR6 receptor variants. Therefore, THP-1 cells were used for further analysis of the physiological relevance of the CXCR6-DRF motif.

4.1.2.2 **Expression and ligand binding of human CXCR6 variants by THP-1 cells**

Expression and ligand-receptor interaction patterns may differ between cell types. Therefore, the expression of the CXCR6 variants after lentiviral transduction as well as the principle interaction with the ligand were again investigated in THP-1 cells to validate this model. The mRNA expression level for each receptor variant was analysed by RT-qPCR analysis. As shown in Figure 15, endogenous expression of human CXCR6 mRNA in THP-1-EV cells was very low. By contrast, there was a strong expression of receptor mRNA in THP-1 cells after transduction with the receptor variants. Importantly, no differences in the expression level were detected

between the CXCR6 variants. Thus, THP-1 cells can be regarded as a suitable expression system for functional analysis of CXCR6 variants.

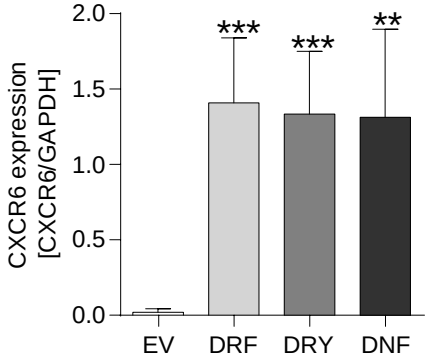

Figure 15 Expression of CXCR6 variant mRNA in THP-1 cells
THP-1 cells were transduced with lentivirus encoding human CXCR6 variants (wild type (DRF), F128Y (DRY), R127N (DNF)) or with empty vector control (EV). Three weeks after lentiviral transduction of THP-1 cells with pLVX-IRES-Neo overexpression vectors and G418 selection, mRNA expression was quantified by RT-qPCR and normalised to expression of GAPDH. Statistical analysis was performed by one tailed Student's t-test and corrected for multiple comparison by FDR, comparing expression of variants to expression in THP-1-EV cells (n=3; **p<0.01, ***p<0.001).

Next, THP-1 cells expressing the different CXCR6 variants were investigated for ligand binding using the CXCL16-Fc fusion protein. As shown by flow cytometry analysis (Figure 16A), THP-1-EV and THP-1 cells expressing CXCR6-DNF cells did not bind CXCL16-Fc, whereas THP-1 cells expressing CXCR6-DRF or -DRY were able to bind CXCL16-Fc. Simultaneous treatment with an excess of soluble CXCL16 (100 nM) blocked the binding of CXCL16-Fc. Thus, CXCL16 was competing with CXCL16-Fc for binding of CXCR6 demonstrating the specificity of CXCR6-CXCL16 interaction. Interestingly, ligand binding was only observed at 37 °C and was clearly inhibited at 4 °C. The temperature affects the signalling ability of enzymatic reactions, which is minimised at 4 °C. This indicated that CXCL16-Fc binding by THP-1 cells might require temperature sensitive CXCL16-induced intracellular processes. This is in line with the observation that THP-1 cells expressing the signalling-dead mutant CXCR6-DNF did not bind CXCL16-Fc. Together, these findings suggest that binding of CXCL16 to CXCR6 on THP-1 cells depends on activation of the G protein. Of note, the corresponding experiments with HEK293 cells had demonstrated that CXCR6-mediated binding of CXCL16 on these cells does not require G protein activation. These observations led to the hypothesis that ligand binding to CXCR6 can involve distinct mechanisms in HEK293 and THP-1 cells.

4.1.2.3 **Influence of CXCR6 expression on basal cell functions**

The expression of CXCR6 variants in THP-1 cells could have general effects on basal cell

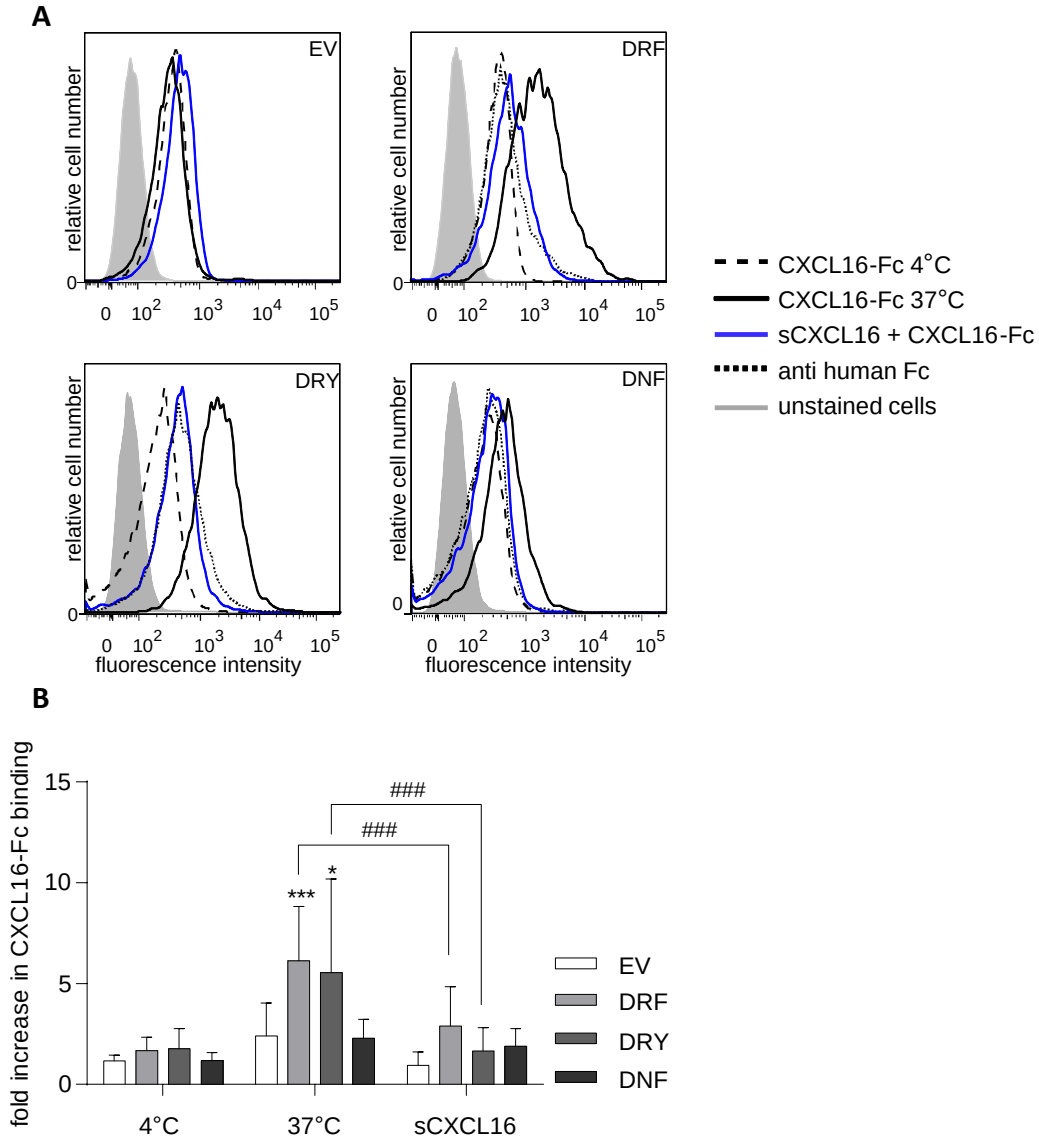

Figure 16 CXCL16 binding by THP-1 cells expressing CXCR6 variants
THP-1 cells were transduced with lentivirus encoding human CXCR6 variants. Ligand binding ability of receptor mutants was analysed via incubation with CXCL16-Fc fusion protein and following antibody staining against human-Fc fragments. Cells were either incubated at 4 °C or 37 °C to investigate temperature and active signalling dependency. Treatment with 100 nM soluble CXCL16 (sCXCL16) simultaneous to application of CXCL16-Fc fusion protein served as specificity control. A) Representative histograms of flow cytometry analysis showing the distribution of fluorescence signals. B) CXCL16-Fc binding was measured as geomean of fluorescence signal. Signals were expressed in relation to binding of anti human-Fc and data are shown as mean + SD (n=5-7). Statistical analysis was performed by one tailed Student's t-test and corrected for multiple comparison by FDR. Asterisks indicate differences to THP-1-EV cells (*p<0.05, ***p<0.001) and hashes indicate differences in comparison to simultaneous sCXCL16 treatment (###p<0.001).

functions. This would influence the analysis of chemokine receptor specific responses, including adhesion, calcium signalling and migration. To exclude such potential influence, transduced THP-1 cells were investigated for cell proliferation, cell survival, integrin expression and cytoskeletal rearrangement.

First, proliferation and viability of THP-1 cells expressing the different CXCR6 variants were tested. Cell density showed an approx. 4-fold increase in THP-1 cells after 72 h of incubation (Figure 17A), which was neither changed by overexpression of CXCR6 nor by mutation of the DRF motif. Further, neither CXCL16 application nor CXCL16 neutralisation by anti-human CXCL16 antibody treatment showed any effect on cell proliferation. Next, viability of THP-1 cells expressing the different CXCR6 receptor variants was analysed. Percentage of apoptotic cells was quantified via Annexin V and 7-AAD staining and apoptosis was provoked by presence of 100 mU/ml bleomycin for 24 h, as shown exemplary in density plots of flow cytometry analysis (Figure 17B and C). 3.4% of untreated cells were positively stained for Annexin V, which indicates early apoptotic processes in a small amount of cells. Furthermore, 13.3% of untreated cells were double positive for Annexin V and the viability dye 7-AAD, which indicates late stage apoptosis. When cells were treated with 100 mU/ml bleomycin, the percentage of early and late stage apoptotic cells increased (22.2% and 20.5% respectively, Figure 17D). However, neither CXCR6 expression nor DRF mutation affected cell survival. This was also confirmed by the finding that depletion of soluble CXCL16 by application of anti-human CXCL16 antibody had no effect on apoptosis (Figure 17D).

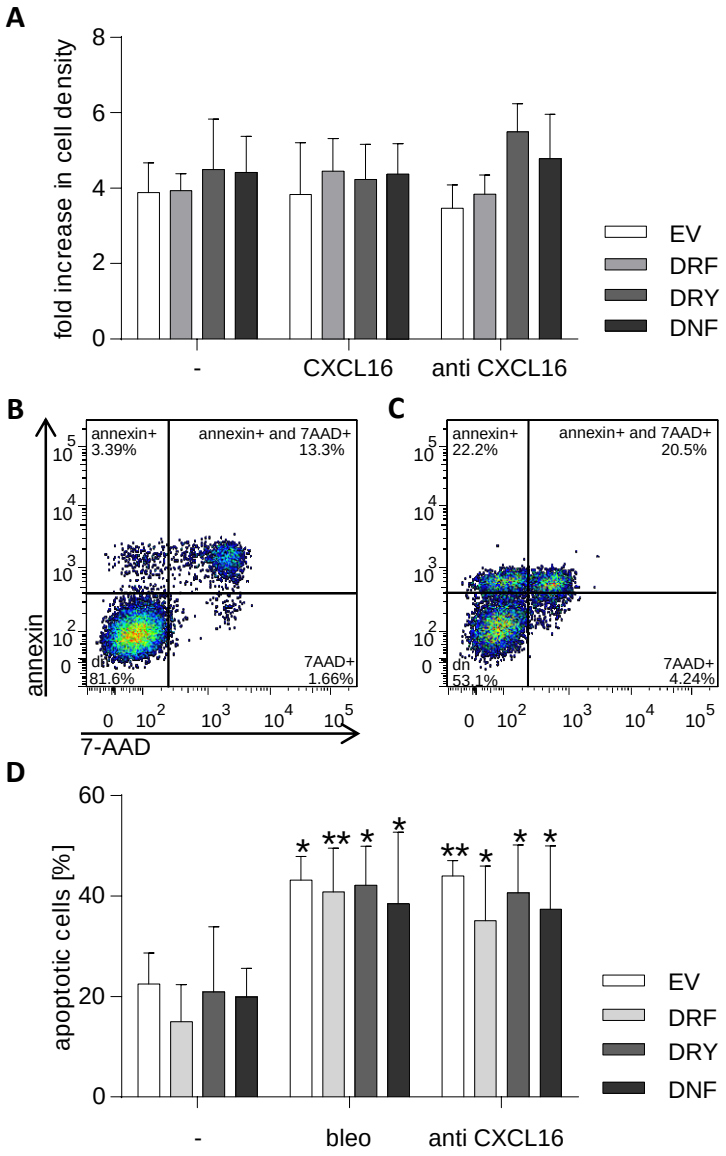

Figure 17 Proliferation and survival of THP-1 cells expressing CXCR6 variants
THP-1 cells were transduced with lentivirus encoding human CXCR6 variants A) Proliferation was determined using the IncuCyte Zoom microscope. Measurement was performed for 72 h in the presence or absence of either 10 nM CXCL16 or 50 ng/ml anti-human CXCL16 antibodies. Data are shown as fold increase after 72 h of proliferation, measured by cell density. B – C) Representative density plots of annexin V and 7-AAD staining to identify apoptotic cells. THP-1-EV cells were either left untreated (B) or treated with 100 mU/ml bleomycin (bleo, C) for 24 h. D) CXCR6 variants expressing THP-1 cells were treated with 100 mU/ml bleomycin or with 100 mU/ml bleomycin plus 50 ng/ml anti-human CXCL16 antibody (indicated as "anti CXCL16") for 24 h. Apoptosis was analysed by Annexin V and 7-AAD staining and flow cytometry. Apoptotic cells were defined as cells positive for Annexin V plus cells positive for Annexin V and 7-AAD and are expressed as % of all cells + SD (n=3-5). A and D: Statistical analysis was performed by two way ANOVA (treatment: $p<0.001$ and genotype= not significant, interaction: not significant) with Bonferroni post-test. Asterisks indicate significant differences to untreated cells (*$p<0.05$, **$p<0.01$).

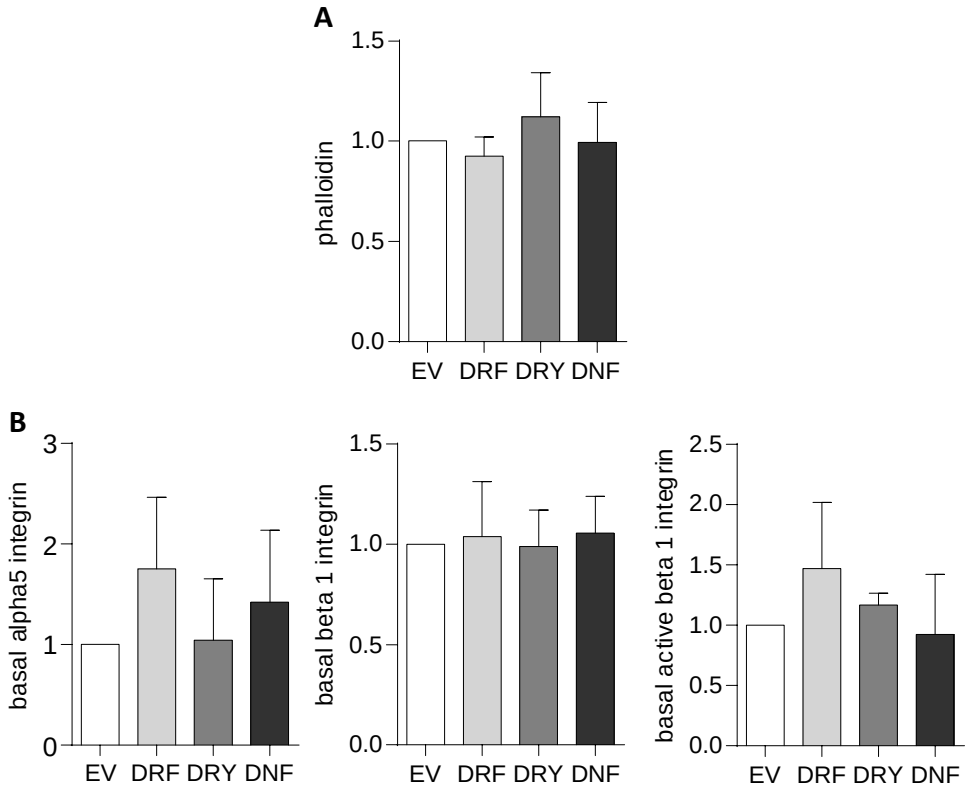

Figure 18 F-actin and integrin analysis of THP-1 cells expressing CXCR6 variants
THP-1 cells were transduced with lentivirus encoding human CXCR6 variants. **A)** THP-1 cells were stained with phalloidin Alexa488 to analyse intracellular F-actin amount dependent on CXCR6 receptor variant expression. Cells were stained and fluorescence signal was measured by flow cytometry. Phalloidin binding was measured as geomean of fluorescence signal. Signals were expressed in relation to THP-1-EV cells and data of three independent experiments are shown as mean + SD. **B)** Integrin surface expression was characterised by specific antibody staining, analysed by flow cytometry and measured as geomean of fluorescence signal. Signals were expressed in relation to THP-1-EV cells and data of three independent experiments are shown as mean + SD. A and B: Statistical analysis was performed by one sample t-tests (hypothetical value = 1). No significant differences were observed.

The migration of cells strongly depends on rearrangement of the cytoskeleton, which is linked to the regulation of integrins[101]. Cytoskeletal rearrangement was analysed by quantification of the polymerisation of filamentous actin (F-actin) via flow cytometry analysis using fluorescently labelled phalloidin. CXCR6 overexpression in THP-1 cells did not change basal F-actin polymerisation in comparison to THP-1-EV. In addition, no influence of CXCR6 mutation was observed (Figure 18A). Furthermore, no basal differences concerning the surface expression pattern of alpha5 integrin, beta1 integrin or activated beta1 integrin were detected (Figure 18B). Therefore, neither overexpression of CXCR6-WT in THP-1 cells nor mutation of the endogenous DRF motif of CXCR6 did have an impact on basal cell functions like proliferation, apoptosis, basal F-actin polymerisation or integrin expression.

4.1.2.4 **Involvement of CXCR6 in Akt activation**

Adhesion and migration processes involve a huge variety of signalling processes, including the phosphorylation of the kinases p38, ERK1/2 and Akt. A previous study showed that the CXCR6/CXCL16 axis activates the Akt/mTOR pathway[53]. With respect to functional consequences, Akt phosphorylation in THP-1 cells after stimulation with CXCL16 was measured dependent on mutations of the endogenous DRF motif of CXCR6. All tested THP-1 cell lines showed increased amounts of phosphorylated Akt in response to MCP-1 stimulation when compared to buffer control (Figure 19A and B). In THP-1 cells expressing CXCR6 wild type and DRY mutant, stimulation with 10 nM CXCL16 for 1, 5 and 10 min increased phosphorylation of Akt to a similar extent (Figure 19A and C), whereas this response was absent in THP-1-EV and THP-1 cells expressing the signalling-dead DNF mutant. Thus, CXCR6-DRF and -DRY induced rapid phosphorylation of Akt whereas the signalling-dead DNF-mutant was not able to induce Akt activation.

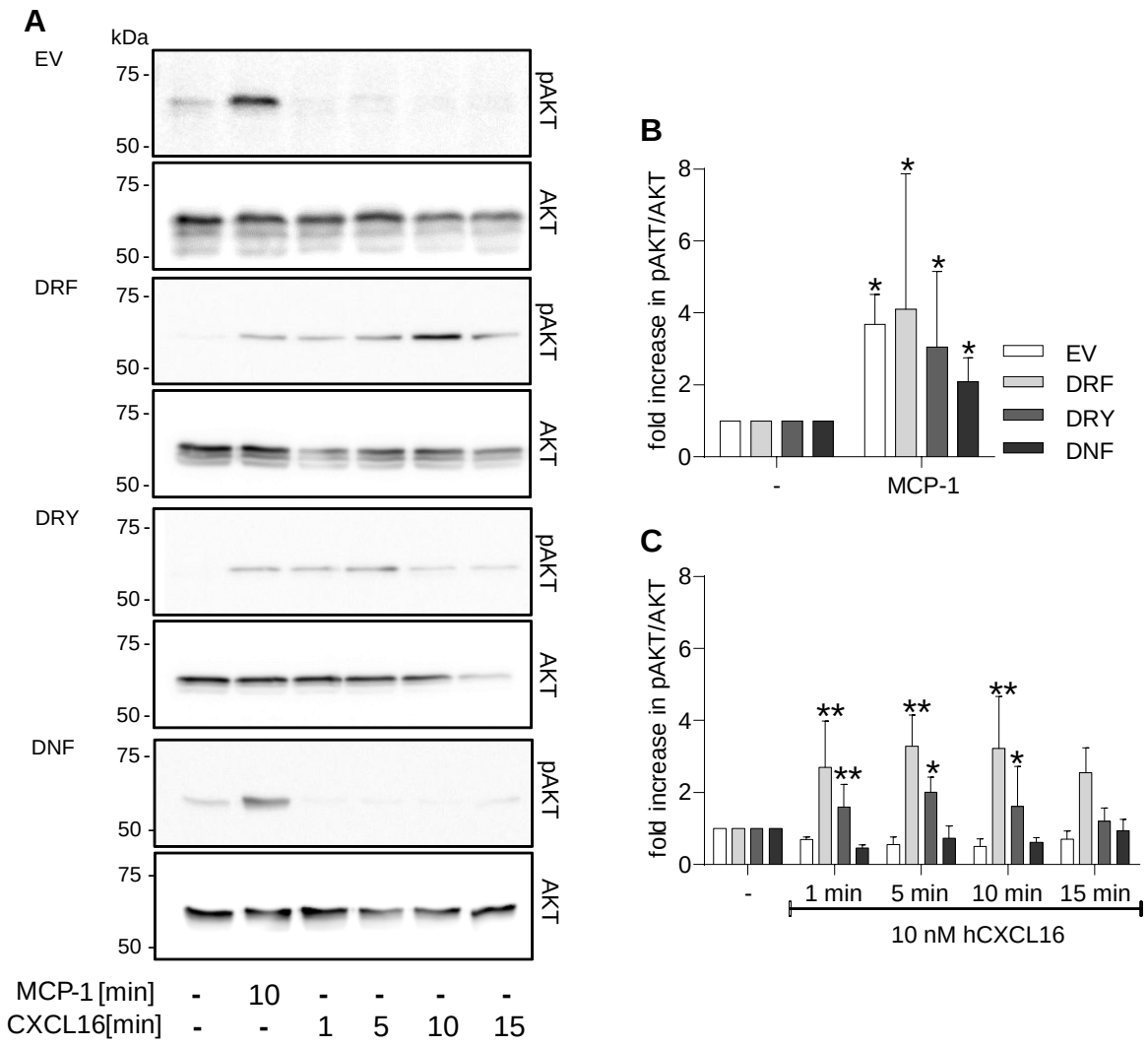

Figure 19 Phosphorylation of Akt in THP-1 cells expressing CXCR6 variants
THP-1 cells were transduced with lentivirus encoding human CXCR6 variants. For phosphorylation analysis, cells were stimulated with 10 nM CXCL16 for the indicated period of time. As positive control, cells were stimulated with 3 nM MCP-1 for 10 min and as a negative control cells were stimulated with buffer alone. Western blots were stained for phosphorylated Akt first (upper panel). Afterwards, antibodies were stripped and membranes were reprobed with antibodies against total Akt (lower panel). A) Representative Western blots of three independent experiments. B and C) Signals in A were quantified by densitometry. For better visability, MCP control stimulation and CXCL16 stimulation were plotted in different graphs. The signal of phosphorylated Akt was normalised to that of total Akt and then expressed in relation to unstimulated cells. Data represent mean + SD (n=3). For statistical analysis pAkt/Akt ratios (not normalised to unstimulated control) were used and subjected to Student's t-test and corrected for multiple comparison by FDR. Asterisks indicate significant differences from untreated cells (*p<0.05, **p<0.01).

4.1.2.5 **CXCR6-mediated adhesion of THP-1 cells to immobilised CXCL16**

The previous experiments revealed that CXCR6 expression did not change basal cell functions of THP-1 cells. CXCR6 was reported to play a role in cell recruitment to sites of inflammation[45,62], which includes adhesive and migratory processes. It was already shown for HEK293 cells that CXCR6 is capable of mediating adhesion to its endogenous ligand CXCL16 (see section 4.1.1.3). Next, THP-1 cells expressing CXCR6 variants were investigated for adhesion to immobilised CXCL16-Fc. For such an experiment it has to be taken into account that monocytic cells express different Fc-receptors, which could interact with the anti-human-Fc antibody that was used for the immobilisation of CXCL16-Fc. Therefore, the basal adhesion of THP-1 cells to anti-human-Fc was determined. Adhesion to anti-human-Fc was 1.5% to 2% of the total number of loaded cells. This represents a low level of basal adhesion, which was not changed by CXCR6 overexpression (Figure 20A). In the next step adhesion to immobilised CXCL16-Fc fusion protein was analysed (Figure 20B). EV-expression did not show altered adhesion of THP-1 cells to immobilised CXCL16 compared to adhesion to anti-human-Fc. By contrast, CXCR6-DRF and DRY expressing cells showed an approx. 3.5-fold increase in adhesion to immobilised CXCL16-Fc. This adhesion could be inhibited by preincubation of THP-1 cells with 20 nM soluble CXCL16, which could either block the access of CXCR6 to immobilised CXCL16-Fc due to internalisation of the receptor or due to competitive effects. This finding indicated specific CXCR6-CXCL16 interaction resulting in adhesion. Importantly, THP-1 cells expressing human CXCR6-DNF mutant did not adhere to immobilised CXCL16-Fc. This was in contrast to the observation with HEK293 cells, since HEK293 cells expressing CXCR6-DNF showed significant adhesion and binding to immobilised CXCL16-Fc and to soluble CXCL16-Fc. As mentioned in 4.1.1.3, the murine receptor variants were used in the adhesion assays with HEK293 cells. To exclude species specific effects, the adhesion assays were repeated with THP-1 cells expressing murine CXCR6 receptor variants (Figure 20C). Again, adhesion to murine CXCL16-Fc was increased by expression of CXCR6-DRF and -DRY (1.7 and 2.0-fold), but not by expression of CXCR6-DNF or EV. As reported above for the ligand binding experiments, also adhesion of CXCR6 to immobilised CXCL16-Fc seems to involve different mechanisms in HEK293 and THP-1 cells.

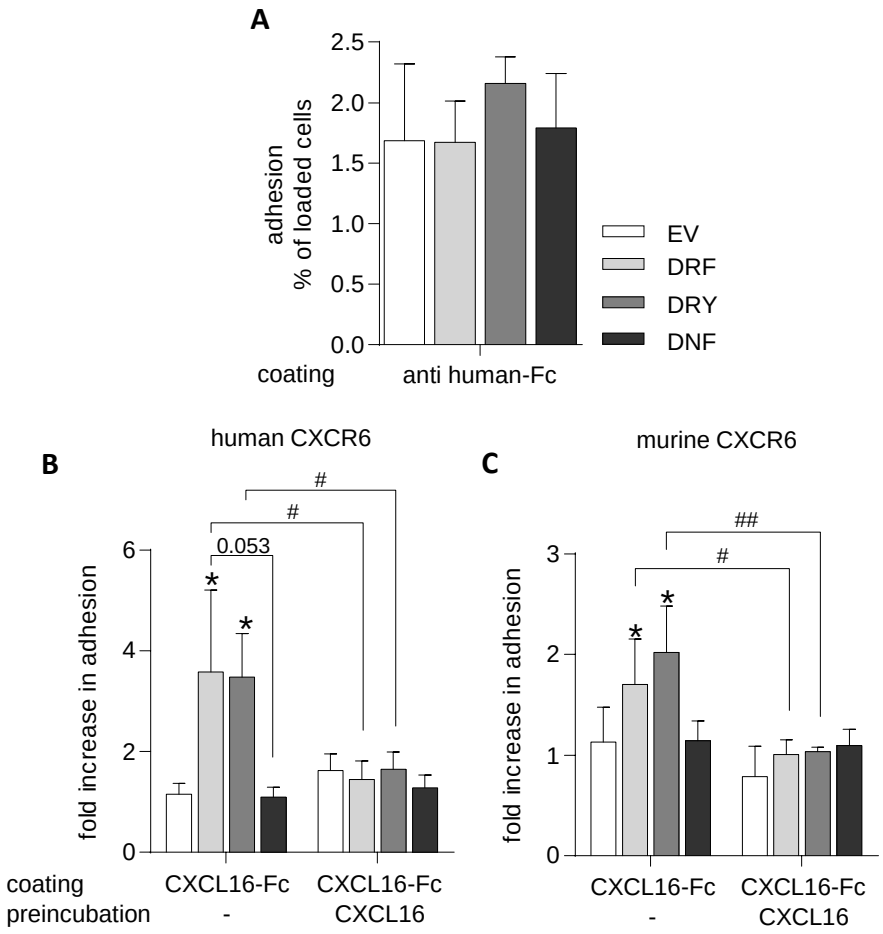

Figure 20 Adhesion dependent on CXCR6 DRF variants
THP-1 cells were transduced with lentivirus encoding human (A/B) or murine (C) CXCR6 variants. **A)** Adhesion of THP-1 cells to anti-human-Fc. Data show per cent of remaining cells after three washing steps and are expressed as mean +SD (n=4). B-C) Adhesion of THP-1 cells expressing human (B) or murine (C) CXCR6 mutants to immobilised human (B)/murine (C) CXCL16-Fc. Data are expressed as mean + SD of data normalised to cells adhering to anti-human-Fc (n(hCXCR6)=4, n(mCXCR6)=3). Statistic to compare adhesion to CXCL16-Fc and anti-human-Fc was performed by one sample t-test (hypothetical value = 1) and is indicated by asterisks (*$p<0.05$). To compare adhesion to CXCL16 and adhesion to CXCL16 after preincubation, Student's t-test with Welch's correction was used and results are indicated by hashes (#$p<0.05$, ##$p<0.01$). All p-values were corrected for multiple comparison by FDR.

It might be that adhesion of THP-1 cells expressing CXCR6 to immobilised CXCL16 is more dependent on interaction of CXCR6 with the $G\alpha_i$ protein. To test this hypothesis, THP-1 cells expressing human CXCR6 variants were treated with PTX prior to adhesion to immobilised CXCL16-Fc. Indeed, CXCR6-mediated adhesion was decreased to background levels by PTX pretreatment of THP-1 cells (Figure 21A). One explanation for reduced adhesion could be enhanced apoptosis by PTX treatment. However, PTX did not change the cell survival of THP-1 cells (Figure 21B), supporting the hypothesis of $G\alpha_i$ protein involvement in CXCR6-CXCL16 interaction in THP-1 cells.

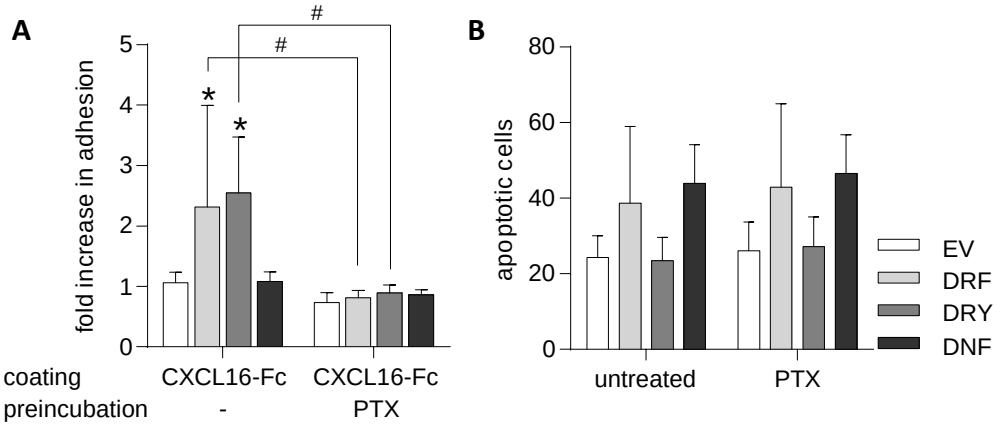

Figure 21 Involvement of Gα_i-mediated signalling in adhesion of THP-1 cells expressing CXCR6 variants

THP-1 cells were transduced with lentivirus encoding human CXCR6 variants. A) Adhesion to immobilised CXCL16-Fc fusion protein was analysed with THP-1 cells without and with pretreatment with 50 ng/ml PTX for 4 h. Data are expressed as mean + SD of data normalised to cells adhering to anti-human-Fc (n=5-8). B) Cells were treated with 50 ng/ml PTX or left untreated for 4 h. Apoptosis was quantified by annexin V and 7-AAD staining via flow cytometry analysis. Apoptotic cells were defined as cells positive for annexin V together with cells positive for annexin V and 7-AAD and are expressed as percentage of all cells + SD (n=3). Statistic to compare adhesion to CXCL16-Fc and to anti-human-Fc was performed by one sample t-test and is indicated by asterisks (hypothetical value: 1). To compare adhesion to CXCL16 and adhesion after PTX treatment, Student's t-test with Welch's correction and FDR was used and results are indicated by hashes (# $p<0.05$, ##$p<0.01$). Statistical analysis of B was performed by Student's t-test with Welch's correction. No statistical differences were observed in B.

4.1.2.6 Calcium signalling and chemotactic migration of THP-1 cells expressing CXCR6 variants

The involvement of the DRF motif in calcium signalling has been shown for HEK293 cells expressing CXCR6 receptor variants in section 0. In HEK293 cells, the DRF and DRY variants mediated calcium influx in response to CXCL16 stimulation, whereas the DNF mutant did not. Since THP-1 cells and HEK293 cells showed differences in CXCR6-DNF-mediated cell adhesion to CXCL16-Fc, the calcium response was again investigated in THP-1 cells expressing the different CXCR6 variants. CXCL16 exposure of THP-1-EV and THP-1-DRF cells induced a transient increase in the calcium signal, which peeked 10 to 12 s after CXCL16 application and strongly decreased after 50 s. This response of THP-1 cells was similar to that observed for HEK293 cells (Figure 22A, compare Figure 12). Again, the CXCR6-DNF mutant did not show calcium influx after CXCL16 application. THP-1 cells expressing DRF or DRY variants clearly showed different signalling levels. The maximal fluorescence signal in THP-1 cells induced by

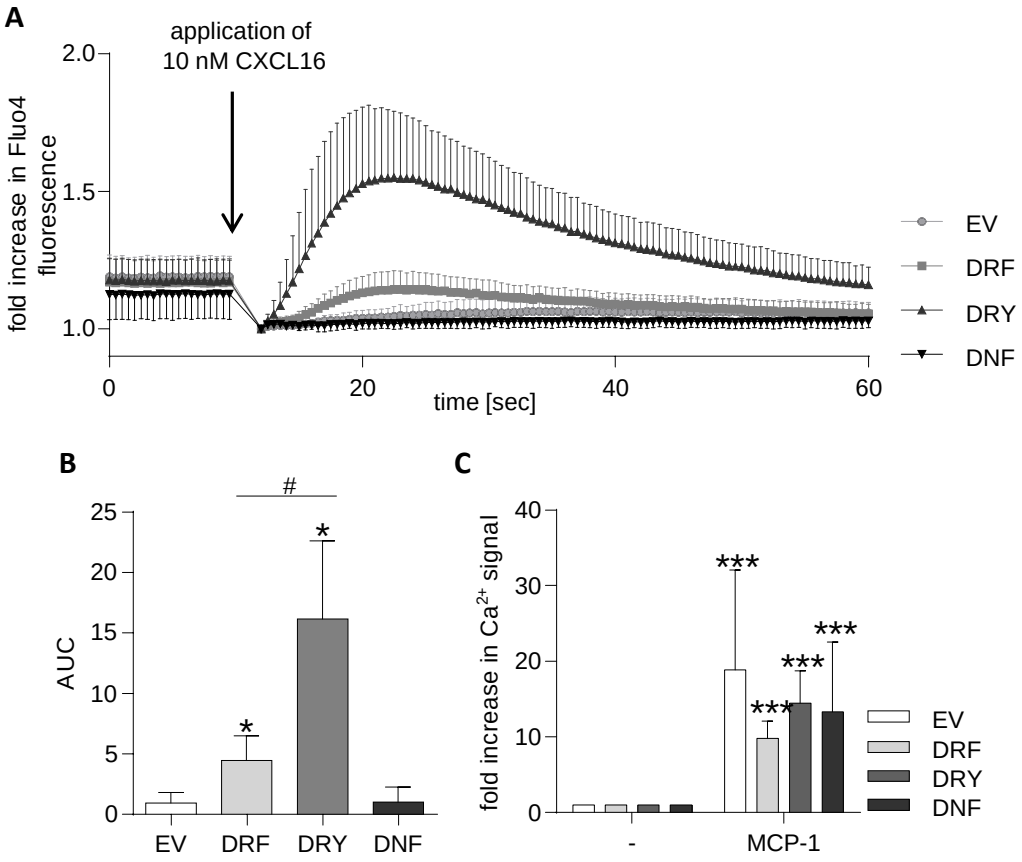

Figure 22 Intracellular calcium signalling in THP-1 cells expressing CXCR6 variants
THP-1 cells were transduced with lentivirus encoding human CXCR6 variants. A) Fluo-4-AM loaded THP-1 cells were stimulated with 10 nM CXCL16 and data represent fluorescence signalling in dependence on receptor expression and time (8 sec prior to and 51 sec after application of CXCL16). To simplify comparison of signalling curves, data are normalised to signals at 9 sec and expressed as means ± SD. B) AUC of signalling curves shown in A. Statistic was performed by Student's t-test and corrected for multiple comparison by FDR. Asterisks indicate differences from response of EV transduced THP-1 cells (*$p<0.05$) and hashes indicate differences between cell mutants (#$p<0.05$). C) THP-1 cells were stimulated with 3 nM MCP-1. Data were expressed in relation to buffer control and represent mean + SD (n=3). Raw data were box-cox-transformed and statistical analysis was performed by Student's t-test and corrected for multiple comparison by FDR. Asterisks indicate significant differences from each buffer control (***$p<0.001$).

CXCR6-DRY was about 3-fold higher than that induced by CXCR6-DRF (Figure 22B). By contrast, the MCP-1-induced calcium response was not different (Figure 22C), indicating that there was no general difference in responsiveness between the cell lines. Thus, the effect was due to the different functionality of CXCR6-DRF and -DRY in THP-1 cells.

To further evaluate this difference, THP-1-EV and THP-1 cells carrying the different receptor variants were stimulated with increasing concentrations of CXCL16 (Figure 23A). Even low concentrations of CXCL16 (1 nM and 2 nM) resulted in calcium influx in THP-1 cells expressing CXCR6-DRF and -DRY variants, which further increased with higher CXCL16 concentrations.

Interestingly, the level of the calcium response induced by CXCR6-DRY was approx. 3-fold higher than that induced by CXCR6 DRF. Thus, there seemed to be an influence of the mutation from DRF to DRY in CXCR6 on intracellular calcium signalling in THP-1 cells. Interestingly, this difference was not seen in HEK293 cells as described above.

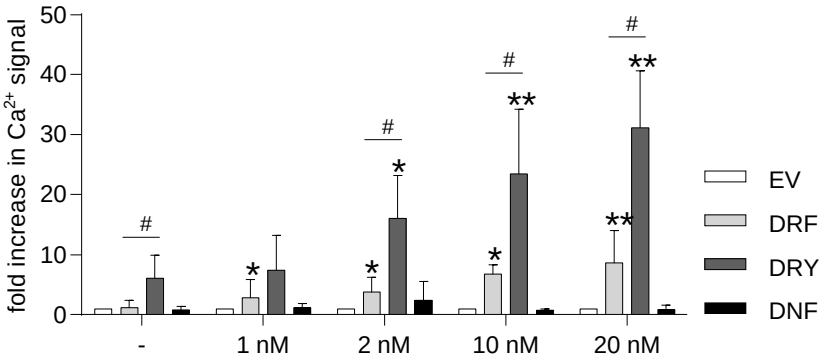

Figure 23 CXCL16 concentration dependency of calcium signalling
THP-1 cells were transduced with lentivirus encoding human CXCR6 variants. Cells were stimulated with increasing concentrations (0 to 20 nM) of human CXCL16. For each calcium response the maximal fluorescence intensity was determined and baseline fluorescence intensity was subtracted (mean of signals in the period between 50 and 60 sec). Data were expressed in relation to the response of THP-1-EV cells for each stimulation and represent mean + SD (n=4). Asterisks indicate significant differences from each buffer control (*p<0.05, **p<0.01) and hashes indicate differences between DRF and DRY variants (#p<0.05). Raw data were box-cox-transformed and statistical analysis was performed by Student's t-test and corrected for multiple comparison by FDR.

Intracellular calcium flux represents a critical signalling event in cell migration. Therefore, chemotactic migration of THP-1 cells expressing receptor variants in response to increasing concentrations of CXCL16 was tested in a *Boyden chamber* assay. In this setup about 7 – 8% of loaded THP-1 cells migrated in the lower compartment of the chamber in the absence of a chemotactic stimulus. This random migration did not differ between the different receptor variants (Figure 24A). Further, all THP-1 cells showed significant chemotactic migration in response to 3 nM MCP-1, which served as a positive control in every assay (Figure 24B). Thus, there was no general difference in cell migration between the differently transduced cells. As expected, control cells treated with EV did not show a chemotactic response when stimulated with CXCL16. Interestingly, those cells expressing CXCR6-DRF showed only weak chemotaxis, which was only significant at 1 nM CXCL16 and absent at other concentrations. In contrast, CXCR6-DRY expressing cells clearly showed a typical Gauss distribution of the chemotactic response to CXCL16 peaking at 3 nM CXCL16. Moreover, there was no detectable migration of

THP-1-EV and THP-1 cells expressing signalling-dead CXCR6-DNF in response to CXCL16. As reported above, very similar observations were made for the calcium response in THP-1 cells which is more efficiently induced in CXCR6-DRY cells than in CXCR6-DRF cells. Therefore, mutating the endogenous CXCR6 from DRF into DRY seemed to increase both calcium signalling downstream of the intracellular G protein as well as cell migration

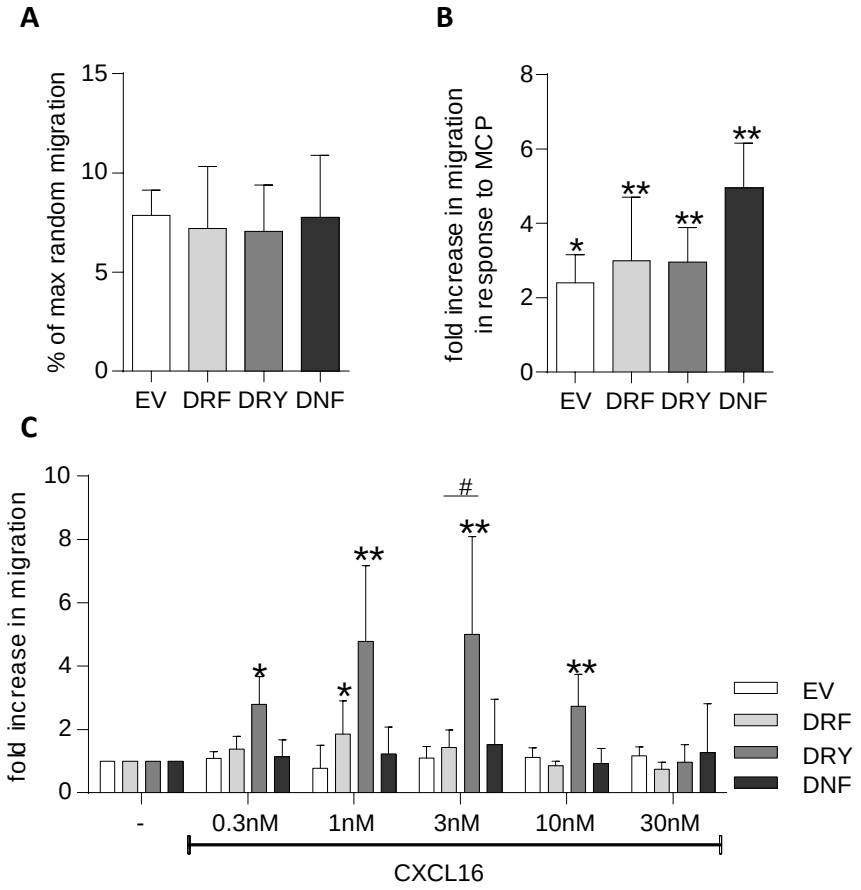

Figure 24 Chemotactic migration of THP-1 cells expressing CXCR6 variants
THP-1 cells were transduced with lentivirus encoding human CXCR6 variants. A) Chemotactic migration of THP-1 cells expressing the different CXCR6 receptor variants were tested in a Boyden chamber. Random migration of cells into the lower compartment was assessed in the absence of chemotactic stimulus after 2 h and expressed as percentage of cells added to the upper compartment. B) Chemotaxis in response to 3 nM MCP-1 served as positive control in every Boyden chamber assay. C) Cell migration against increasing concentrations of CXCL16 was quantified as number of migrated cells in the presence of chemotactic stimulus in relation to the number determined in the absence of a chemokine. Data are expressed as mean + SD (n=5-6). Statistical analysis was performed with raw data using Student's t-test following correction of multiple comparison by FDR. Asterisks indicate significant differences from migration of unstimulated cells (*$p<0.05$, **$p<0.001$) and the hash indicates difference between DRF and DRY variants (#$p<0.05$).

4.1.3 Mutation of the endogenous DRY motif of CX_3CR1 into DRF

The finding reported above suggest that CXCR6 is only a weak chemoattractant for THP-1 cells which may be explained by the presence of the endogenous DRF motif. By contrast, other chemokine receptors such as CX_3CL1 carry an endogenous DRY motif and have been described as potent chemoattractants. The only known ligand for CX_3CR1 is CX_3CL1 (also called fractalkine), which is the only other transmembrane chemokine besides CXCL16. Transmembrane CX_3CL1 also induces firm adhesion to its receptor CX_3CR1[35], which is expressed on leukocytes. To investigate the importance of the DRY in CX_3CR1, this motif was mutated into DRF and DNF. As THP-1 cells endogenously express the human chemokine receptor CX_3CR1, the murine CX_3CR1 receptor was mutated and overexpressed in this study to minimize the influence of endogenous receptors on ligand binding, adhesion and migration. Murine CX_3CL1 was used as a ligand, which does not or only weakly bind human CX_3CR1.

4.1.3.1 Expression of CX_3CR1 variants and ligand binding

Overexpression of the different CX_3CR1 receptor variants (DRY, DRF and DNY) in THP-1 cells was achieved by lentiviral transduction as described for CXCR6 receptor variants. Overexpression of receptor mutants was detected by using the murine CX_3CL1-Fc fusion protein[51] via flow cytometry analysis. All cells transduced with murine CX_3CR1 overexpression vectors were able to bind murine CX_3CL1-Fc to a similar extent on their surface indicating that all CX_3CR1 variants were expressed at a similar level. By contrast, THP-1-EV cells showed low binding of murine CX_3CL1-Fc (Figure 25), indicating weak interaction with endogenous CX_3CR1. The CX_3CR1-DNY mutant was capable of binding its ligand, and incubation of THP-1 cells with the CX_3CL1-Fc fusion protein at 4 °C did not prevent binding. Further, incubation at 37 °C resulted in decreased surface staining with CX_3CL1-Fc and anti-Fc antibody, which may be due to internalisation processes of the ligand-receptor complex after binding. These results are in contrast to the results obtained with the CXCR6 variants which indicated that CXCL16 binding to its receptor on THP-1 cells is dependent on CXCR6 signalling. CXCL16 binding to CXCR6 on THP-1 cells was only observed after incubation at 37°C and was completely inhibited at 4°C (Figure 16).

The role of $G\alpha_i$-protein signalling mechanisms on adhesion of CX_3CR1 DRY cells to immobilised CX_3CL1-Fc was further analysed by PTX treatment. In parallel, THP-1 cells were treated with soluble CX_3CL1 to analyse the specificity. Again, adhesion to coated anti-human-Fc

without immobilised CX_3CL1 served as internal control. All cells showed a minimal adhesion to anti-human-Fc alone (THP-1 CX_3CR1-DRY: 5.6%, THP-1-EV: 4.4%). Overexpression of the CX_3CR1-DRY receptor enhanced adhesion to immobilised CX_3CL1 (39% of loaded THP-1-CX_3CR1-DRY cells) in comparison to THP-1-EV cells (8%) (Figure 25C). Preincubation of THP-1 cells with soluble CX_3CL1 clearly decreased the number of adherent CX_3CR1 cells. The adhesion of CX_3CR1 expressing THP-1 cells was not inhibited by PTX treatment. Thus, in contrast to CXCR6 which requires a functional G protein for ligand binding, the chemokine receptor CX_3CR1 does not require intracellular interaction with the G protein for stable interaction with its ligand CX_3CL1.

4.1.3.2 **Chemotactic migration of CX_3CR1 DRY and DRF variants**

Analysis of CXCR6 variants revealed that the mutation of CXCR6-DRF into CXCR6-DRY resulted in increased CXCL16-induced migration of THP-1 cells overexpressing this receptor variant. To further compare the different motifs in CXCR6 and CX_3CL1, CX_3CR1-DRY and -DRF cells were analysed for CX_3CL1-induced migration. It was already shown that murine CX_3CL1 did not bind to the endogenously expressed human CX_3CR1. However, there could be still a contribution to migratory processes. Therefore, the migration of THP-1-WT cells in response to human and murine CX_3CL1 was tested. No migration in response to murine CX_3CL1 was observed in wild type THP-1 cells, whereas significant migration was detectable in response to human CX_3CL1 (Figure 26A). Therefore, the overexpression of murine CX_3CR1 variants in THP-1 cells was a suitable model to analyse the influence of DRY mutation to DRF on migration induced by murine CX_3CL1. As shown in Figure 26B, THP-1 cells expressing murine CX_3CR1-DRY (wild type) showed chemotactic migration in response to 0.3, 1, 3 and 10 nM CX_3CL1. In contrast, cells expressing murine CX_3CR1 DRF mutant only showed weak but significant migration in response to 3 nM CX_3CL1. The comparison of DRY and DRF expressing CX_3CR1 variants showed a significant difference at 1 nM CX_3CL1. Thus, as observed for CXCR6 the mutation of the DRY motif into DRF results in a reduced migration in response to the chemokine ligand. These data suggest that the DRY motif in CX_3CR1 makes CX_3CL1 a strong chemoattractant of monocytic cells whereas the DRF motif in CXCR6 explains the weak chemotactic activity of CXCL16.

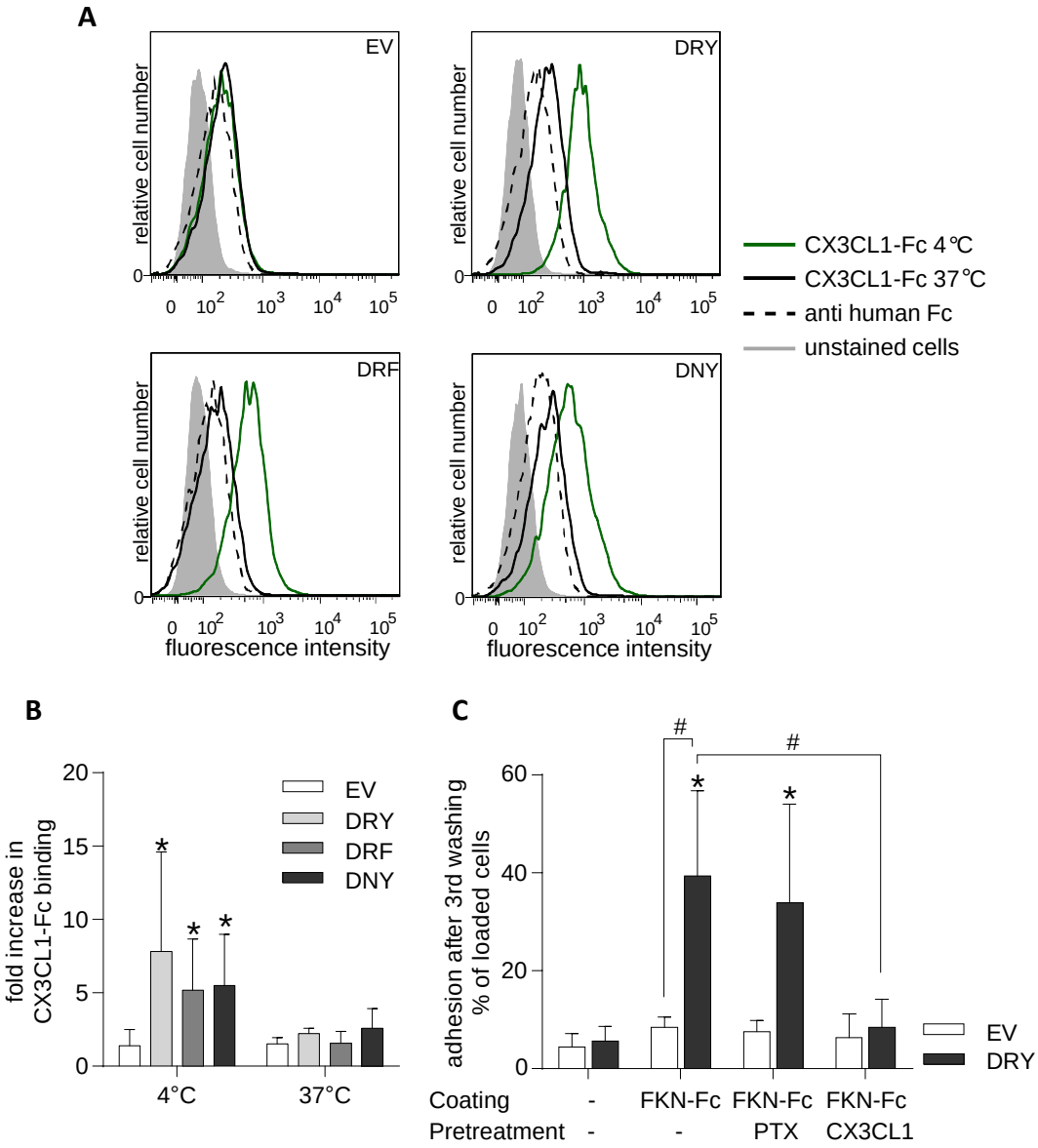

Figure 25 CX_3CL1 binding by THP-1 cells expressing CX_3CR1 variants
THP-1 cells were transduced with lentivirus encoding murine CX_3CR1 variants (wild type (DRY), Y129F (DRF), R128N (DNY)) or with empty vector control (EV). Ligand binding ability of receptor mutants was analysed via incubation with CX_3CL1-Fc fusion protein and following antibody stain against human-Fc fragment. Binding ability was tested at 4° and 37 C during incubation with CX_3CL1-Fc. A) Representative histograms B) CX_3CL1-Fc binding was measured as geomean of fluorescence signal. Signals were expressed in relation to binding of anti human-Fc and data are shown as mean + SD (n=5-7). Statistical analysis was performed by Student's t-test and FDR. Asterisks indicate differences to THP-1-EV cells (*p<0.05, ***p<0.001). C). Adhesion of CX_3CR1 expressing THP-1 cells to immobilised CX_3CL1-Fc (FKN-Fc). Cells were treated either with 50 ng/ml PTX for 4 h, or were preincubated with 10 nM soluble CX_3CL1 for 15 min (preinc) prior to adhesion to immobilised CX_3CL1-Fc (FKN-Fc). Data represent mean + SD of percentages of adherent cells in relation to loaded cells. Statistical analysis was performed by one tailed Student's t-test with Welch's correction and corrected for multiple comparison by FDR. Asterisks indicate differences to cells adhering to anti-human-Fc alone (*p<0.05) and hashes indicate differences between groups (#p<0.05).

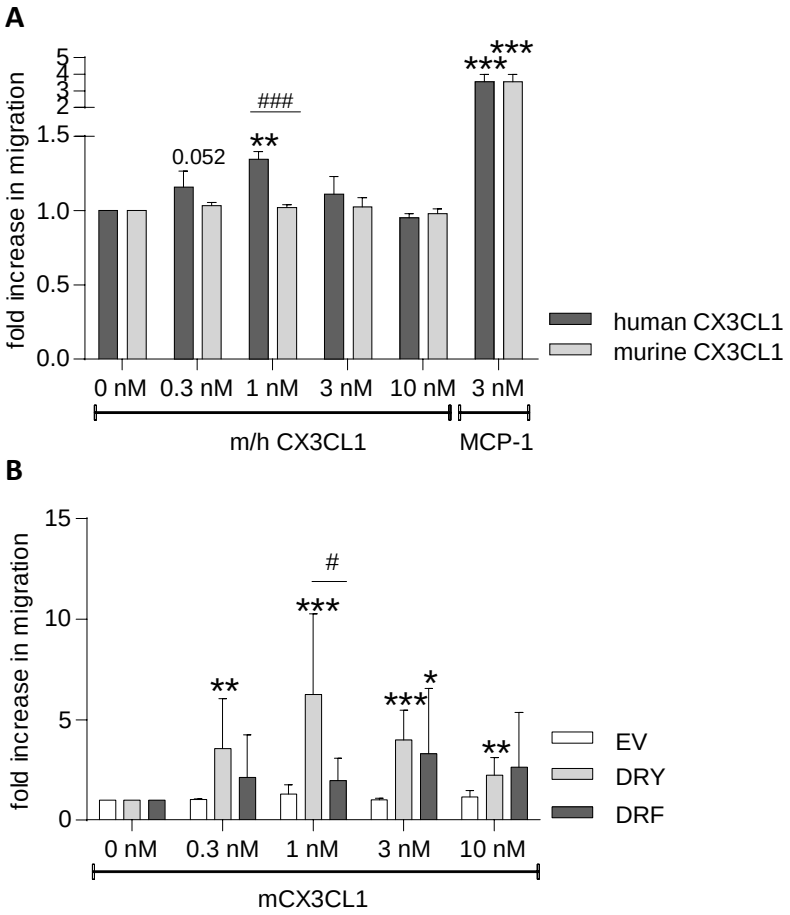

Figure 26 Chemotactic migration of THP-1 cells expressing CX_3CR1 variants
THP-1 cells were transduced with lentivirus encoding murine CX_3CR1 variants. A) Migration of THP-1-WT cells in response to human or murine CX_3CL1. Cell migration was quantified as number of migrated cells in the presence of chemotactic stimulus in relation to the number determined in the absence of chemokine. The assay was performed for 2 h using transwells with 8 µm pores. B) Migration of THP-1-EV cells and cells expressing CX_3CR1-DRY or CX_3CR1-DRF variant in response to increasing concentrations of CX_3CL1 was tested in a *Boyden chamber* for 2 h. Data are expressed as mean + SD (n=3-7). Statistical analysis was performed with raw data using Student's t-test and corrected for multiple comparison by FDR. Asterisks indicate significant differences from migration of unstimulated cells (*p<0.05, **p<0.01, ***p<0.001) and hashes indicate difference between groups (#p<0.05).

4.1.4 Molecular modelling of the DRF motif of CXCR6

Molecular studies of CXCR6 and CX_3CR1 revealed an essential contribution of the DRF/DRY motif to the receptor activity. In the present study, it was shown that the endogenous DRF motif of CXCR6 and the mutation of the more common DRY motif of CX_3CR1 into DRF led to decreased chemotactic migration in comparison to DRY expressing receptor variants. One possible explanation for these observations could be an altered three-dimensional structure of the receptors resulting in different activation states. To analyse this, Dr. Xavier Deupi from the Paul

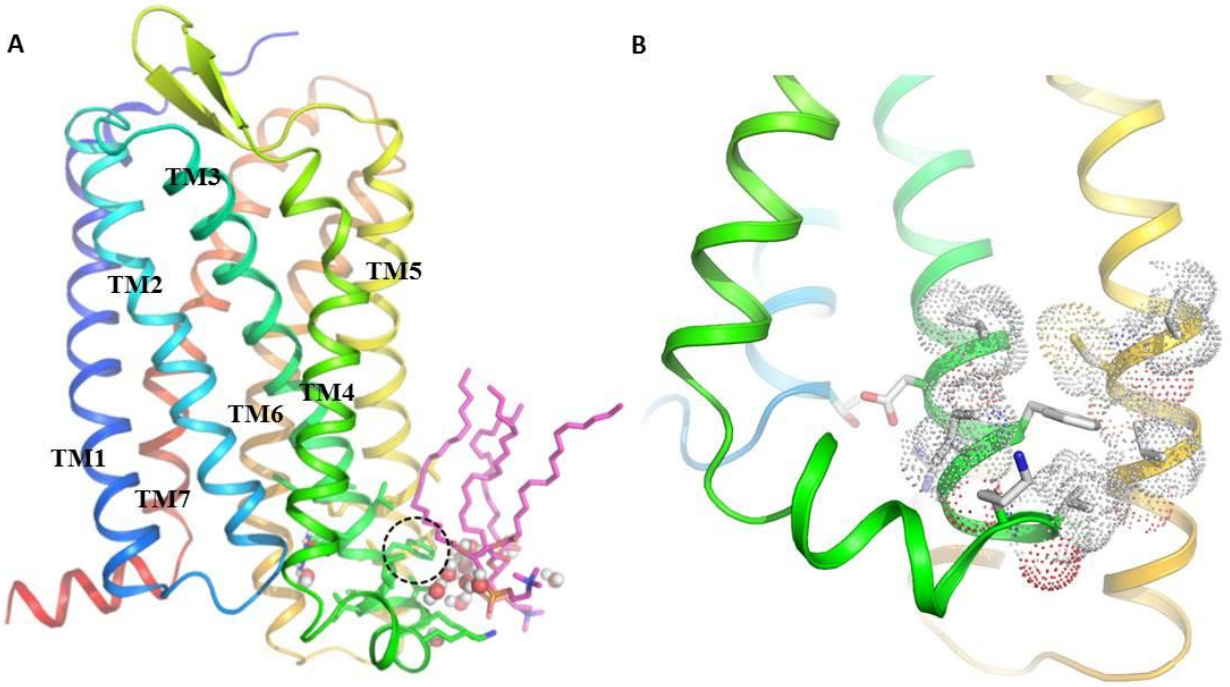

Figure 27 Modelling of CXCR6 and the DRF motif in its environment
Human CXCR6 was modelled using the crystal structure of human CCR5 (PDBid: 4MBS) as a template. A) $F^{3.51}$ of human CXCR6 (in black dotted circle) is located in the surface of the receptor at the interface between the lipid bilayer (lipids are indicated in purple) and the cytoplasm. Transmembrane helixes are numbered (TM1-TM7). B) $F^{3.51}$ is surrounded by a cluster of hydrophobic residues in TM-III and TM-V. Hydrophobic residues surrounding $F^{3.51}$ are represented as sticks and dots, to better depict their volume). Blue residues: nitrogen, red residues: oxygen, yellow residue: sulphur. Analysis performed by Dr. X. Deupi from the Paul Scherrer Institut in Villigen, Switzerland.

Scherrer Institute in Switzerland was asked to perform molecular modelling studies. The available crystal structure of human CCR5[102] was used as a template for CXCR6.

First, the molecular structure of human CXCR6 was investigated. The receptor showed the typical 7-TM structure, including a short helical bundle at the C-terminal end, sometimes termed helix 8. The molecular investigation focused on the environment of the DRF motif of CXCR6 at the interface of TM-III and the second intracellular loop, with F at position 3.51 of the receptor (see dotted circle in Figure 27A). The model showed that $F^{3.51}$ of the DRF motif in CXCR6 is located at the surface of the receptor, roughly at the interface between the lipid bilayer and the cytoplasm, where it can interact with water molecules and the phospholipid head groups (Figure 27A). Therefore, a potentially critical lipid-receptor interaction at this site could be one mechanism for activity regulation of CXCR6. In addition to the membrane and water environment, $F^{3.51}$ is surrounded by a cluster of hydrophobic residues of TM-III and TM-V (Figure 27B). Since all other chemokine receptors except CXCR6 express Y at position 3.51, the

importance of this amino acid was analysed in more detail in CCR5 (Figure 28). CCR5 was analysed, since a 2.7 Å resolution crystal structure of human CCR5 has been published[102]. Indeed, in CCR5 the $Y^{3.51}$ of the DRY motif is located at hydrogen bond distance to $H^{3.56}$, a basic amino acid located about one helical turn downstream of $Y^{3.51}$. In fact, a basic amino acid at position 3.56 seems to be conserved in many peptide GPCRs. In CXCR6, $K^{3.56}$ is located five residues downstream of $F^{3.51}$. Therefore, the lack of a possible hydrogen bond interaction, caused by expression of $F^{3.51}$ instead of $Y^{3.51}$ in CXCR6, might affect receptor conformation and activity.

In summary, there are different possible impacts of DRY/DRF on the conformation and activity of chemokine receptors and other GPCRs.

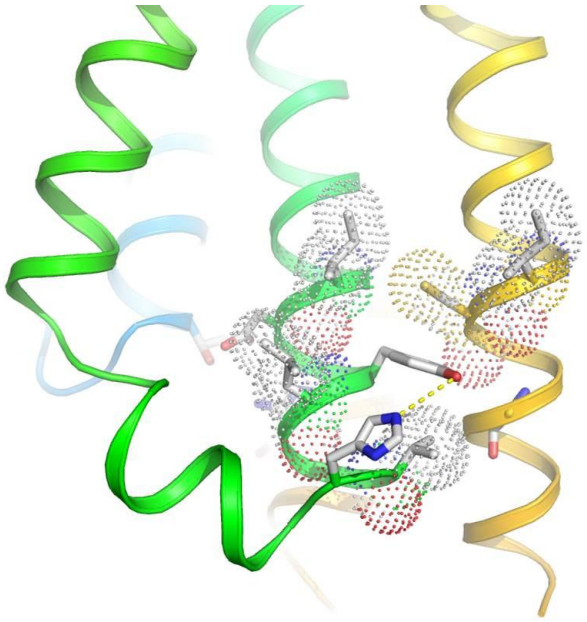

Figure 28 Hydrogen bond of $Y^{3.51}$ to $H^{3.56}$ in CCR5
In CCR5, there is a conserved basic residue ($H^{3.56}$) about one helical turn (five residues) downstream of $Y^{3.51}$. $Y^{3.51}$ is capable of interacting with this residue via hydrogen bonds (indicated by the yellow dotted line). Blue residues: nitrogen, red residues: oxygen, yellow residue: sulphur. Analysis performed by Dr. X. Deupi**.**

4.2 Role of CXCR6 during ovalbumin-induced lung inflammation

In the first part of this study it was shown that the DRF motif of CXCR6 is necessary for adhesion and calcium signalling upon CXCL16 exposure in monocytic cells, whereas it mediates only a weak chemotactic response. Several reports exist that CXCR6 is important for different inflammatory diseases, e.g. during inflammation of the liver[45]. During this disease, CXCR6 was shown to mediate the recruitment of immune cells, including T cell subsets and macrophages[45,61]. Chronic lung inflammation is strongly influenced by the recruitment of immune cells, like eosinophils as well as different T cell subsets and to some degree also macrophages[103]. Therefore, the impact of the chemokine receptor CXCR6 on the development of chronic lung disease was investigated at two different stages of experimental asthma using CXCR6-deficient mice. The 35-days ovalbumin (OVA) model was used to mimic the subchronic phase indicated by recruitment of leukocytes and cytokine accumulation, whereas the 110-days model was chosen to study the chronic state of lung inflammation, which was in depth investigated by physiological lung measurements and histology to focus on remodelling processes.

4.2.1 Basal analysis of CXCR6$^{+/GFP}$ and CXCR6$^{GFP/GFP}$ mice

In this study mice were used, in which the CXCR6 gene was replaced by the fluorescent protein GFP, which is then expressed under the control of the CXCR6 promotor (CXCR6$^{GFP/GFP}$)[94], a so called knock-out through knock-in. Heterozygous mice expressing GFP in addition to CXCR6 (CXCR6$^{+/GFP}$) served as control mice. These mice were first investigated for basal differences in CXCL16 mediated chemotaxis of blood leukocytes due to the altered expression of CXCR6 and the expression of GFP. Furthermore cell composition of blood, spleen and lung tissue were analysed, while focusing on expression of CXCR6 in different immune cell subsets under homeostatic conditions in both mice strains.

Blood leucocytes of CXCR6$^{GFP/GFP}$ and CXCR6$^{+/GFP}$ mice were tested for their chemotactic response to soluble CXCL16. Blood cells of CXCR6$^{+/GFP}$ showed migration in response to 3 and 10 nM CXCL16, whereas blood cells of CXCR6$^{GFP/GFP}$ did not (Figure 29). This confirmed the relevance of CXCR6 for CXCL16-induced cell migration and furthermore showed the functional knock-out of CXCR6 in cells of CXCR6$^{GFP/GFP}$ mice.

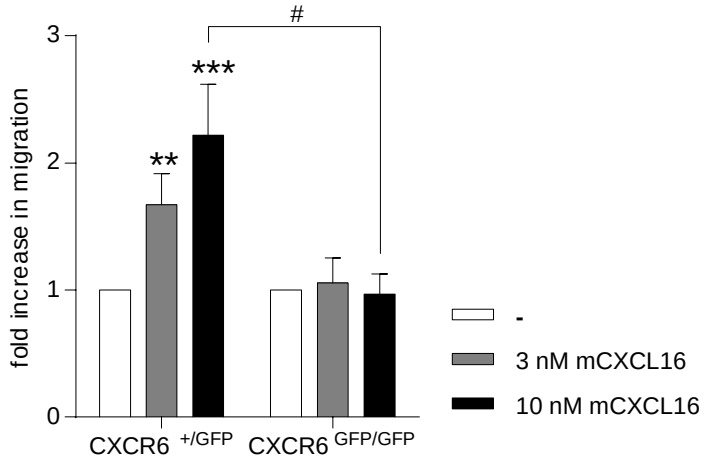

Figure 29 Migration of blood cells of CXCR6$^{+/GFP}$ and CXCR6$^{GFP/GFP}$ mice in response to CXCL16
Blood of mice was isolated and erythrocytes were lysed as described. Remaining leukocytes were analysed for migration against recombinant murine CXCL16 using transwells with 8 µm pores for 2 h. Data are expressed as mean + SD (n=3). Statistical analysis was performed with raw data using Student's t-test followed by correction for multiple comparison via FDR. Asterisks indicate significant differences from migration of unstimulated cells (**p<0.01, ***p<0.001).

.

Next, the cellular composition of blood of CXCR6$^{+/GFP}$ and CXCR6$^{GFP/GFP}$ mice was analysed with special focus on CXCR6 expression by leukocyte subsets, which can be easily identified by GFP fluorescence (see Figure 30). Blood cells of the innate immune system were analysed and divided into different classes. CD45 and CD11b-positive cells, identified as eosinophils (Figure 30A), included 9.5 - 16% GFP/CXCR6-positive cells. Neutrophils, identified as F4/80-negative and Ly6G-positive cells, showed GFP/CXCR6 expression in 90% of cells (Figure 30C). Monocytic cells were characterised as F4/80-positive and Ly6G-negative cells (Figure 30B), and 44 – 59% of these cells showed GFP/CXCR6 expression. The numbers of monocytic cells and neutrophils appeared to be slightly decreased in blood of CXCR6$^{GFP/GFP}$ mice. However statistical analysis revealed that there were no significant differences between CXCR6$^{+/GFP}$ and CXCR6$^{GFP/GFP}$ mice in any of the tested cell populations.

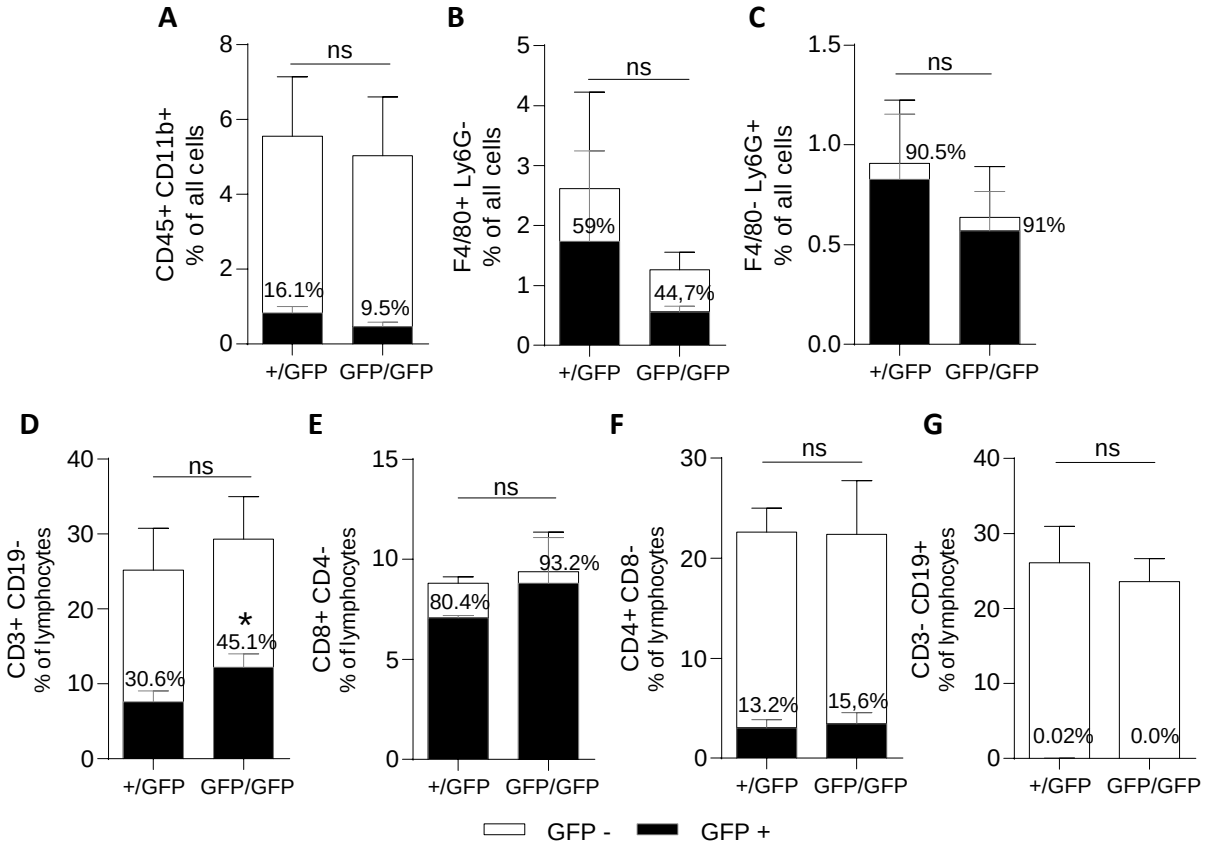

Figure 30 Expression of CXCR6 in blood cells of CXCR6$^{+/GFP}$ and CXCR6$^{GFP/GFP}$ mice
A-G: Cells were isolated from blood and stained with different antibodies. During flow cytometry analysis, cells were distinguished by different size (FSC) and granularity (SSC) and characterised by antibody staining. A) Granulocytes positive for CD45 and CD11b (eosinophils). B) Blood cells positive for F4/80 and negative for Ly6G (monocytic cells). C) Granulocytes negative for F4/80 and positive for Ly6G (neutrophils). D) Lymphocytes positive for CD3 and negative for CD19 (T lymphocytes). E) Lymphocytes positive for CD8 and negative for CD4 (cytotoxic T lymphocytes). F) Lymphocytes positive for CD4 and negative for CD8 (T helper cells). G) Lymphocytes negative for CD3 and positive for CD19 (B cells). Black bars incorporated in larger bars, indicate the percentage of cells (also given by numbers), expressing GFP, which indicates potential CXCR6 expression. Data are expressed as mean + SD (n=3) of all cells in A-C and of lymphocytes in D-G. Statistical analysis was performed using Student's t-test. No significant differences were observed.

Next, blood lymphocytes were distinguished and analysed for their GFP/CXCR6 expression (Figure 30D-G). CD3-positive and CD19-negative T lymphocytes of blood from CXCR6$^{GFP/GFP}$ mice showed slightly increased amounts of GFP/CXCR6-positive cells (45%) compared to CXCR6$^{+/GFP}$ (31%). CD4-positive and CD8-negative lymphocytes were positive for GFP in 13-15% of cells, whereas the majority of CD8-positive lymphocytes expressed GFP/CXCR6 (80-93%). There was no expression of GFP/CXCR6 in B cells, which were characterised as CD3-negative and CD19-positive lymphocytes. Thus, neither GFP/CXCR6 expression nor the general lymphocyte composition showed significant differences between CXCR6$^{+/GFP}$ and CXCR6$^{GFP/GFP}$

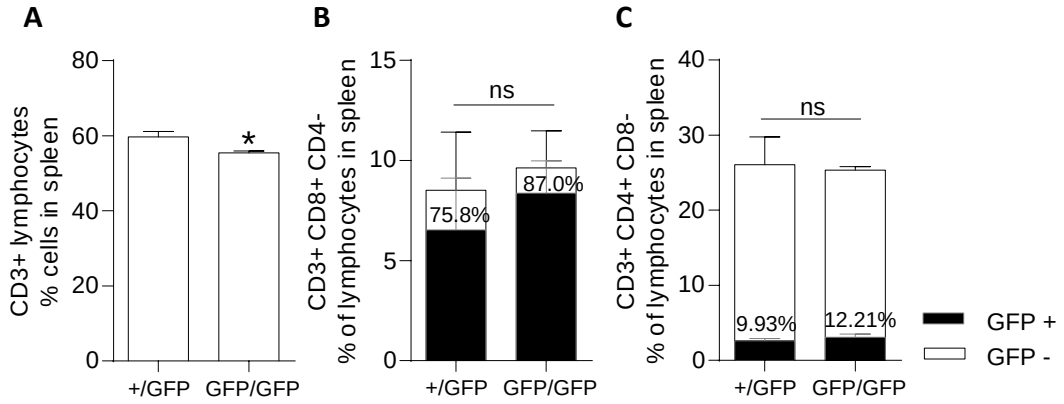

Figure 31 Expression of CXCR6 by splenic lymphocytes of CXCR6$^{+/GFP}$ and CXCR6$^{GFP/GFP}$ mice.
Cells were isolated from spleen and stained with different antibodies. During flow cytometry analysis, the lymphocytes cell gate was determined by FSC/SSC and the lymphocyte subtypes characterised by antibody staining. A) Lymphocytes positive for CD3 (T lymphocytes). No measurement of GFP expression in A. B) Lymphocytes positive for CD3 and CD8 and negative for CD4 (cytotoxic T lymphocytes). C) Lymphocytes positive for CD3 and CD4 and negative for CD8 (T helper cells). Black bars incorporated in larger bars indicate the percentage of cells (also given by numbers), which indicates potential CXCR6 expression. Data are expressed as mean + SD (n=3). Statistical analysis was performed using Student's t-test.

mice.

The antigen-specific activation and differentiation of T-lymphocytes is one of the first steps during the development of asthmatic disease. Therefore, T cell subpopulations in the spleen were also investigated (Figure 31). There was a weak decrease of CD3-positive T lymphocytes in the spleen of CXCR6$^{GFP/GFP}$ mice. As already seen for peripheral lymphocytes, CD3/CD8-positive cells showed a higher amount of GFP/CXCR6 expressing cells compared to CD3/CD4-positive cells. However, the analysis of CD3/CD4-positive cells (T helper cells) and CD3/CD8-positive cells (cytotoxic T cells) did not show differences in the distribution between CXCR6$^{+/GFP}$ and CXCR6$^{GFP/GFP}$ mice.

As this study aimed to analyse the role of CXCR6 during lung inflammatory disease, the cellular composition of lung tissue was analysed in a next step. Eosinophils, characterised by morphology and CD11b expression, represented about 10–12% of cells in lung tissue (Figure 32A). About 9–12% of eosinophils from lung tissue were GFP/CXCR6-positive. F4/80-positive monocytic cells in lung tissue contained about 58–70% GFP/CXCR6-positive cells. Furthermore, Ly6G-positive neutrophils were GFP-positive in 58–69% of cells in lung tissue. However, no differences between CXCR6$^{+/GFP}$ and CXCR6$^{GFP/GFP}$ mice were observed.

The analysis of lung tissue lymphocytes revealed a similar general pattern of GFP/CXCR6 expression in CD4-and CD8-positive lymphocytes (Figure 33A and B) as shown for blood and spleen before. CD4-positive lymphocytes expressed GFP/CXCR6 in 9 – 10% of cells and in case of CD8-positive lymphocytes, 42-64% of cells expressed GFP/CXCR6. The population of CD4 positive lymphocytes was then further divided into IFNγ (Figure 33C) and ST2 (Figure 33D) expressing cells, which indicates T helper cells type 1 (T_H1) and T helper cells type 2 (T_H2), respectively. Almost no GFP expression was detectable in CD4/IFNγ-positives cells. In contrast, 5–12% of CD4/ST2-positive lymphocytes showed GFP expression. CXCR6 dependent NKT cell recruitment has been shown during development of liver fibrosis[45]. NKT cells were characterised by CD3/NK1.1 expression and indeed, 13–18% of these cells located in lung tissue, showed GFP expression. Again, the analysis of lung lymphocyte subtypes showed no differences in their relative distribution between $CXCR6^{+/GFP}$ and $CXCR6^{GFP/GFP}$ mice.

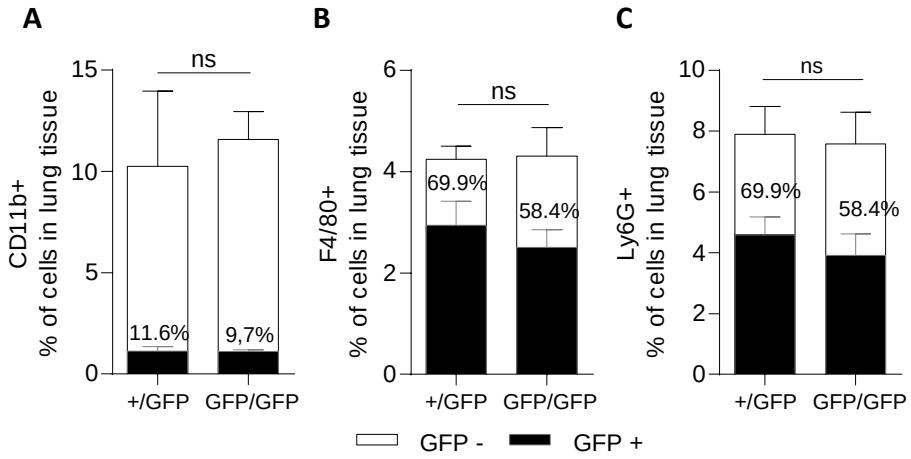

Figure 32 Expression of CXCR6 by lung tissue cells of $CXCR6^{+/GFP}$ and $CXCR6^{GFP/GFP}$ mice
Cells were isolated from disintegrated lung tissue and stained with different antibodies. During flow cytometry analysis, cells were distinguished by different size (FSC) and granularity (SSC) and characterised by antibody staining. A) Granulocytes positive for CD11b (eosinophils). B) Cells positive for F4/80 (monocytic cells). C) Granulocytes positive for Ly6G (neutrophils). Black bars incorporated in bigger bars indicate the percentage of cells (also given by numbers) expressing GFP, which indicates potential CXCR6 expression. Data are expressed as mean + SD (n=3). Statistical analysis was performed using Student's t-test. No significant differences were observed.

In conclusion, $CXCR6^{+/GFP}$ and $CXCR6^{GFP/GFP}$ mice did not differ in their basal cell composition of blood, spleen and lung. CXCR6/GFP expression could be detected on several cell populations including eosinophils, neutrophils, monocytic cells and different T cell subpopulations, like CD8-positive cells, T_H2 and NKT cells.

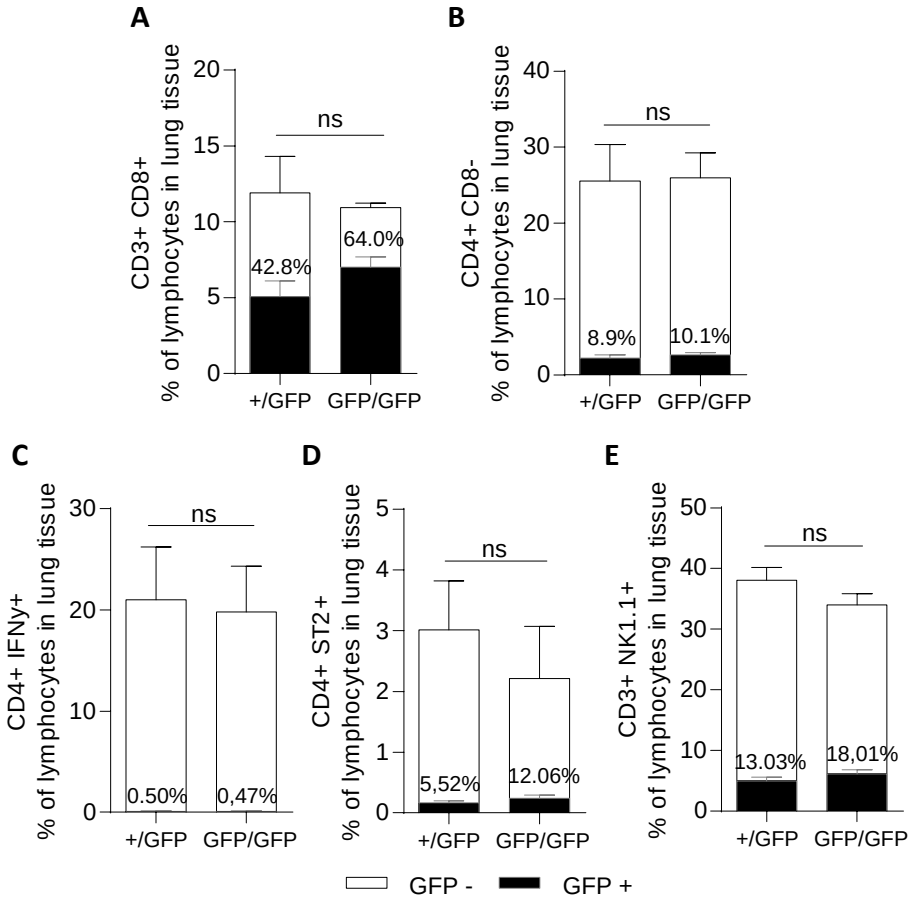

Figure 33 Expression of CXCR6 by lung tissue lymphocytes of CXCR6$^{+/GFP}$ and CXCR6$^{GFP/GFP}$ mice Cells were isolated of disintegrated lung tissue and stained with different antibodies. During flow cytometry analysis, the lymphocytes cell gate was determined by FSC/SSC and the lymphocyte subtypes characterised by antibody staining. A) Lymphocytes positive for CD3 and CD8 (cytotoxic T lymphocytes). B) Lymphocytes positive for CD4 and negative for CD8 (T helper cells). C) Lymphocytes positive for CD4 and IFNγ (T helper cells type 1). D) Lymphocytes positive for CD4 and ST2 (T helper cells type 2). E) Lymphocytes positive for CD3 and NK1.1 (natural killer T cell). Black bars incorporated in bigger bars indicate the percentage of cells (also given by numbers) expressing GFP, which indicates CXCR6 expression. Data are expressed as mean + SD (n=3). Statistical analysis was performed using Student's t-test. No significant differences were observed.

4.2.2 Visualisation of GFP expressing cells in lungs of CXCR6$^{+/GFP}$ and CXCR6$^{GFP/GFP}$ mice

As mentioned above, CXCR6$^{GFP/GFP}$ and CXCR6$^{+/GFP}$ mice both express GFP in CXCR6-expressing cells. Both genotypes did not show any significant differences in the amount of GFP/CXCR6-expressing cells under homeostatic conditions. However, this does not exclude differences in the distribution of cells in the lung tissue or between control and asthmatic mice. To compare the presence of GFP/CXCR6 positive cells in asthmatic and control treated lungs, the model of OVA-induced experimental asthma was performed. Therefore, mice were treated either

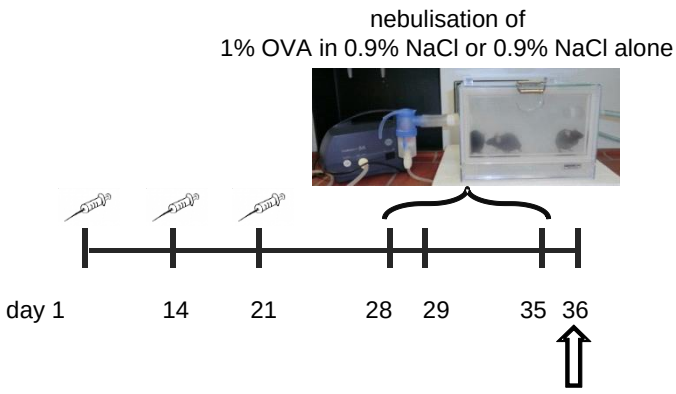

Figure 34 Sensitisation protocol for OVA-induced asthma (35-days)
I.p. injections of either OVA in aluminium hydroxide or aluminium hydroxide alone were performed on day 1, 14 and 21. On day 28, 29 and 35 mice were nebulised with 1% OVA or 0.9% NaCl (vehicle control) alone. Mice were sacrificed on day 36.

with OVA or with NaCl for 35 days as shown in Figure 34. Lung tissue was then analysed in collaboration with Dr. Reinhard Windoffer using the *Lightsheet microscope.* This allows three dimensional analysis of tissues without special preparation, which often decreases endogenous GFP signals. GFP/CXCR6-positive cells were detected as strongly green fluorescent cells in both untreated and control treated lungs of $CXCR6^{+/GFP}$ and $CXCR6^{GFP/GFP}$ mice (Figure 35). As lung tissue shows some background fluorescence, it was even possible to recognise tissue structures. Upon treatment with OVA, the amount of GFP/CXCR6-positive cells seemed to increase in lungs of $CXCR6^{+/GFP}$ and $CXCR6^{GFP/GFP}$ mice. As only one animal per group was analysed, statistical quantification could not be performed.

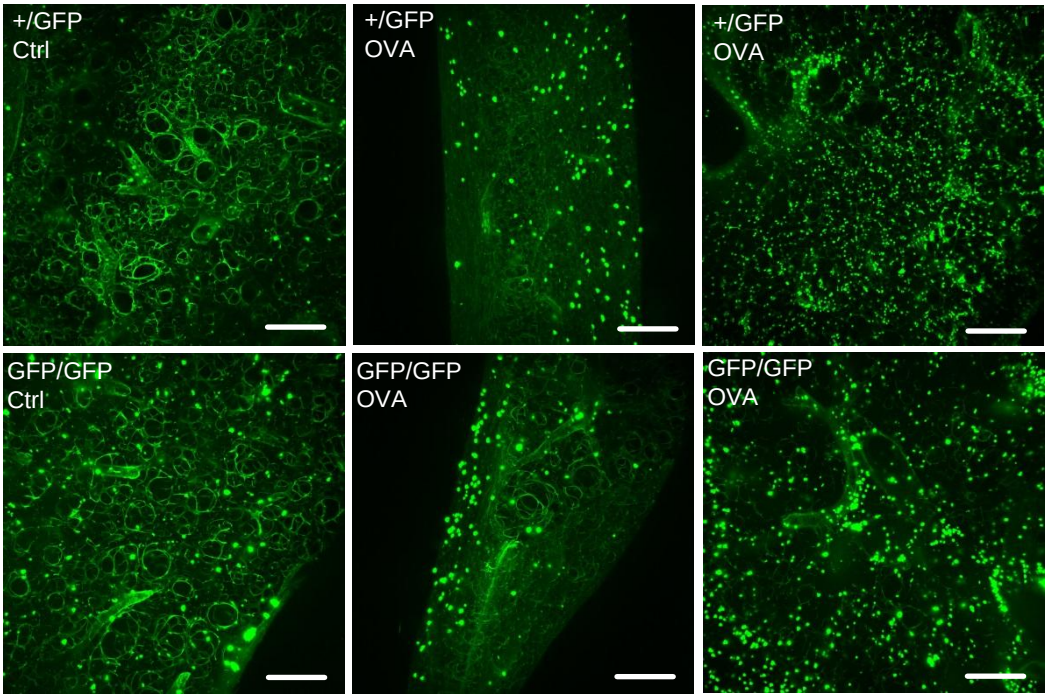

Figure 35 GFP positive cells in lung of CXCR6$^{+/GFP}$ and CXCR6$^{GFP/GFP}$ mice
Mice were either control treated or treated with OVA as described for 35 days of OVA sensitisation. Afterwards lungs were isolated and observed by the *Lightsheet Z.1* microscope. Left: lung slices of the right lobe of control-treated mice. Middle and right panels: lung tissue of OVA treated mice. Middle panels show tissue of the post-caval lobe, whereby tissue was partially truncated. Right panels show tissue slices of the right lobe. White bars indicate a length of 200 µm.

4.2.3 Analysis of the development of subchronic asthma in CXCR6$^{+/GFP}$ and CXCR6$^{GFP/GFP}$ mice

As shown above, CXCR6 is expressed by different T cell subpopulations and eosinophils in the lung. Furthermore, it has been shown that lung tissue displays as strong CXCL16 expression[11], which might be relevant for cell recruitment during inflammation. Therefore, the impact of CXCR6 on asthma development was investigated using the 35-days model of OVA-induced experimental asthma. For this purpose, CXCR6$^{+/GFP}$ and CXCR6$^{GFP/GFP}$ mice were treated as already shown in Figure 34. First, the level of IgE in serum was analysed to confirm successful sensitisation (Figure 36A). Untreated mice (day 0) showed less than 50 ng/ml of IgE in serum (Figure 36A). After 35 days of treatment, there was a strong increase of IgE in serum of OVA treated mice (up to 1000 ng/ml IgE), which was absent in control treated mice and did not differ between CXCR6$^{+/GFP}$ and CXCR6$^{GFP/GFP}$ mice. Thus, successful sensitisation was achieved in both mice strains. One marker of lung inflammation is the increase of vascular permeability and oedema formation, indicated by influx of proteins into the alveolar space. As shown in Figure 36B, there was a 2-fold increase in protein concentration in BAL-fluid of OVA treated mice in

comparison to control treated mice. Due to high standard deviation the increase in heterozygous mice was not significant. Nevertheless, tendencies were identical between CXCR6$^{+/GFP}$ and CXCR6$^{GFP/GFP}$ mice.

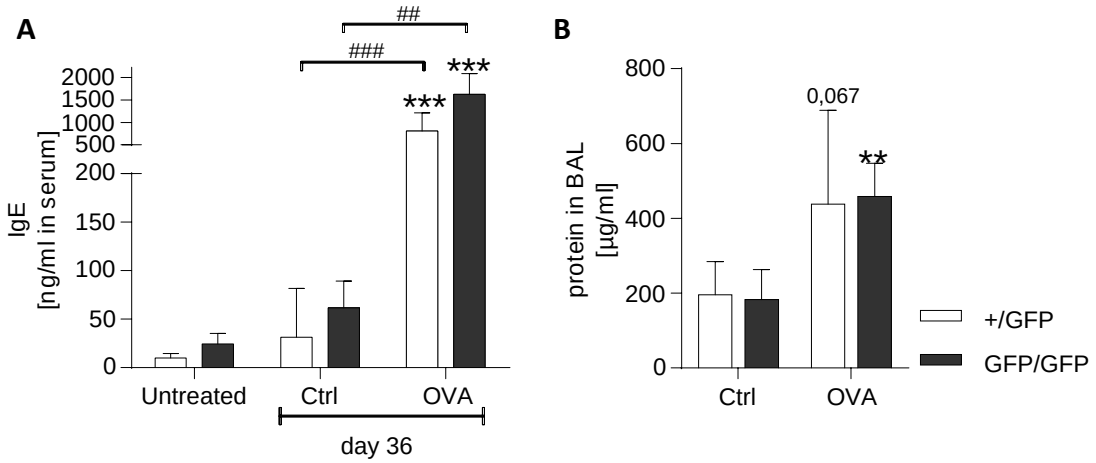

Figure 36 Sensitisation of CXCR6$^{+/GFP}$ and CXCR6$^{GFP/GFP}$ mice for 35 days
A) Concentration of IgE in serum of OVA and control treated mice as well as untreated mice (before start of sensitisation) were measured by ELISA specific for mouse IgE. Asterisks indicate differences from untreated mice (***p<0.001) and hashes indicate differences as shown (##p<0.01, ###p<0.001). B) Protein concentrations of BAL-fluid were measured by BCA assay. Data are shown as mean + SD (n=4-6). Statistical analysis was performed by Student's t-test and FDR. Asterisks indicate differences from control mice (**p<0.01).

4.2.3.1 Cell recruitment into lung of OVA treated CXCR6$^{+/GFP}$ and CXCR6$^{GFP/GFP}$ mice

Lung inflammation is further marked by a strong influx of leukocytes, which is dominated by eosinophils and lymphocyte recruitment in asthmatic disease. The cellular composition of BAL cells was determined by antibody staining and flow cytometry analysis. The global distinction of cell populations was performed by FSC and SSC gating as exemplarily shown in Figure 37. Quantification of the total BAL cell number revealed an significant increase in total leukocyte count upon OVA-treatment (Figure 36B) in comparison to control treatment (Figure 36A), which did not differ between CXCR6$^{+/GFP}$ and CXCR6$^{GFP/GFP}$ mice (Figure 37C). Despite this similarity and due to the fact that differences may occur in distinct subpopulations, the two most prominently increased cell populations, the granulocytes and the lymphocytes, were further distinguished by special surface markers.

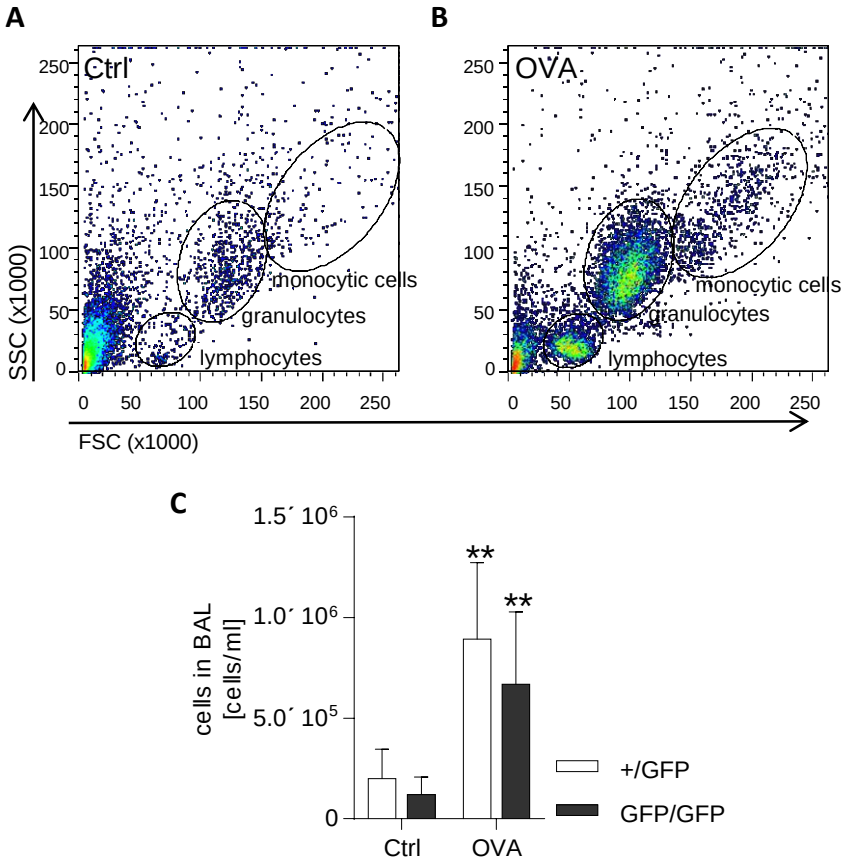

Figure 37 Flow cytometry analysis of cells in BAL-fluid of CXCR6$^{+/GFP}$ and CXCR6$^{GFP/GFP}$ mice
Mice were sensitised and nebulised with OVA or control treated for 35 days and analysed on day 36. A and B) Representative flow cytometry dot blot of BAL-fluid cells of heterozygous CXCR6$^{+/GFP}$ control (Ctrl) (A) and OVA (B) treated mice. Cell populations were distinguished by size (FSC) and granularity (SSC) and characterised more precisely by antibody staining as indicated. C) Total amount of cells in BAL-fluid after 35 days of treatment. Data represent mean + SD and statistical analysis was performed by Student's t-test and corrected for multiple comparison by FDR (n=4-6). Asterisks indicate differences from control mice (**p<0.01).

First, the recruitment of granulocytes and monocytic cells was analysed. OVA-treated mice showed a strong recruitment of eosinophils (Figure 38A), neutrophils (Figure 38B) and monocytic cells (Figure 38) in comparison to control treated mice, which did not differ between CXCR6$^{+/GFP}$ and CXCR6$^{GFP/GFP}$ mice.

T lymphocytes are critically involved in the development of asthmatic disease. T cell recruitment due to OVA-sensitisation was obvious in both mice strains

Figure 39). CD4-positive lymphocytes, identified as T helper cells, showed a 12-fold increase in BAL-fluid of OVA-treated mice in comparison to control treated mice in both CXCR6$^{+/GFP}$ and CXCR6$^{GFP/GFP}$ mice. About one third of these T cells were positive for GFP/CXCR6 expression. The population of CD4-positive T helper cells was further divided into T_H1 (CD4+ IFN+), T_H2

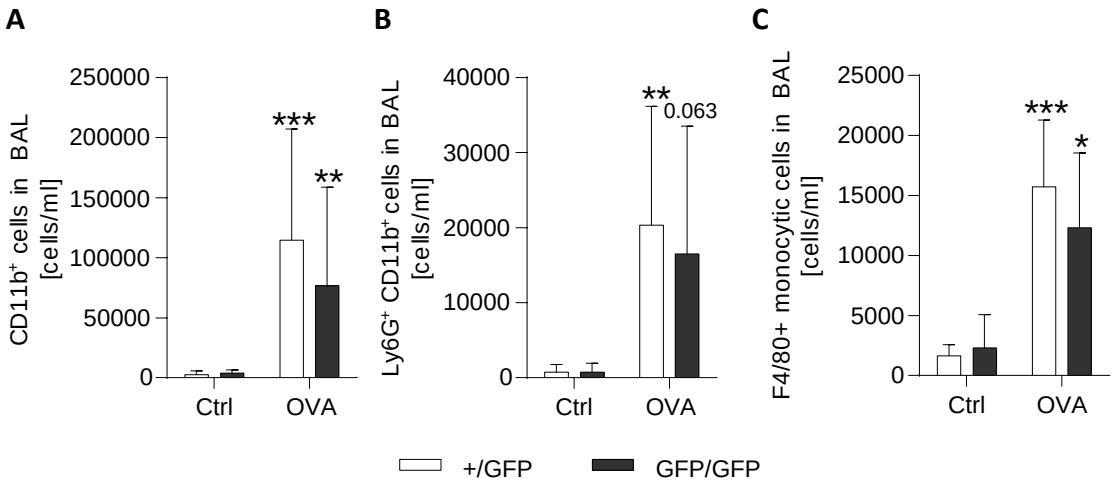

Figure 38 Granulocyte and monocytic cells in BAL-fluid of CXCR6$^{+/GFP}$ and CXCR6$^{GFP/GFP}$ mice
During flow cytometry analysis, the cell gates were determined by FSC/SSC and the lymphocyte subtypes characterised by antibody staining A) Number of CD11b-positive granulocytes (eosinophils). B) Number of neutrophils in BAL-fluid characterised by morphology and Ly6G- and CD11b-positive staining. C) Number of monocytic cells in BAL-fluid characterised by morphology and F4/80-positive staining. Data represent mean + SD and statistical analysis was performed by Student's t-test and corrected for multiple comparison by FDR (n=4-6). Asterisks indicate differences from control mice (*p<0.05; **p<0.01, ***p<0.001).

(CD4+ ST2+) and regulatory T cells (Treg; CD4+ CD25+). Again, the number of all these T cell subpopulations was increased in OVA-treated mice in comparison to control-treated mice and did not differ between the two genotypes. In comparison to T helper cells, CD3/CD8-positive lymphocytes, identified as cytotoxic T cells, were 8-times less abundant, but showed a similar increase in number upon OVA-treatment. Again, this effect was genotype independent. One further T cell subpopulation which is discussed to be strongly involved in asthma development, is the lymphocyte subset of NKT cells[45]. As shown in Figure 40, NKT cells were characterised as CD3- and NK1.1-positive lymphocytes. There was a similar 20-fold increase of NKT cells after OVA-treatment compared to control treatment in both mice strains. About 50% of the detected NKT cells showed GFP/CXCR6 expression.

In summary, recruitment of cells of the innate and adaptive immune system into the alveolar space could be observed due to OVA-treatment, but this recruitment was independent of CXCR6 as no differences were observed between CXCR6$^{+/GFP}$ and CXCR6$^{GFP/GFP}$ mice.

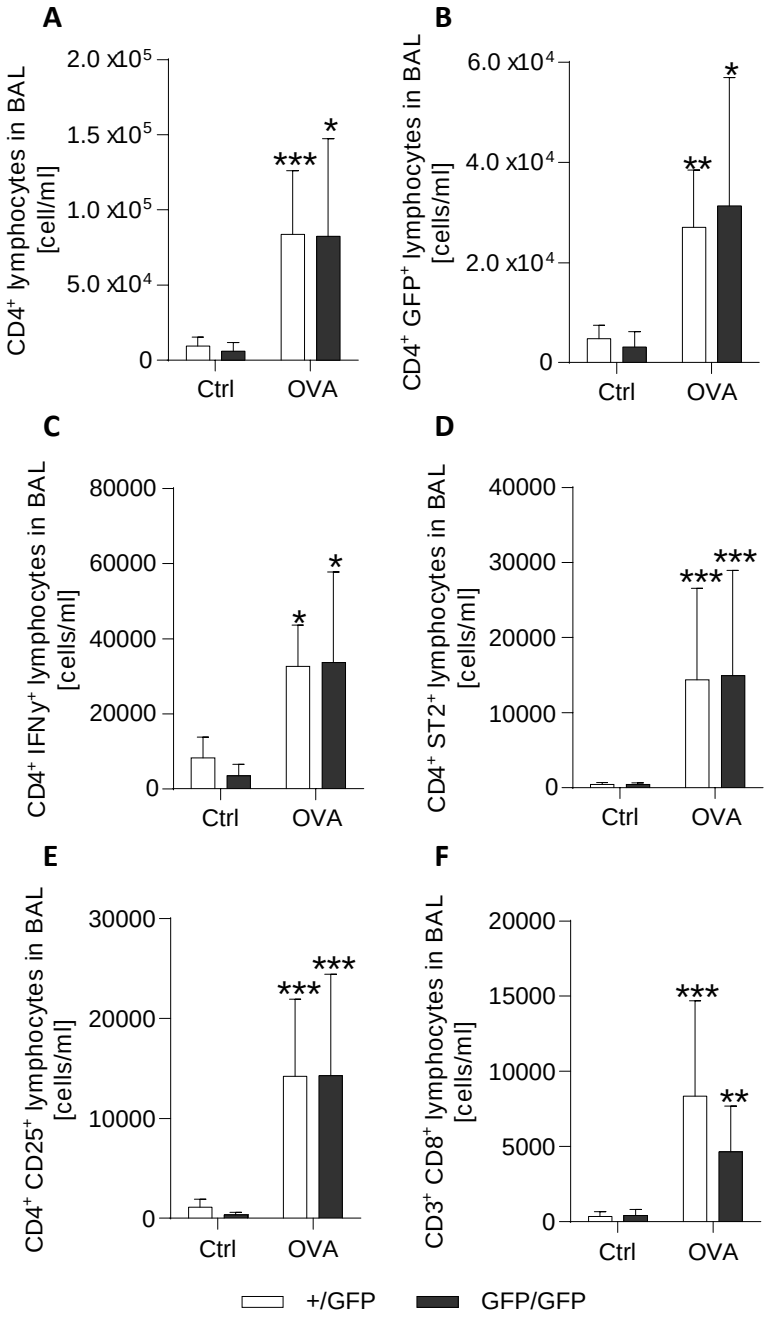

Figure 39 Lymphocytes in BAL-fluid of CXCR6$^{+/GFP}$ and CXCR6$^{GFP/GFP}$ mice
During flow cytometry analysis, the lymphocytes cell gate was determined by FSC/SSC and the lymphocyte subtypes characterised by antibody staining. A) Number of CD4-positive lymphocytes. B) Number of CD4- and CXCR6-positive lymphocytes. C) Number of CD4- and IFNγ-positive lymphocytes (T_H1 cells). D) Number of CD4- and ST2-positive lymphocytes (T_H2 cells). E) Number of CD4- and CD25-positive lymphocytes (regulatory T cells). F) Number of CD3- and CD8-positive lymphocytes (cytotoxic T cells). Data represent mean + SD and statistical analysis was performed by Student's t-test and corrected for multiple comparison by FDR (n=4-6). Asterisks indicate differences from control mice (*p<0.05, **p<0.01, ***p<0.001).

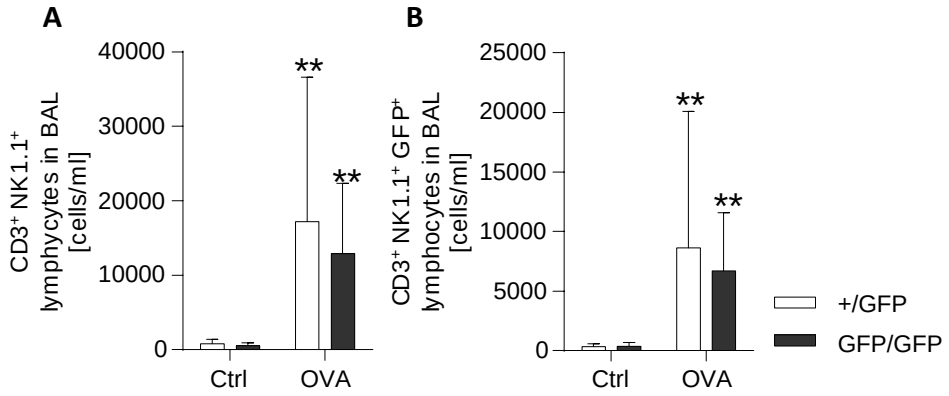

Figure 40 NKT cells in BAL-fluid of CXCR6$^{+/GFP}$ and CXCR6$^{GFP/GFP}$ mice
During flow cytometry analysis, the lymphocytes cell gate was determined by FSC/SSC and the lymphocyte subtypes characterised by antibody staining. A) Number of CD3- and NK1.1-positive lymphocytes (NKT cells). B) Number of CD3- and NK1.1-positive lymphocytes expressing GFP (NKT cells potentially expressing CXCR6). Data represent mean + SD and statistical analysis was performed by Student's t-test and corrected for multiple comparison by FDR (n=4-6). Asterisks indicate differences from control mice (**p<0.01).

4.2.3.2 **Cytokine content of BAL-fluid and serum after 35 days of OVA-treatment**

During asthma development, cytokines are released from epithelial cells as well as resident and recruited leukocytes. Interleukin-4 (IL-4), interleukin-5 (IL-5), interleukin-13 (IL-13), and eotaxin are most prominent to be found in BAL-fluid of human and mice suffering from asthma[104–107]. The concentration of IL-5 showed a 20-fold increase in BAL-fluid and a 5-fold increase in serum of OVA-treated mice in comparison to control treated mice (Figure 41A, B). No differences comparing BAL-fluid of CXCR6$^{+/GFP}$ and CXCR6$^{GFP/GFP}$ mice were detectable. The IL-4 concentration in BAL-fluid was less high in comparison to IL-5, but still there was an increase of IL-4 upon OVA-treatment in both mice strains (Figure 41C). Furthermore, a 2-fold increase of TGFβ concentration in BAL-fluid was observed after OVA-treatment (Figure 41D). The so far analysed cytokines did not differ in their concentrations between CXCR6$^{+/GFP}$ and CXCR6$^{GFP/GFP}$ mice, which was true for control treated as well as OVA treated groups.

CXCR6 function is regulated via its unique ligand CXCL16, which was measured in BAL-fluid and serum as well. BAL-fluid of untreated mice contained approx. 250 ng/ml CXCL16 in both CXCR6$^{+/GFP}$ and CXCR6$^{GFP/GFP}$ mice. Upon OVA-treatment, CXCL16 concentration in BAL-fluid increased only in case of CXCR6$^{GFP/GFP}$ mice. Furthermore CXCR6$^{GFP/GFP}$ mice showed increased serum CXCL16 levels in comparison to CXCR6$^{+/GFP}$ mice in both OVA treated and

control treated mice. This increased concentration might be explained by reduced uptake of the chemokine due to complete CXCR6 deficiency in CXCR6$^{GFP/GFP}$ mice.

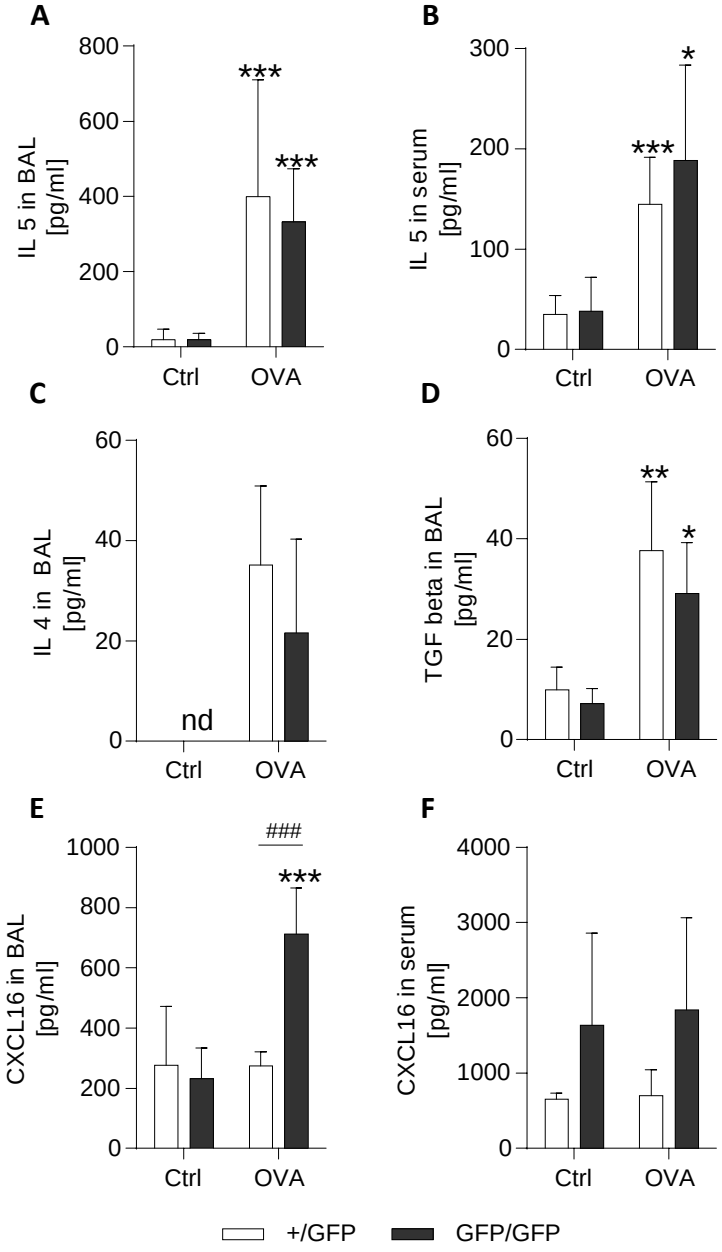

Figure 41 Cytokine levels in BAL-fluid and serum
Cytokine concentrations in BAL-fluid (A, C, D, E) and serum (B, F) were measured by ELISA. A) and B) IL-5. C) IL-4. D) Transforming growth factor beta (TGFβ). E) and F) CXCL16. Data represent mean + SD and statistical analysis was performed by Student's t-test and corrected for multiple comparison by FDR (n=4-6). Asterisks indicate differences from control mice (*p<0.05, **p<0.01, ***p<0.001) and hashes indicate differences between CXCR6$^{+/GFP}$ and CXCR6$^{GFP/GFP}$ mice (###p<0.001).

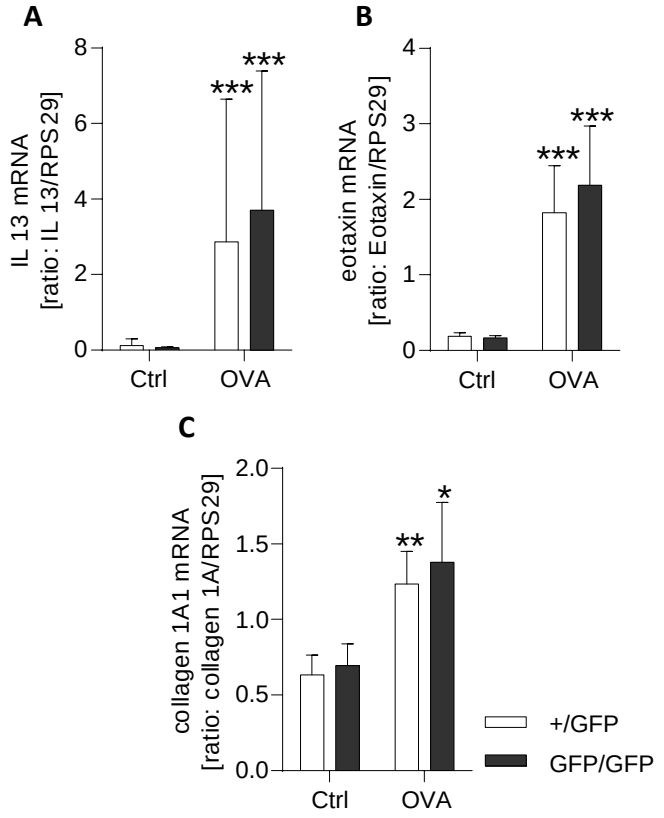

Figure 42 mRNA expression of inflammatory and fibrotic markers in lung tissue
Quantification of mRNA expression in lung tissue was performed by RT-qPCR and expressed in relation to the housekeeping gene RPS29. A) Interleukin 13 (IL-13) mRNA expression B) Eotaxin mRNA expression C) Collagen 1A1 mRNA expression in lung tissue. Data represent mean + SD and statistical analysis was performed by student's t-test and corrected for multiple comparison by FDR (n=4-6). Asterisks indicate differences from control mice (*p<0.05, **p<0.01, ***p<0.001).

IL-13, eotaxin and collagen type I-accumulation were quantified by RT-qPCR as shown in Figure 42. All three genes showed increased expression pattern caused by OVA-treatment in comparison to control treatment. However, no differences in CXCR6$^{+/GFP}$ and CXCR6$^{GFP/GFP}$ mice were detectable.

In summary, both CXCR6$^{+/GFP}$ and CXCR6 $^{GFP/GFP}$ mice showed a normal response to OVA-sensitisation, characterised by increased IgE levels in serum, protein influx into the alveolar space, cell recruitment into the alveolar space and increased chemokine secretion and expression in OVA-treated mice. Interestingly, the comparison of CXCR6$^{+/GFP}$ and CXCR6 $^{GFP/GFP}$ mice in the 35-days model of OVA-sensitisation did not show an obvious role of the chemokine receptor CXCR6 in subchronic (moderate) asthma.

4.2.4 Chronic asthma in CXCR6$^{+/GFP}$ and CXCR6$^{GFP/GFP}$ mice after 110 days of sensitisation

The pathogenesis of asthma develops over many years in human patients, which finally leads to strong remodelling processes in the lung tissue, causing airway hyperresponsiveness. This remodelling does not occur within the used subchronic model of experimental asthma. Therefore, the model was prolonged to a period of 110 days, and beside leukocyte recruitment, tissue remodelling was analysed by lung function measurement and histology. Mice were sensitised as illustrated in Figure 43. Since pathological changes are expected to have a functional impact after 110 days the focus of the investigations was on the analysis of functional lung measurements and the investigation of histological modifications.

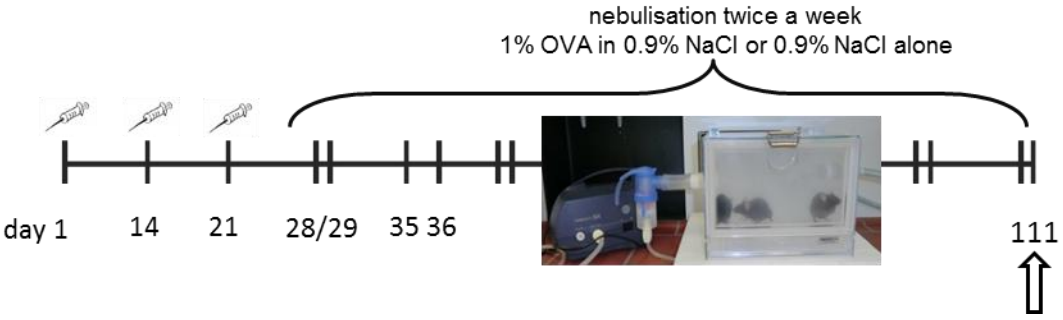

Figure 43 Sensitisation protocol for OVA-induced asthma (110 days)
I.p. injection of either OVA in aluminium hydroxide or aluminium hydroxide alone (vehicle control) were performed on day 1, 14 and 21. On day 28/29, 35/36, 42/43, 49/50, 56/57, 63/64, 70/71, 77/78, 84/85, 91/92, 98/99 105/106 and 110 mice were ventilated with 1% OVA in 0.9% NaCl or 0.9% NaCl alone (vehicle control). Mice were sacrificed on day 111.

4.2.4.1 Physiological lung measurements and histological evaluation of remodelling processes after 110 days of treatment

Measurements of respiratory mechanics were performed using the *flexiVent* ventilation setup. In this study, different parameters were measured, which allowed parametric distinction between airway and tissue mechanics. Using the single frequency forced oscillation technique, the total respiratory system resistance and elastance were analysed, reflecting the level of constriction and the stiffness of the lung. The respiratory system input impedance was analysed using the low frequency oscillation technique. By fitting the respiratory system input impedance to the constant phase model, the resistance of central and conducting airways (called newtonian resistance) and the resistance of small bronchioles (called tissue damping), could be distinguished. Each of these

parameters was first analysed in basal state and then, evolved airway hyperresponsiveness was analysed by challenging the mice with increasing concentrations of acetylcholine (AcCh).

Basal resistance and elastance of the whole lung tissue seemed to be marginally increased after OVA-treatment in CXCR6$^{GFP/GFP}$ mice in comparison to CXCR6$^{GFP/GFP}$ control treated mice (Figure 44). CXCR6 $^{+/GFP}$ mice did not show differences in total lung resistance or elastance comparing OVA and control treatment. Differentiation between the resistance of central airways (newtonian resistance) and small bronchioles (tissue damping) indicated stronger differences between CXCR6$^{+/GFP}$ and CXCR6$^{GFP/GFP}$ mice upon OVA-treatment. Newtonian resistance and

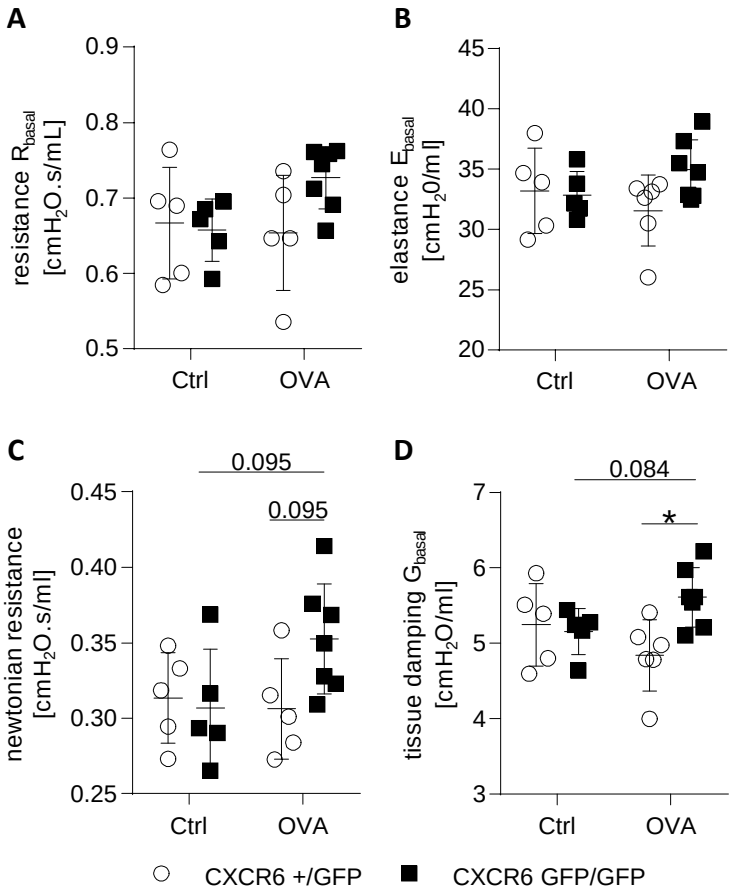

Figure 44 Basal physiological measurements of lung function
Lung function parameters were recorded every 30 seconds for a period of 30 min. A) Basal resistance of lungs. B) Basal elastance of lung tissue. C) Basal newtonian resistance of the central airways. D) Basal tissue damping of the lungs, reflecting energy dissipation in the lungs. Results for every mouse are shown and mean values ± SD are indicated (n=5-7). Statistical analysis was performed by Student's t-test and corrected for multiple comparison by FDR (*p<0.05).

tissue damping were increased in case of CXCR6$^{GFP/GFP}$ mice after 110 days of OVA-treatment, whereas both parameters were unchanged for CXCR6$^{+/GFP}$ mice. Although lung tissue might show changes in a basal state, the airway hyperresponsiveness to unspecific stimuli is a more characteristic indicator of asthma. Therefore, the responsiveness of lung tissue to increasing concentrations of AcCh was analysed in the next step. OVA-treated mice showed a tendency of increased responsiveness to AcCh for all parameters in comparison to control-treated mice (Figure 45). In case of elastance of the lung tissue and restriction of the bronchioles (tissue damping), the increased responsiveness was significant for OVA-treated CXCR6$^{+/GFP}$ mice. In the group of CXCR6$^{GFP/GFP}$ mice, huge variations of the mean values prevented significance, although the mean values for all parameters were slightly increased in comparison to values of CXCR6$^{+/GFP}$ mice.

Constriction of central and peripheral airways is a result of remodelling processes caused by inflammation. In asthma, remodelling is characterised by increased amounts of subepithelial collagen and increased mucus secretion of epithelial cells. Therefore, these parameters were analysed by histological stainings. Collagen amount and mucus secretion were visualised by Ladewig's trichrome (TRC) and Periodic acid–Schiff (PAS) staining, respectively, whereas overall changes in the tissue were observed by hematoxylin-eosin (HE)-staining. HE-staining allows differentiation of cells in tissue and provides an overview of possible remodelling processes. Both OVA-treated CXCR6$^{+/GFP}$ and CXCR6$^{GFP/GFP}$ mice seemed to show an increase of the thickness of septa in comparison to control treated animals (Figure 46, left panel). The quantification revealed that only CXCR6$^{GFP/GFP}$ mice showed significantly increased thickness after 110 days of OVA-treatment (Figure 47A). Enhanced thickness of septa may be accompanied by enhanced oedema formation, which was determined by wet-to-dry ratio. Indeed, a significant increase of this parameter was only detected in OVA-treated CXCR6$^{GFP/GFP}$ mice in comparison to control treated animals (Figure 47D), whereas OVA-treated CXCR6$^{+/GFP}$ mice showed normal values. TRC-staining of bronchial tissue (Figure 46, middle panel) revealed that OVA-treatment increased the thickness of airways' collagen surrounding (blue colour). Again, only the increase for CXCR6$^{GFP/GFP}$ mice was significant after quantification (Figure 47C). Mucus secreting cells are stained in darker purple than other cells in PAS-staining. Such cells were detectable in OVA treated mice, but not in control treated mice (Figure 46, right panel).

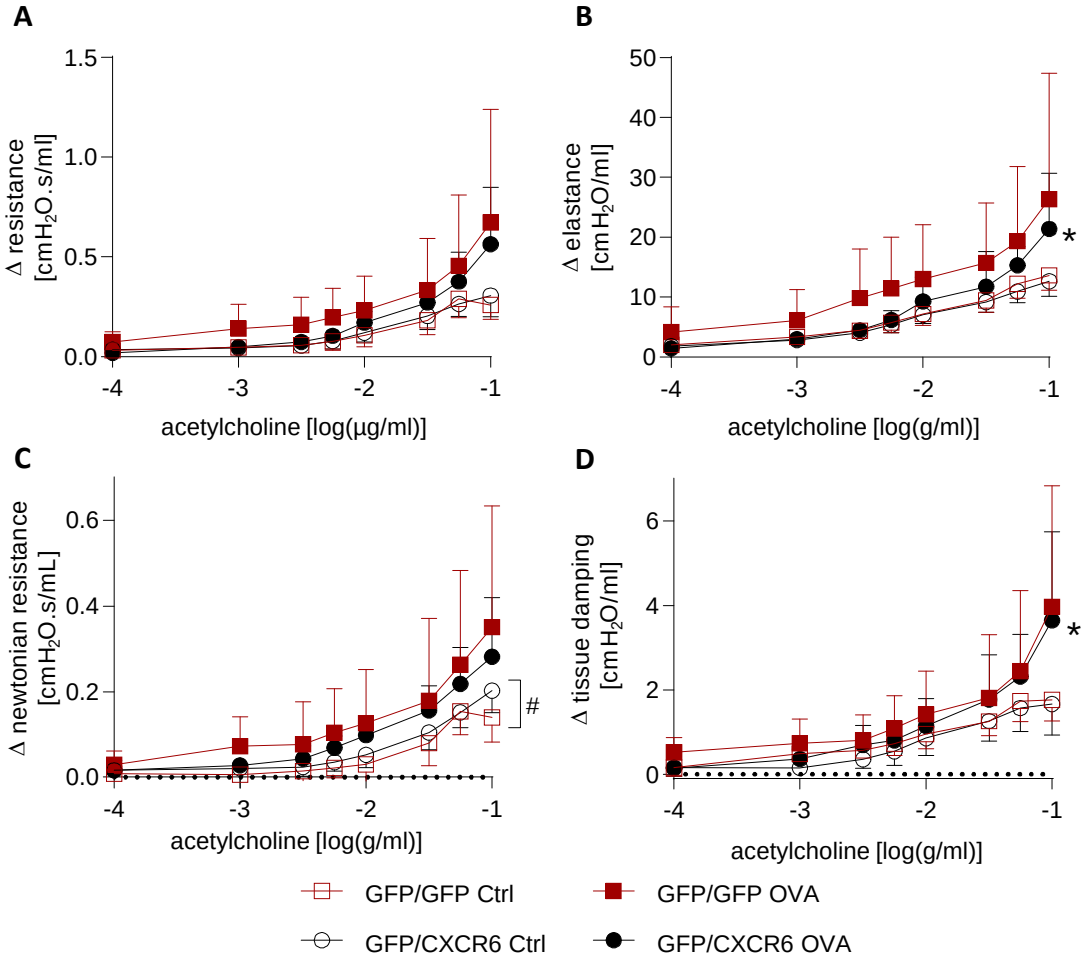

Figure 45 Measurement of airway hyperresponsiveness
To exclude basal differences for each parameter, means of data after application of 0.0 g/ml acetylcholine were subtracted from every data point, which results in Δ values for every parameter. A) Δ Resistance of lungs. B) Δ Elastance of lung tissue. C) Δ Newtonian resistance of the central airways. D) Δ Tissue damping of the lungs. Results for every mouse are shown and mean values ± SD are indicated. Statistical analysis was performed by comparing the reactions to every AcCh concentration by Student's t-test and corrected for multiple comparison by FDR using *SAS* software. Asterisks indicate significant differences for challenging with 100 ng/ml AcCh in comparison to Ctrl treated mice of the corresponding genotype (*p<0.05).

Quantification revealed that both CXCR6$^{+/GFP}$ and CXCR6$^{GFP/GFP}$ mice showed a similar increase of mucus producing cells (Figure 47C) upon OVA-treatment.

In summary, both CXCR6$^{+/GFP}$ and CXCR6 $^{GFP/GFP}$ mice developed airway hyperresponsiveness after OVA-treatment and showed increased mucus production and collagen deposition, which seemed to be almost independent of CXCR6-expression. However, further analysis revealed that

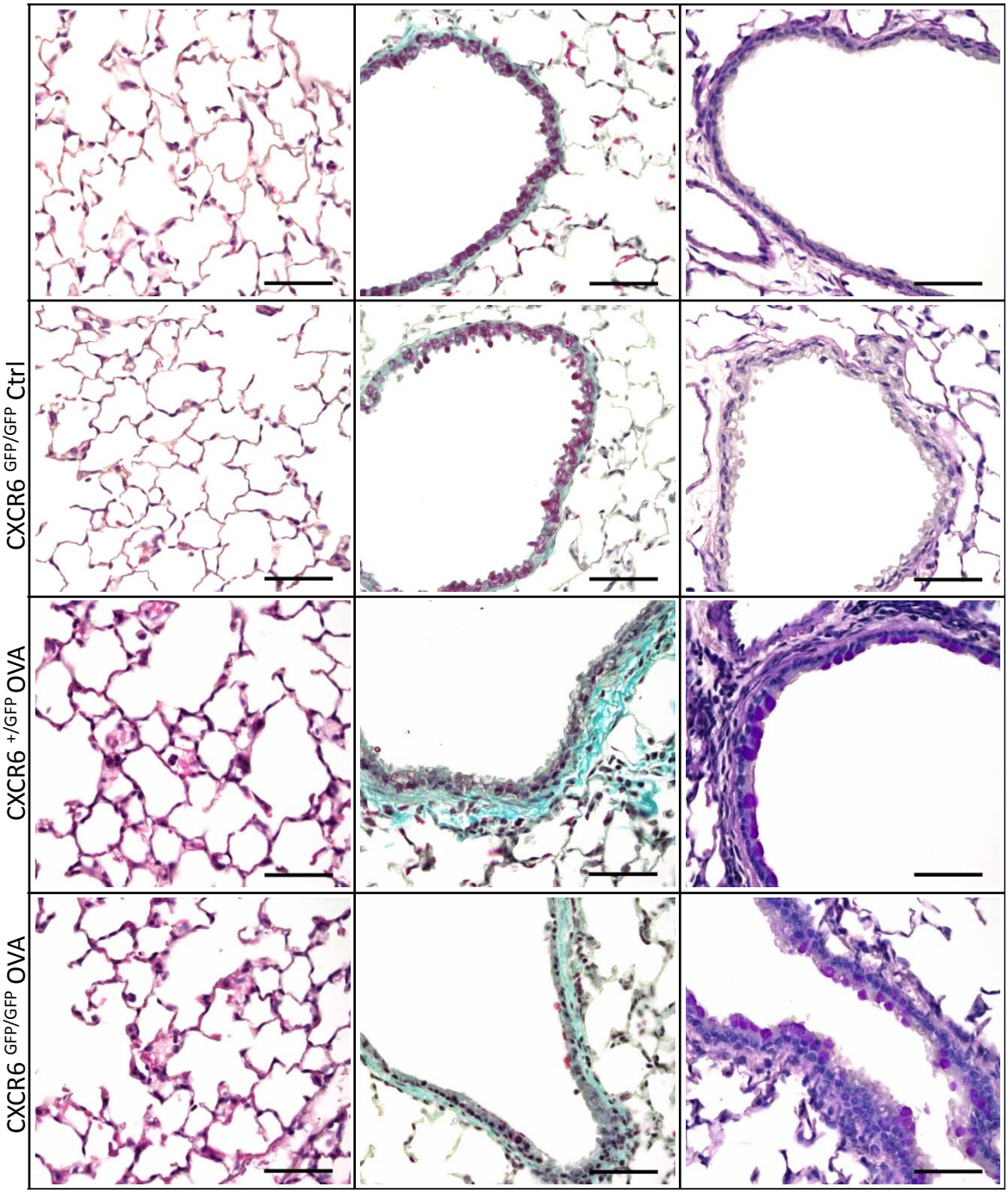

Figure 46 Histological analysis of lung tissue after sensitisation for 110 days
Fixated lung tissue was dehydrated and paraffin embedded prior to performance of 3 µm sections. Lung sections were stained with HE (left), TRC to visualise collagen fibres (blue) and by PAS to visualise mucus secreting cells (dark purple). HE-stainings show overviews of the alveolar space, whereas in the middle and right panel bronchioles are highlighted. Representative pictures for every treatment group, out of at least 5 pictures per animal and staining, were depicted. Black scales indicate a length of 50 µm.

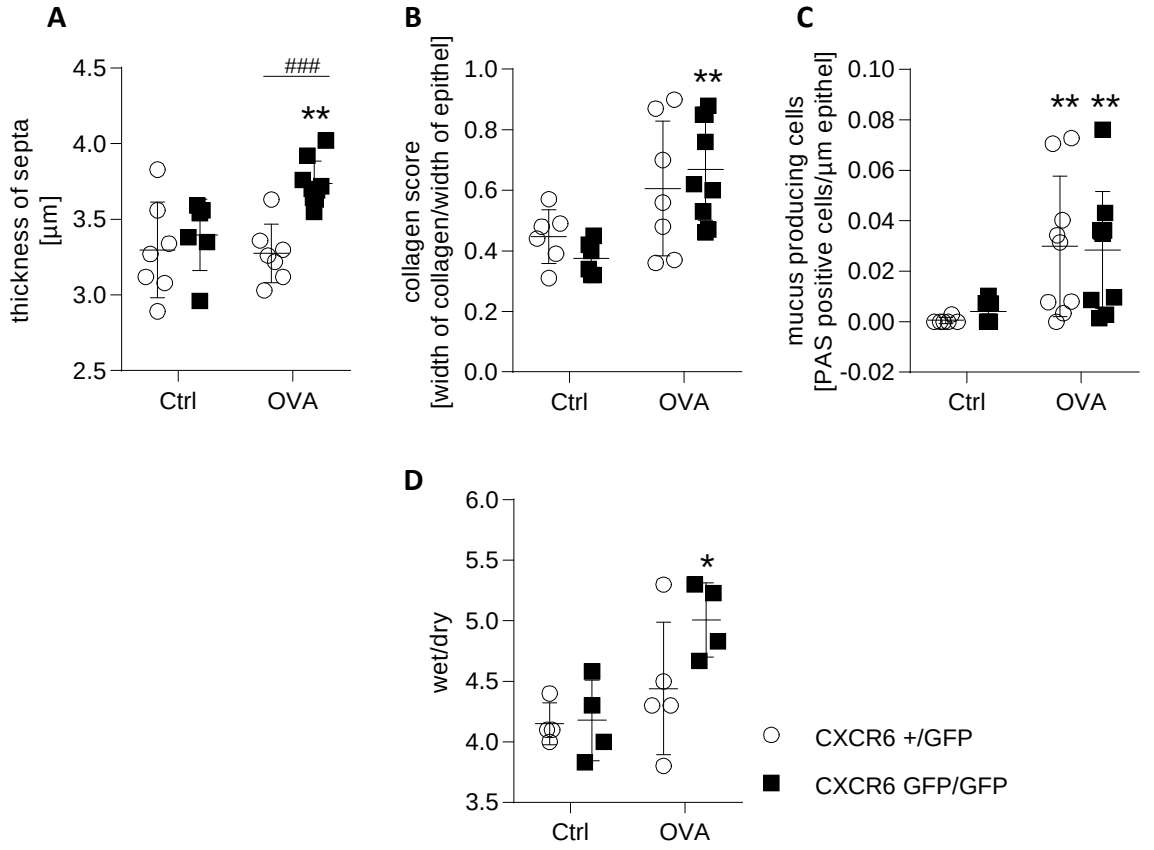

Figure 47 Histological analysis and oedema formation in lung tissue within the 110-days-model
A) Thickness of septa, measured at least in 10 regions of 5 pictures per animal of HE-stained sections. B) Collagen score expressed as ratio of the width of collagen and the width of epithelial cell layer. Ratios were measured at least in 5 regions of 5 pictures per animal of TCR-stained sections C) PAS positive cells per µm epithelium. Positive cells were measured at the length of all bronchioles and the bronchus of each lung slice of all animals. D) Wet-to-dry ratio of lung tissue. Animals were treated as indicated for a period of 110 days. Wet-to-dry ratio was determined using the Post-caval lobe. The value for each animal is shown. Error bars and lines represent mean values ± SD (n=4-5). Statistical analysis was performed by Student's t-test and corrected for multiple comparison by FDR. Asterisk indicates difference from control mice (*$p<0.05$) and hashes indicate differences between $CXCR6^{+/GFP}$ and $CXCR6^{GFP/GFP}$ mice (###$p<0.001$).

after 110 days of OVA-treatment basal constriction of small bronchioles (tissue damping) and oedema formation were more increased in the lungs of $CXCR6^{GFP/GFP}$ mice than in lungs of $CXCR6^{+/GFP}$ mice.

4.2.4.2 **Cell recruitment after 110 days of treatment**

The development of asthmatic disease involves a strong interplay between recruited and resident cells. This was obvious after 35 days of OVA-sensitisation, when cell recruitment into the alveolar space was strongly increased (Figure 37). After 110 days, the general recruitment of leukocytes (Figure 48A) into the alveolar space was less obvious. $CXCR6^{+/GFP}$ mice showed a 3-fold increase in the number of leukocytes into the alveolar space, but this was not significant. In $CXCR6^{GFP/GFP}$ mice, the number of leukocytes was not increased after 110 days of treatment. Furthermore, OVA-treated $CXCR6^{+/GFP}$ mice showed a significant 4-fold increase of eosinophils in BAL-fluid in comparison to control-treated animals (Figure 48B), whereas the number of monocytic cells was not increased after 110 days of OVA treatment (Figure 48C). Similar number of eosinophils was detectable in OVA-treated $CXCR6^{GFP/GFP}$ mice after 110 days. However, this increase was not significant due to higher number of eosinophils in lungs of control treated mice caused by one outlier (according to Grupps's test). The analysis of CD4-positive lymphocytes revealed interesting differences comparing $CXCR6^{+/GFP}$ and $CXCR6^{GFP/GFP}$ mice. There was a clear 2-fold increase of the number of CD4-positive and of CD4- and GFP-positive lymphocytes in $CXCR6^{+/GFP}$ mice after OVA-treatment, which was not detectable in BAL-fluid of OVA-treated $CXCR6^{GFP/GFP}$ mice (Figure 48D and E). Control treated animals of $CXCR6^{+/GFP}$ and $CXCR6^{GFP/GFP}$ mice did not differ in their number of CD4-postive lymphocytes in BAL-fluid. Since the weak increase of T_H2 cells (CD4+, ST2+) in both mice groups after OVA-treatment was not significant in comparison to control animals (Figure 48F), another CD4-positive subset of lymphocytes should be responsible for the observed differences. Finally, insignificant lower number of CD4-, GFP- and NK1.1-positive cells (NKT cells) was detected in the BAL-fluid of $CXCR6^{GFP/GFP}$ mice in comparison to BAL-fluid of $CXCR6^{+/GFP}$ mice after OVA-treatment (Figure 48G). Upon OVA-treatment, number of NKT cells showed 2-fold increase in BAL-fluid of $CXCR6^{+/GFP}$ mice, whereas the number of NKT cells in BAL-fluid of $CXCR6^{GFP/GFP}$ mice was not elevated after 110 days of treatment.

In summary, $CXCR6^{+/GFP}$ and $CXCR6^{GFP/GFP}$ mice did not show any differences in the development of subchronic asthma (35 days model). In contrast, after 110 days of OVA-treatment, the basal tissue damping and the oedema formation were increased in $CXCR6^{GFP/GFP}$ mice in comparison to $CXCR6^{+/GFP}$ mice, whereas the CD4-positive cell number was decreased in $CXCR6^{GFP/GFP}$ mice.

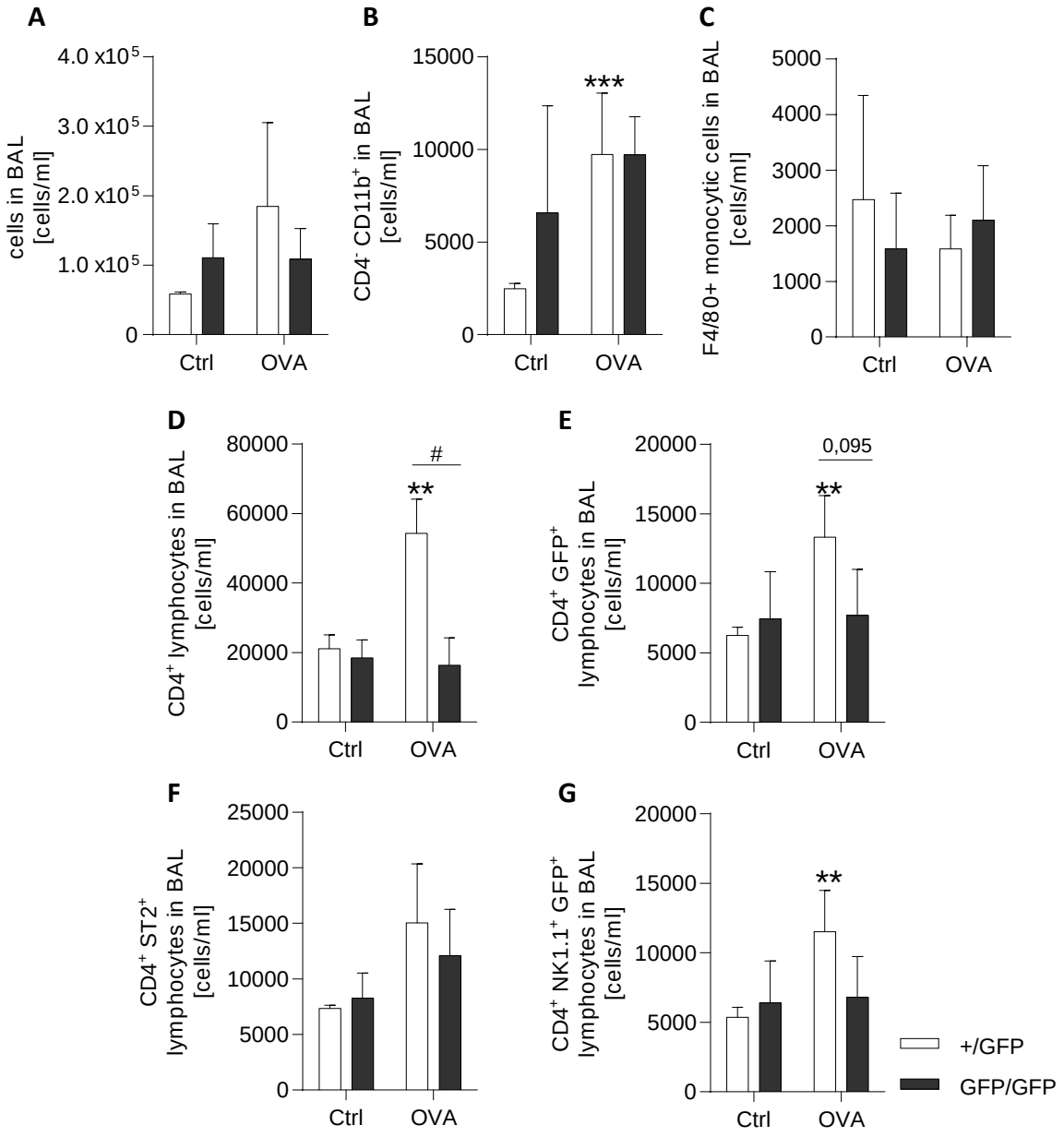

Figure 48 Cell recruitment into BAL after 110 days of treatment
During flow cytometry analysis, the different cell gates were determined by FSC/SSC and the leucocyte subtypes characterised by antibody staining. A) Number of all cells in BAL. B) Number of CD11b-positive cells (eosinophils). C) Number of F4/80-positive monocytic cells. D) Number of CD4-positive lymphocytes (T helper cells). E) Number of CD4- and GFP-positive lymphocytes (T helper cells potentially expressing CXCR6). F) Number of CD4- and ST2-positive lymphocyte (T_H2 cells). G) Number of CD4- and NK1.1-positive lymphocytes (NKT cells). Data represent mean + SD and statistical analysis was performed by Student's t-test and corrected for multiple comparison by FDR (n=4-5). Asterisks indicate differences from control mice (**p<0.01, ***p<0.001) and hashes indicate differences between $CXCR6^{+/GFP}$ and $CXCR6^{GFP/GFP}$ mice (#p<0.05).

4.3 Role of endothelial ADAM10 in development of OVA-induced asthma in mice

The endogenous ligand of CXCR6, the chemokine CXCL16 is expressed as a transmembrane protein and can be shed by ADAM10. Furthermore, the activation of endothelial ADAM10 leads to the release of a huge variety of soluble factors and the cleavage of junction and adhesion molecules, e.g. CX_3CL1 and VE-cadherin, which are mediators of leukocyte recruitment and endothelial permeability[81]. Thus, ADAM10 may affect inflammatory events in the lung by several more pathways than only via CXCL16. So far, the cell-specific function of ADAM10 in asthmatic disease was only investigated in B cells[80]. In the present study the role of endothelial ADAM10 during the development of subchronic asthma (35-days model) was analysed by the investigation of Tie2 *Adam10*$^{-/-}$ (endothelial knock-out of ADAM10) and ADAM10flox/flox mice (littermates).

4.3.1 Responsiveness of Tie2 *Adam10*$^{-/-}$ mice and littermates to 35 days of OVA sensitisation

First, the responsiveness of mice to the sensitisation process was verified by analysis of the IgE-concentration in serum. Both Tie2 *Adam10*$^{-/-}$ mice and littermates showed approx. 100 ng/ml IgE in serum after OVA treatment, which is a significant 5-fold increase in IgE concentration in serum compared to control-treatment. This indicated no differences in sensitisation due to endothelial ADAM10-deficiency (Figure 49A). Furthermore, the protein amount in BAL-fluid of

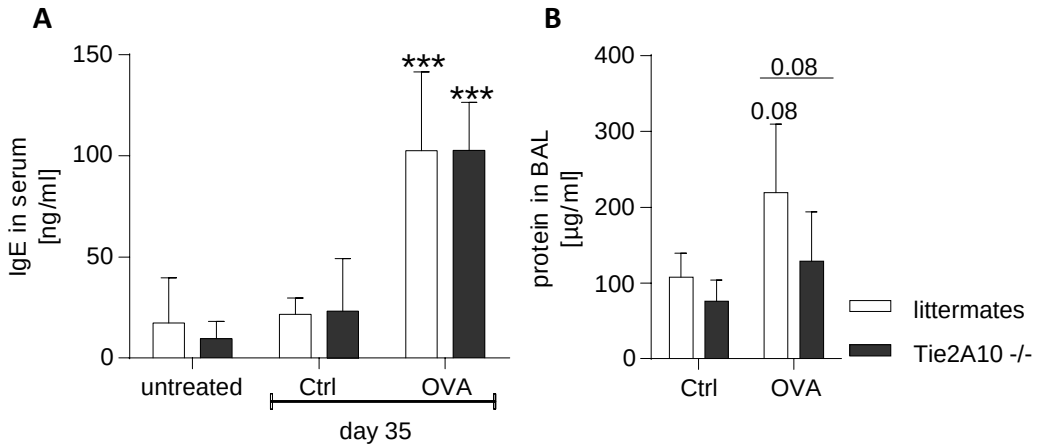

Figure 49 Sensitisation of Tie2 *Adam10*$^{-/-}$ mice and littermates for 35 days
Animals were treated as shown in Figure 36. A) Concentration of IgE in serum of OVA and control treated mice were measured by ELISA specific for mouse IgE. B) Protein concentrations of BAL-fluid were measured by BCA assay. Data are shown as mean + SD (n=5-6). Statistical analysis was performed by Student's t-test and corrected for multiple comparison by FDR. Asterisks indicate differences from control mice (***p<0.001).

OVA and control treated mice was measured (Figure 49B). There was a 2-fold increase of protein concentration in BAL-fluid of OVA-treated littermates in comparison to control-treated animals, which was absent in Tie2 *Adam10*$^{-/-}$ mice. These results indicated a successful sensitisation of both OVA-treated mice groups.

4.3.2 Histological analysis of Tie2 *Adam10*$^{-/-}$ mice and littermates within the 35-days model

Lung tissue sections were analysed for remodelling processes, including the thickness of septa (HE-stained slices), collagen deposition (TCR-stained slices), and the number of mucus producing cells (PAS-stained slices) (Figure 50 and Figure 51). 35 days of OVA-treatment did neither result in increase of septa thickness nor in enhanced collagen deposition (Figure 51A, B) in Tie2 *Adam10*$^{-/-}$ or littermate mice in comparison to control animals. However, there was a 10-fold increase in the number of mucus producing cells, identified as PAS positive cells, in littermates treated with OVA in comparison to control-treated mice. This increase was not significant, due to high variances. However, Tie2 *Adam10*$^{-/-}$ mice did not show increased number of PAS positive cells in the epithelial cell layer (Figure 51C).

As mentioned above, 35 days of OVA-treatment mimic the development of subchronic asthma, which lacks massive tissue remodelling at this disease stage. Therefore, the analysis of Tie2 *Adam10*$^{-/-}$ mice and littermates focused on cell recruitment and cytokine secretion.

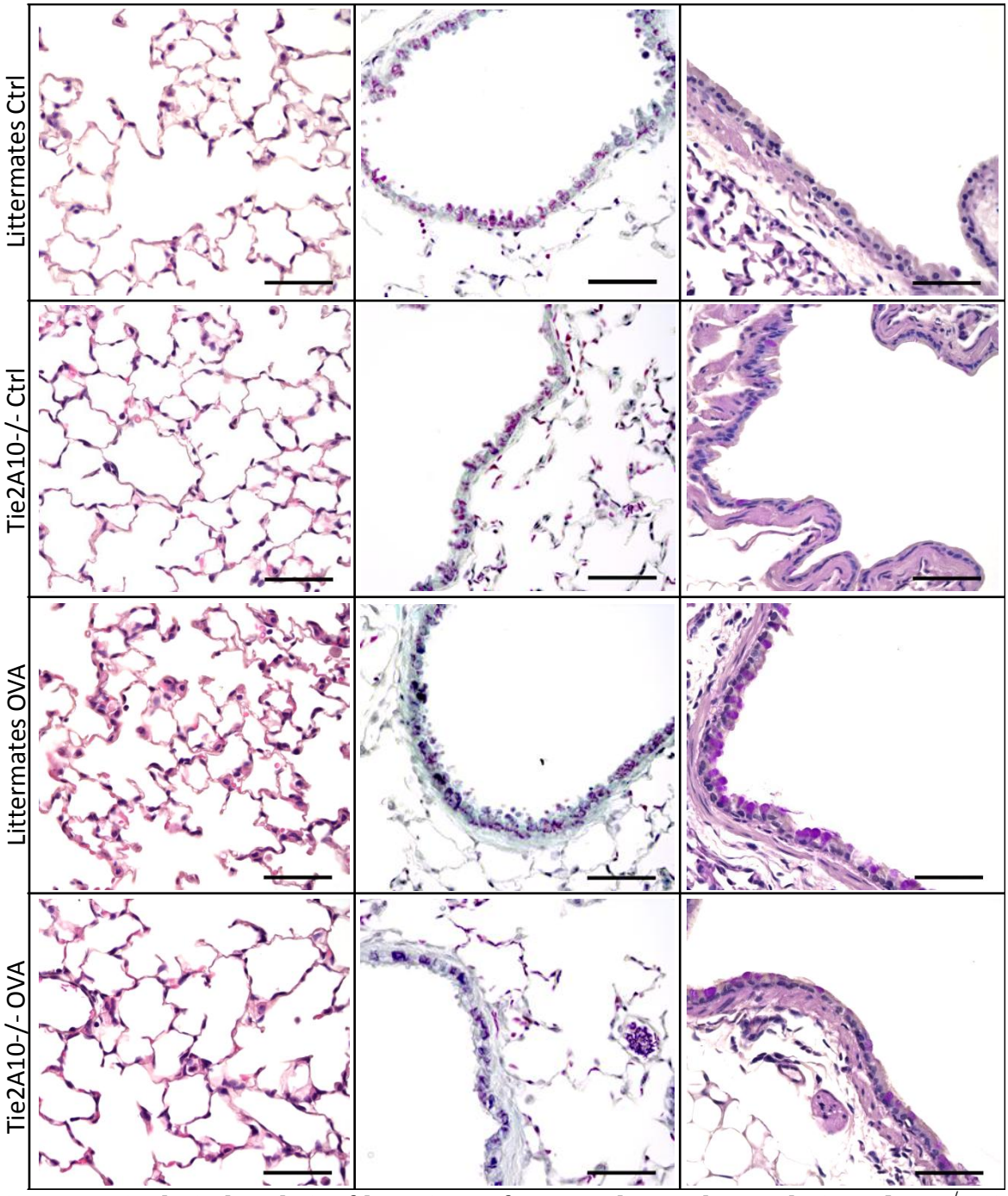

Figure 50 Histological analysis of lung tissue of OVA and control treated Tie2 *Adam*10$^{-/-}$ mice and littermates

Fixated lung tissue was dehydrated and paraffin embedded prior to performance of 3 µm sections. Lung sections were stained with HE (left), TRC to visualise collagen fibres (blue) and by PAS to visualise mucus secreting cells (dark purple). HE-stainings show overviews of the alveolar space, whereas in the middle and right panel bronchioles are highlighted. Representative pictures for every treatment group, out of at least 5 pictures per animal and staining. Black scales indicate a length of 50 µm.

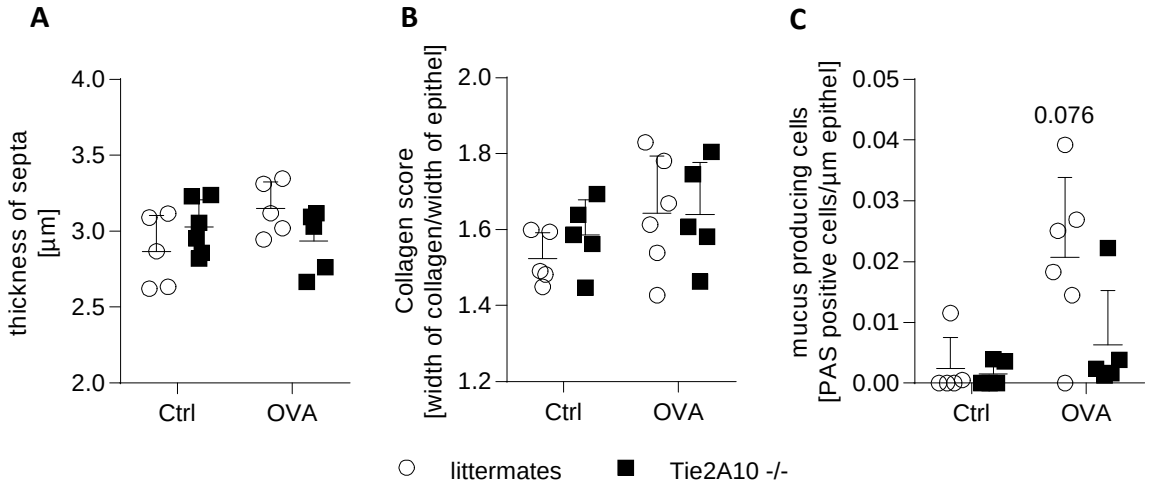

Figure 51 Quantification of histological analysis of lung tissue after 35 days of OVA and control treatment

A) Thickness of septa, measured at least in 10 regions of 5 pictures per animal of HE-stainings B) Collagen score expressed as ratio of the width of collagen and the width of epithelial cell layer. Ratios were measured at least in 10 regions of 5 pictures per animal of TCR-staining. C) PAS positive cells per µm epithelium. Positive cells were measured at the length of all bronchioles and the bronchus of each lung slice of all animals. The average value for each animal is shown. Error bars and lines represent mean values ± SD (n=5-6). Statistical analysis was performed by Student's t-test and corrected for multiple comparison by FDR. No significant differences were observed.

4.3.2.1 **Role of endothelial ADAM10 in cell recruitment and cytokine expression**

The investigation of cell recruitment after 35 days of sensitisation served to analyse the differences between Tie2 *Adam10*$^{-/-}$ mice and littermates, which were indicated by slight differences in protein amount in BAL-fluid and the number of PAS positive cells. Therefore, the total number of leukocytes in BAL-fluid was analysed first. There was a slightly enhanced amount of leukocytes in BAL-fluid of OVA-treated littermate mice, not reaching significance due to high variations (Figure 52A). In contrast, in Tie2 *Adam10*$^{-/-}$ mice the leukocyte number in BAL-fluid was not changed upon OVA-treatment. Moreover, the detailed analysis of accumulated granulocytes and monocytic cells (Figure 52B-D) in BAL-fluid showed significant differences comparing OVA treated Tie2 *Adam10*$^{-/-}$ mice and littermates. In littermates there was a 7-fold increase of the number of eosinophils, a 3-fold increase of the number of neutrophils and a 5-fold increase in the number of monocytic cells upon OVA-treatment in comparison to control treated littermates. These increases were absent in OVA treated Tie2 *Adam10*$^{-/-}$ mice. The number of eosinophils and monocytic cells increased (1.5- and 2.5-fold, respectively) in BAL-fluid of Tie2 *Adam10*$^{-/-}$ mice upon OVA-treatment in comparison to control treatment. However, these increases were weak and significantly lower than the recruitment into the alveolar space of OVA-treated littermates.

Lymphocytes, especially T helper cells, play an important role in asthma development. Therefore, the BAL lymphocyte composition was analysed in more detail. The increase of the total number of CD4-positive lymphocytes was not significant for either of the OVA treated mice groups (Figure 52E) in comparison to control treated mice. Despite this fact, CD4-positive lymphocyte subpopulations were further distinguished. Interestingly, the number of T_H2 cells was 5-fold increased in OVA-treated Tie2 *Adam10*$^{-/-}$ mice (Figure 52F) in comparison to control mice, whereas in BAL-fluid of OVA-treated littermates the number of T_H2 cells increased only 2-fold. Additionally, the number of T_H1 cells was equally increased in lungs of littermates and Tie2 *Adam10*$^{-/-}$ mice. Both mice groups showed insignificant 2-fold increases of T_H1 cells in BAL-fluid upon OVA-treatment in comparison to control treatment. Furthermore, no significant differences were observed, depending on endothelial ADAM10 expression with regard to recruitment of CD4-positve lymphocyte subpopulations.

Leukocyte recruitment and tissue damage are mediated by cytokine production, which was analysed by RT-qPCR of lung tissue and ELISA of BAL-fluid and serum (Figure 53). Although the expression of IL-5 was not significantly increased upon OVA-treatment, there was a tendency of higher IL-5 expression in OVA-treated littermates in comparison to Tie2 *Adam10*$^{-/-}$ mice (Figure 53A). Furthermore, mRNA expression of eotaxin (Figure 53B) and IL-13 (Figure 53C) were significantly increased in lung tissue of littermates after OVA-treatment in comparison to control mice. In lung tissue of OVA-treated littermates, eotaxin expression was approx. 9-fold increased and IL-13 expression was 8-fold increased. In contrast, lung tissue of OVA-treated Tie2 *Adam10*$^{-/-}$ showed less increased expression levels of eotaxin and IL13 (4-fold and 2-fold, respectively). In case of OVA-induced eotaxin expression, differences between Tie2 *Adam10*$^{-/-}$ mice and littermates were significant. The mRNA expression of collagen 1A1 was slightly increased in both Tie2 *Adam10*$^{-/-}$ and littermate mice after OVA-treatment, but this did not reach significance (Figure 53D).

Finally the accumulation of CXCL16 in serum and BAL was analysed. Serum levels were very weakly, but not significantly increased in both Tie2 *Adam10*$^{-/-}$ and littermate mice after OVA-treatment in comparison to the respective control mice. Analysis of BAL-fluid concentration of CXCL16 revealed only a slight enhancement in Tie2 *Adam10*$^{-/-}$ mice upon OVA-treatment. However, no significant changes were observed for any treatment group or genotype.

In summary, mice deficient in endothelial ADAM10 showed slight protection against increased permeability of the vascular system measured by protein amount in BAL-fluid and the tendency of increased mucus production by epithelial bronchial cells in comparison to littermate mice. Together with the significant lower amounts of granulocytes and monocytic cells and the weaker expression of eotaxin and IL-13, these data indicate a protection of Tie2 *Adam10*$^{-/-}$ mice during the development of OVA-induced subchronic asthma.

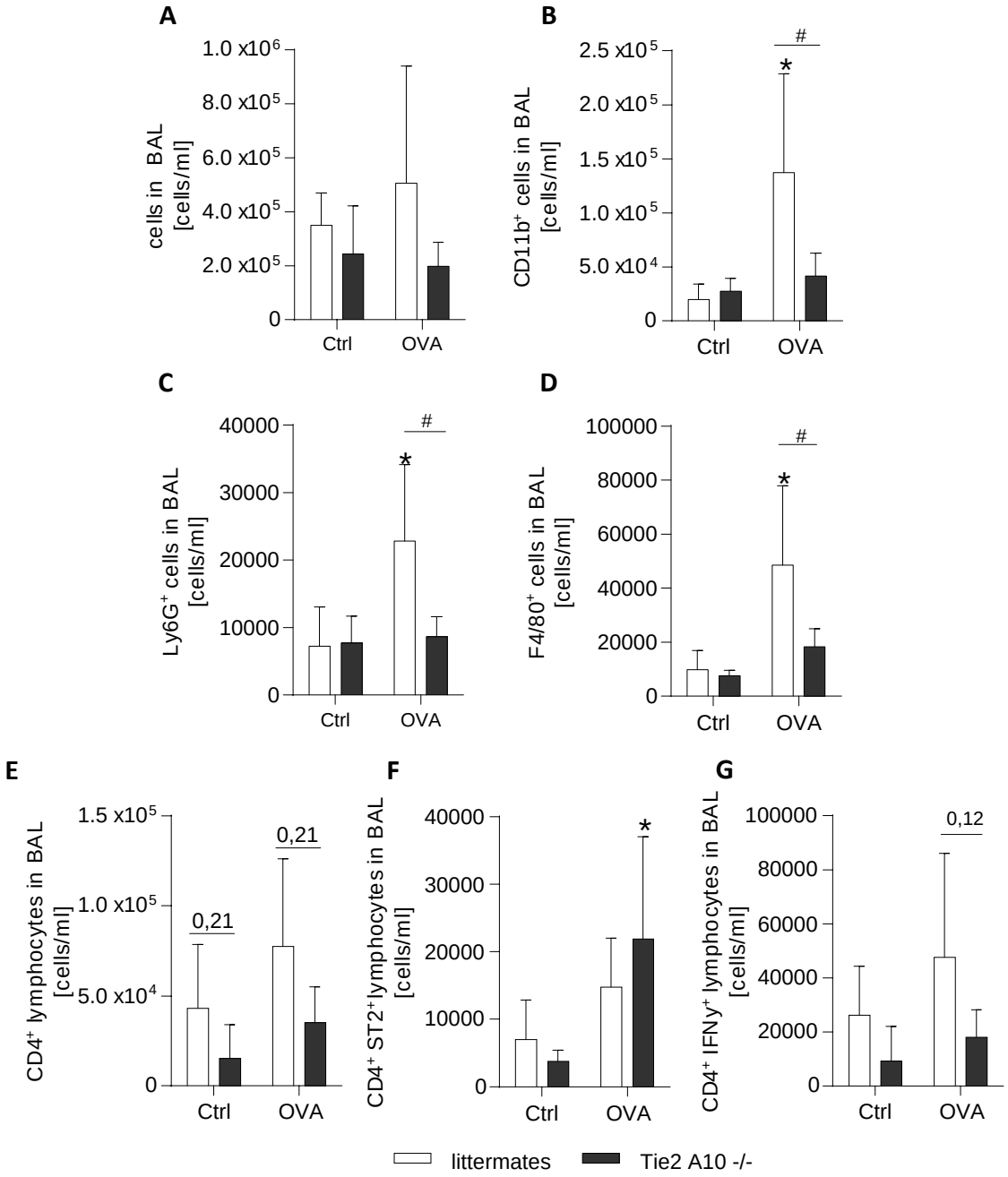

Figure 52 Cells in BAL-fluid of Tie2 *Adam*10$^{-/-}$ mice and littermates after 35 days of treatment
A) Number of all cells in BAL-fluid. During flow cytometry analysis, the granulocytes, monocytic and lymphocytes cell gates were determined by FSC/SSC and subtypes were characterised by antibody staining. B) Number of CD11-positive cells (eosinophils). C) Number of Ly6G-positive cells (neutrophils). D) Number of F4/80-positive cells (monocytic cells). E) Number of all CD4-positive lymphocytes in BAL. F) CD4- and ST2-positive lymphocytes (T_H2 cells). G) Number of CD4- and IFNγ-positive cells (T_H1 cells). Data represent mean + SD and statistical analysis was performed by Student's t-test and corrected for multiple comparison by FDR (n=5-6). Asterisks indicate differences from control mice (**p<0.01) and hashes indicate differences between CXCR6$^{+/GFP}$ and CXCR6$^{GFP/GFP}$ mice (#p<0.05).

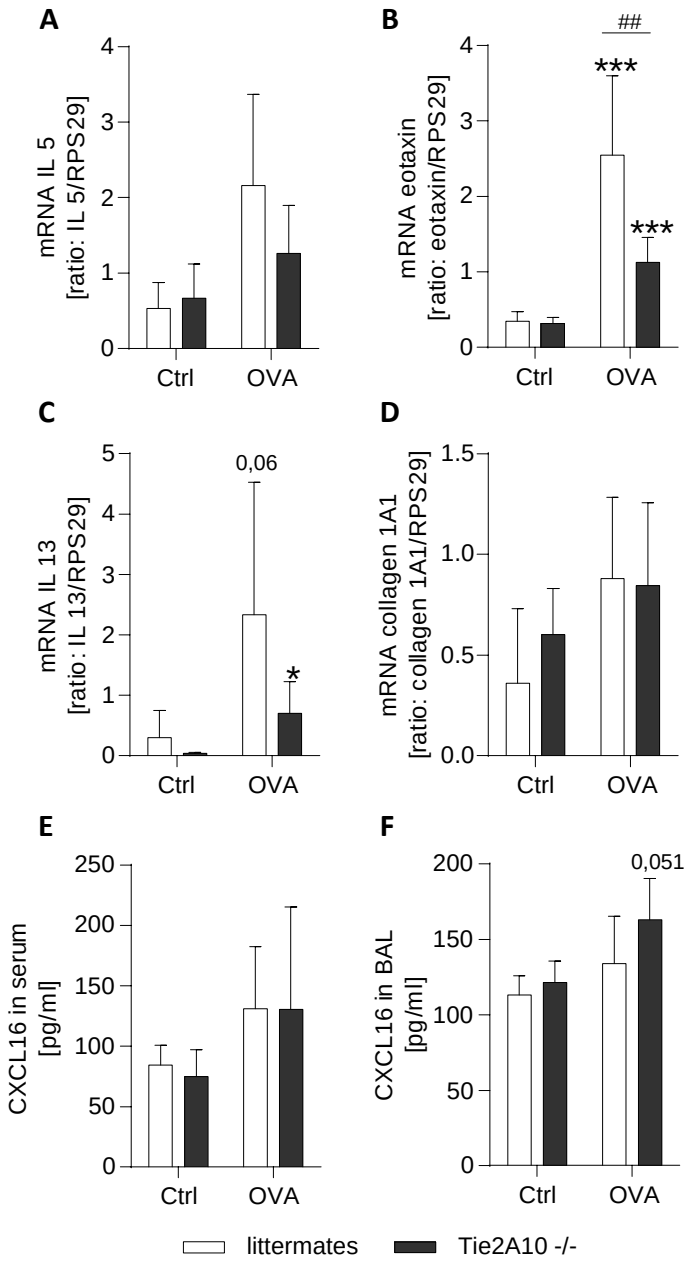

Figure 53 mRNA expression of inflammatory and fibrotic markers in lung tissue and CXCL16 levels in BAL-fluid and serum

A-D) Quantification of mRNA expression in lung tissue was performed by RT-qPCR and expressed in relation to the housekeeping gene RPS29. A) IL-5 expression in lung tissue. B) Eotaxin expression in lung tissue. C) IL-13 expression. D) Collagen 1A1 expression. E-F) Accumulation of CXCL16 in serum and BAL. Chemokine concentrations were measured by ELISA. Data represent mean + SD and statistical analysis was performed by Student's t-test and corrected for multiple comparison by FDR (n=4-6). Asterisks indicate differences from control mice (***$p<0.001$) and hashes indicate differences between $CXCR6^{+/GFP}$ and $CXCR6^{GFP/GFP}$ mice (##$p<0.01$).

5 Discussion

The mammalian chemokine receptor CXCR6 is unique in the GPCR family of chemokine receptors, as it endogenously expresses a DRF motif instead of the common DRY motif at the interface of transmembrane region three and the second intracellular loop. CXCR6 is involved in the recruitment of different leukocytes to sites of inflammation and in progression of different inflammatory diseases[45,46,108]. Since transmembrane chemokine CXCL16 which is the only known ligand for CXCR6 is constitutively expressed by lung epithelial[11] and endothelial cells, it was thought the receptor may be relevant for homing of leukocytes into lung tissue[11].

The present thesis investigates these specialised functions of CXCR6 on the molecular level and in an *in vivo* model of allergic lung inflammation. In the first part, the physiological importance of the unique DRF motif of CXCR6 was analysed and compared with CXCR6 variants expressing the more common DRY motif or a signalling-dead DNF motif. *Vice versa* CX_3CR1 was analysed for importance of the endogenous DRY motif in comparison to mutants carrying DRF or DNY. In a second part, the relevance of CXCR6 in murine experimental asthma was investigated. Two different asthma models (35-days and 110-days model) were used and lung tissue and the recruitment of inflammatory cells were analysed. In a third part, the impact of endothelial ADAM10 on experimental murine asthma was investigated. ADAM10 is the protease, which is most relevant for shedding of the transmembrane chemokine CXCL16. Therefore, Tie2 *ADAM10*$^{-/-}$ mice were analysed within the 35-days model of OVA-induced asthma.

5.1 *In vitro* analysis of the DRF motif of CXCR6 shows that $F^{3.51}Y$ decreases maximal signalling levels and migration

First, the endogenous ^{126}DRF motif of CXCR6 was investigated for its importance on signalling and cell migration. This was analysed and compared in two different experimental expression systems (HEK293 and THP-1 cells). The results are summarised in Table 8. CXCR6-WT was modified into the more common DRY motif and into the signalling-dead DNF motif. Expression, ligand binding, internalisation and recycling processes were analysed in HEK293 cells and were not affected by both mutations of the DRF motif. In contrast, analysis of CXCR6 variants expressed by the monocytic cell line THP-1 uncovered increased activity of the receptor in calcium and chemotaxis assays when expressing the DRY instead of the DRF motif. Notably, in

THP-1 cells, CXCR6-CXCL16 interaction lead to firm binding and adhesion of the DRY or DRF variants and this was abrogated by the DNF mutation. This indicates that these receptor functions were dependent on CXCR6-mediated signalling or G protein interaction. By contrast, adhesion and ligand binding were independent from intracellular signalling in HEK293 cells. Mutation of the endogenous DRY motif in CX_3CR1 into DRF demonstrated that both motifs promote ligand binding. The activity of CX_3CR1 in terms of the induction of cell migration was lower in the mutated DRF variant in comparison to the wild type receptor expressing the endogenous DRY motif (Table 9). These functional aspects of CXCR6-CXCL16 interaction and CXCR6-mediated signalling as well as differences between CXCR6 and other chemokine receptors will be discussed in detail in the following paragraphs.

Table 8 Summary of the analysis of DRF motif alterations in CXCR6
Each receptor variant was analysed in comparison to the wild type receptor CXCR6-DRF. Symbol description: no change (=); not analysed (n.a.); increase: ↑; decrease: ↓.

chemokine receptor function	**protein and expression system**	**results of the indicated mutation in comparison to wild type**	
		$R^{3.50}N$	**$F^{3.51}Y$**
expression	CXCR6 in HEK293 cells	=	=
ligand binding		=	=
internalisation		=	=
recycling		=	=
adhesion		=	=
calcium signalling		↓	=
expression	CXCR6 in THP-1 cells	=	=
ligand binding		↓	=
adhesion		↓	=
Akt signalling		↓	=
calcium signalling		↓	↑
chemotactic migration		↓	↑

Table 9 Summary of the analysis of DRY motif alterations in CX_3CR1
Each receptor variant was analysed in comparison to the wild type receptor CX3CR1-DRY. Symbol description: no change (=); not analysed (n.a.); increase: ↑; decrease: ↓.

chemokine receptor function	protein and expression system	results of the indicated mutation in comparison to wild type	
		$R^{3.50}N$	$Y^{3.51}F$
expression	CX_3CR1 THP-1 cells	=	=
ligand binding		=	=
adhesion		(=)[35]	n.a.
migration		n.a.	↓

CXCL16-induced trafficking of CXCR6 in HEK293 cells is independent of DRF modifications

Trafficking of CXCR6 variants was analysed in terms of constitutive surface expression, CXCL16-induced internalisation and recycling to the cell surface in HEK293 cells. Surface expression was not affected by any mutation of the receptor. Surface expression analysis of CXCR6 variants after CXCL16 stimulation showed that internalisation of CXCR6 occurred in a DRF independent manner (Figure 54). The dynamin-inhibitor dynasore blocked internalisation of CXCR6 indicating that ligand binding of all CXCR6 variants induced internalisation into vesicles via dynamin-mediated formation of clathrin-coated pits or dynamin dependent caveolae-mediated endocytosis[109,110]. Usually this is followed by a rapid transport to the endosomal compartment. In fact, this is the most common pathway for chemokine receptor internalisation[98]. For several other chemokine receptors it has been shown that receptor internalisation is independent of G protein activation but dependent on intracellular phosphorylation of the receptors' C-terminus and intracellular ß-arrestin recruitment to the receptor[98,111]. The present thesis demonstrates that CXCR6 is internalised rapidly after ligand binding, but does not require the relevant motif for G protein coupling. This indicates that trafficking of CXCR6 is similar to that of other chemokine receptors. Beside internalisation pathways via clathrin-coated pits or caveolae, chemokine receptor internalisation mediated by lipid rafts has also been discussed in literature[98]. But since dynasore inhibited internalisation of CXCR6 completely, it is likely that lipid rafts may not be of relevance for the internalisation of CXCR6.

After internalisation, GPCRs and chemokine receptors are either subjected to lysosomal degradation or recycled to the cell surface. For recycling, endocytosed receptors are processed by endosomal-associated proteins and return back to the cell surface via the perinuclear recycling compartment[98]. Involved regulatory proteins include phosphatases, Rab GTPases (Rab: "Ras-related in brain) and β-arrestin. Some members of the Rab family are associated with either the rapid recycling pathway (Rab4) or the slow recycling pathway (Rab11). In case of chemokine receptors, different mechanisms have been reported. Interaction with the slow Rab11 pathway has been reported for CXCR2, which colocalises with Rab11 in the perinuclear compartment[111]. For CXCR4 colocalisation with both Rab4 and Rab11 was shown[112]. Regarding CXCR6, this study indicates that the receptor is partially recycled in a rapid way, since the receptor was detected on the cell surface 5 min after ligand removal. Moreover, recycling of CXCR6 via the slow recycling pathway might be relevant as well, since recycling was not completed after 30 min of analysis. Therefore, interaction of CXCR6 with Rab4 in addition to Rab11 is possible and further studies could investigate this issue in more detail. Nevertheless, the DRF motif mutation did not affect CXCR6 recycling in HEK293 cell (Figure 54).

It has also been demonstrated that dissociation of β-arrestin from the receptor is necessary for recycling to occur[98] and that the binding affinity of β-arrestin to receptors negatively correlates with receptor recycling velocity[98]. It has been proposed that the DRY motif of chemokine receptors can influence the interaction of the receptor with β-arrestin which would then affect chemotactic signalling of the receptor [31]. In contrast to these findings, the present study could not obtain evidence for a role of endogenous DRF or DRY in trafficking of CXCR6. Even the signalling-dead mutant DNF was still capable of interacting with the ligand CXCL16 and inducing rapid internalisation and recycling. Therefore, in case of HEK293 cells it seems unlikely that the DRF motif of CXCR6 is involved in interaction mechanisms with β-arrestin or other proteins involved in rapid protein trafficking. This thesis focussed on CXCR6 trafficking in HEK293 cells but it may be worthwhile to include THP-1 cells in further studies to investigate potential cell specific effects of $F^{3.51}Y$ mutation on trafficking. This could reveal different cell specific effects of this mutation on the chemotactic response.

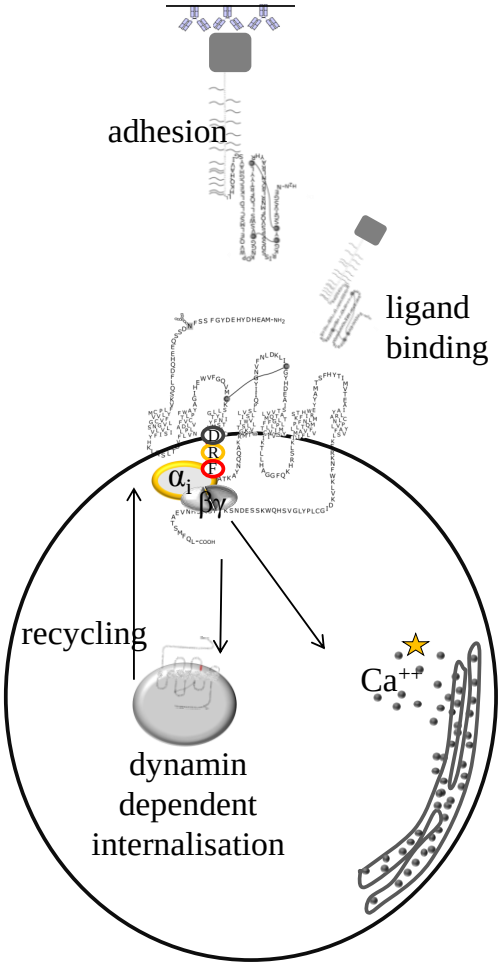

Figure 54 Relevance of the DRF motif of CXCR6 in HEK293 cells
CXCR6 variants were expressed in HEK293 cells. Adhesion to immobilised CXCL16-Fc and binding of soluble CXCL16-Fc as well as dynamin dependent internalisation and recycling were DRF motif independent. In HEK293 cells, only calcium signalling was shown to be DRY motif-dependent as it was abrogated due to $R^{3.50}N$ mutation (indicated by yellow star).

Signalling dependency of CXCL16-CXCR6-mediated adhesion is cell type specific

In HEK293 cells all receptor variants mediated firm adhesive interactions with immobilised CXCL16-Fc (Figure 54). These interactions were specific for CXCR6-CXCL16 interaction, since preincubation of HEK293 cells with soluble CXCL16, which led to ligand binding and subsequent internalisation of the receptor, prevented adhesion. As already shown for receptor internalisation, even the signalling-dead mutant CXCR6-DNF mediated adhesion of HEK293 cells to CXCL16-Fc. Furthermore, PTX pretreatment of HEK293 cells did not affect adhesion. Thus, CXCR6-mediated adhesion of HEK293 cells is independent of the DRF motif and intracellular signalling events activated by the chemokine receptor and its interaction with the G protein. These observations are in line with the view that chemokine binding to their receptors

does not require intracellular signalling mechanisms due to receptor activation[113–115]. In the two step model of chemokine receptor-ligand interaction, the extracellular loops and the N-terminus of the receptor are important for the interaction with the N-loop region of the core domain of the chemokine (site-I). This leads to interactions of the chemokine N-terminal part with the transmembrane and extracellular domains of the receptor (site-II), finally leading to activation. Site I alone was reported to be strong enough to generate binding for many chemokine–chemokine receptor interactions. For example, analysis of chimeras of the receptors CCR1 and CCR3, revealed that N-terminal domains of the chemokine receptors were sufficient for interaction with the respective chemokine, independent of any activation ability[114]. For CXCR6, experiments were performed in L1.2 cells in a previous study[115], showing that CXCR6-mediated CXCL16 binding is unaffected by PTX treatment. This report is well in line with the results of the present thesis analysing CXCR6 in HEK293 cells.

In contrast to the congruent findings in HEK293 cells and murine pre-B cells (L1.2), the present study indicates a cell-type specific signalling dependency of CXCR6-CXCL16-mediated adhesion in monocytic THP-1 cells. In THP-1 cells, ligand binding occurred temperature dependent, and adhesion was disrupted by CXCR6-DNF mutation or PTX pretreatment. These results suggest that G protein activation is required for ligand binding in THP-1 cells (Figure 56). Notably, regulation of ligand binding by intracellular receptor interaction with the G protein has been reported for the α2a adrenergic receptor[116]. This process depends on signalling mediated by an intact DRY motif. Moreover, in case of the β2 adrenergic receptor, G protein coupling resulted in increased agonist binding[117], which is in accordance with the ternary complex model[118]. This model proposes the formation of an agonist-promoted high affinity complex of agonist, receptor and G protein resulting in cooperative interactions among the different proteins. Coupling of the receptor to the G protein results in an active state of the receptor that binds agonist with high affinity, whereas the uncoupled receptor is inactive and exhibits low affinity for its agonist[119]. Interestingly, in the case of CXCR6, adhesion and ligand binding were not affected by $F^{3.51}Y$ mutation, indicating that the endogenous DRF motif does not result in reduced ligand binding due to impaired G protein activation. By contrast, the chemokine receptor CX_3CR1, which also promotes firm adhesion to its immobilised ligand CX_3CL1, did not show signalling dependency of ligand binding or adhesion processes when expressed by THP-1 cells. Further, ligand binding was not affected by mutation of the DRY motif in CX_3CR1 into DRF or DNY. Compared to

CX_3CR1, it has already been speculated that CXCR6 might show special binding-characteristics[38]. It has been proposed that CXCR6 might differ from CX_3CR1 by acquiring distinct conformations when binding of the soluble CXCL16 chemokine domain or the transmembrane chemokine. This model was supported by the identification of a glutamic acid residue within TM-VII of CXCR6 which was critical for binding of the soluble but not the transmembrane form of CXCL16[115]. This has not been reported for CX_3CR1 so far. Furthermore, the mutation of N-terminal acidic residues of CXCR6 did not have an impact on the interaction of the receptor with soluble CXCL16[115]. This was unexpected as basic residues located in the chemokine domain of CXCL16 were shown to be important for receptor interaction, since CXCL16 induced migration was reduced when these residues were replaced by alanine[48]. The loss of N-terminal posttranslational modifications like glycosylation did not result in signalling inhibition, as it was shown for CCR5, CX_3CR1 and CXCR1[120,121]. Furthermore, an extension of the chemokine N-terminal domain resulted in antagonism for chemokine receptors like CCR5, whereas the CXCR6-CXCL16 interaction was not affected[115]. Additionally, CXCR6 lacks a second disulphide bond between the N-terminal site and the extracellular loop 3. This second disulphide bond is common for all other chemokine receptors and an important consequence of this second disulfide bond is the formation of an additional extracellular loop, which shapes the entrance of the ligand-binding pocket[47]. Thus, in contrast to other chemokine receptors CXCR6 might hold an exceptional nature with regard to the ligand binding mechanism involving G protein activation (Figure 55).

Cell biased signalling of GPCRs has been reported before[122,123]. This may be explained on the level of cell type specific conformational states of the GPCR or the interaction with the G protein and G protein-associated molecules. Distinct conformational changes and the structural differences in comparison to other chemokine receptors described above may result in different accessibility modes of the receptor. This could explain the observed cell-type specific differences in surface antibody staining of CXCR6. Surface expression could be easily detected on HEK293 cells via anti-human CXCR6 antibodies. In contrast, surface staining of CXCR6 was not possible on THP-1 cells, although the receptor variants DRF and DRY could be detected via ligand binding assays. Therefore, the receptor might occur in different cell type specific states, which result in different antibody staining. A possible regulatory step influencing ligand binding may be the interaction with the G protein.

A recent study showed that CXCR6-induced calcium and migration responses can be different in HEK293T cells on the one hand and in human leukaemic T cells (Jurkats E6-1) on the other hand[60]. It has been assumed, that the interaction of CXCR6 with different $G\alpha_{i/o}$-subunits might be the reason for cell type specific observations, since the expression pattern of those subunits is cell type specific. Indeed, a role in the selectivity of $G\alpha_{i/o}$-subunits use of the DRY/DRF motif of CXCR6 was shown. However, the factors leading to cell type specificity could not be identified, since interaction patterns of CXCR6 variants with $G\alpha_{i/o}$-subunits in different cell types were not in line with different expression patterns of $G\alpha_{i/o}$-subunits in these cell lines. Additionally, cell type dependent properties of CXCR6 could also result from other cell type specific regulators such as the regulators of G protein signalling (RGS) or GPCR kinases (GRKs). RGS proteins

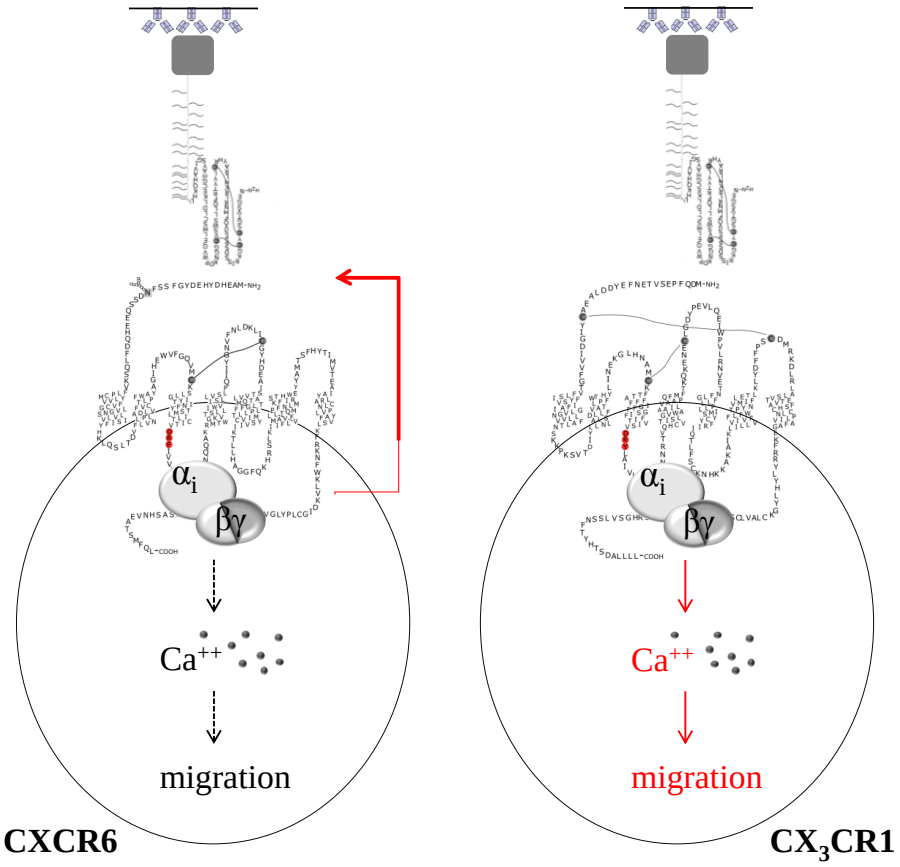

Figure 55 Predominant functions of CXCR6 and CX_3CR1 in monocytic cells
Adhesion of CXCR6 expressing THP-1 cells (left) was shown to depend on G protein coupling (as indicated by red arrow), since PTX treatment, low temperature and DNF expression inhibited binding of soluble and immobilised CXCL16. In contrast, CX_3CR-mediated adhesion of THP-1 cells (right) did not depend on G protein activation. For CX_3CR1 a strong effect on calcium influx and migration was shown (highlighted in red), whereas CXCR6 mediated only weak calcium influx and migration (dotted lines). Location of DRY and DRF motifs are highlighted in red and disulphide bonds are indicated by grey lines.

contribute to signal termination without interacting with the receptor itself, but by regulating activation of the Gα-subunit[124]. It still remains unknown, which mechanisms might be involved in the regulation of activation, inactivation and accessibility of CXCR6 in a cell-biased manner. Therefore, the cell type specific expression pattern of different RGS should be analysed, as it has been performed for different $G\alpha_{i/0}$-subsets[60]. Subsequently, overexpression and gene silencing studies of the identified RGS and $G\alpha_{i/0}$-subsets could be performed to uncover the molecular reasons for cell type specific CXCR6 functions

Intracellular signalling and migration of CXCR6 expressing THP-1 cells is DRF dependent

It has been reported for other chemokine receptors, such as CX_3CR1[125,126], that receptor activation leads to enhanced proliferation and cell survival. In case of CX_3CR1, cell survival was shown to be increased due to protection against apoptotic stress. CX_3CL1-CX_3CR1 interaction reduced intracellular levels of reactive oxygen species via an unknown mechanism and promoted cell survival of monocyte subsets[126]. Further, the phosphatidylinositide 3-kinases (PI3K)/Akt pathway was shown to promote CX_3CL1 mediated cell survival in prostate cancer cells[127]. In contrast, CXCR6-CXCL16 interaction did neither increase cell survival after bleomycin treatment nor proliferation of THP-1 cells in the present study. Nevertheless, CXCL16 stimulation of THP-1 cells led to activation of Akt signalling, which was dependent on active signal transduction as CXCL16-induced Akt phosphorylation was absent in CXCR6-DNF expressing cells (Figure 56). This is well in line with the activation of the PI3K/AKT signalling pathway described for CXCL16 stimulation of CXCR6 expressing platelets[53]. Interestingly, previous studies showed that Akt phosphorylation is partly dependent on β-arrestin activation[32]. In addition to their role as desensitisers of G protein-mediated signalling, β-arrestins may directly serve as signal transducers. β-Arrestin-dependent engagement of many seven transmembrane receptor-coupled signalling systems and the regulation of essential cellular processes by these β-arrestin-mediated pathways has been reported[32]. The atypical chemokine receptor CXCR7 was shown to interact with β-arrestin exclusively, which resulted in Akt phosphorylation and migration[128,129]. Since CXCR7 is an atypical chemokine receptor, no G protein interaction is involved in this signalling process. As described above, also CXCR6 shows several atypical features in comparison to the typical structure of GPCRs, which could include β-arrestin interaction. However, the observed lack of Akt phosphorylation due to DNF mutation shows a

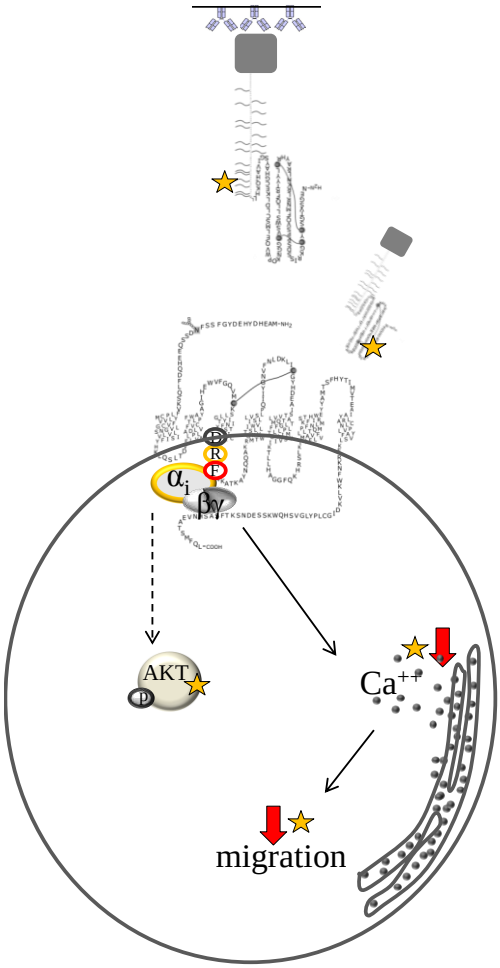

Figure 56 Relevance of the DRF motif of CXCR6 in THPs cells
CXCR6 variants were expressed in THP-1 cells. Adhesion to immobilised CXCL16-Fc and binding of soluble CXCL16-Fc were investigated and shown to be DRF dependent as $R^{3.50}N$ mutation abrogated CXCL16 binding. In addition, Adhesion, Akt phosphorylation, calcium influx and migration were shown to dependent on DRF/DRY motif-mediated signalling. Interestingly, calcium influx and migration showed reduced activity of CXCR6-DRF-WT in comparison to CXCR6-DRY variant. Yellow stars indicate relevance of DRF dependent processes (abrogated due to $R^{3.50}N$ mutation), red arrow indicate reduced activity of CXCR6-DRF-WT in comparison to CXCR6-DRY variant ($F^{3.51}Y$ mutation).

strong involvement of G protein coupled signalling in case of CXCR6. The slight enhancement of Akt phosphorylation in DRF expressing cells could be due to G protein independent interaction with β-arrestin enhancing the G protein mediated signalling cascade. To solve this question, effects on the phosphorylation of Akt by inhibition of β-arrestin activity or silencing of β-arrestin expression could be analysed in follow up studies.

Calcium influx is an important rapid intracellular signal induced by CXCL16-CXCR6 interaction[60]. As shown for chemokine receptors, calcium influx is mediated by activation of phospholipase C (PLC)[130,131]. PLC cleaves the phospholipid phosphatidylinositol 4,5-bisphosphate (PIP_2) into diacyl glycerol and inositol 1,4,5-trisphosphate (IP_3). IP_3 then diffuses

through the cytosol to bind to IP_3 receptors, particularly calcium channels in the smooth endoplasmic reticulum, which leads to calcium influx into the cytoplasm[132,133]. Both the analysis of HEK293 and THP-1 cells demonstrated that the CXCL16-induced calcium influx is G protein dependent (Figure 55, Figure 54 and Figure 56). Notably, also for the calcium response a cell biased signalling character of CXCR6 was observed in the two cell types. In HEK293, no differences between CXCR6-DRF and -DRY motif expressing cells were observed. In contrast, THP-1 cells expressing CXCR6-DRY showed stronger increase of the cytoplasmic calcium response after CXCL16 stimulation in comparison to CXCR6-DRF (Figure 56). In line with the view that migration and calcium signalling are closely linked cellular responses to chemokines[134], CXCR6-DRY expressing THP-1 cells showed higher migration in response to CXCL16 in comparison to CXCR6-DRF expressing cells (Figure 56). Small intracellular calcium signals, also called calcium flickers, are responsible for the regulation of migratory mechanisms and the activation of diverse regulator proteins like myosin, F-actin polymerisation and the calcium sensitive protease calpain. All mechanisms drive protrusion-retraction-adhesion cycles of lamellipodia and filopodia at the front of migrating cells[134]. Interestingly, there were no detectable differences in basal F-actin polymerisation of THP-1 cells due to CXCR6 expression or the mutation of the DRF motif. It might be that other mechanisms than F-actin polymerisation, like myosin activation or the calcium sensitive activation of different proteases or kinases, are responsible for the difference in DRF/DRY mediated chemotaxis. To confirm this hypothesis, CXCL16 stimulated F-actin polymerisation could be analysed in future studies. However, THP-1 cells expressing CXCR6-DRY variants showed a stronger chemotactic migration in response to soluble CXCL16 than CXCR6-DRF expressing cells. Notably $F^{128}Y$ mutation increased calcium signalling as well as migration only in response to high concentrations but not to low concentrations of CXCL16. This may indicate that the ligand binding affinity of the receptor is not altered but rather its effectiveness in transducing signals towards the G protein. To further study the functional relevance of the endogenous DRY motif in other chemokine receptors, CX_3CR1 variants carrying the endogenous DRY or the varied DRF motif, were analysed for mediating CX_3CL1-induced cell migration. Indeed, THP-1 cells expressing CX_3CR1-DRF, showed decreased chemotactic migration in comparison to CX_3CR1-DRY, which confirms the effects of CXCR6-DRF variation. In contrast, it was recently shown that CXCR6-DRY was less active than the CXCR6-DRF, when receptor variants were expressed in HEK293T cells as measured by calcium influx and cell migration[60]. However, when receptor variants were

expressed in Jurkats E6-1 cells, no differences concerning calcium signalling and migration were observed in that study. Although these previous results again demonstrated the cell-biased character of CXCR6, they are contrary to the present study which did observe increased calcium influx and migration when CXCR6-DRY was expressed in THP-1 cells instead of CXCR6-DRF. Moreover, analysis of another chemokine receptor CCR6 performed by the same authors, did show a negative effect on cell activation caused by $Y^{3.51}F$ mutation, since the endogenous DRY motif-mediated higher activity than a DRF mutant[60]. The authors propose a change in TM-IV length and rotation to be responsible for altered activities after ligand stimulation, which might be affected by mutations altering the endogenous and optimised receptor conformation. In contrast, the present study proposes a model in which the DRY/DRF motif interacts with different domains of the receptor and the environment of the receptor, as will be described below. The observation of these potential interactions might uncover mechanisms of DRF/DRY mediated activation, which are possibly shared by all chemokine receptors, including CXCR6, CCR6[60] and CX_3CR1.

DRY/DRF motif is potentially important for interaction with the receptor environment or for molecular interactions of TM-III with different receptor domains

The DRY/DRF motif in the chemokine receptor family of GPCRs is directly involved in ligand-induced signalling since the mutation of $R^{3.50}N$ results in decreased activity levels[34–36]. Furthermore, the present study uncovers an activity regulating relevance of the third amino acid of the DRY/DRF motif. The molecular modelling analysis of the environment of the DRF motif of CXCR6 indicated that this motif is localised at the intracellular surface of the receptor, where interactions with the phospholipid head groups of the lipid bilayer and water molecules are possible. The interaction of GPCRs with different phospholipids was recently analysed for the β2 adrenergic receptor[135]. It was reported that phospholipids act as direct allosteric modulators for ligand binding and activity of this receptor. This effect is driven by the nature of the head group of phospholipids, whereby ionic interactions between receptor and different head groups might be relevant. In case of chemokine receptors, the interaction with different phospholipid head groups could be influenced differently due to expression of either DRY or DRF. This motif is localised closely to the head groups of surrounding phospholipids and $Y^{3.51}$ or $F^{3.51}$ expression directly affects the polarity of this specific motif. Furthermore, the amino acid at position 3.51 is surrounded by a cluster of hydrophobic amino acids of TM-III and TM-V. As described in the

introduction of this thesis, the conformational changes leading to activation of GPCRs are driven by a network of highly conserved residues and non-covalent interactions, which are similar in all GPCRs of the rhodopsin like family. Therefore, different polar characteristics of the DRF/DRY motif might have critical impact on the interactions of different residues in such a hydrophobic environment.

The role of the more common $Y^{3.51}$ is not yet clear. Therefore, in the present study molecular analysis of the canonical $Y^{3.51}$ of the chemokine receptor CCR5 was performed. The available crystal structure of CCR5 was used as a template, since CCR5 endogenously expresses the DRY motif. Therein, it was obvious that $Y^{3.51}$ of the DRY motif is in hydrogen bond distance of a basic residue at position 3.56. This interaction would be directly affected by $Y^{3.51}F$ mutation. Furthermore, in some non-peptide GPCRs (M2 muscarinic receptor, β2 adrenergic receptor, rhodopsin) there is a possible interaction of $Y^{3.51}$ with a basic residue on TM-V (5.60), which would be affected by $Y^{3.51}F$ mutation as well. Although chemokine receptors lack this basic amino acid at 5.60, this observation highlights the importance of the third amino acid of the DRY motif. Tyrosine is capable of interacting with basic amino acids in the environment of the DRY motif and $Y^{3.51}F$ mutations could directly affect these interactions. The importance of $Y^{3.51}$, has been suggested by other studies as well. The rat cytomegalovirus R33 gene, which is similar to chemokine receptors was analysed by altering the endogenous NRY motif into NRF, and indeed slightly decreased activity of this receptor could be observed[136]. Interestingly, the majority of seven-transmembrane viral chemokine receptors, which often are homologous to mammalian chemokine receptors, show polar/hydrophilic residues in position 3.51[137], as the canonical DRY motif is often altered to DRC, DRT or DRW. It is known that viral seven-transmembrane receptors show a vast divergence in their signalling capacity, ligand specificity and basal activity. Furthermore, viral receptors are very often constitutively active and signal promiscuously through many pathways. This is an additional example for increased receptor activity when amino acids with unipolar side chains like phenylalanine in position 3.51 are replaced by amino acids with a polar side chain, like tyrosine.

Beside the non-covalent interaction of $Y/F^{3.51}$ with different regions of GPCRs, there could exist another possibility how this residue might affect GPCR signalling. It has been reported that the chemokine receptor CCR2 gets phosphorylated at position $Y^{3.51}$ upon signalling, which was supposed to involve the Januskinase/signalling transducer and activator of transcription

(JAK/STAT) pathway[43]. Induction of $Y^{3.51}A$ mutation in CCR2 inhibited receptor phosphorylation at tyrosine in position 3.51, which inhibited calcium influx after ligand binding. Furthermore, an involvement of the JAK/STAT pathway has been reported for CXCR4[100], since inhibition of the JAK/STAT pathway reduced CXCL12 stimulated signalling of CXCR4. But in contrast to strongly decreased signalling of CCR2 due to $Y^{3.51}A$ mutation, the chemokine receptor CXCR4 still interacted with the intracellular G protein when the same mutation was generated[44]. Furthermore, it has been shown recently that CX_3CR1 activates the JAK/STAT/ERK signalling cascade, resulting in chemotactic migration[138]. Pharmacological inhibition or transcriptional silencing of the JAK/STAT pathway decreased CX_3CL1 mediated migration, without blocking migration completely. This mechanism of decreased signalling might be relevant for CXCR6 as well. The mutation of the common DRY motif into DRF might be an adaption of CXCR6 to prevent an involvement of the JAK/STAT signalling pathway, whereas interaction with the G protein, adhesion and weak migration are still possible. This could explain the differences observed between the enhancements of the migratory potential in CXCR6-DRY cells in comparison to CXCR6-DRF expressing cells, whereas ligand binding and adhesion were not affected. However, there is another Y at the intracellular loop 2 in position 4.31 of CXCR6, which might also be targeted by JAK. Therefore, further studies need to investigate the involvement of JAK/STAT during CXCR6-mediated signalling. For this purpose, potential phosphorylations at tyrosine-residues in both positions (3.51 and 4.31) of CXCR6 need to be investigated in detail.

The physiological relevance of the expression of a less active DRF motif in CXCR6 combined with the cell type specific effect of adhesion mechanisms and activity reduction is not easy to understand. Cell migration studies with human PBMCs and murine blood cells indicated that CXCL16 can induce migration of these cells to some degree confirming an endogenous chemotactic function of the receptor. However, there is a study describing CXCR6 as a weak mediator of chemoktaxis[22]. Cancer cells, e.g. breast cancer cells often show increased migration in response to soluble CXCL16, regulated by increased CXCR6 expression[58,139,140]. CXCL16 is constitutively expressed in endothelial and epithelial cells and up-regulated during cancer progression[141]. Therefore, decreased CXCR6 sensitivity to CXCL16 might be an adaptation of the mammalian organism to restrict metastasis. Additionally, the alteration of the DRY motif into DRF in CXCR6 might be an evolutionary adaptation towards a conformation, which is specified

for adhesion rather than migration. Interestingly, in human GPCRs of the rhodopsin like family 66% of receptors express DRY, but 11% also express DRF or even other motifs (10% C, 4% H, 4% W, 5% others at position 3.51). Most of these DRF expressing GPCRs (e.g. dopamine D4 receptor, histamine H3 receptor, proteinase-activated receptor 1 (PAR-1), C5a anaphylatoxin receptor) are not specialised for migration. The presented data suggest that the DRF motif of wild type CXCR6 is not optimised for induction of cell migration. Thus, CXCR6 might be more relevant for other functions than mediating cell migration. The present thesis also showed that CXCR6-mediated adhesion cannot be further optimised by mutating the DRF motif into DRY. This indicates that adhesion by interaction with transmembrane CXCL16 could be an important function of the receptor. Furthermore, as shown in the present study, CXCR6-mediated ligand binding and adhesion can be signalling dependent in some cells such as monocytic THP-1 cells but not in HEK293 cells. Cell biased signalling has been reported for CXCR6 in different cell lines transfected to express CXCR6[60] and as shown here, calcium influx and adhesion processes are regulated differently in different expression systems. Therefore, the chemokine receptor CXCR6 might be optimised for cell biased signalling as well.

5.2 In chronic asthma CXCR6 deficiency reduces leukocyte recruitment but increases tissue remodelling

In the second part of this thesis, the role of the chemokine receptor CXCR6 during experimental murine asthma was investigated. For this purpose, CXCR6/GFP knock-in mice, expressing GFP instead ($CXCR6^{GFP/GFP}$) or in addition to CXCR6 ($CXCR6^{+/GFP}$) were analysed in a subchronic (35 days) and chronic (110 days) model of OVA-induced asthma. $CXCR6^{GFP/GFP}$ and $CXCR6^{+/GFP}$ mice did not differ in the development of subchronic asthmatic disease (35 days) but showed differences in the level of remodelling after developing chronic asthma (110 days) (Table 10).

After 35 days of OVA treatment, the only difference among all measured parameters was observed in CXCL16 secretion. $CXCR6^{GFP/GFP}$ mice showed increased BAL-fluid levels of soluble CXCL16 (Figure 57 step 1 and Table 10). This increase can be explained by the absent binding and uptake of the chemokine by CXCR6 expressing cells. In serum, slight differences in CXCL16 concentration were detectable as well. $CXCR6^{GFP/GFP}$ mice showed increased levels of CXCL16 in healthy and asthmatic mice in comparison to $CXCR6^{+/GFP}$ mice. Thus, differences

were already observed in the constitutive release of CXCL16 in healthy mice and asthmatic mice did not show increased serum CXCL16 levels. A strong constitutive expression of CXCL16 even under healthy conditions has been reported by other studies for human bronchial epithelial cells and also for human lung tissue[11,67]. Due to the strong constitutive production of CXCL16 by bronchial epithelial cells the additional induction of the chemokine in other cell types under asthmatic conditions may not become detectable when BAL levels of CXCL16 in $CXCR6^{+/GFP}$ mice are studied.

In contrast to the subchronic model, the chronic model with 110 days of treatment demonstrated a protective role of CXCR6 during chronic asthma development in mice. Decreased accumulation of CD4-positive cells and increased remodelling processes in CXCR6 deficient mice were detectable (Table 10). These findings indicate a potentially antifibrotic relevance of CXCR6 in late chronic asthma. $CXCR6^{+/GFP}$ and $CXCR6^{GFP/GFP}$ mice showed characteristic features of asthma, like airway hyperresponsiveness, increased mucus production by epithelial cells, subepithelial collagen accumulation and moderate cell recruitment (Figure 57). Interestingly, levels of airway hyperresponsiveness provoked by acetylcholine were similar comparing $CXCR6^{+/GFP}$ and $CXCR6^{GFP/GFP}$ mice, but parameters for tissue remodelling like basal tissue damping and septa thickness were more increased in $CXCR6^{GFP/GFP}$ mice. Remodelling processes and constriction of the small bronchioles influence lung physiology during chronic inflammation in asthmatic diseases[142,143]. The parameter of tissue damping is correlated with the restriction of the small airways and the peripheral tissue. This may indicate a higher susceptibility of $CXCR6^{GFP/GFP}$ in comparison to $CXCR6^{+/GFP}$ mice to prolonged OVA treatment[49].

Table 10 Comparison of CXCR6$^{+/GFP}$ and CXCR6$^{GFP/GFP}$mice in the subchronic and chronic model of OVA-induced asthma

Results are expressed as change in CXCR6$^{GFP/GFP}$ mice in relation to CXCR6$^{+/GFP}$ mice: Symbol description: no change (=); not analysed (n.a.); increase: ↑; decrease: ↓; differences, which are not significant: (↑)/(↓).

analysed mice	sensitisation-model	analysed parameter		Results after OVA treatment compared to CXCR6$^{+/GFP}$
CXCR6$^{GFP/GFP}$ mice	35-days model	IgE in serum		=
		protein in BAL		=
		granulocytes/ monocytic cells in BAL	eosinophils neutrophils monocytic cells	= = =
		leukocytes in BAL	CD4+ T cells CD8+ T cells NKT	= = =
		cytokines in BAL/ cytokine expression in lung tissue	IL-5 eotaxin CXCL16	= = ↑
	110-days model	basal lung function	resistance n-resistance elastance tissue damping	(↑) (↑) (↑) ↑
		AHR	resistance n-resistance elastance tissue damping	= = = =
		tissue remodelling	septa thickness collagen mucus w/d	↑ = = (↑)
		granulocytes/ monocytic cells in BAL	eosinophils monocytic cells	= =
		leukocytes in BAL	CD4+ T cells NKT	↓ (↓)

The question whether chronic inflammation and remodelling progress are parallel or sequential events is controversy discussed[144]. There exist reports showing that inflammatory parameters increase before signs of tissue remodelling are visible[145]. Such a more sequential development could explain the observations made in the present study. Cell recruitment processes were especially observed in the acute phase and in fact leukocytes are very important indicators of the

acute phase of asthma. As mentioned above CXCR6$^{GFP/GFP}$ and CXCR6$^{+/GFP}$ mice did not differ in these early responses. In later stages, tissue modifications and remodelling processes were more prominent and less leukocytes could be observed. This was indicated by the higher amount of remodelling and lower levels of eosinophils and monocytic cells in long-term treated mice. Again there was no difference in the recruitment of eosinophils and monocytic cells between CXCR6$^{GFP/GFP}$ and CXCR6$^{+/GFP}$ mice. Interestingly, after 110 days number of CD4-positive lymphocytes was more profoundly decreased in the alveolar space of CXCR6$^{GFP/GFP}$ mice compared to CXCR6$^{+/GFP}$ mice (Table 10). Moreover, lung tissue of CXCR6$^{GFP/GFP}$ mice showed enhanced remodelling compared to CXCR6$^{+/GFP}$ mice. Taken together, it seems that the transit from the acute inflammation to the remodelling phase is faster in CXCR6$^{GFP/GFP}$ than in CXCR6$^{+/GFP}$ mice.

During asthma, recruitment of leukocytes into the lung tissue and the alveolar space are driven by different cytokines and chemokines, which are released by epithelial cells, macrophages, dendritic cells, T_H cells and others[72,107,144]. During recruitment, leukocytes adhere to endothelial cells via adhesion molecules and also via chemokine receptors and then transmigrate through the endothelial cell layer[146,147]. Further migration through tissue cells is coordinated by chemokine gradients and ensures the recruitment of immune cells to sites of inflammation and the alveolar space. Potential migration of white blood cells in response to soluble CXCL16 was shown in this study and was verified by others[45,76,148]. CXCL16-induced migration is mediated by activation of the only receptor for CXCL16, CXCR6. Furthermore, expression of transmembrane CXCL16 suppressed the migration of cultured cancer cells in response to other chemokines[141]. Suppression of cell migration by CXCL16 was also observed *in vivo* and is thought to be mediated by specific adhesion of migrating CXCR6 expressing cells to transmembrane CXCL16, expressed by cells of the surrounding tissue[141]. As shown in the *in vitro* part of the present thesis, CXCR6-CXCL16 interaction can be G protein dependent and independent, depending on the cell type and these properties can represent a special adaptation of this chemokine receptor.

Different subsets of leukocytes were shown to express CXCR6 as indicated by the analysis of tissue from normal healthy mice. Eosinophils, neutrophils, monocytic cells and different T cell subpopulations, like CD8-positive cells, CD4-positive cells, T_H2 and NKT cells of the lung tissue showed GFP/CXCR6 expression. However, there were no differences with regard to the recruitment of leukocytes into the alveolar space of asthmatic mice after 35 days of OVA

treatment. CXCR6 might not be essential for the migration and invasion of the mentioned cells during acute lung inflammation. In contrast, after 110 days of treatment there were less CD4-positive lymphocytes in the alveolar space of $CXCR6^{GFP/GFP}$ mice. Since the recruitment of CD4-positive cells after 35 days was identical, the receptor might influence the long-term retention or survival of these cells in the lung, which results in detectable differences after 110 days of treatment. It has been reported that CXCR6 influences long-term survival of CD8-positive T cells [149], by inhibiting apoptosis of these cells, without influencing proliferation. Similar results were obtained for NKT and NK cells in the liver[150,151]. In the *in vitro* part of this study, no effect of CXCL16 or CXCR6 on apoptosis could be detected as shown by CXCR6 expression and CXCL16 application. Therefore, another possible mechanism should be considered. The adhesive interaction of CXCR6 with transmembrane CXCL16 might affect retention of CD4-positive cells in lung tissue. As mentioned, high constitutive expression of CXCL16 by lung epithelial cells was reported[11] and CXCR6 expressing cells were shown to adhere to immobilised CXCL16 (see *in vitro* part of this study). Thus, adhesion might result in retention of CXCR6 expressing cells in the inflamed tissue (Figure 57, step 4). In line with this, CXCL16-CXCR6 interaction was reported to mediate retention and positioning in healthy and inflamed liver[152]. Also, CX_3CL1 can serve as retention signal for leucocytes to the interstitium during renal inflammatory responses[153]. As mentioned above, the inflammatory and the remodelling phase of subchronic and chronic asthma can represent sequential steps of disease development. Therefore, the inhibited egress from lung tissue of CD4-positive lymphocytes due to CXCR6 expression might delay the transit from the inflammatory to the remodelling phase of asthma. This might explain the more severe remodelling in lung tissue of CXCR6 deficient mice, which might enter the remodelling phase earlier. For further analysis, the CD4-positive lymphocyte subset which remains in lungs of $CXCR6^{+/GFP}$ mice but not in lungs of $CXCR6^{GFP/GFP}$ mice has to be identified, since lymphocyte subsets analysed in this study (chronic phase: T_H2, NKT) did not differ significantly.

When CXCR6 expression and its role during inflammation are discussed, NKT cells are mentioned frequently[45,59,76,150]. Beside CD4-positive cells, NKT cells were found to express CXCR6 and after 110 days of OVA treatment these cells were slightly less abundant in the BAL-fluid of $CXCR6^{GFP/GFP}$ than in BAL-fluid of $CXCR6^{+/GFP}$ mice. NKT cells have often been reported to support the T_H2 specific response in the on-going phase of asthma, by rapid secretion

of T_H2 specific cytokines[154,155]. Recruitment of NKT cells to sites of inflammation has been reported to be mediated by CXCR6 dependent chemotaxis, especially during liver inflammation[45,61]. However, other chemokine receptors than CXCR6 may be responsible for the recruitment of NKT cells during subchronic lung inflammation. In the present study, there were no significant differences comparing $CXCR6^{+GFP}$ and $CXC6^{GFP/GFP}$ mice after 35 or 110 days of OVA treatment, although a slight decrease of NKT cells was detectable after 110 days in BAL-fluid of $CXCR6^{GFP/GFP}$ mice. In fact, the receptor CCR4 and its ligands CCL17 and CCL22 have been reported to mediate the recruitment of NKT cells into lung tissue during experimental murine asthma[156]. This was combined with development of airway hyperresponsiveness by direct activation of NKT cells, which was absent in CCR4 knock-out mice. Additionally, the mentioned study provided evidence that in CXCR6 knock-out mice, the recruitment of NKT cells during subchronic asthma was not disturbed[156]. Therefore, these results are in line with the results of the present study. However, it is still possible that retention of NKT cells in lung tissue is regulated by CXCR6-CXCL16 adhesion (Figure 57, step 4), although differences in NKT cell number comparing $CXCR6^{+/GFP}$ and $CXCR6^{GFP/GFP}$ mice was not significant. Interestingly, despite the pro-asthmatic effect of NKT cells, during bleomycin-induced fibrotic lung disease, NKT cells can act anti-fibrotic, which was associated with strong secretion of the T_H1 cytokine IFNγ and resulting down-regulation of TGFβ-synthesis[157]. Therefore, NKT cell subsets in lungs of long-term-treated $CXCR6^{+/GFP}$ and $CXCR6^{GFP/GFP}$ mice should be analysed in more detail and the identification of NKT cells should be differentiate between mature NK1.1-positive and immature NK1.1-negative NKT cells, since both forms are present in the periphery[76].

One hallmark of remodelling is the airway wall thickening, which is driven by epithelial cell alterations, increased airway smooth muscle mass, increased airway vascularisation and subepithelial fibrosis[158]. These processes are mediated by different cytokines and chemokines secreted by inflammatory cells and resident lung tissue cells. As such, IL-13, TGFβ and collagen are important modulators of airway wall thickening[107,159–161]. Expression of IL-13, TGFβ and collagen, were increased after 35 days of OVA treatment in both mice strains. One result of collagen 1A1 expression was subepithelial fibrosis, which becomes clearly detectable by thickening of the lamina reticularis[159,162].

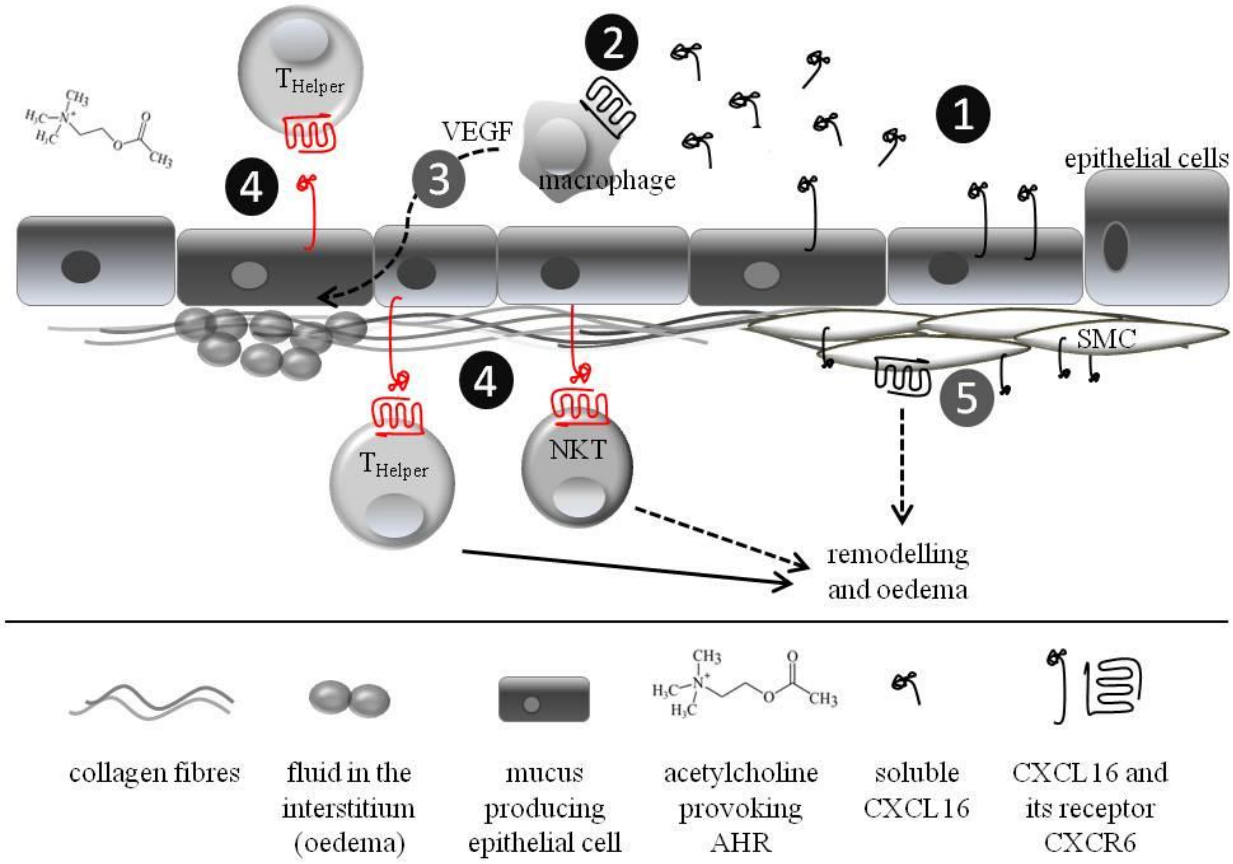

Figure 57 CXCR6-mediated mechanisms during tissue remodelling after 110 days of OVA treatment

All mice showed characteristic features of asthma after 110 days of OVA treatment. CXCL16/CXCR6 related processes during inflammation and remodelling are shown by numbers (black circles: demonstrated in this study, grey circles/dotted lines: hypothesised). (1) CXCL16 is constitutively expressed and released into the alveolar space. (2) CXCL16 can be cleared by CXCR6-mediated endocytosis by e.g. macrophages. (3) Macrophages possibly release VEGF, which could induces subepithelial oedema formation. (4) CXCL16 is not required for recruitment of immune cells but for adhesion and retention (highlighted in red) of CD4-positive lymphocytes in the alveolar space and in the lung tissue. (5) CXCL16 and CXCR6 might affect smooth muscle cell migration. Release of regulatory factors and cytokines by lymphocytes and SMCs can affect lung function, remodelling processes and oedema formation.

This collagenous layer increased after 110 days of treatment which was shown for $CXCR6^{+/GFP}$ and $CXCR6^{GFP/GFP}$ mice. This is a result of extracellular matrix deposition, primarily collagen I, III and V[160]. As shown later for Tie2 *Adam10*$^{-/-}$ and littermates, thickening of the collagen layer is not prominent but slightly increased after 35 days of OVA treatment. This shows again that the inflammation during the acute and subchronic phase of OVA-induced asthma is predominantly characterised by cell recruitment into the lung tissue and these processes result in remodelling mechanisms which are not obvious until chronic asthma has developed. However, CXCR6

expression did not affect thickening of the lamina reticularis of the central airways, which was shown here by quantifying histological investigations of the central airways and big bronchioles. Despite this, thickening of the airway wall might be different in small airways. As shown by the parameter tissue damping, basal constriction of the terminal and small bronchioles was more increased in lungs of $CXCR6^{GFP/GFP}$ mice. Basal constriction might be a result of increased remodelling processes, also driven by increased subepithelial fibrosis causing airway thickening. Therefore, remodelling processes of the terminal bronchioles need to be investigated in more detail.

Despite the expression of CXCR6 by leukocytes and especially lymphocytes, its expression by tissue cells might be relevant in terms of remodelling processes. It has been reported that CXCR6 or CXCL16 are expressed by aortic smooth muscle cells[64,163], fibroblasts[46], epithelial cells[11] and endothelial cells progenitors[164]. Besides thickening of the lamina reticularis, increased proliferation and migration of airway smooth muscle cells are markers for remodelling in asthma[165]. Since aortic smooth muscle cells express CXCR6, expression by airway smooth cells seems possible. In addition, endothelial cell progenitors express CXCR6. Therefore it might be possible, that under healthy conditions CXCL16-CXCR6-mediated adhesive mechanisms supress the migration of smooth muscle cells (Figure 57 step 5) or endothelial cells. Under disease conditions these events could be regulators of remodelling, angiogenesis and oedema formation[88,166]. When the receptor is not expressed, the migration-inhibiting effect of transmembrane CXCL16 expression by other tissue cells[141], which was mentioned above, might be reduced and different cells might show increased migration and invasion leading to a more severe asthmatic phenotype. This has to be investigated in more detail to specify any possible mechanisms. Therefore, proliferation and migration of endothelial cells and smooth muscle cells depending on CXCL16 expression could be analysed *in vitro* and consequences on remodelling and angiogenesis could be analysed *in vivo*. Fibroblasts, as another tissue cell subtype might be interesting too, since these cells express CXCR6 and migrate to sites of renal inflammation in dependence on CXCR6[46]. In addition, TGFβ induces fibroblasts to express α-smooth muscle actin and thereby drives fibrosis[167]. As mentioned, TGFβ secretion is up-regulated to a similar extent in BAL-fluid of $CXCR6^{+/GFP}$ and $CXCR6^{GFP/GFP}$ mice after 35 days of treatment. This demonstrates the fibrotic character of asthma and indicates that TGFβ secretion is not directly influenced by CXCR6 deficiency. Still, recruitment and transition of fibroblast-to-myofibroblast

phenotype during asthma development[168] was not investigated in this study and might be analysed in future experiments.

Angiogenesis and oedema formation also regulate airway wall thickening[152]. The latter was shown to be increased in CXCR6$^{GFP/GFP}$ mice in comparison to CXCR6$^{+/GFP}$ mice after 110 days of OVA treatment. Both, angiogenesis and oedema formation can be regulated by vascular endothelial growth factor (VEGF), which was shown to be increased in sputum of asthmatic patients'[170]. Furthermore, it could be demonstrated that overexpression of VEGF induced an asthmatic phenotype in mice resulting in inflammation, remodelling, mucus metaplasia, airway hyper-responsiveness and oedema formation[171]. Different cells in lung tissue are capable of secreting VEGF. As such, alveolar macrophages are supposed to be an important source of VEGF secretion during asthma development[172] and macrophages were reported to be sensible for CXCL16-induced migration and VEGF secretion[61,164] (Figure 57 step 2 and 3). In addition, a prostate cancer cell line was shown to secrete VEGF as a result of CXCL16 stimulation[57]. Therefore, CXCL16 might be a regulator of VEGF release by alveolar macrophages. However, the amount of these cells did not differ comparing recruitment patterns of CXCR6$^{+/GFP}$ and CXCR6$^{GFP/GFP}$ mice after 35 or 110 days of OVA treatment. Notably, there were more CD4-positive T cells in lung tissue of CXCR6$^{+/GFP}$ and these cells are capable of secreting VEGF as well[172,173]. Nevertheless, this cannot explain the more increased oedema formation in CXCR6$^{GFP/GFP}$ mice since these mice showed weaker CD4-positive cell accumulation. Still, it might be promising to analyse VEGF secretion of alveolar macrophages and CD4-positive T cells during chronic asthma and thereby investigating development of oedema formation in lungs of CXCR6$^{+/GFP}$ and CXCR6$^{GFP/GFP}$ mice in more detail.

Different aspects of remodelling processes have been discussed, but still, it is difficult to find the most likely mechanisms by which remodelling and oedema formation are increased in CXCR6$^{GFP/GFP}$ mice. Since the differences comparing CXCR6$^{+/GFP}$ and CXCR6$^{GFP/GFP}$ mice were only detectable in some parameters measured here, it might be beneficial to analyse the role of CXCR6 expression in a more fibrotic lung disease. This could lead to a more prominent phenotype of CXCR6 deficiency, mediated by pro-fibrotic mechanisms.

There are diverse mice strains, which can react differently to induction of experimental asthma[174]. When mice with a C57BL/6 background and mice with a genetical BALB/c background were

treated to provoke experimental asthma, different disease outcomes were obviuos[174]. BALB/c mice displayed greater levels of airway hyperresponsiveness and exhibited higher number of mast cells in lung tissue than C57BL/6 mice. On the contrary, eosinophil and neutrophil counts in BAL-fluid were greater in C57BL/6[174]. During the basal analysis of cell composition of lung tissue and during analysis of BAL cells after induction of subchronic asthma, the amount of IFNγ producing CD4-positive lymphocytes were higher than the amount of ST2 expressing CD4-positive cells. This confirmed the more T_H1 biased character of mice of the C57BL/6 strain, as reported previously[175]. Thus, to further study how CXCR6 can influence T_H2 based immunologic mechanisms of airway hyperresponsiveness, it seems advisable to include mice with a genetical BALB/c background.

In summary, the chemokine receptor CXCR6 probably influences retention and maintenance of CD4-positive cells in asthmatic lung tissue, which increases anti-fibrotic mechanisms. The CXCL16-CXCR6 axis might influence VEGF secretion by alveolar macrophages or CD4-positive lymphocytes, which possibly affects oedema formation. Moreover, CXCR6-CXCL16 interaction mediated adhesion of lung tissue cells (e.g. smooth muscle cells) might influence migration and proliferation patterns, which affects airway wall thickening. Nevertheless, differences between $CXCR6^{+/GFP}$ and $CXCR6^{GFP/GFP}$ are only detectable in some parameters of tissue remodelling and cell recruitment. Therefore, the chemokine receptor CXCR6 plays a minor role in the regulation of asthma development, but might still be more important during the development of fibrotic lung diseases.

5.3 Endothelial ADAM10 acts pro-asthmatic during subchronic lung inflammation

In the last part of this thesis, the importance of endothelial ADAM10 during asthma development was investigated. This protease is responsible for shedding of the CXCR6 ligand CXCL16. Also EGF, neuregulin, VE-cadherin, CD23, Notch and others are shed by ADAM10[80,81]. The present study could show that endothelial ADAM10 is crucial for the recruitment of leukocytes, especially granulocytes and monocytic cells, into lung tissue in the 35-days model of subchronic asthma. Furthermore, the concentration and expression of asthma specific cytokines, like eotaxin, were decreased in mice lacking endothelial ADAM10 (Table 11).

Table 11 Results of *in vivo* analysis of OVA-induced asthma in Tie2 *Adam*10$^{-/-}$ mice and littermates
Symbol description: no change compared to control (=); not analysed (n.a.); increase compared to wild type control: ↑; decrease compared to wild type control: ↓; differences, which are not significant: (↑)/(↓). Also compare Figure 58.

analysed mice	sensitisation-model	analysed parameter		Results after OVA treatment compared to littermates
Tie2 *Adam*10$^{-/-}$	35-days model	IgE		=
		protein in BAL		(↓)
		tissue remodelling	septa thickness collagen mucus	= = (↓)
		granulocytes in BAL	eosinophils neutrophils monocytic cell	↓ ↓ ↓
		leukocytes in BAL	CD4+ T cells	(↓)
		cytokines expression in lung tissue	IL-5 eotaxin cxcl16	(↓) ↓ =

In the present study, a pro-asthmatic role of endothelial ADAM10 during the acute phase of OVA-induced asthma development could be shown. In this early phase, the recruitment of leukocytes into the lung tissue and the alveolar space is the most characteristic process for asthma. Since no actual tissue damage was provoked in this OVA-induced asthma model, the recruited leukocytes are predominantly responsible for most histopathologic and functional changes. This leukocyte recruitment includes the adhesion of peripheral leukocytes to the endothelium, transmigration of leukocytes through the endothelial cell layer into the tissue and

the migration of leukocytes mediated by chemokine gradients[176]. The extravasation of leukocytes from the blood stream into lung tissue depends on different adhesion molecules on the endothelial cell surface. Several of these molecules are regulated by proteolytic shedding. Thus, transendothelial extravasation can be strongly affected by the deficiency of ADAM10 in endothelial cells (Figure 58)[84,90].

CXCL16 is one of the ADAM10 substrates expressed on endothelial cells that have been shown to mediate leukocyte adhesion and recruitment. However, as indicated in the previous part, CXCR6 deficiency does not lead to altered leukocyte recruitment in the early phase of asthma, suggesting that the CXCL16-CXCR6 axis is of minor relevance for transendothelial leukocyte extravasation. Therefore, it is questionable whether the protection against asthmatic lung inflammation by endothelial ADAM10 deficiency is linked to the suppression of CXCL16 shedding from endothelial cells.

It has been shown for *in vitro* experiments that LPS-induced inflammation in endothelial cells lead to up-regulated expression and activity of ADAM10 and that ADAM10 is required for the control of microvasculature permeability under those inflammatory conditions[177]. Vascular endothelial (VE-) cadherin is a substrate of ADAM10, and shedding of this important cell-cell interaction protein results in increased permeability due to the formation of trans cellular gaps[178]. This enables transmigration of leukocytes into inflamed lung tissue (Figure 58, step 4). This might be an important mechanism, limiting leukocyte recruitment in case of endothelial ADAM10 deficiency, as shown in this study. In fact, *in vitro* it was shown that genetical silencing of ADAM10 and also ADAM17 in endothelial cells is sufficient to abrogate transmigration of neutrophils through endothelial cell layers. These findings were extended to *in vivo* analyses, where vascular permeability and leukocyte recruitment was inhibited by pharmacological inhibition of ADAM10 and ADAM17[177]. It was furthermore shown, that pharmacological inhibition of the protease activity *in vivo* inhibited shedding and the release of the transmembrane chemokine CX_3CL1[177], which might be important for the recruitment and the adhesion of leukocytes to the endothelial cell layers (Figure 58, step 3).

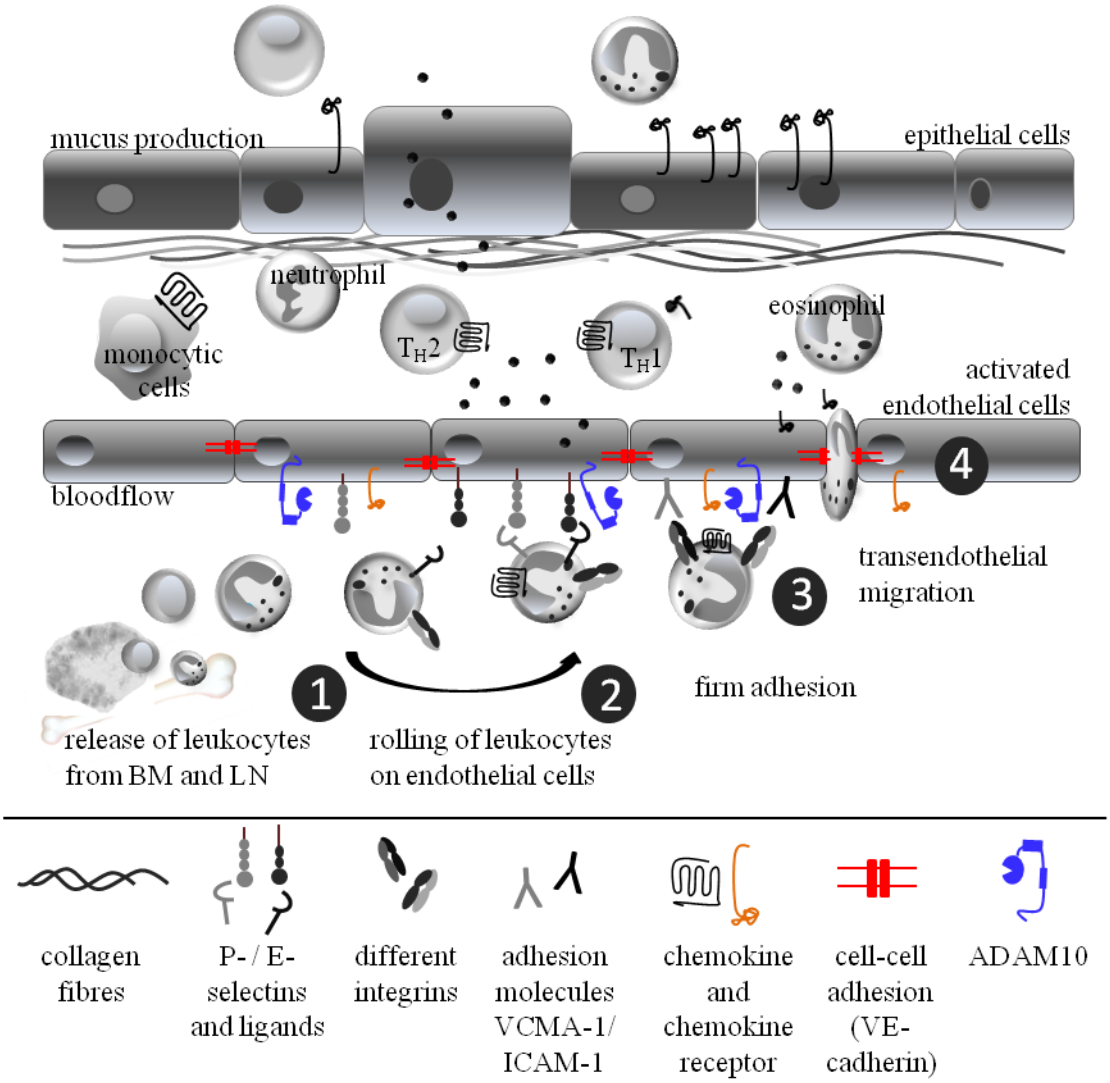

Figure 58 Transendothelial migration during acute asthma
Recruitment of leukocytes into the lung tissue and the alveolar space are crucial in the acute and early phase of asthma. Additionally, mucus production increases and processes leading to subepithelial fibrosis (e.g. production of collagen fibres) are about to start. (1) For the recruitment of leukocytes from the bone marrow (BM) and from neighbouring lymph nodes (LN), the release of cytokines and chemokines by different cells is important. Additionally the endothelium gets activated. Leukocytes of the vasculature interact via adhesion molecules with the adhesion molecules of the activated endothelium (P-/E-selectins). (2) This initiates the leukocytes' process of slow rolling on the endothelium. (3) The interaction of leukocytic integrins with endothelial adhesion molecules (vascular cell adhesion molecule 1 (VCAM-1), intercellular adhesion molecule 1 (ICAM-1)) and the interaction of leukocytic chemokine receptors with endothelial chemokines (CXCL16/CX_3CL1) leads to firm adhesion of the leukocytes. (4) The increased permeability of the endothelium, which is one effect of ADAM10 activity and resulting VE-cadherin shedding, facilitates the subsequent transendothelial migration of leukocytes. Endothelial ADAM10 protease and substrates are highlighted in colour.

As mentioned above, pharmacological inhibition of ADAM proteases reduced inflammation in an *in vivo* model of LPS-induced lung inflammation. This inhibition did not result in a specific inhibition of endothelial ADAM10, but in the inhibition of ADAM10 protease expressed by different cells, like smooth muscle cells and epithelial cells. In fact, recent *in vitro* and *in vivo* studies could show, that ADAM10 also regulates migration of leukocytic cells[84]. THP-1 cells, primary human neutrophils and murine bone marrow derived macrophages require ADAM10 for efficient chemotactic migration and transmigration[84]. Furthermore, signalling and adhesion events that are linked to chemotaxis such as F-actin polymerisation, adhesion to fibronectin and up-regulation of α_5 integrin were also dependent on ADAM10 expression and activity[84]. The lack of leukocytic ADAM10 resulted in an incomplete cell migration due to reduced adhesion to matrix components. *In vivo* it was further shown that ADAM10 expressed by leucocytes is essential for recruitment of these cells into the alveolar space in the lung[84] and into atherosclerotic plaques[179], which confirmed the in *vitro* analysis.

Interestingly, endothelial ADAM10 is not only important for the regulation of vascular permeability due to VE-cadherin shedding, but also for the migration and chemotaxis of endothelial cells[178,179]. It has been shown that endothelial ADAM10 is important for VEGF-induced endothelial cell function due to the interaction and shedding of the VEGF-receptor2 (VEGFR2)[178]. This may also affect angiogenesis processes, which are important during remodelling processes in later stages of murine asthma[158]. Therefore, the effect of endothelial ADAM10 deficiency needs to be further analysed in a more chronic asthma model.

In summary, the protease ADAM10 is very important in many different pathways that contribute to asthma development. Recruitment of leucocytes to sites of inflammation and resulting remodelling processes, e.g. mediated by angiogenesis, are related to expression and activity of ADAM10 by endothelial cells as shown here as well as by other cells, as shown elsewhere.

6 Outlook

The chemokine receptor CXCR6 is unique in the family of chemokine receptors, since it expresses a DRF motif instead of the more common DRY motif at the interface of the TM-III and the second intracellular loop. The present thesis describes the endogenous DRF motif as an adaption of the CXCR6 receptor still allowing adhesion but decreasing calcium signalling and induction of migration in monocytic cells. Still, questions are remaining regarding the cell-biased character of these functions and the activity regulating aspects of the DRY/DRF motif.

Chemokine receptors are activated by ligand binding, but may also obtain basal and ligand-independent activation[180,181]. Further, cell biased and tissue biased signalling has been reported before[60,122,182] but the mechanisms of cell biased regulation of CXCR6 activity and accessibility remain elusive. During this study, HEK293 and THP-1 cells were used as expression systems and different assay were performed with each cell type. It was shown that adhesion and ligand binding as well as calcium signalling was differently regulated in HEK293 and THP-1 cells. To further investigate cell biased mechanisms, all assays need to be performed in each of the cell lines for easier comparison. Cell biased signalling could be influenced by different basal activation states of CXCR6 in different cell types. Therefore, radiolabeled non-hydrolysable GTP-γ^{35}S could be utilized to study G-protein activation. Ligand-independent as well as ligand induced activity and G-protein activation by CXCR6 should be analysed to detect potential differences of the DRF and DRY variants. Recently different interaction of CXCR6 variants with different $G\alpha_{i/0}$ subunits has been described, but the question of cell specificity of CXCR6 functions was not addressed[60]. With regard to cell biased signalling and activity, different $G\alpha_i$ proteins or other regulators of activity could be differently expressed in different cell types. Future studies could study the cell specific coupling to different $G\alpha_i$-proteins or cell specific interactions with regulatory proteins such as GRKs and RGS mediating intracellular receptor phosphorylation and the activity of the Gα-subunit. Besides receptor phosphorylation also glycosylation or sulphation of the receptor could be studied. Both glycosylation and sulphation were shown to influence chemokine receptor activity[180].

It is not yet clear why the DRF expressing CXCR6 or CX_3CR1 have reduced chemotactic activity in comparison to DRY expressing receptors. Underlying mechanisms still need to be

investigated. Specific inhibitors of the JAK pathway have been found to block CXCR4 induced cell functions[100]. These inhibitors could be used to study whether the JAK pathway differentially contributes towards signalling of CXCR6 or CX_3CR1 variants. Cells expressing the DRY motif might show reduced signalling and migration within the range of DRF-receptor expressing cells, when treated with inhibitors of the JAK pathway. In contrast, DRF expressing receptors may not respond to inhibitor treatment as the JAK pathway is already blocked due to the $F^{3.51}Y$ mutation. In line with this, phosphorylation of the hydroxyl groups of $Y^{3.51}$ and $Y^{4.31}$ of CXCR6-DRY and –DRF variant could be investigated in the presence and absence of CXCL16. Furthermore, the interaction of the amino acid at position 3.51 of chemokine receptors with basic residues at position 3.56 should be investigated to clarify the importance of hydrophobic interactions within TM-III of the class of chemokine receptors. Point mutations of the basic amino acid at position $K^{3.56}$ of CXCR6 would be one possible approach to investigate this aspect. Recent studies showed that GPCR activation may involve the interaction with phospholipid head groups of the lipid bilayer[135]. It could therefore be investigated whether these interaction depend on the third amino acid of the DRY/DRF motif, For this analysis, purified chemokine receptors could be reconstituted in high-density lipoparticles to systematically characterize the effect of phospholipids and their head groups on receptor activity, as shown for the β2-adrenergic receptor[135].

The *in vivo* analysis of this study indicated that CXCR6 is relevant for chronic asthma. It was demonstrated that the recruitment of leukocytes in subchronic asthma is not CXCR6 dependent. However, the receptor is relevant for the long-term retention of lymphocytes in the lung tissue. This possibly results in anti-fibrotic mechanisms in the lung, becoming relevant at later stages of chronic asthmatic disease. However, the underlying mechanisms of this anti-fibrotic effect are not yet clear. It would be helpful to analyse the time course of leukocyte recruitment and the fate of individual cells during experimental asthma to specify the tissue infiltration retention and survival of leukocytes in more detail. This analysis should also focus on the smooth muscle cell and myofibrobast proliferation and on the expression of pro- and anti-fibrotic cytokines (IL-10, IFNγ, TGFβ) by different cell subsets. Moreover, the relevance of CXCR6 during lung inflammation might be more obvious in models of more severe lung fibrosis, such as bleomycin induced fibrosis.

With regard to the analysed mice, it might be beneficial for further studies to include mice with a genetical BALB/c background, as they characteristically display a natural T_H2 bias[174] which has been made responsible for more severe asthma development in these mice . Moreover, it was reported that CXCR6$^{+/GFP}$ mice expressing only one CXCR6 allele can differ from wild type mice expressing both alleles for CXCR6[76]. NKT cells of CXCR6$^{+/GFP}$ mice showed reduced migration in comparison to cells of WT-mice, whereas both cell types showed higher CXCL16-induced migration compared to NKT cells of CXCR6$^{GFP/GFP}$ mice. Therefore, asthma development in CXCR6$^{GFP/GFP}$ and CXCR6$^{+/GFP}$ mice should also be compared to that in wild type mice expressing both alleles for CXCR6..

The only known ligand of CXCR6, the transmembrane chemokine CXCL16, is constitutively cleaved by ADAM10, and ADAM10 was reported to be important for cell migration and recruitment[84,177]. A pro-asthmatic role of endothelial ADAM10 could be experimentally shown in the present thesis. In subchronic murine experimental asthma, mice lacking endothelial ADAM10 were protected and this could be underlined by *in vitro* studies performed by other groups[177,84]. Unpublished data indicate that ADAM10 may act protective during the chronification phase of LPS-induced inflammation and bleomycin-induced fibrosis (D. Dreymueller and J. Schumacher (Institute of Pharmacology and Toxicology of the University Hospital Aachen) personal communication and published data[183]). It was already reported that angiogenesis may be impaired by endothelial knock out of ADAM10[178], resulting in reduced remodelling processes. To specify the role of endothelial ADAM10 in asthmatic disease, the chronic phase (110-days model) of asthma should be investigated and analysis of the physiological lung function of OVA- and control-treated mice after induction of chronic asthma should be included.

7 Summary

The chemokine receptor CXCR6 mediates recruitment of T-lymphocytes, plasma cells and macrophages to sites of inflammation and cancer. The only known ligand of CXCR6 is the CXC-chemokine CXCL16, which exists as a transmembrane variant mediating cell-cell adhesion and as a soluble variant acting as a chemoattractant. Like all chemokine receptors, CXCR6 is a heptahelical G protein-coupled receptor. G protein coupling is usually mediated by a $D^{3.49}R^{3.50}Y^{3.51}$ motif at the interface of the third transmembrane region and the second intracellular loop of chemokine receptors. However, CXCR6 carries a unique $D^{3.49}R^{3.50}F^{3.51}$ motif at this position. Yet, the relevance of the DRF motif in CXCR6 and the function of the receptor in the development of asthmatic lung inflammation remain unclear.

The present thesis investigated the importance of the DRF motif of CXCR6 particularly with regard to signalling processes resulting in cell migration. Human embryonic kidney HEK293 cells and monocytic THP-1 cells were transduced to express three different receptor variants carrying different motifs: the natural DRF motif, a DNF mutation, which is thought to disrupt G protein binding, and a mutant with the canonical DRY motif of the other chemokine receptors. In HEK293 cells CXCR6-CXCL16 interaction mediated adhesion and dynamin-dependent internalisation, followed by rapid recycling of the receptor back to the cell surface. Neither of these mechanisms required the DRF motif. In contrast, CXCL16-induced calcium influx was abrogated when DRF was mutated in DNF. In THP-1 cells CXCR6 carrying the DRF motif mediated cell adhesion to immobilized CXCL16, Akt signalling, calcium influx and cell migration in response to CXCL16. All three responses were abrogated by the DNF mutation. Notably, the DRY mutation increased calcium influx and migration induced by CXCL16, but did not affect ligand binding or Akt signalling compared to the DRF variant. *Vice versa* replacement of the endogenous DRY motif in CX_3CR1 by DRF led to decreased cell migration in response to CX_3CL1 without influencing binding to CX_3CL1. However, in contrast to CXCR6, adhesion via CX_3CL1 was not affected by the inhibition of G protein coupling. Thus, the presence of the DRF motif in CXCR6 might represent an adaptation of the receptor for predominantly mediating retention of immune cells to tissues via adhesion to immobilized CXCL16 rather than induction of cell migration in response to soluble CXCL16.

In vivo studies addressed the role of CXCR6 in subchronic (35-days model) and chronic (110-days models) experimental murine asthma. After provoking Ovalbumin (OVA)-induced asthma in a subchronic way, $CXCR6^{+/GFP}$ and $CXCR6^{GFP/GFP}$ mice showed equal responses to OVA. In both mice genotypes increased IgE serum levels, cell recruitment into the alveolar space and similar cytokine release and expression were detectable. In contrast, after induction of chronic asthma, remodelling of lung tissue was more severe in $CXCR6^{GFP/GFP}$ mice than in $CXCR6^{+/GFP}$ mice. Especially septa thickness and the construction of bronchioles and small airways were more increased in lungs of $CXCR^{GFP/GFP}$ mice. Furthermore, $CXCR6^{GFP/GFP}$ mice showed decreased levels of CD4-positive lymphocyte in BAL-fluid. Taken together, CXCR6 does not influence the recruitment of lymphocytes into the lung during the acute phase of asthma, but seems to mediate retention of CD4-positive lymphocytes in the chronic phase. This might influence the remodelling process in lung tissue during the chronification of murine asthma.

Since CXCL16 is cleaved by ADAM10 on endothelial cells, this study additionally addressed the question whether and how endothelial ADAM10 affects the development of subchronic murine asthma. After 35 days of OVA treatment, lungs of Tie2 $Adam10^{-/-}$ mice showed reduced markers of lung inflammation. Reduction in cell recruitment, cytokine release and mucus production in Tie2 $Adam10^{-/-}$ mice compared to littermates were detectable. Therefore, the present thesis uncovered a pro-asthmatic role of endothelial ADAM10. This pro-asthmatic effect was evident already during the acute phase of asthma, in which CXCR6 plays no role, and altered CXCL16 shedding was not observed. This suggests that cleavage of other ADAM10 substrates on endothelial cells, like VE-cadherin could promote endothelial permeability and also increase cell recruitment into the alveolar space.

Thus, CXCR6 is unique within the chemokine receptor family with respect to the function of its DRF motif in cell recruitment and adhesion. The adhesive function of the receptor could be required for the retention of CD4-positive cells to cells expressing transmembrane CXCL16 and promote inflammation in the late phase of asthma. In contrast, to CXCR6, endothelial ADAM10 acts pro-asthmatic already in the acute phase most probably by mediating shedding of other substrates than transmembrane CXCL16.

8 Zusammenfassung

Der Chemokinrezeptor CXCR6 vermittelt die Rekrutierung von T-Lymphozyten, Plasmazellen und Makrophagen in Entzündungsreaktionen und Krebserkrankungen. Das CXC-Chemokin CXCL16 ist der einzig bekannte Ligand des CXCR6 und kann als Adhäsion-vermittelnde transmembrane Variante sowie als chemotaktisch aktive soluble Variante an den Rezeptor binden. Wie alle anderen Chemokinrezeptoren ist CXCR6 ein heptahelikaler G Protein gekoppelter Rezeptor. Die Kopplung des G Proteins wird durch das sogenannte $D^{3.49}R^{3.50}Y^{3.51}$ Motiv vermittelt. CXCR6 trägt jedoch ein für Chemokinrezeptoren einzigartiges DRF-Motiv. Bisher wurde die physiologische Bedeutung dieser natürlichen $Y^{3.51}F$ Mutation im CXCR6 und die Funktion des Rezeptors während der Ausbildung asthmatischer Lungenentzündung nicht näher untersucht.

Die vorliegende Arbeit untersuchte die Relevanz des DRF-Motivs des CXCR6 mit speziellem Fokus auf Signalkaskaden, welche zur Zellmigration führen. Humane embryonale Nieren–Zellen (HEK293) und monozytäre THP-1 Zellen wurden transduziert, um unterschiedliche CXCR6-Varianten zu exprimieren: eine DRF-Variante, welche das endogene Motiv exprimierte, eine Variante, welche ein DNF-Motiv trug, von dem angenommen wird, dass es die Kopplung des G Proteins unterbindet, und eine Variante, welche das in anderen Chemokinrezeptoren exprimierte DRY-Motiv enthielt. In HEK293 Zellen führte die CXCR6-CXCL16 Interaktion zur Adhäsion und zur Dynamin-abhängigen Internalisierung, gefolgt vom Recycling des Rezeptors zurück an die Zelloberfläche. Keiner dieser Mechanismen wurde durch Modifikationen des DRF-Motivs beeinflusst. Hingegen wurde der CXCL16-induzierte Calciumeinstrom durch die Mutation des DRF- zu einem DNF-Motiv unterbunden. In THP-1 Zellen vermittelte das natürliche DRF-Motiv Zelladhäsion, Akt Phosphorylierung, Calciumeinstrom und Zellmigration. Alle diese Prozesse wurden durch die DNF Mutation inhibiert. Auffällig war die Verstärkung des intrazellulären Calciumeinstroms und die verstärkte CXCL16-induzierte Migration bei Expression der DRY-Variante, wobei die Liganden-Bindung und Akt Phosphorylierung, verglichen mit der DRF Variante, unverändert blieben. *Vice versa* Veränderungen des endogenen DRY-Motivs des Chemokinrezeptors CX_3CR1 verringerten die CX_3CL1-stimulierte Zellmigration. Anders als beim CXCR6, wurde die CX_3CR1-vermittelte Adhäsion an CX_3CL1 nicht durch eine Inhibition der G Protein Kopplung herabgesetzt. Daher könnte die Expression

des DRF-Motivs im CXCR6 möglicherweise eine spezielle Adaptation darstellen, die den Rückhalt von Immunzellen im Gewebe durch Adhäsion an membranständiges CXCL16 ermöglicht, ohne dabei verstärkte Zellmigration durch lösliches CXCL16 auszulösen.

Durch *in vivo* Studien wurde die Rolle des CXCR6 in subchronischem (35-Tage Modell) und chronischem (110-Tage Modell) murinen Asthma untersucht. Nach Ausbildung von subchronischem OVA-induziertem Asthma zeigten $CXCR6^{+/GFP}$ und $CXCR6^{GFP/GFP}$ Mäuse keine Unterschiede bezüglich IgE-Serumgehalt, Leukozytenrekrutierung in den Alveolarraum oder Zytokin-Expression. Nach der Induktion chronischen Asthmas zeigten sich jedoch verstärkte Remodellierungsprozesse im Lungengewebe von $CXCR6^{GFP/GFP}$ Mäusen im Vergleich zu $CXCR6^{+/GFP}$ Mäusen. Vor allem die Septendicke und die basale Konstriktion kleiner Atemwege und Bronchiolen waren in $CXCR6^{GFP/GFP}$ Mäusen erhöht. Weiterhin zeigten $CXCR6^{GFP/GFP}$ Mäuse eine verringerte Anzahl an CD4-positiven Lymphozyten im Alveolarraum. Insgesamt zeigte sich, dass CXCR6 die Rekrutierung von Immunzellen in die Lunge während der akuten Phase des Asthmas nicht beeinflusst, wohingegen die Retention von CD4-positiven Zellen CXCR6-vermittelt zu sein scheint. Letzteres vermag Remodellierungsprozesse in der Lunge während der Chronifikation murinen Asthmas zu beeinflussen.

Da CXCL16 auf Endothelzellen durch ADAM10 proteolytisch prozessiert wird, wurde untersucht, inwiefern endotheliales ADAM10 die Ausbildung subchronischen murinen Asthmas beeinflusst. Nach 35 Tagen der OVA-Behandlung zeigten Lungen von Tie2 $Adam10^{-/-}$ Mäusen reduzierte Charakteristika der Entzündung. Auffällig waren vor allem die reduzierte Zellrekrutierung, Zytokinfreisetzung und Mukusproduktion in Lungen der Tie2 $Adam10^{-/-}$ Mäuse. Damit zeigte die vorliegende Arbeit eine pro-asthmatische Funktion endothelialer ADAM10. Diese pro-asthmatische Funktion war schon in der akuten Phase des Asthmas offensichtlich, während CXCR6 zu diesem Zeitpunkt keine detektierbare Relevanz hatte und eine erhöhte Freisetzung von solublen CXCL16 nicht beobachtet werden konnte. Dies lässt vermuten, dass andere ADAM10-Substrate auf endothelialen Zellen, wie VE-Cadherin, die endotheliale Permeabilität und die Rekrutierung von Immunzellen in den Alveolarraum fördern.

Es konnte gezeigt werden, dass CXCR6 im Hinblick auf die Funktion des DRF-Motivs in der Zellrekrutierung und –Adhäsion einzigartig in der Familie der Chemokinrezeptoren ist. Die besondere Funktion der Adhäsion könnte essentiell für die Retention von CD4-positiven Zellen

an CXCL16 exprimierenden Zellen sein und dadurch inflammatorische Prozesse während der späten Phase des Asthmas beeinflussen. Im Gegensatz dazu übt endotheliales ADAM10 seine pro-asthmatische Wirkung schon in der frühen Phase des Asthmas aus, wofür die Prozessierung von anderen Substraten als CXCL16 von Bedeutung zu sein scheint.

9 Collaborations

The following experiments and analyses were performed by or in collaboration with the indicated scientists.

- The experiment investigating G protein signaling dependency of CXCR6-mediated adhesion of HEK293 cells (chapter 4.1.1.3, Figure 11) was performed by Dr. Daniela Dreymueller (Institute of Pharmacology and Toxicology of the University Hospital Aachen). Planning, statistical investigation and interpretation was performed in cooperation with Dr. Dreymueller.
- The experiment analysing a physiological relevance of CXCR6 in monocytic cells (chapter 4.1.2, Figure 14) was planned and performed by Dr. Dreymueller. Interpretation and statistical investigation was performed in cooperation with Dr. Dreymueller.
- Molecular modelling of the CXCR6 receptor on the basis of the known crystal structure of CCR5 was performed by Dr. Xavier Deupi (Paul Scherrer Institute Villigen, Switzerland). Dr. Deupi generated both molecular models for human CXCR6 and CCR5 shown in Figure 27 and Figure 28 (chapter 4.1.4). Furthermore, Dr. Deupi contributed to the interpretation of the results.
- The analysis of murine lung tissue after OVA sensitisation by the Lightsheet microscope (chapter 4.2.2, Figure 35) was performed together with Dr. Reinhard Windoffer (Institute of Molecular and Cellular Anatomy of the University Hospital Aachen). Dr. Windoffer introduced me in the operation of the microscope and the Zen software

The collaborations are also mentioned in the corresponding chapters. All other experiments were planned, performed, analysed and interpreted by myself.

10 References

1. Reig, G., Pulgar, E. & Concha, M. L. Cell migration: from tissue culture to embryos. *Dev. Camb. Engl.* 141, 1999–2013 (2014).
2. Yamaguchi, H. & Condeelis, J. Regulation of the actin cytoskeleton in cancer cell migration and invasion. *Biochim. Biophys. Acta BBA - Mol. Cell Res.* 1773, 642–652 (2007).
3. Huang, C.-W. *et al.* Shear Stress Induces Differentiation of Endothelial Lineage Cells to Protect Neonatal Brain from Hypoxic-Ischemic Injury through NRP1 and VEGFR2 Signaling. *BioMed Res. Int.* 2015, 862485 (2015).
4. Zhang, Z. *et al.* Fibroblast-derived tenascin-C promotes Schwann cell migration through β1-integrin dependent pathway during peripheral nerve regeneration. *Glia* (2015). doi:10.1002/glia.22934
5. Schneider, L. *et al.* Directional Cell Migration and Chemotaxis in Wound Healing Response to PDGF-AA are Coordinated by the Primary Cilium in Fibroblasts. *Cell. Physiol. Biochem.* 25, 279–292 (2010).
6. Welf, E. S. & Haugh, J. M. Signaling pathways that control cell migration: models and analysis. *Wiley Interdiscip. Rev. Syst. Biol. Med.* 3, 231–240 (2011).
7. Wang, J. & Knaut, H. Chemokine signaling in development and disease. *Dev. Camb. Engl.* 141, 4199–4205 (2014).
8. Bachelerie, F. *et al.* International Union of Basic and Clinical Pharmacology. LXXXIX. Update on the Extended Family of Chemokine Receptors and Introducing a New Nomenclature for Atypical Chemokine Receptors. *Pharmacol. Rev.* 66, 1–79 (2014).
9. Palomino, D. C. T. & Marti, L. C. Chemokines and immunity. *Einstein São Paulo Braz.* 13, 469–473 (2015).
10. Eberlein, J. *et al.* Comprehensive assessment of chemokine expression profiles by flow cytometry. *J. Clin. Invest.* 120, 907–923 (2010).
11. Day, C., Patel, R., Guillen, C. & Wardlaw, A. J. The chemokine CXCL16 is highly and constitutively expressed by human bronchial epithelial cells. *Exp. Lung Res.* 35, 272–283 (2009).
12. Rosito, M. *et al.* Trasmembrane chemokines CX3CL1 and CXCL16 drive interplay between neurons, microglia and astrocytes to counteract pMCAO and excitotoxic neuronal death. *Front. Cell. Neurosci.* 8, 193 (2014).
13. Brouty-Boyé, D., Pottin-Clémenceau, C., Doucet, C., Jasmin, C. & Azzarone, B. Chemokines and CD40 expression in human fibroblasts. *Eur. J. Immunol.* 30, 914–919 (2000).
14. Speyer, C. L. & Ward, P. A. Role of endothelial chemokines and their receptors during inflammation. *J. Investig. Surg. Off. J. Acad. Surg. Res.* 24, 18–27 (2011).
15. Abel, S. *et al.* The transmembrane CXC-chemokine ligand 16 is induced by IFN-gamma and TNF-alpha and shed by the activity of the disintegrin-like metalloproteinase ADAM10. *J. Immunol. Baltim. Md 1950* 172, 6362–6372 (2004).
16. Ludwig, A., Berkhout, T., Moores, K., Groot, P. & Chapman, G. Fractalkine is expressed by smooth muscle cells in response to IFN-gamma and TNF-alpha and is modulated by metalloproteinase activity. *J. Immunol. Baltim. Md 1950* 168, 604–612 (2002).

17. Hundhausen, C. *et al.* Regulated shedding of transmembrane chemokines by the disintegrin and metalloproteinase 10 facilitates detachment of adherent leukocytes. *J. Immunol. Baltim. Md 1950* 178, 8064–8072 (2007).
18. Keeley, E. C., Mehrad, B. & Strieter, R. M. CXC chemokines in cancer angiogenesis and metastases. *Adv. Cancer Res.* 106, 91–111 (2010).
19. Weber, K. S., von Hundelshausen, P., Clark-Lewis, I., Weber, P. C. & Weber, C. Differential immobilization and hierarchical involvement of chemokines in monocyte arrest and transmigration on inflamed endothelium in shear flow. *Eur. J. Immunol.* 29, 700–712 (1999).
20. Middleton, J., Patterson, A. M., Gardner, L., Schmutz, C. & Ashton, B. A. Leukocyte extravasation: chemokine transport and presentation by the endothelium. *Blood* 100, 3853–3860 (2002).
21. Slauenwhite, D., Gebremeskel, S., Doucette, C. D., Hoskin, D. W. & Johnston, B. The chemokine receptor CXCR6 regulates cytokine polarization and T cell recruitment to inflamed paws in collagen-induced arthritis. *Arthritis Rheumatol.* n/a–n/a (2014). doi:10.1002/art.38816
22. Latta, M., Mohan, K. & Issekutz, T. B. CXCR6 is expressed on T cells in both T helper type 1 (Th1) inflammation and allergen-induced Th2 lung inflammation but is only a weak mediator of chemotaxis. *Immunology* 121, 555–564 (2007).
23. Hall, R. A., Premont, R. T. & Lefkowitz, R. J. Heptahelical Receptor Signaling: Beyond the G Protein Paradigm. *J. Cell Biol.* 145, 927–932 (1999).
24. Ulvmar, M. H., Hub, E. & Rot, A. Atypical chemokine receptors. *Exp. Cell Res.* 317, 556–568 (2011).
25. Rot, A. & von Andrian, U. H. Chemokines in innate and adaptive host defense: basic chemokinese grammar for immune cells. *Annu. Rev. Immunol.* 22, 891–928 (2004).
26. Han, X., Feng, Y., Chen, X., Gerard, C. & Boisvert, W. A. Characterization of G protein coupling mediated by the conserved D1343.49 of DRY motif, M2416.34, and F2516.44 residues on human CXCR1. *FEBS Open Bio* 5, 182–190 (2015).
27. Scholten, D. *et al.* Pharmacological modulation of chemokine receptor function. *Br. J. Pharmacol.* 165, 1617–1643 (2012).
28. Rajagopalan, L. & Rajarathnam, K. Structural Basis of Chemokine Receptor Function—A Model for Binding Affinity and Ligand Selectivity. *Biosci. Rep.* 26, 325–339 (2006).
29. Venkatakrishnan, A. J. *et al.* Molecular signatures of G-protein-coupled receptors. *Nature* 494, 185–194 (2013).
30. Nygaard, R., Frimurer, T. M., Holst, B., Rosenkilde, M. M. & Schwartz, T. W. Ligand binding and micro-switches in 7TM receptor structures. *Trends Pharmacol. Sci.* 30, 249–259 (2009).
31. Huttenrauch, F., Nitzki, A., Lin, F.-T., Höning, S. & Oppermann, M. Beta-arrestin binding to CC chemokine receptor 5 requires multiple C-terminal receptor phosphorylation sites and involves a conserved Asp-Arg-Tyr sequence motif. *J. Biol. Chem.* 277, 30769–30777 (2002).
32. Kovacs, J. J., Hara, M. R., Davenport, C. L., Kim, J. & Lefkowitz, R. J. Arrestin Development: Emerging Roles for β-arrestins in Developmental Signaling Pathways. *Dev. Cell* 17, 443–458 (2009).
33. Sun, Y., Cheng, Z., Ma, L. & Pei, G. Beta-arrestin2 is critically involved in CXCR4-mediated chemotaxis, and this is mediated by its enhancement of p38 MAPK activation. *J. Biol. Chem.* 277, 49212–49219 (2002).
34. Rovati, G. E., Capra, V. & Neubig, R. R. The Highly Conserved DRY Motif of Class A G Protein-Coupled Receptors: Beyond the Ground State. *Mol. Pharmacol.* 71, 959–964 (2007).

35. Schwarz, N. *et al.* Requirements for leukocyte transmigration via the transmembrane chemokine CX3CL1. *Cell. Mol. Life Sci.* 67, 4233–4248 (2010).
36. Leschner, J. *et al.* Interruption of the Ionic Lock in the Bradykinin B2 Receptor Results in Constitutive Internalization and Turns Several Antagonists into Strong Agonists. *J. Pharmacol. Exp. Ther.* 344, 85–95 (2013).
37. Ballesteros, J. A. & Weinstein, H. in *Methods in Neurosciences* (ed. Sealfon, S. C.) 25, 366–428 (Academic Press, 1995).
38. Nomiyama, H. & Yoshie, O. Functional roles of evolutionary conserved motifs and residues in vertebrate chemokine receptors. *J. Leukoc. Biol.* 97, 39–47 (2015).
39. Omasits U, Ahrens CH, Mueller S & Wollscheid B. Protter: interactive protein feature visualization and integration with experimental proteomic data. *Bioinformatics* (2014).
40. Springael, J.-Y. *et al.* The activation mechanism of chemokine receptor CCR5 involves common structural changes but a different network of interhelical interactions relative to rhodopsin. *Cell. Signal.* 19, 1446–1456 (2007).
41. Burger, M. *et al.* Point Mutation Causing Constitutive Signaling of CXCR2 Leads to Transforming Activity Similar to Kaposi's Sarcoma Herpesvirus-G Protein-Coupled Receptor. *J. Immunol.* 163, 2017–2022 (1999).
42. Lagane, B. *et al.* Mutation of the DRY Motif Reveals Different Structural Requirements for the CC Chemokine Receptor 5-Mediated Signaling and Receptor Endocytosis. *Mol. Pharmacol.* 67, 1966–1976 (2005).
43. Mellado, M. *et al.* The Chemokine Monocyte Chemotactic Protein 1 Triggers Janus Kinase 2 Activation and Tyrosine Phosphorylation of the CCR2B Receptor. *J. Immunol.* 161, 805–813 (1998).
44. Berchiche, Y. A. *et al.* Direct Assessment of CXCR4 Mutant Conformations Reveals Complex Link between Receptor Structure and Gαi Activation. *J. Biol. Chem.* 282, 5111–5115 (2007).
45. Wehr, A. *et al.* Chemokine receptor CXCR6-dependent hepatic NK T Cell accumulation promotes inflammation and liver fibrosis. *J. Immunol. Baltim. Md 1950* 190, 5226–5236 (2013).
46. Chen, G. *et al.* CXCL16 recruits bone marrow-derived fibroblast precursors in renal fibrosis. *J. Am. Soc. Nephrol. JASN* 22, 1876–1886 (2011).
47. Szpakowska, M., Perez Bercoff, D. & Chevigné, A. Closing the ring: a fourth extracellular loop in chemokine receptors. *Sci. Signal.* 7, pe21 (2014).
48. Shimaoka, T. *et al.* Chemokines Generally Exhibit Scavenger Receptor Activity through Their Receptor-binding Domain. *J. Biol. Chem.* 279, 26807–26810 (2004).
49. Gough, P. J. *et al.* A disintegrin and metalloproteinase 10-mediated cleavage and shedding regulates the cell surface expression of CXC chemokine ligand 16. *J. Immunol. Baltim. Md 1950* 172, 3678–3685 (2004).
50. Ludwig, A. *et al.* Enhanced expression and shedding of the transmembrane chemokine CXCL16 by reactive astrocytes and glioma cells. *J. Neurochem.* 93, 1293–1303 (2005).
51. Andrzejewski, M. G. *et al.* Distinct role of the intracellular C-terminus for subcellular expression, shedding and function of the murine transmembrane chemokine CX3CL1. *Biochem. Biophys. Res. Commun.* 395, 178–184 (2010).
52. Jovanović, I. *et al.* CXCL16 in Vascular Pathology Research: from Macro Effects to microRNAs. *J. Atheroscler. Thromb.* 22, 1012–1024 (2015).

53. Borst, O. *et al.* The Inflammatory Chemokine CXC Motif Ligand 16 Triggers Platelet Activation and Adhesion Via CXC Motif Receptor 6–Dependent Phosphatidylinositide 3-Kinase/Akt Signaling. *Circ. Res.* 111, 1297–1307 (2012).
54. Hofnagel, O., Engel, T., Severs, N. J., Robenek, H. & Buers, I. SR-PSOX at sites predisposed to atherosclerotic lesion formation mediates monocyte-endothelial cell adhesion. *Atherosclerosis* 217, 371–378 (2011).
55. Meyer Dos Santos, S. *et al.* Platelets from flowing blood attach to the inflammatory chemokine CXCL16 expressed in the endothelium of the human vessel wall. *Thromb. Haemost.* 114, 297–312 (2015).
56. Deng, L., Chen, N., Li, Y., Zheng, H. & Lei, Q. CXCR6/CXCL16 functions as a regulator in metastasis and progression of cancer. *Biochim. Biophys. Acta* 1806, 42–49 (2010).
57. Wang, J. *et al.* CXCR6 induces prostate cancer progression by the AKT/mammalian target of rapamycin signaling pathway. *Cancer Res.* 68, 10367–10376 (2008).
58. Xiao, G. *et al.* CXCL16/CXCR6 chemokine signaling mediates breast cancer progression by pERK1/2-dependent mechanisms. *Oncotarget* 6, 14165–14178 (2015).
59. Yang, S. H. *et al.* NKT cells inhibit the development of experimental crescentic glomerulonephritis. *J. Am. Soc. Nephrol. JASN* 19, 1663–1671 (2008).
60. Singh, S. P. *et al.* Selectivity in the Use of Gi/o Proteins Is Determined by the DRF Motif in CXCR6 and Is Cell-Type Specific. *Mol. Pharmacol.* 88, 894–910 (2015).
61. Wehr, A. *et al.* Pharmacological inhibition of the chemokine CXCL16 diminishes liver macrophage infiltration and steatohepatitis in chronic hepatic injury. *PloS One* 9, e112327 (2014).
62. Xia, Y., Yan, J., Jin, X., Entman, M. L. & Wang, Y. The chemokine receptor CXCR6 contributes to recruitment of bone marrow–derived fibroblast precursors in renal fibrosis. *Kidney Int.* (2014). doi:10.1038/ki.2014.64
63. Burns, A. & Ciborowski, P. Acute exposure to methamphetamine alters TLR9-mediated cytokine expression in human macrophage. *Immunobiology* 221, 199–207 (2016).
64. Wågsäter, D., Olofsson, P. S., Norgren, L., Stenberg, B. & Sirsjö, A. The chemokine and scavenger receptor CXCL16/SR-PSOX is expressed in human vascular smooth muscle cells and is induced by interferon gamma. *Biochem. Biophys. Res. Commun.* 325, 1187–1193 (2004).
65. Hattermann, K., Ludwig, A., Gieselmann, V., Held-Feindt, J. & Mentlein, R. The chemokine CXCL16 induces migration and invasion of glial precursor cells via its receptor CXCR6. *Mol. Cell. Neurosci.* 39, 133–141 (2008).
66. Schramme, A. *et al.* Characterization of CXCL16 and ADAM10 in the normal and transplanted kidney. *Kidney Int.* 74, 328–338 (2008).
67. Morgan, A. J. *et al.* Expression of CXCR6 and its ligand CXCL16 in the lung in health and disease. *Clin. Exp. Allergy J. Br. Soc. Allergy Clin. Immunol.* 35, 1572–1580 (2005).
68. Atamas, S. P., Chapoval, S. P. & Keegan, A. D. Cytokines in chronic respiratory diseases. *F1000 Biol. Rep.* 5, 3 (2013).
69. Wang, W., Li, J. J., Foster, P. S., Hansbro, P. M. & Yang, M. Potential therapeutic targets for steroid-resistant asthma. *Curr. Drug Targets* 11, 957–970 (2010).
70. Pichavant, M. *et al.* Ozone exposure in a mouse model induces airway hyperreactivity that requires the presence of natural killer T cells and IL-17. *J. Exp. Med.* 205, 385–393 (2008).
71. Bhakta, N. R. & Woodruff, P. G. Human asthma phenotypes: from the clinic, to cytokines, and back again. *Immunol. Rev.* 242, 220–232 (2011).

72. Lambrecht, B. N. & Hammad, H. The airway epithelium in asthma. *Nat. Med.* 18, 684–692 (2012).
73. Thomas, S. Y., Banerji, A., Medoff, B. D., Lilly, C. M. & Luster, A. D. Multiple chemokine receptors, including CCR6 and CXCR3, regulate antigen-induced T cell homing to the human asthmatic airway. *J. Immunol. Baltim. Md 1950* 179, 1901–1912 (2007).
74. Conroy, D. M. & Williams, T. J. Eotaxin and the attraction of eosinophils to the asthmatic lung. *Respir. Res.* 2, 150 (2001).
75. Chang, Y.-J., DeKruyff, R. H. & Umetsu, D. T. The role of type 2 innate lymphoid cells in asthma. *J. Leukoc. Biol.* 94, 933–940 (2013).
76. Germanov, E. *et al.* Critical Role for the Chemokine Receptor CXCR6 in Homeostasis and Activation of CD1d-Restricted NKT Cells. *J. Immunol.* 181, 81–91 (2008).
77. Kim, H. Y., DeKruyff, R. H. & Umetsu, D. T. The many paths to asthma: phenotype shaped by innate and adaptive immunity. *Nat. Immunol.* 11, 577–584 (2010).
78. Humbles, A. A. *et al.* The murine CCR3 receptor regulates both the role of eosinophils and mast cells in allergen-induced airway inflammation and hyperresponsiveness. *Proc. Natl. Acad. Sci. U. S. A.* 99, 1479–1484 (2002).
79. Lukacs, N. W., Berlin, A., Schols, D., Skerlj, R. T. & Bridger, G. J. AMD3100, a CxCR4 Antagonist, Attenuates Allergic Lung Inflammation and Airway Hyperreactivity. *Am. J. Pathol.* 160, 1353–1360 (2002).
80. Mathews, J. A. *et al.* A potential new target for asthma therapy: A Disintegrin and Metalloprotease 10 (ADAM10) involvement in murine experimental asthma. *Allergy* 66, 1193–1200 (2011).
81. Dreymueller, D., Uhlig, S. & Ludwig, A. ADAM-family metalloproteinases in lung inflammation: potential therapeutic targets. *Am. J. Physiol. - Lung Cell. Mol. Physiol.* 308, L325–L343 (2015).
82. Hartmann, D. *et al.* The disintegrin/metalloprotease ADAM 10 is essential for Notch signalling but not for alpha-secretase activity in fibroblasts. *Hum. Mol. Genet.* 11, 2615–2624 (2002).
83. Becker, R. E. N., Berube, B. J., Sampedro, G. R., DeDent, A. C. & Bubeck Wardenburg, J. Tissue-specific patterning of host innate immune responses by Staphylococcus aureus α-toxin. *J. Innate Immun.* 6, 619–631 (2014).
84. Pruessmeyer, J. *et al.* Leukocytes require the metalloproteinase ADAM10 but not ADAM17 for cell migration and for inflammatory leukocyte recruitment into the alveolar space. *Blood* (2014). doi:10.1182/blood-2013-09-511543
85. Post, S. *et al.* ADAM10 mediates the house dust mite-induced release of chemokine ligand CCL20 by airway epithelium. *Allergy* (2015). doi:10.1111/all.12730
86. Lassalle, P. *et al.* Modulation of adhesion molecule expression on endothelial cells during the late asthmatic reaction: role of macrophage-derived tumour necrosis factor-alpha. *Clin. Exp. Immunol.* 94, 105–110 (1993).
87. Li, X. & Wilson, J. W. Increased vascularity of the bronchial mucosa in mild asthma. *Am. J. Respir. Crit. Care Med.* 156, 229–233 (1997).
88. Asosingh, K. *et al.* Nascent Endothelium Initiates TH2 Polarization of Asthma. *J. Immunol. Baltim. Md 1950* 190, 3458–3465 (2013).
89. Wanner, A. & Mendes, E. S. Airway Endothelial Dysfunction in Asthma and Chronic Obstructive Pulmonary Disease. *Am. J. Respir. Crit. Care Med.* 182, 1344–1351 (2010).
90. Schulz, B. *et al.* ADAM10 regulates endothelial permeability and T-Cell transmigration by proteolysis of vascular endothelial cadherin. *Circ. Res.* 102, 1192–1201 (2008).

91. Andreas Ludwig *et al.* in *B27. BALANCING ACT: NOVEL FUNCTIONS OF THE PROTEASE AND ANTIPROTEASES IN THE LUNG* A2630–A2630 (American Thoracic Society, 2012). at <http://www.atsjournals.org/doi/abs/10.1164/ajrccm-conference.2012.185.1_MeetingAbstracts.A2630>
92. Babendreyer, A. Etablierung von Methoden zur Untersuchung der Interaktion des Chemkonis CXCL16 mit seinem Rezeptor CXCR6 unter physiologischen Bedingungen. (2012).
93. Schulte, A. Zum Vorkommen und zur Regulation der transmembranen Chemokine CXCL16 und CX3CL1. (2015).
94. Unutmaz, D. *et al.* The primate lentiviral receptor Bonzo/STRL33 is coordinately regulated with CCR5 and its expression pattern is conserved between human and mouse. *J. Immunol. Baltim. Md 1950* 165, 3284–3292 (2000).
95. Jorissen, E. *et al.* The Disintegrin/Metalloproteinase ADAM10 Is Essential for the Establishment of the Brain Cortex. *J. Neurosci.* 30, 4833–4844 (2010).
96. Kisanuki, Y. Y. *et al.* Tie2-Cre transgenic mice: a new model for endothelial cell-lineage analysis in vivo. *Dev. Biol.* 230, 230–242 (2001).
97. Glomski, K. *et al.* Deletion of Adam10 in endothelial cells leads to defects in organ-specific vascular structures. *Blood* 118, 1163–1174 (2011).
98. Neel, N. F., Schutyser, E., Sai, J., Fan, G.-H. & Richmond, A. Chemokine receptor internalization and intracellular trafficking. *Cytokine Growth Factor Rev.* 16, 637–658 (2005).
99. van der Voort, R. *et al.* An alternatively spliced CXCL16 isoform expressed by dendritic cells is a secreted chemoattractant for CXCR6+ cells. *J. Leukoc. Biol.* 87, 1029–1039 (2010).
100. Soriano, S. F. *et al.* Chemokines integrate JAK/STAT and G-protein pathways during chemotaxis and calcium flux responses. *Eur. J. Immunol.* 33, 1328–1333 (2003).
101. Delon, I. & Brown, N. H. Integrins and the actin cytoskeleton. *Curr. Opin. Cell Biol.* 19, 43–50 (2007).
102. Tan, Q. *et al.* Structure of the CCR5 chemokine receptor – HIV entry inhibitor Maraviroc complex. *Science* 341, (2013).
103. Balhara, J. & Gounni, A. S. The alveolar macrophages in asthma: a double-edged sword. *Mucosal Immunol.* 5, 605–609 (2012).
104. Farahani, R., Sherkat, R., Hakemi, M. G., Eskandari, N. & Yazdani, R. Cytokines (interleukin-9, IL-17, IL-22, IL-25 and IL-33) and asthma. *Adv. Biomed. Res.* 3, (2014).
105. Pease, J. E. & Williams, T. J. Eotaxin and asthma. *Curr. Opin. Pharmacol.* 1, 248–253 (2001).
106. Steinke, J. W. & Borish, L. Th2 cytokines and asthma — Interleukin-4: its role in the pathogenesis of asthma, and targeting it for asthma treatment with interleukin-4 receptor antagonists. *Respir. Res.* 2, 66–70 (2001).
107. Wills-Karp, M. Interleukin-13 in asthma pathogenesis. *Immunol. Rev.* 202, 175–190 (2004).
108. Wuttge, D. M. *et al.* CXCL16/SR-PSOX is an interferon-gamma-regulated chemokine and scavenger receptor expressed in atherosclerotic lesions. *Arterioscler. Thromb. Vasc. Biol.* 24, 750–755 (2004).
109. Macia, E. *et al.* Dynasore, a cell-permeable inhibitor of dynamin. *Dev. Cell* 10, 839–850 (2006).
110. Henley, J. R., Krueger, E. W., Oswald, B. J. & McNiven, M. A. Dynamin-mediated internalization of caveolae. *J. Cell Biol.* 141, 85–99 (1998).

111. Fan, G.-H., Lapierre, L. A., Goldenring, J. R. & Richmond, A. Differential regulation of CXCR2 trafficking by Rab GTPases. *Blood* 101, 2115–2124 (2003).
112. Zhang, Y. *et al.* Intracellular localization and constitutive endocytosis of CXCR4 in human CD34+ hematopoietic progenitor cells. *Stem Cells Dayt. Ohio* 22, 1015–1029 (2004).
113. Shimaoka, T. *et al.* Cell surface-anchored SR-PSOX/CXC chemokine ligand 16 mediates firm adhesion of CXC chemokine receptor 6-expressing cells. *J. Leukoc. Biol.* 75, 267–274 (2004).
114. Pease, J. E., Wang, J., Ponath, P. D. & Murphy, P. M. The N-terminal Extracellular Segments of the Chemokine Receptors CCR1 and CCR3 Are Determinants for MIP-1α and Eotaxin Binding, Respectively, but a Second Domain Is Essential for Efficient Receptor Activation. *J. Biol. Chem.* 273, 19972–19976 (1998).
115. Petit, S. J., Chayen, N. E. & Pease, J. E. Site-directed mutagenesis of the chemokine receptor CXCR6 suggests a novel paradigm for interactions with the ligand CXCL16. *Eur. J. Immunol.* 38, 2337–2350 (2008).
116. Chung, D. A. *et al.* Mutagenesis and peptide analysis of the DRY motif in the alpha2A adrenergic receptor: evidence for alternate mechanisms in G protein-coupled receptors. *Biochem. Biophys. Res. Commun.* 293, 1233–1241 (2002).
117. Whorton, M. R. *et al.* A monomeric G protein-coupled receptor isolated in a high-density lipoprotein particle efficiently activates its G protein. *Proc. Natl. Acad. Sci. U. S. A.* 104, 7682–7687 (2007).
118. De Lean, A., Stadel, J. M. & Lefkowitz, R. J. A ternary complex model explains the agonist-specific binding properties of the adenylate cyclase-coupled beta-adrenergic receptor. *J. Biol. Chem.* 255, 7108–7117 (1980).
119. Park, P. S.-H., Lodowski, D. T. & Palczewski, K. Activation of G Protein–Coupled Receptors: Beyond Two-State Models and Tertiary Conformational Changes. *Annu. Rev. Pharmacol. Toxicol.* 48, 107–141 (2008).
120. Farzan, M. *et al.* Tyrosine Sulfation of the Amino Terminus of CCR5 Facilitates HIV-1 Entry. *Cell* 96, 667–676 (1999).
121. Bannert, N. *et al.* Sialylated O-glycans and sulfated tyrosines in the NH2-terminal domain of CC chemokine receptor 5 contribute to high affinity binding of chemokines. *J. Exp. Med.* 194, 1661–1673 (2001).
122. Steen, A., Larsen, O., Thiele, S. & Rosenkilde, M. M. Biased and G Protein-Independent Signaling of Chemokine Receptors. *Front. Immunol.* 5, (2014).
123. Cox, M. A. *et al.* Human Interferon-Inducible 10-kDa Protein and Human Interferon-Inducible T Cell α Chemoattractant Are Allotopic Ligands for Human CXCR3: Differential Binding to Receptor States. *Mol. Pharmacol.* 59, 707–715 (2001).
124. Patel, J., Channon, K. M. & McNeill, E. The Downstream Regulation of Chemokine Receptor Signalling: Implications for Atherosclerosis. *Mediators Inflamm.* 2013, (2013).
125. Landsman, L. *et al.* CX3CR1 is required for monocyte homeostasis and atherogenesis by promoting cell survival. *Blood* 113, 963–972 (2009).
126. White, G. E., McNeill, E., Channon, K. M. & Greaves, D. R. Fractalkine promotes human monocyte survival via a reduction in oxidative stress. *Arterioscler. Thromb. Vasc. Biol.* 34, 2554–2562 (2014).
127. Shulby, S. A., Dolloff, N. G., Stearns, M. E., Meucci, O. & Fatatis, A. CX3CR1-fractalkine expression regulates cellular mechanisms involved in adhesion, migration, and survival of human prostate cancer cells. *Cancer Res.* 64, 4693–4698 (2004).

128. Rajagopal, S. *et al.* β-arrestin- but not G protein-mediated signaling by the 'decoy' receptor CXCR7. *Proc. Natl. Acad. Sci.* 107, 628–632 (2010).
129. Torossian, F. *et al.* CXCR7 participates in CXCL12-induced CD34+ cell cycling through β-arrestin–dependent Akt activation. *Blood* 123, 191–202 (2014).
130. Cronshaw, D. G. *et al.* Evidence that phospholipase-C-dependent, calcium-independent mechanisms are required for directional migration of T-lymphocytes in response to the CCR4 ligands CCL17 and CCL22. *J. Leukoc. Biol.* 79, 1369–1380 (2006).
131. Shirakawa, A.-K. *et al.* Pathway-selective suppression of chemokine receptor signaling in B cells by LPS through downregulation of PLC-β2. *Cell. Mol. Immunol.* 7, 428–439 (2010).
132. Bach, T. L. *et al.* Phospholipase cbeta is critical for T cell chemotaxis. *J. Immunol. Baltim. Md 1950* 179, 2223–2227 (2007).
133. Mikoshiba, K. IP3 receptor/Ca2+ channel: from discovery to new signaling concepts. *J. Neurochem.* 102, 1426–1446 (2007).
134. Tsai, F.-C., Kuo, G.-H., Chang, S.-W. & Tsai, P.-J. Ca2+ signaling in cytoskeletal reorganization, cell migration, and cancer metastasis. *BioMed Res. Int.* 2015, 409245 (2015).
135. Dawaliby, R. *et al.* Allosteric regulation of G protein-coupled receptor activity by phospholipids. *Nat. Chem. Biol.* (2015). doi:10.1038/nchembio.1960
136. Gruijthuijsen, Y. K. *et al.* Mutational analysis of the R33-encoded G protein-coupled receptor of rat cytomegalovirus: identification of amino acid residues critical for cellular localization and ligand-independent signalling. *J. Gen. Virol.* 85, 897–909 (2004).
137. Jensen, A.-S. M., lleskov, Sparre-Ulrich, A. H., Davis-Poynter, N. & Rosenkilde, M. M. Structural Diversity in Conserved Regions Like the DRY-Motif among Viral 7TM Receptors—A Consequence of Evolutionary Pressure? *Adv. Virol.* 2012, e231813 (2012).
138. Zhang, Y. *et al.* Fractalkine promotes chemotaxis of bone marrow-derived mesenchymal stem cells towards ischemic brain lesions through Jak2 signaling and cytoskeletal reorganization. *FEBS J.* 282, 891–903 (2015).
139. Triplett, A., Sharma, P., Singh, R., Lillard, J. & Singh, S. CXCR6 mediates migration and invasion of breast cancer cells in a Src, FAK, and ERK1/2 dependent fashion. *J. Immunol.* 184, 133.6 (2010).
140. Darash-Yahana, M. *et al.* The Chemokine CXCL16 and Its Receptor, CXCR6, as Markers and Promoters of Inflammation-Associated Cancers. *PLoS ONE* 4, (2009).
141. Fang, Y. *et al.* Chemokine CXCL16 Expression Suppresses Migration and Invasiveness and Induces Apoptosis in Breast Cancer Cells. *Mediators Inflamm.* 2014, (2014).
142. Tulic, M. K., Christodoulopoulos, P. & Hamid, Q. Small airway inflammation in asthma. *Respir. Res.* 2, 333–339 (2001).
143. Corren, J. Small airways disease in asthma. *Curr. Allergy Asthma Rep.* 8, 533–539 (2008).
144. Murdoch, J. R. & Lloyd, C. M. Chronic inflammation and asthma. *Mutat. Res.* 690, 24–39 (2010).
145. Di Valentin, E. *et al.* New asthma biomarkers: lessons from murine models of acute and chronic asthma. *Am. J. Physiol. Lung Cell. Mol. Physiol.* 296, L185–197 (2009).
146. Beck, G. C. *et al.* Fractalkine is not a major chemoattractant for the migration of neutrophils across microvascular endothelium. *Scand. J. Immunol.* 58, 180–187 (2003).
147. Lassalle, P., Delneste, Y., Gosset, P., Tonnel, A. B. & Capron, A. Potential implication of endothelial cells in bronchial asthma. *Int. Arch. Allergy Appl. Immunol.* 94, 233–238 (1991).
148. Singh, A. K. *et al.* Natural Killer T Cell Activation Protects Mice Against Experimental Autoimmune Encephalomyelitis. *J. Exp. Med.* 194, 1801–1811 (2001).

149. Heesch, K. *et al.* The Function of the Chemokine Receptor CXCR6 in the T Cell Response of Mice against Listeria monocytogenes. *PLoS ONE* 9, e97701 (2014).
150. Geissmann, F. *et al.* Intravascular Immune Surveillance by CXCR6+ NKT Cells Patrolling Liver Sinusoids. *PLoS Biol* 3, e113 (2005).
151. Paust, S. *et al.* Critical role for the chemokine receptor CXCR6 in NK cell-mediated antigen-specific memory of haptens and viruses. *Nat. Immunol.* 11, 1127–1135 (2010).
152. Heydtmann, M. *et al.* CXC Chemokine Ligand 16 Promotes Integrin-Mediated Adhesion of Liver-Infiltrating Lymphocytes to Cholangiocytes and Hepatocytes within the Inflamed Human Liver. *J. Immunol.* 174, 1055–1062 (2005).
153. Chakravorty, S. J., Cockwell, P., Girdlestone, J., Brooks, C. J. & Savage, C. O. S. Fractalkine expression on human renal tubular epithelial cells: potential role in mononuclear cell adhesion. *Clin. Exp. Immunol.* 129, 150–159 (2002).
154. Paget, C. & Trottein, F. Role of type 1 natural killer T cells in pulmonary immunity. *Mucosal Immunol.* 6, 1054–1067 (2013).
155. Umetsu, D. T. & DeKruyff, R. H. Current Perspectives: focused commentary: Key cells in asthma. *J. Allergy Clin. Immunol.* 125, 975–979 (2010).
156. Meyer, E. H. *et al.* iNKT Cells Require CCR4 to Localize to the Airways and to Induce Airway Hyperreactivity. *J. Immunol.* 179, 4661–4671 (2007).
157. Kimura, T. *et al.* Treatment with alpha-galactosylceramide attenuates the development of bleomycin-induced pulmonary fibrosis. *J. Immunol. Baltim. Md 1950* 172, 5782–5789 (2004).
158. Shifren, A., Witt, C., Christie, C. & Castro, M. Mechanisms of remodeling in asthmatic airways. *J. Allergy* 2012, 316049 (2012).
159. Postma, D. S. & Timens, W. Remodeling in asthma and chronic obstructive pulmonary disease. *Proc. Am. Thorac. Soc.* 3, 434–439 (2006).
160. Homer, R. J. & Elias, J. A. Airway remodeling in asthma: therapeutic implications of mechanisms. *Physiol. Bethesda Md* 20, 28–35 (2005).
161. Coutts, A. *et al.* Release of biologically active TGF-beta from airway smooth muscle cells induces autocrine synthesis of collagen. *Am. J. Physiol. Lung Cell. Mol. Physiol.* 280, L999–1008 (2001).
162. Manso, L., Reche, M., Padial, M. A., Valbuena, T. & Pascual, C. Diagnostic tools assessing airway remodelling in asthma. *Allergol. Immunopathol. (Madr.)* 40, 108–116 (2012).
163. Patel, D. N. *et al.* TLR4-NOX4-AP-1 signaling mediates lipopolysaccharide-induced CXCR6 expression in human aortic smooth muscle cells. *Biochem. Biophys. Res. Commun.* 347, 1113–1120 (2006).
164. Isozaki, T. *et al.* Evidence That CXCL16 Is a Potent Mediator of Angiogenesis and Is Involved in Endothelial Progenitor Cell Chemotaxis: Studies in Mice With K/BxN Serum–Induced Arthritis. *Arthritis Rheum.* 65, 1736–1746 (2013).
165. Lazaar, A. L. & Panettieri, R. A. Airway smooth muscle: a modulator of airway remodeling in asthma. *J. Allergy Clin. Immunol.* 116, 488–495; quiz 496 (2005).
166. Bergeron, C., Tulic, M. K. & Hamid, Q. Airway remodelling in asthma: From benchside to clinical practice. *Can. Respir. J. J. Can. Thorac. Soc.* 17, e85–e93 (2010).
167. Duvernelle, C., Freund, V. & Frossard, N. Transforming growth factor-β and its role in asthma. *Pulm. Pharmacol. Ther.* 16, 181–196 (2003).
168. Wójcik, K. A. *et al.* Apigenin inhibits TGF-β1 induced fibroblast-to-myofibroblast transition in human lung fibroblast populations. *Pharmacol. Rep. PR* 65, 164–172 (2013).

169. Chetta, A. *et al.* Vascular endothelial growth factor up-regulation and bronchial wall remodelling in asthma. *Clin. Exp. Allergy J. Br. Soc. Allergy Clin. Immunol.* 35, 1437–1442 (2005).
170. Kristan, S. S. *et al.* Airway angiogenesis in patients with rhinitis and controlled asthma. *Clin. Exp. Allergy J. Br. Soc. Allergy Clin. Immunol.* 39, 354–360 (2009).
171. Lee, C. G. *et al.* Vascular endothelial growth factor (VEGF) induces remodeling and enhances TH2-mediated sensitization and inflammation in the lung. *Nat. Med.* 10, 1095–1103 (2004).
172. Song, C., Ma, H., Yao, C., Tao, X. & Gan, H. Alveolar macrophage-derived vascular endothelial growth factor contributes to allergic airway inflammation in a mouse asthma model. *Scand. J. Immunol.* 75, 599–605 (2012).
173. Marek, N. *et al.* Increased spontaneous production of VEGF by CD4+ T cells in type 1 diabetes. *Clin. Immunol. Orlando Fla* 137, 261–270 (2010).
174. Gueders, M. M. *et al.* Mouse models of asthma: a comparison between C57BL/6 and BALB/c strains regarding bronchial responsiveness, inflammation, and cytokine production. *Inflamm. Res. Off. J. Eur. Histamine Res. Soc. Al* 58, 845–854 (2009).
175. Schulte, S., Sukhova, G. K. & Libby, P. Genetically Programmed Biases in Th1 and Th2 Immune Responses Modulate Atherogenesis. *Am. J. Pathol.* 172, 1500–1508 (2008).
176. Schnoor, M., Alcaide, P., Voisin, M.-B. & van Buul, J. D. Crossing the Vascular Wall: Common and Unique Mechanisms Exploited by Different Leukocyte Subsets during Extravasation. *Mediators Inflamm.* 2015, 946509 (2015).
177. Dreymueller, D. *et al.* Lung endothelial ADAM17 regulates the acute inflammatory response to lipopolysaccharide. *EMBO Mol. Med.* 4, 412–423 (2012).
178. Donners, M. M. P. C. *et al.* A disintegrin and metalloprotease 10 is a novel mediator of vascular endothelial growth factor-induced endothelial cell function in angiogenesis and is associated with atherosclerosis. *Arterioscler. Thromb. Vasc. Biol.* 30, 2188–2195 (2010).
179. van der Vorst, E. P. C. *et al.* Myeloid A disintegrin and metalloproteinase domain 10 deficiency modulates atherosclerotic plaque composition by shifting the balance from inflammation toward fibrosis. *Am. J. Pathol.* 185, 1145–1155 (2015).
180. Bennett, L. D., Fox, J. M. & Signoret, N. Mechanisms regulating chemokine receptor activity. *Immunology* 134, 246–256 (2011).
181. Gilliland, C. T., Salanga, C. L., Kawamura, T., Trejo, J. & Handel, T. M. The chemokine receptor CCR1 is constitutively active, which leads to G protein-independent, β-arrestin-mediated internalization. *J. Biol. Chem.* 288, 32194–32210 (2013).
182. Corbisier, J., Galès, C., Huszagh, A., Parmentier, M. & Springael, J.-Y. Biased Signaling at Chemokine Receptors. *J. Biol. Chem.* 290, 9542–9554 (2015).
183. Dreymueller, D. *et al.* ADAM10 as therapeutic target in acute lung inflammation. Presented as a poster at the 81st Annual Congress of the DGPT (German Society for Experimental and Clinical Pharmacology and Toxicology). (2015).

11 Appendix

11.1 Abbreviations

7AAD	7-Aminoactinomycin
AcCh	acetylcholine
Alu	aluminium hydroxide
Akt	(Proteinkinase B)
ADAM	a disintegrin and metalloproteinase
AHR	airway hyper responsiveness
AM	acetoxymethylesther
Amp	ampicillin
ANOVA	analysis of variances
APC	allophycocyanin
APC	antigen presenting cell
approx. .	approximately
bp(s)	base pairs
BAL	bronchoalveolar lavage
BCA	bicin choninic assay
BSA	bovine serum albumin
°C	degrees Celsius
CD	cluster of differentiation
cDNA	complementary DNA
Cy	cyanin
CCL	[C C motif] ligand
CXCL	[CXC motif] ligand
CX3CL	[CX3C motif] ligand
CCR	[C C motif] receptor
CXCR	[CXC motif] receptor
CX3CR	[CX3C motif] receptor
Ctrl	control
Da	Dalton
DAG	Diacylglycerol
DC	dendritic cell
DMEM	Dulbecco´s modified Eagle´s medium
DMSO	dimethyl sulfoxid
DNA	deoxyribonucleic acid
E-caherin	epithelial cadherin
EDTA	ethylenediaminetetraacetic acid
EGF	epidermal growth factor
Erk	extracellular-signal regulated kinase

E-Selectin	endothelial selectin
e.g.	*exempli gratia* (for example)
et al.	et alii
FACS	fluorescence activated cell sorter
FBS	fetal bovine serum
Fc	fragment crystallisable region: the tail region of an antibody
FCS	fetal calf serum
FDR	false discovery rate
FOT	forced oscillation technique
g	g-force
G	gauge
GAPDH	glyceraldehyde 3-phosphate dehydrogenase
GDP	guanosine diphosphate
GTP	guanosine triphosphate
GFP	green fluorescent protein
GPCR	G protein coupled receptor
h	hour
HEK293 cells	human embryonic kidney cells
ICAM-1	intercellular adhesion molecule-1
IgE	immunoglobulin E
IgG	immunoglobulin G
JAK	Januskinase
IFN-γ	interferon-γ
IL	Interleukin
IP3	Inositol-1,4,5- trisphosphate
i.p.	intraperitoneal
LPS	lipopolysaccharide
mAb	monoclonal antibody
MAPK	mitogen-activated protein kinase
MCP-1	monocyte chemotactic protein 1
min	minute
ml	millilitre
mM	millimolar
mRNA	messenger RNA
mTOR	mammalian target of rapamycin
NKT cell	natural killer T cell
nm	nanometer
OVA	ovalbumin
p	probability
PacBlue	pacific blue
PAGE	polyacrylamide gel electrophoresis

PBS	phosphate buffered saline
PCR	polymerase chain reaction
PE	phycoerythrin
PFA	paraformaldehyde
pg	picogramm
PI3K	phosphatidylinositide 3-kinases
PIP_2	phosphoinositol-4,5-bisphosphate
PLC	phospholipase C
P/S	penicillin/streptomycin
P-Selectin	platelet-selectin
PTX	pertussis toxin
PVDF	polyvinylidene difluorid
RT-qPCR	quantitative real-time polymerase chain reaction
RNA	ribonucleic acid
mRNA	messenger RNA
RPE	R-Phycoerythrin
rpm	rounds per minute
RPS29	40S ribosomal protein S29
RT	room temperature
SD	standard deviation
SDS	sodium dodecyl sulphate
STAT	signalingtransducer and activator of transcription
TE	trypsin/EDTA
T_H	T helper cell
THP-1	human monocytic cell line
TGF	transforming growth factor
TNF	tumour necrosis factor
TM	transmembrane domain
TSLP	thymic stromal lymphopoietin
VE-cadherin	Vascular endothelial cadherin
WT	wild type
X	any amino acid
α	alpha
β	beta
γ	gamma
µ	micro
µg	microgram
µl	microliter
µm	micrometer

11.2 Amino acids

To name amino acids, the one letter-code was used in this study.

A alanine (Ala)	G glycine (Gly)	M methionine (Met)	S serine (Ser)
C cysteine (Cys)	H histidine (His)	N asparagine (Asn)	T threonine (Thr)
D aspartic acid (Asp)	I isoleucine (Ile)	P proline (Pro)	V valine (Val)
E glutamic acid (Glu)	K lysine (Lys)	Q glutamine (Gln)	W tryptophane (Trp)
F phenylalanine (Phe)	L leucine (Leu)	R arginine (Arg)	Y tyrosine (Tyr)

11.3 List of figures

11.4 List of tables

11.5 Plasmid maps

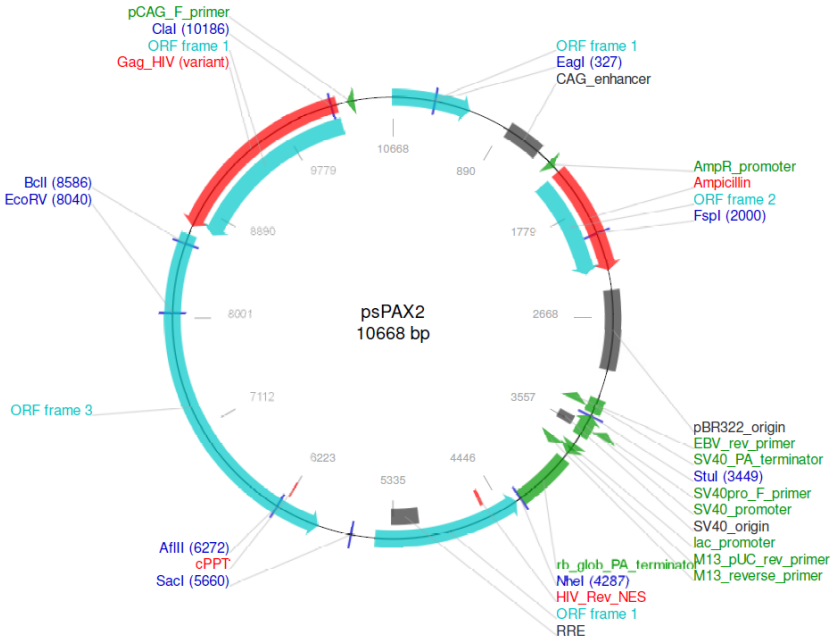

Figure 59 Plasmid map of psPAX2
Source: from addgene.com. psPax2 is a second generation lentiviral packaging plasmid. Can be used with lentiviral vectors and envelope expressing plasmid, e.g. pMD2.G (Addgene number: 12260).

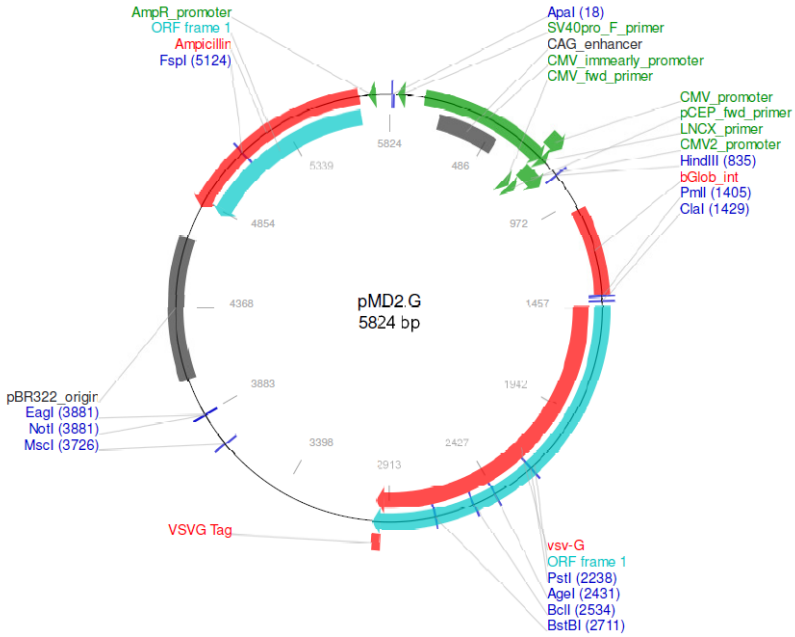

Figure 60 Plasmid map of pMD2.G
Source from addgene.com. pMD2.G is the VSV-G envelope expressing plasmid. Addgene number: 12259.

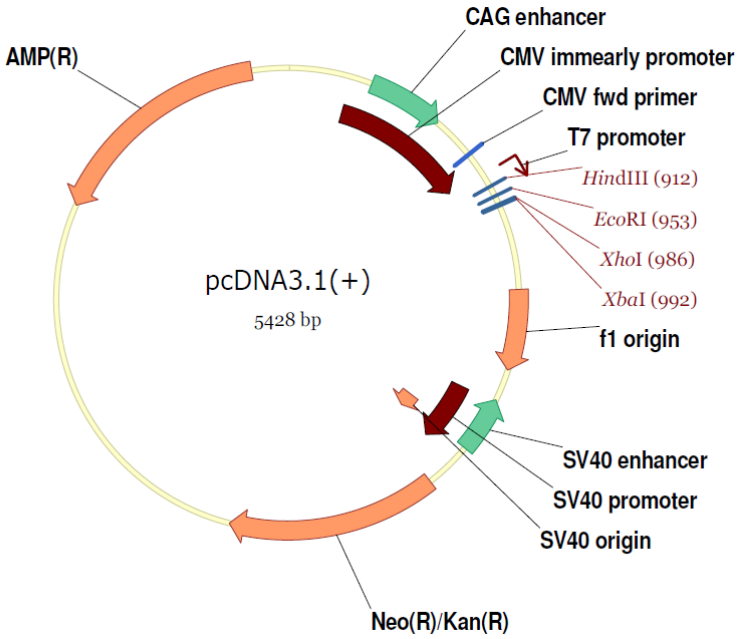

Figure 61 Plasmid map of pcDNA3.1+

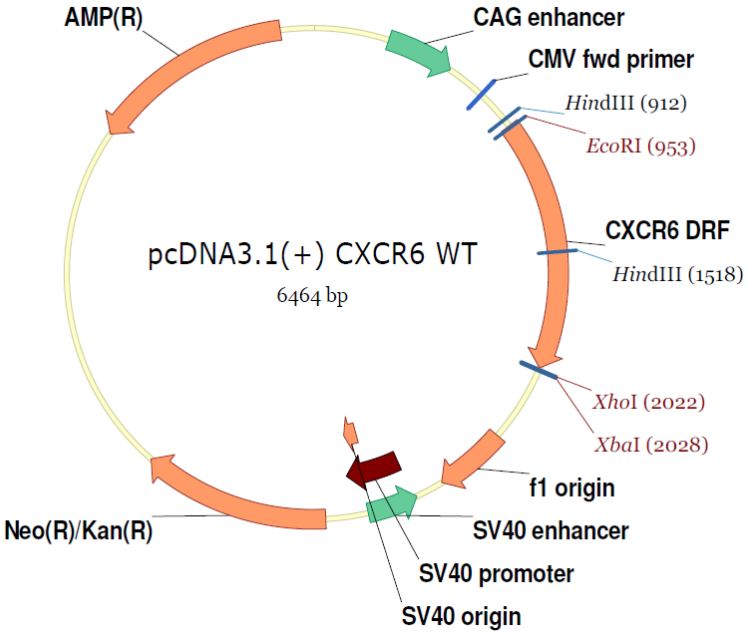

Figure 62 Plasmid map of pcDNA3.1+ encoding for CXCR6 variants
Restriction sites EcoRi and XbaI were used to excise CXCR6 sequences.

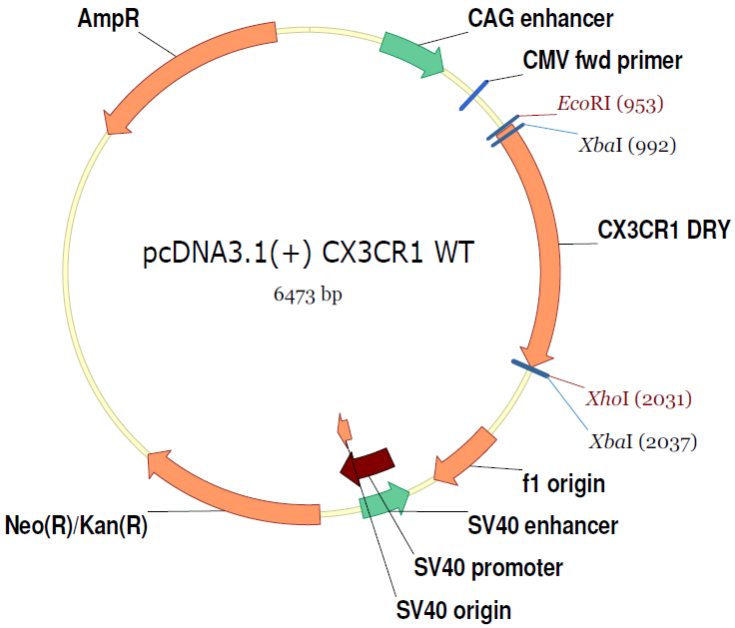

Figure 63 Plasmid map of pcDNA3.1+ encoding murine CX3CR1 variants
Restriction sites EcoRi and XhoI were used to excise CX_3CR1 sequences.

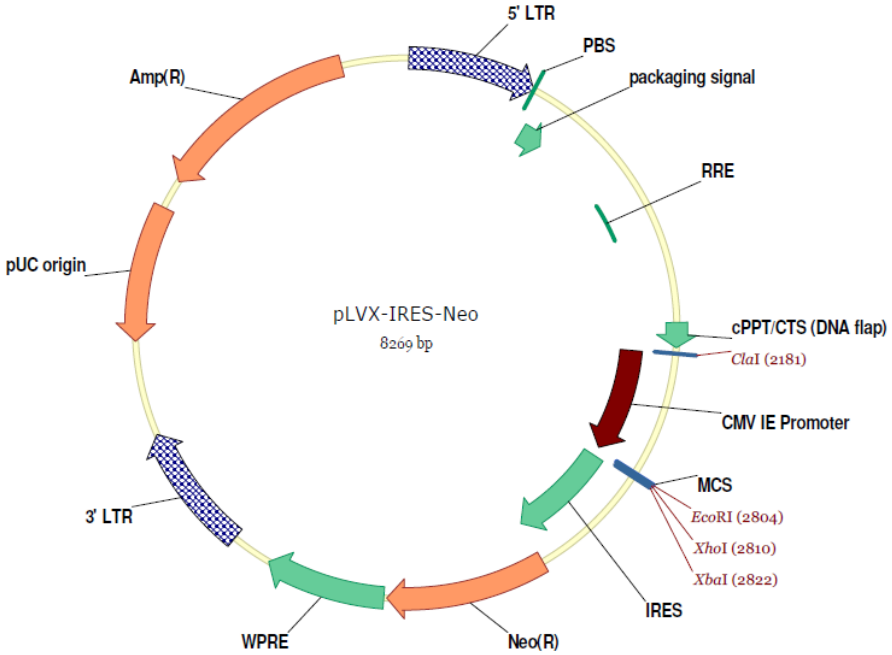

Figure 64 Plasmid map of pLVX-IRES-Neo (EV)
HIV-1-based, lentiviral expression vector.

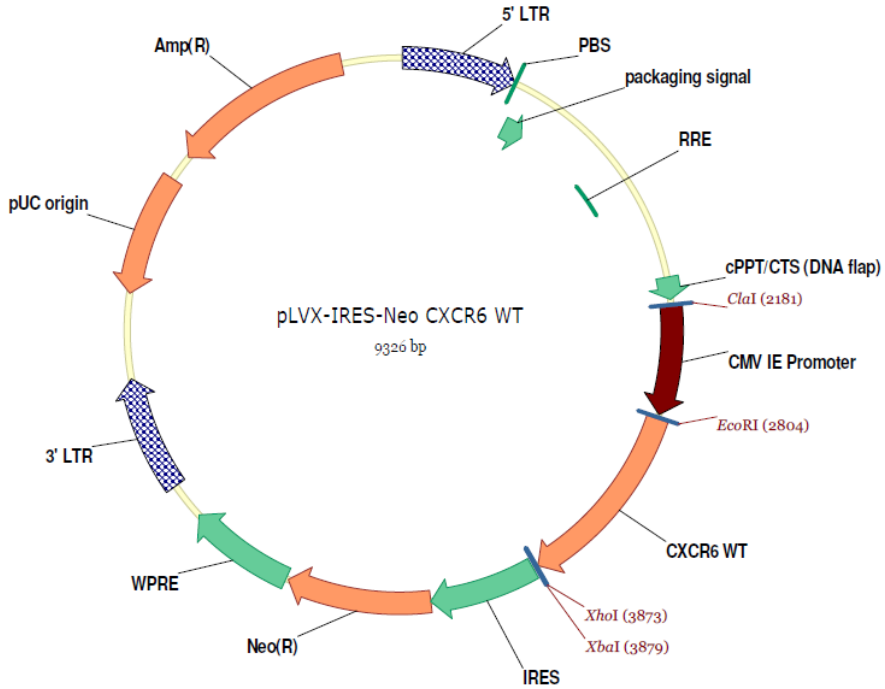

Figure 65 Plasmid map of pLVX-IRES-Neo encoding CXCR6 variants
Restriction sites EcoRi and XbaI were used to insert CXCR6 sequences.

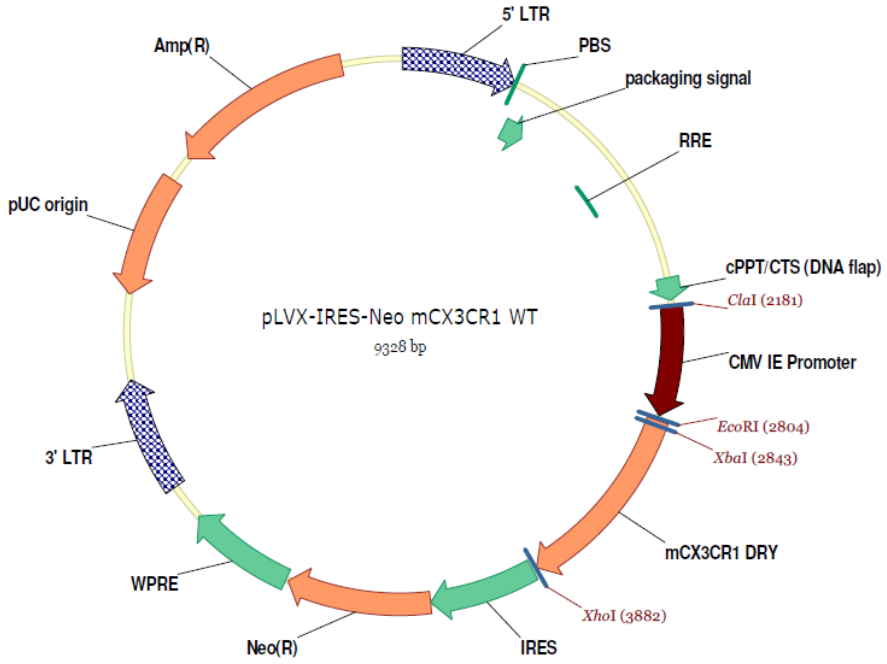

Figure 66 Plasmid map of pLVX-IRES-Neo encoding murine CX_3CR1 variants
Restriction sites EcoRi and XhoI were used to excise CX_3CR1 sequences.

11.6 Nucleotide sequences

All sequences were verified by sequencing (MWG Biotech, Ebersberg, Germany) and showed no mutations (yellow marks codons encoding the DRF/DRY motif of each sequence). Oligonucleotides shown in **Table 4** were used for site directed mutagenesis.

Human CXCR6 WT

ATGGCAGAGCATGATTACCATGAAGACTATGGGTTCAGCAGTTTCAATGACAGCAGC
CAGGAGGAGCATCAAGACTTCCTGCAGTTCAGCAAGGTCTTTCTGCCCTGCATGTAC
CTGGTGGTGTTTGTCTGTGGTCTGGTGGGGAACTCTCTGGTGCTGGTCATATCCATCT
TCTACCATAAGTTGCAGAGCCTGACGGATGTGTTCCTGGTGAACCTACCCCTGGCTG
ACCTGGTGTTTGTCTGCACTCTGCCCTTCTGGGCCTATGCAGGCATCCATGAATGGGT
GTTTGGCCAGGTCATGTGCAAGAGCCTACTGGGCATCTACACTATTAACTTCTACAC
GTCCATGCTCATCCTCACCTGCATCACTGTGGATCGTTTCATTGTAGTGGTTAAGGCC
ACCAAGGCCTACAACCAGCAAGCCAAGAGGATGACCTGGGGCAAGGTCACCAGCTT
GCTCATCTGGGTGATATCCCTGCTGGTTTCCTTGCCCCAAATTATCTATGGCAATGTC
TTTAATCTCGACAAGCTCATATGTGGTTACCATGACGAGGCAATTTCCACTGTGGTTC
TTGCCACCCAGATGACACTGGGGTTCTTCTTGCCACTGCTCACCATGATTGTCTGCTA
TTCAGTCATAATCAAAACACTGCTTCATGCTGGAGGCTTCCAGAAGCACAGATCTCT
AAAGATCATCTTCCTGGTGATGGCTGTGTTCCTGCTGACCCAGATGCCCTTCAACCTC
ATGAAGTTCATCCGCAGCACACACTGGGAATACTATGCCATGACCAGCTTTCACTAC
ACCATCATGGTGACAGAGGCCATCGCATACCTGAGGGCCTGCCTTAACCCTGTGCTC
TATGCCTTTGTCAGCCTGAAGTTTCGAAAGAACTTCTGGAAACTTGTGAAGGACATT
GGTTGCCTCCCTTACCTTGGGGTCTCACATCAATGGAAATCTTCTGAGGACAATTCCA
AGACTTTTTCTGCCTCCCACAATGTGGAGGCCACCAGCATGTTCCAGTTA

Murine CXCR6 WT

ATGGATGATGGGCATCAAGAGTCAGCTCTGTACGATGGGCACTACGAGGGAGATTTC
TGGCTCTTCAACAATTCCAGTGATAACAGCCAGGAGAACAAACGCTTCCTAAAGTTC
AAGGAGGTCTTTTTGCCCTGTGTGTACCTGGTAGTGTTTGTCTTTGGACTGCTAGGAA
ACTCCCTGGTTCTGATTATATACATTTTCTACCAGAAGCTGAGGACTCTGACAGATGT
GTTTCTGCTGAACTTGCCCCTGGCTGACCTGGTGTTTGTCTGTACTCTGCCCTTTTGGG
CCTATGCAGGCACCTATGAGTGGGTCTTTGGCACAGTCATGTGCAAAACTCTTCGAG
GCATGTATACAATGAACTTCTACGTGTCCATGCTCACTCTCACCTGCATCACAGTGGA
TCGTTTCATTGTAGTGGTCCAGGCTACCAAGGCCTTCAACCGGCAGGCTAAGTGGAA
GATCTGGGGCCAAGTCATTTGCTTGCTCATTTGGGTGGTCTCCCTGTTGGTTTCTTTG
CCACAGATCATCTATGGCCATGTTCAAGATATTGACAAGCTTATCTGTCAGTACCAC
AGTGAGGAGATATCCACTATGGTTCTTGTTATACAGATGACTCTGGGGTTCTTCCTGC
CATTGCTCACTATGATTCTGTGCTACTCAGGCATTATCAAGACCTTGCTTCATGCTCG
AAACTTCCAGAAGCACAAATCTCTAAAGATCATCTTCCTTGTAGTGGCTGTGTTCCTG
CTGACCCAGACACCCTTCAACCTTGCCATGTTAATCCAAAGTACAAGCTGGGAGTAC
TATACCATAACCAGCTTTAAGTATGCCATCGTAGTGACAGAGGCTATAGCATACTTT
CGGGCTTGCCTTAACCCTGTACTTTATGCCTTTGTTGGCTTAAAGTTCCGGAAGAACG
TCTGGAAACTTATGAAGGATATCGGCTGCCTCTCTCACCTGGGAGTCTCAAGTCAAT
GGAAGTCTTCTGAGGACAGTTCCAAGACTTGTTCTGCCTCCCACAATGTAGAGACCA
CCAGTATGTTCCAATTG

Murine CX_3CR1 WT

ATGTCCACCTCCTTCCCTGAACTGGATCTAGAGAATTTTGAGTATGACGATTCTGCTG
AGGCCTGTTATTTGGGCGACATTGTGGCCTTTGGAACCATCTTCCTGTCCGTCTTCTA
CGCCCTCGTCTTCACGTTCGGTCTGGTGGGAAATCTGTTGGTGGTCCTCGCTCTCACC
AACAGCCGGAAGCCCAAGAGCATCACTGACATCTACCTCCTGAACCTGGCCTTGAGC
GACCTGCTCTTTGTGGCCACCTTGCCCTTCTGGACTCACTACCTCATCAGCCATGAGG
GCCTCCACAATGCCATGTGCAAGCTCACGACTGCCTTCTTCTTCATTGGCTTCTTTGG
GGGCATATTCTTCATCACCGTCATCAGCATCGACCGGTACCTTGCCATCGTCCTGGCC
GCCAACTCCATGAACAACCGGACAGTGCAGCACGGTGTCACCATTAGTCTGGGCGTC
TGGGCGGCGGCCATCTTAGTGGCGTCACCCCAGTTCATGTTCACAAAGAGAAAGGAC
AACGAGTGTCTGGGTGACTACCCCGAGGTCCTGCAGGAAATGTGGCCCGTGCTCCGC
AACTCGGAAGTCAACATCCTGGGCTTCGCCCTGCCCTTGCTTATCATGAGCTTTTGCT
ACTTCCGCATCATCCAGACGCTGTTTTCCTGCAAGAATCGCAAGAAGGCCAGAGCCG
TCAGACTCATCCTCCTGGTGGTCTTTGCCTTCTTCCTCTTCTGGACACCATACAACAT
CATGATTTTCCTGGAGACTCTCAAGTTCTACAACTTCTTCCCCAGTTGTGACATGAAG
AGGGACCTGAGGTTGGCCCTCAGTGTGACGGAGACAGTGGCGTTCAGCCACTGTTGC
CTCAACCCCTTTATCTACGCCTTTGCCGGGGAAAAGTTCAGAAGATACCTGGGACAC
CTGTATAGGAAGTGCCTGGCCGTCCTGTGCGGTCATCCTGTCCACACCGGCTTCTCGC
CAGAGTCCCAGAGGAGCAGGCAGGACAGCATTCTGAGCAGTTTCACTCACTACACA
AGCGAGGGAGATGGGTCTCTCCTGCTC

12 Publication

Published article:

A cytoplasmic C-terminal fragment of syndecan-1 is generated by sequential proteolysis and antagonizes syndecan-1 dependent lung tumor cell migration

Tobias Pasqualon, Jessica Pruessmeyer, Vera Jankowski, Aaron Babendreyer, Esther Groth, Julian Schumacher, Andrea Koenen, Sarah Weidenfeld, Nicole Schwarz, Bernd Denecke, Holger Jahr, Daniela Dreymueller, Joachim Jankowski, Andreas Ludwig

Abstracts/Poster:

Andrea Koenen, Aaron Babendreyer, Andreas Ludwig, Daniela Dreymueller

Role of the DRF motif for CXC-chemokine receptor 6 (CXCR6)

81nd Annual Congress of the German Society for Experimental and Clinical Pharmacology and Toxicology, Kiel, Germany, 2015

13 Declaration (Eidesstattliche Erklärung)

Hiermit erkläre ich, Andrea Koenen, dass ich die vorliegende Arbeit selbstständig und nur mit Hilfe der angegebenen Hilfsmittel und Quellen unter Anleitung meiner akademischen Lehrer angefertigt habe.

Diese Dissertation wurde bisher keiner anderen Fakultät vorgelegt.

Ich erkläre, bisher kein anderes Promotionsverfahren ohne Erfolg beendet zu haben und dass keine Aberkennung eines bereits erworbenen Doktorgrades vorliegt.

Ort, Datum _____ Unterschrift _____

14 Acknowledgement (Danksagung)

An erster Stelle danke ich Herrn Prof. Dr. Andreas Ludwig herzlich für die Betreuung meiner Doktorarbeit. Danke, dass deine Türe immer offen stand und du mir stets beratend und diskussionsfreudig zur Seite gestanden hast. Außerdem danke ich dir für das Schärfen meines kritischen „Wissenschaftlerblickes“ auf Belange innerhalb und außerhalb des Labors.

Bei Herrn Prof. Dr. Hermann Wagner möchte ich mich für die Übernahme des Zweitgutachtens recht herzlich bedanken.

Ganz besonders danke ich Frau Dr. Daniela Dreymüller. Danke für deine intensive Betreuung, und die vielen wissenschaftlichen Erfahrungen die ich in den letzten Jahren sammeln durfte. Durch deinen positiven Blick auf die Dinge hast du mir so manche Analyse versüßt. Des Weiteren gebührt verschiedenen Helfern Dank. Danke an Silvia Roubrocks und Nadine Ruschke für die Hilfe bei den *FlexiVent* Messungen und danke an Dr. Reinhard Windoffer für die große Hilfe bei der Arbeit an dem *Lightsheet* Mikroskop. Weiterer Dank gebührt Melanie Esser und Tanja Woopen für die viele Hilfe im Labor und für die tausend Kleinigkeiten die ihr jeden Tag für uns erledigt. Ich danke Esther für ihr Talent des Zuhörens und Verstehens in so vielen verschiedenen Momenten, wissenschaftlich und privat. Ich danke weiterhin Julian, dem besten Sitznachbarn den ich mir hätte vorstellen können. Danke, dass du dir für jede einzelne Frage die ich an dich gerichtet habe Zeit genommen hast. Danke auch an „I love science“- Toby, für deine nicht enden wollende Begeisterung und für unzählige witzige Momente. Ebenso danke ich Aaron für seine manchmal niederschmetternde und dennoch erheiternde Komik die meinen Forscheralltag erheiterte. Ich danke der gesamten Arbeitsgruppe für viele geistreiche, lehrreiche ebenso wie witzige Momente im und um das Labor herum.

Ein riesen Dank gilt meinen Freunden daheim und in Aachen. Vor allem danke ich Kathrin und Christoph die in den vergangenen 10 Jahren immer da waren und mit denen ich die Universität in all ihren Facetten gemeinsam erkunden durfte. Es ist so schön mit euch.

Tiefer Dank gilt meinen Eltern und Geschwistern für ihre Unterstützung und Ermunterungen. Ihr seid mein Ruhepol und die Wurzeln die ich nur jedem wünschen kann. Danke Frederik, für jedes ermutigende Wort während der gesamten Promotionszeit und für vieles mehr.